Mechanistic Studies on the Oxidation of Short Peptides with Relevance to Hair Damage

Nikolaos Vagkidis

Doctor of Philosophy

University of York

Chemistry

March 2023

Abstract

The main purpose of this project was the mechanistic study of the aerobic oxidation of short peptides with relevance to hair protein damage. It is well-established that oxidation of biological matter leads to formation of intermediate hydroperoxides. It was hypothesised that accumulation and subsequent decomposition of hydroperoxides would lead to enhanced protein damage. This theory was tested in short peptides that were used as protein mimics. In Chapter 2 it was demonstrated that the combined damage of two insults (UV and heat) is greater than the sum of the two, thus confirming that the two insults act in synergy. Evidence for the role of intermediate hydroperoxides in the process were collected.

In Chapter 3 the antioxidant effect of four catechol-based antioxidants derived from natural extracts was described. Protein damage in hair is known to occur *via* radical reactions. Antioxidants derived from natural sources have received attention in various industries as they have been shown to retard the oxidation of organic compounds. It was demonstrated that all four antioxidants offer significant protection against the $HO^{\bullet}$-mediated oxidation of two protected amino acids. By detecting degradation products formed on the antioxidants, reaction pathways were proposed to corroborate their antioxidant mechanism.

Radical intermediates formed during protein oxidation are challenging to detect with the current detection methods, as their steady state concentration is usually too low. Recently, a new method for trapping and detecting radical intermediates was developed in our group, and this method was applied with success to many different areas of chemistry (e.g., atmospheric, synthetic). In Chapter 4, the scope of application of this method was further expanded. A great number of biological intermediate radicals (both C- and O-centred) generated *via* different oxidants, were successfully characterised. The exact identify of these radicals was further elucidated by well-established isotope-exchange experiments.

Contents

List of Schemes

List of Figures

Acknowledgments

First and foremost, I would like to thank my supervisor Prof Victor Chechik, who guided and supported me throughout my research and writing, but also during the unprecedented pandemic times. His kind and encouraging nature, as well as his scientific insight helped me to grow, both personally and professionally, and build confidence in my work and my capabilities.

I am also very thankful for the exceedingly supportive and encouraging environment created by Dr Jennifer Marsh, my P&G supervisor. I would also like to thank my IPM advisor, Dr Chris Spicer, for his detailed feedback, advice, encouragement, and for making me feel comfortable that I could reach out to him at any point.

Thank you to the academic support staff who provided training and guidance with performing experiments and measurements, including Karl Heaton (MS) and Heather Fish (NMR spectroscopy). A special and heartfelt thanks must go to the eternally kind and helpful Ed Bergstrom (MS), who so patiently helped me every time a problem arose and guided me in times of uncertainty.

Next, I would like to thank the whole of the Chechik group (VC bros!), past and current members, for making the everyday life so much nicer. It was a very demanding period; however, the group made it extremely fun and exciting.

A special warm thanks goes to my four dearest friends Peter, who had been with me since my first day in York, and has helped me integrate into the Chechik group so smoothly, Jonathan and William for the stimulating coffee breaks and discussions, especially during the lockdown period, and finally Ivan who since joining the group has been my best mate, and we have shared so much together (and will definitely share more). Thank you all for the countless pints and laughs we shared together. All of you have been amazing friends both in and out of the lab.

Finally, I would like to thank my family, for supporting me from abroad all these years, and making everything in their power to make it easier for me, and of course, my brother Chris and my best mate Alex, who even though far away, always listened to my problems and concerns, supported me, and made me feel like I never left.

Declaration

I declare that this thesis is a presentation of original work, and I am the sole author. I also declare that in the event the work of others has been used, this has been fully acknowledged in the text and as references. All of the human hair experiments and analysis (Sections 5.5.11 and 5.5.12) were carried out by Procter and Gamble. This work has not previously been presented for an award at this, or any other, University. All sources are acknowledged as References.

Some of the research outlined in this thesis has been published in the following paper:

N. Vagkidis, L. Li, J. M. Marsh, and V. Chechik, *J*. *Photochem*. *Photobiol*. A *Chem.*, 2023, **439**, 114627-114637.

Chapter 1: Introduction

1.1 The Haircare and Cosmetics Market

The haircare market is a global industry worth an estimated of 87.9 billion U.S. dollars in 2012.[1] It includes products like shampoos, conditioners, hair dyes, hair oils and sprays, and more recently, products for personal grooming. It is a well networked market and is segmented by various distribution channels that include, but are not limited to supermarkets, hair salons, drug stores and online retail stores, representing a burgeoning compound annual growth rate (CAGR) of 4.7% between 2013 and 2017.[2]

All mammalian hairs are structurally similar to wool,[3] and the earliest investigations into the photo-induced damage to wool can be traced back to the 1950's.[4,5] The drive behind these studies was to understand and prevent the discolouration (photo-yellowing) of white wool.[4,5] Indeed, at the time, it was already evident that light accelerates the yellow discolouration of wool, but it was unclear how it was affecting the internal structure of wool.[6,7]

Since wool and hair are similar, it is not surprising that exposure of human hair to sunlight could also have harmful effects. Today the deleterious effect of solar radiation on hair is well-documented in the literature, and it is widely accepted to lead to tensile strength loss, discolouration, split ends, loss of lustre and embrittlement.[8–12]

Humans, and by natural extension, human hair are exposed daily to sunlight, and this exposure has both beneficial and harmful effects.[13] The elucidation of the processes resulting in hair damage is, of course, of central interest to the haircare industry. Understanding the mechanisms that lead to hair photo-damage, can help develop new, effective technologies and methodologies, that can be incorporated into hair care products in order to reduce or prevent this damage.

In this Chapter the structure and chemical composition of hair will briefly be described, before moving to explore the most important oxidants that are capable of inducing damage to hair. These oxidants are capable of damaging the proteins found in hair both directly and indirectly (from secondary oxidants arising from their reactions). The main body of this Chapter will discuss in-depth the chemistry of these oxidants, and how they react with the amino acids found most frequently in hair. A particular emphasis is given on the formation, stability, reactivity, and detection of hydroperoxides (ROOH) which have been identified as the main intermediate products of the aerobic protein oxidation.

1.2 Chemical Composition of Hair

Human hair is a bio-synthesised material with complex internal structure and is primarily composed of a protein known as keratin.[14–16] The approximate composition of a dry human hair is given in Table 1.

Table 1. Overall chemical composition of dry human hair. Data obtained from reference 16.

Component	Content in % weight
Proteins	95
Lipids	4
Sugars	1
Trace metals, ash, and pigments	<1

Table 1 shows that the major non-water component of hair is proteins (*ca*. 95%). Lipids are mainly present in the cell membrane complexes and separate the remnants of cells in the hair from each other. Different metals are present in hair including copper and iron whose origin in hair is uncertain and likely includes both endogenous (decomposed enzymes) and exogenous (water supply, hair treatment products) sources.[17] Zinc is present at relatively high levels (up to 200 ppm) and is a result of enzymatic processes in the follicle.[16]

A key difference between white hair and black hair is the presence of melanin. Melanin is a particulate pigment, that can exist in as much as 1% by weight. The amount of melanin present in white hair is typically 28 ± 1 ng / mg[18] and can be as high as 7200 ± 1 ng / mg in black hair.[19] Melanin is divided into two different types (eumelanin and pheomelanin; Figure 1), and the ratio between the two determines the hair colour with eumelanin being present at low concentrations and often absent in white hair.[18]

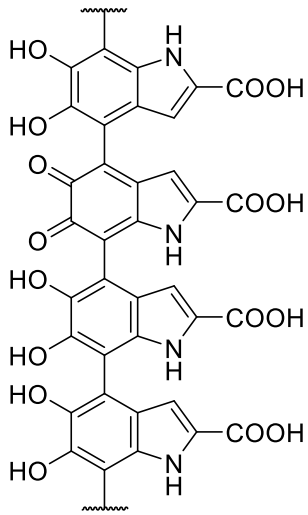

Proposed structure of eumelanin

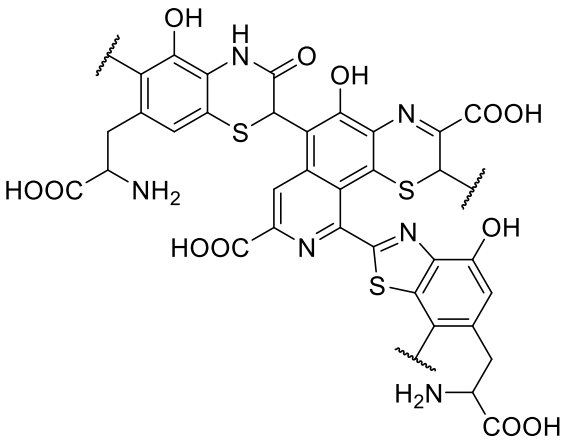

Proposed structure of pheomelanin

Figure 1. Proposed structures of A) eumelanin, and B) pheomelanin.

While melanin is omnipresent in living organisms, it is a highly complex pigment and despite the extensive focus it has received over the years, our understanding of its chemistry and its role is limited.[20] It is, however, accepted that eumelanin acts as a highly efficient UV filter and protects dark brown/black hair from sunlight, while pheomelanin (present in red hair) offer significantly lower protection.[20] It is, therefore, sensible that hair of different colour will respond differently to sunlight. Since the intended purpose of this thesis is to explore the mechanisms of oxidative damage to hair proteins, the presence and effect of melanin will not be further considered, as this would alter the overall reactivity significantly.

1.3 Structure and Properties of Keratin

Rogers in 2004 described the terms keratin and keratin-associated proteins (KAP) to refer to the intermediate filament proteins of the fibre.[21] Keratin proteins have a high sulfur content that distinguishes them from other proteins and are typically, durable, insoluble, and unreactive to the natural environment.[22]

1.3.1 Classification of Keratins

Keratins are categorised in two main groups; the *α*- helices and *β*-sheets keratins and are the two major internal supportive structures of the proteins.[23] *α*-Keratin is found in mammals and is the primary constituent of wool, hair and nails while *β*-keratin is found in reptilian tissues such as feathers and claws.[24] In addition, keratins can be classified based on the amount of sulfur cross links (cystine content).[23] Keratins with lower amount of sulfur are classified as "soft" keratins and are usually weakly consolidated while keratins with higher amount of sulfur are classified as "hard" keratins, have a more coherent structure and can be found in hair and nails.

1.3.2 Molecular Structure of *α*-Keratins

The helix conformation of *α*-keratin as was originally proposed by Pauling and Corey in 1951 is shown in Figure 1.[23,25] Stabilisation of the helical structure due to formation of hydrogen bonds is highlighted (red circle) in Figure 2a, while Figure 1b shows the keratin formation process. Two individual *α*-helix chains spiral together to form a coiled coil, the dimer.[26] To achieve this, the two isolated chains are forming disulfide cross links. In turn, the dimers coil together *via* disulfide bonds to form a tetramer known as protofilament.[27] Two protofilaments associate together into a protofibril and finally four protofibrils combine together to form an intermediate filament.

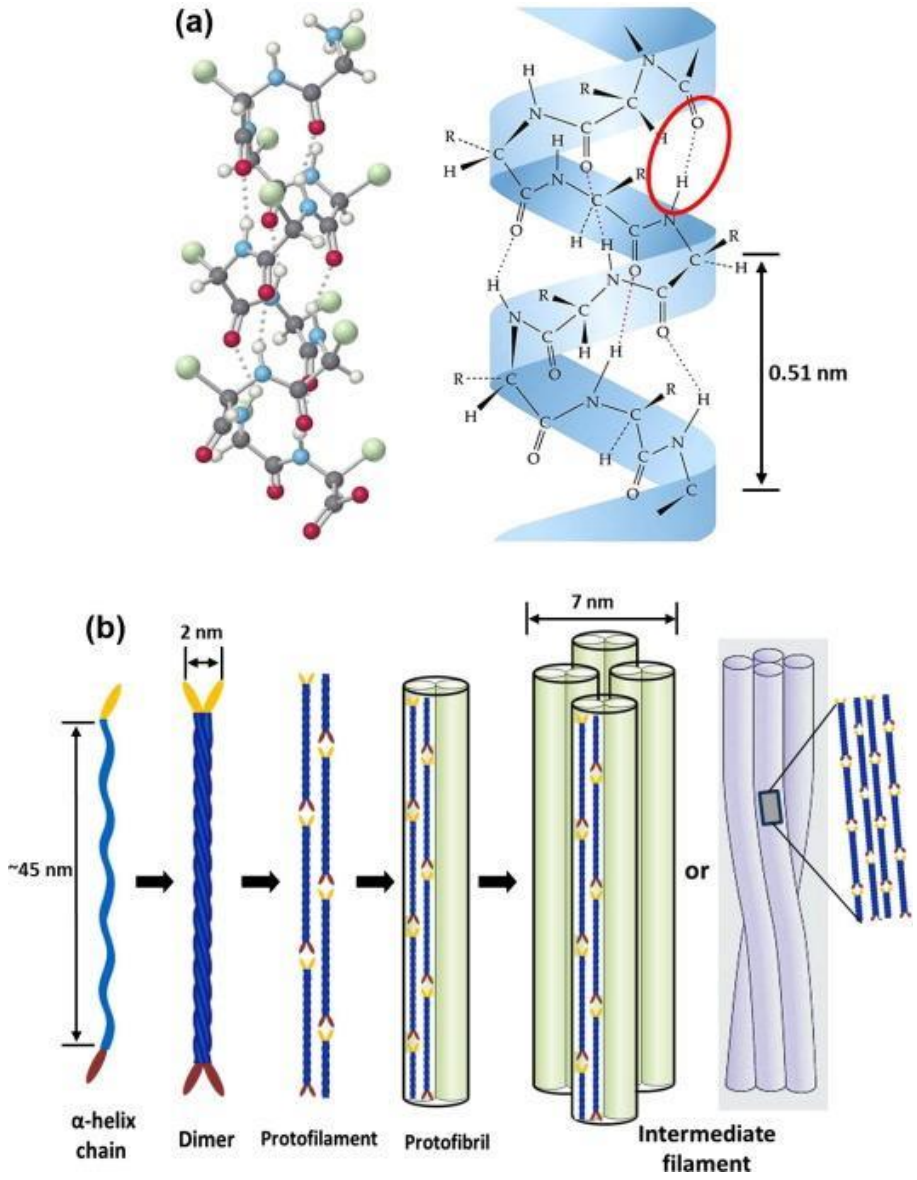

Figure 2. Intermediate filament structure of α-keratin. a) ball-and-stick model of the polypeptide chain, and α-helix showing the location of the hydrogen bonds (red circle) and the 0.51 nm pitch of the helix. b) schematic drawing of the intermediate filament formation: α-helix chains twist to form the dimers, which assemble to form the protofilament. Four protofilamets organise into the intermediate filament. Figure adapted from reference 22. Permission to use the figure was requested and granted.

Hair proteins are potentially major targets for photo-oxidation due to their abundance and their high exposure to solar radiation.[28] Photo-induced damage to hair proteins can occur *via* two major pathways; that are energy transfer and one-electron processes.[29,30] Direct absorption of UVB (and to a lesser extent UVA) radiation by particular amino acid residues in hair keratins (e.g., tryptophan (Trp), tyrosine (Tyr), phenylalanine (Phe), cysteine (Cys) and disulfide bonds (cystine)) results in the formation of electronically-excited states and photo-ionisation reactions. As such, damage induced to hair as a result of sunlight absorption, involves both free radical chain reactions and, energy transfer from the excited states to molecular oxygen yielding singlet oxygen ($^1O_2$).[29]

The extent of the damage depends on the amino acid residues and chromophores present in hair, that are capable of absorbing the incident solar radiation. Therefore, it is instructive to consider the individual amino acid content in human hair.

1.4 Amino Acid Composition of Keratins in Hair

The % composition of the main amino acids of human hair is given in Table 2. Typically, hair keratins are comprised of 18 amino acids, however, the exact amino acid concentration and amino acid sequences can be markedly different; both among different individuals but also within the cortex and the cuticle of the same person.[31]

Table 2. Amino acid composition of human head hair. Data obtained from reference 15.

Amino acid	**Content in residue %**
Cystine	16.73
Glutamic acid	12.95
Serine	11.52
Threonine	7.45
Proline	6.80
Leucine	6.49
Glycine	6.11
Tyrosine	2.14

Of particular note is the high amount of cystine, which amounts for nearly 17% in whole hair but can be as high as 37% in some of hair subcomponents.[32] The variation between cysteine **1.1** and cystine **1.2** (formation of a disulfide bond between two molecules of cysteine; Figure 3) is a topic of interest that has been investigated as early as the 1940.[33]

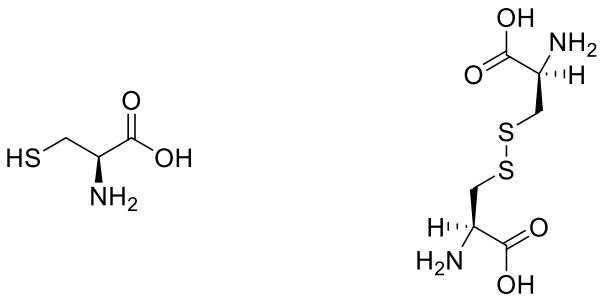

L-Cysteine **1.1**

L-Cystine **1.2**

Figure 3. Chemical structures and difference between cysteine and cystine.

It is noteworthy, that Cys is only present in small traces with the majority being present as cystine. The amount of cystine is important in the chemistry of hair as it is primarily responsible for the structural resilience and the mechanistic properties of hair.[16]

Of all the naturally occurring amino acids that can be found in proteins (including hair keratins), tryptophan (Trp) is the strongest near-UV chromophore exhibiting the highest molar extinction coefficient (ε) and the highest absorption wavelengths (maxima at 280 and 290 nm with a corresponding ε of 5500 and 4500 M^{-1} s^{-1} respectively).[34] In reality however, the high and efficient absorption of Trp is attenuated by its low abundance in proteins (<1% in hair keratins).[35]

Two of the amino acids reported in Table 2 have significant absorption in the near UV-region of the spectrum, that are, cystine and Tyr.[36,37] As such, their photochemistry is of considerable importance when studying the photo-induced hair damage and will be explored further.

1.5 Cystine photochemistry

The absorption maxima and extinction coefficients (ε) for both acidic and alkaline solutions of cystine have been reported in the literature, and little dependence on the pH of the solutions was found.[38] Indeed, in both low and high pH no maximum is observed in the UV absorption spectrum. At 290 and 300 nm, ε values are approximately 40 and 25 M^{-1} cm^{-1}, respectively.[37] The relatively high absorption wavelengths have been assigned to a forbidden n* - σ* transition.[37] However, it is reported that absorption spectra of disulfides are subject to structural differences, and absorption maxima and/or ε values, can in theory, deviate for those reported for free cystine.[37]

The low ε values of cystine when compared to other amino acids (mainly Tyr; *vide infra*), is compensated by the high abundance of cystine in hair keratins (Table 2). Therefore, photoexcitation of cystine, may be qualitatively and quantitatively more important, even though less efficient.

Direct photoexcitation of cystine leads to a singlet state that undergoes rapid homolytic cleavage, to afford mainly two transient thiyl radicals (RS•) that recombine to form the initial disulfide with a $k > 10^9$ M^{-1} s^{-1} (Scheme 1).[39,40]

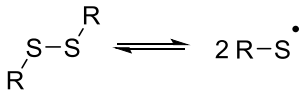

Scheme 1. Photolysis of the (-S-S-) bond via direct absorption of light. The homolysis of the disulfide bond yields two transient thiyl radicals that readily recombine.

However, there is still some debate regarding the identities of the resulting radicals (Scheme 2).[37]

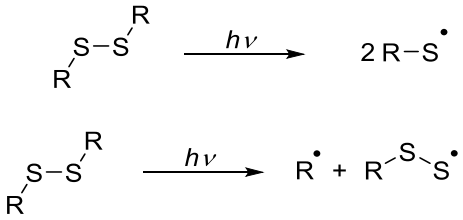

Scheme 2. Photolysis of the disulfide bond. There is evidence for the formation of both a) two thiyl radical as a result of the (-S-S-) cleavage and b) carbon-centred and perthiyl radicals as a result of (-R-S-) bond cleavage.

There is evidence for the formation of both thiyl and perthiyl (RSS•) radicals, as a result of S-S or R-S bond cleavage respectively, with the former being the major pathway. Disproportionation of 2 RS• to yield a free thiol and a thioaldehyde (Scheme 3) occurs and has been reported to be a significant pathway in both Ar- and O_2- saturated solutions.[41]

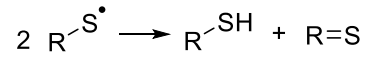

Scheme 3. Disproportionation reaction of two thiyl radicals leading to a stable thiol and thioaldehyde.

The ensuing chemistry of RS• (in addition to radical-radical recombination and disproportionation) is complex and will be briefly discussed now.

1.5.1 Reactivity of thiyl radicals

Another important reaction pathway for a cysteine thiyl radical **1.3** (CysS•) generated in proteins, and in a low O_2 environment, is hydrogen atom abstraction (HAA) from a nearby available $^{\alpha}$C-H bond **1.4** (Scheme 4).

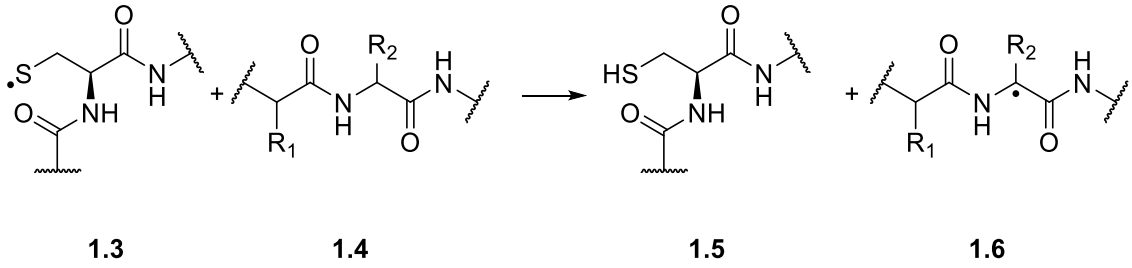

1.3 **1.4** **1.5** **1.6**

Scheme 4. Hydrogen atom abstraction from the α-carbon of a peptide by a thiyl radical, yielding a relatively stable carbon-centred radical and a thiol.

This generates a new carbon-centred radical on the protein **1.6** and a free thiol **1.5**. The absolute rate constants for the HAA reaction by CysS• from different amino acids in deoxygenated solutions were determined by Schöneich and co-workers.[42] The experiments revealed the propensity of the CysS• to abstract a H-atom from the $^{\alpha}$C-H of amino acids with a $k \sim 10^4$ M^{-1} s^{-1}, while the reverse reaction (repair of the carbon-centred radical) is practically negligible owing to the disparity of the bond dissociation enthalpy (BDE) between the S-H and the $^{\alpha}$C-H. Indeed, the BDE for the $^{\alpha}$C-H of alanine has been estimated to be ~ 83.5 kcal mol^{-1},[43] while the BDE for the S-H of Cys is ~ 89.1 kcal mol^{-1} (both calculated for small peptides in a fully planar conformation).[44] The lower BDE value for the $^{\alpha}$C-H is readily explained by the fact that the resulting α-amino radical is further stabilised by electron delocalisation onto the amide and carbonyl functions (see Section 1.7.4.1).[45]

In 2008 Schöneich and co-workers further elucidated the HAA reaction by CysS•, by investigating the intramolecular hydrogen atom transfer from the cysteine thiyl radical and glycine/alanine in model peptides **1.7** (Scheme 5).[46]

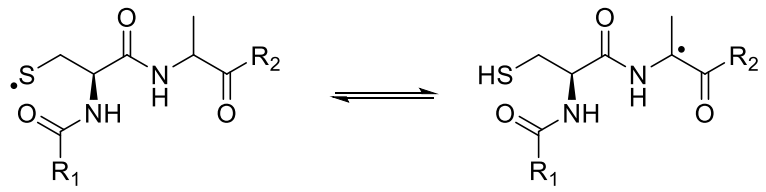

1.7 **1.8**

Scheme 5. Intramolecular hydrogen atom abstraction by a cysteine radical, generating a new carbon-centred radical on the neighbouring alanine residue.

This work revealed that for several glycine and alanine model peptides (up to 6 Gly/Ala amino acid sequence) the forward reaction proceeds with a $k \sim 10^5\ M^{-1}s^{-1}$ with the reverse reaction taking place with $k \sim 10^6\ M^{-1}s^{-1}$. This outcome was inconsistent with the intermolecular HAA reaction previously determined, and with the BDE of the cysteine S-H and the $^{\alpha}$C-H of amino acids (*vide supra*). Based on experimental results, it was proposed that both glycine and alanine, when incorporated into long peptides, assume a different conformation, that is not fully planar and increases the BDE of the $^{\alpha}$C-H to at least > 88.3 kcal mol^{-1}.[46]

A second major reaction pathway that needs to be considered is reaction of a thiyl radical **1.9** with molecular oxygen yielding a thiyl peroxyl radical **1.10** (Scheme 6).

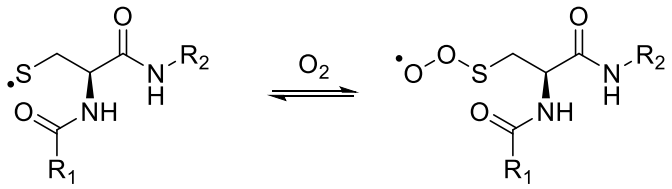

1.9 **1.10**

Scheme 6. Reaction of a cysteine thiyl radical with molecular oxygen generating a thiyl peroxyl radical. The reverse reaction is reasonably efficiently re-generating the thiyl radical.

This reaction is noteworthy as i) O_2 is usually abundantly present in biological environments and in the hair, and ii) the forward reaction is near the diffusion limit ($k \sim 10^9$ M^{-1} s^{-1}).[47] However, the reverse reaction is reasonably fast ($k \sim 10^6$ M^{-1} s^{-1}), and as such, not many products are expected from this reaction pathway. Theoretical calculations predict that even in systems where O_2 availability is sufficiently high, more than 70% of the initial CysS$^\bullet$ are expected to convert to carbon-centred radicals *via* intra- or inter-molecular hydrogen transfer (Scheme 5).[48] This is because once formed carbon-centred radicals, rapidly convert to peroxyl radicals (ROO$^\bullet$). Indeed, reaction of most carbon-centred radicals with O_2 is diffusion controlled and irreversible (see Section 1.8.1).[49] Therefore, thiyl radicals can serve as precursors of protein oxidation, by transferring the radical to a different site in the protein.

1.6 Tyrosine photochemistry

Similarly to Trp and cystine, the UV absorption spectra of Tyr are well-documented in the literature, including the absorption maxima and the associated ε values. Aqueous solutions of free Tyr (at pH 6) exhibit a near-UV region maximum at 270 nm, with a shoulder peak at 280 nm (ε = 1000 and 800 M^{-1} s^{-1} respectively).[50] This absorption band is assigned to a π – π* transition. It has been reported that the ionisation of the phenolic hydroxyl group has a large effect on the efficiency of photon absorption with the phenolate anion of Tyr exhibiting a significantly higher ε of 2100 M^{-1} s^{-1} at 280 nm.[36]

Direct absorption of light by Tyr generates the first singlet excited state, which is unstable and undergoes a rapid intersystem crossing to yield the more stable first triplet excited state (^{3}Tyr).[51] Energy transfer from the singlet and triplet excited state of Tyr to Trp, occurs readily with up to 69% efficiency, generating the corresponding Trp excited state.[52] Due to this high-yielding process, and the higher molecular absorption coefficients that Trp exhibits, Tyr photochemistry has generally received less focus.[36] However, hair keratins contain little to no Trp (*vide supra*). As such, in the context of hair chemistry the alternative reaction pathways for the excited states of Tyr are more significant.

The ^{3}Tyr undergoes rapid electron transfer with suitable electron acceptors (e.g., disulfides; present in high abundance in hair keratins) (Scheme 7).[13] The energy transfer results in the formation of a disulfide radical anion ($RSSR^{-\bullet}$) and a tyrosine radical cation ($Tyr^{+\bullet}$), that rapidly deprotonates to yield a phenoxyl (also called tyrosyl) radical (**1.11** $Tyr^{\bullet}$).[51]

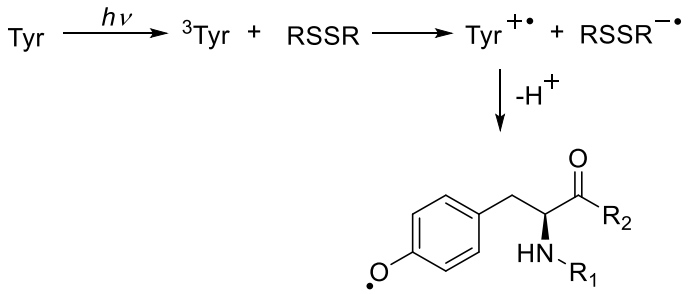

1.11

Scheme 7. Photoexcitation of Tyr yielding a highly stabilised tyrosyl (phenoxyl) radical via energy transfer of the first triplet excited state.

Once formed, $Tyr^{\bullet}$ can undergo a wide range of reactions. Due to delocalisation of the unpaired electron in the aromatic ring, $Tyr^{\bullet}$ is a long-lived radical that reacts slowly with molecular O_2 and a rate constant of $k \sim 10^3$ M^{-1} s^{-1} has been estimated.[53] On the contrary, dimerisation is favoured to give di-tyrosine **1.12** *via* both C-O and C-C linkages, with the latter predominating, with a $2k \sim 5 \times 10^8$ M^{-1} s^{-1} (Scheme 8).[54–56]

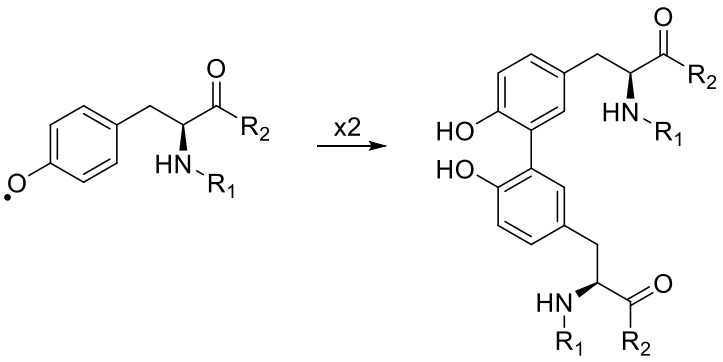

1.11 **1.12**

Scheme 8. Radical-radical recombination of two highly stabilised tyrosyl radicals, producing a dimeric species (dityrosine).

Furthermore, HAA reactions from suitable $^{\alpha}$C-H (both intra- and inter-molecularly) can occur to recover the parent Tyr moiety and transfer the radical along the protein (similarly to CysS$^{\bullet}$).[13] A more in-depth discussion for the overall reactivity Tyr$^{\bullet}$ including reaction with O_2 is given in Section 1.7.

In addition, energy transfer from the first singlet state of Tyr to the ground state of oxygen (O_2) can take place re-generating Tyr, and producing singlet oxygen ($^1O_2$).[52] Singlet oxygen is widely-accepted to be a damaging agent in biological systems as it is capable of reacting with various biological targets, including DNA, RNA and proteins.[57] Unlike energy transfer to Trp, this process is inefficient (low quantum yield).[52] However, once formed, $^1O_2$ reacts rapidly with amino acids, including Tyr ($k \sim 10^7$ M^{-1} s^{-1}), thus making its generation a noteworthy reaction pathway.[58] This reaction is covered in Section 1.7.1, and will only be explored here briefly.

Reaction of Tyr with $^1O_2$ produces hydroperoxides (ROOH) in high yields.[57] The Tyr-associated hydroperoxides are converted to alcohols *via* homolysis of the -O-O- bond. Indeed, it has been reported that amino acid, peptide, and protein hydroperoxides are unstable at elevated temperatures, in presence of redox active metals (e.g., Cu^+, Fe^{2+}), UV light and reductants.[59–64]

Homolysis of the peroxide bond yields reactive alkoxyl (RO$^{\bullet}$) and hydroxyl (HO$^{\bullet}$) radicals, both capable of reacting with proteins with fast rate constants.[65,66] Thus, initial damage incurred to the protein can be exacerbated by formation of hydroperoxides. The chemistry of hydroperoxides (i.e., generation, stability, and reactivity) is complex and will be discussed in-depth in Section 1.10.

It is evident, that even if the initial damage to the protein is photo-initiated by a chromophore, other secondary oxidants, mainly reactive oxygen species (ROS) can be generated and react with proteins. Therefore, the next Section is focused on the reactivity between such species and proteins.

1.7 Reactive Oxygen Species

Of all the ROS the ones that are most relevant to hair chemistry are singlet oxygen ($^1O_2$), superoxide radical anion ($O_2^{\bullet -}$), ozone (O_3) and hydroxyl radicals ($HO^{\bullet}$).

1.7.1 Singlet oxygen

A possible pathway for the generation of $^1O_2$ has already been covered, and it is generally thought that it can be produced both *in vivo* (enzymatic processes) and *in vitro* (sunlight in presence of a chromophore).[67] Proteins are prime targets for $^1O_2$ oxidation due to their high abundance and fast rate of reaction with $^1O_2$.[68,69] Detailed research in the reactivity of $^1O_2$ with peptides containing different amino acids, has shown that it preferentially reacts with tyrosine, tryptophan, cysteine, histidine and methionine.

Initial reaction of Tyr with $^1O_2$ gives rise to an unstable endoperoxide **1.14** that undergoes spontaneous decomposition to give a hydroperoxide **1.15** at the C-1 position (Scheme 9).[58,70]

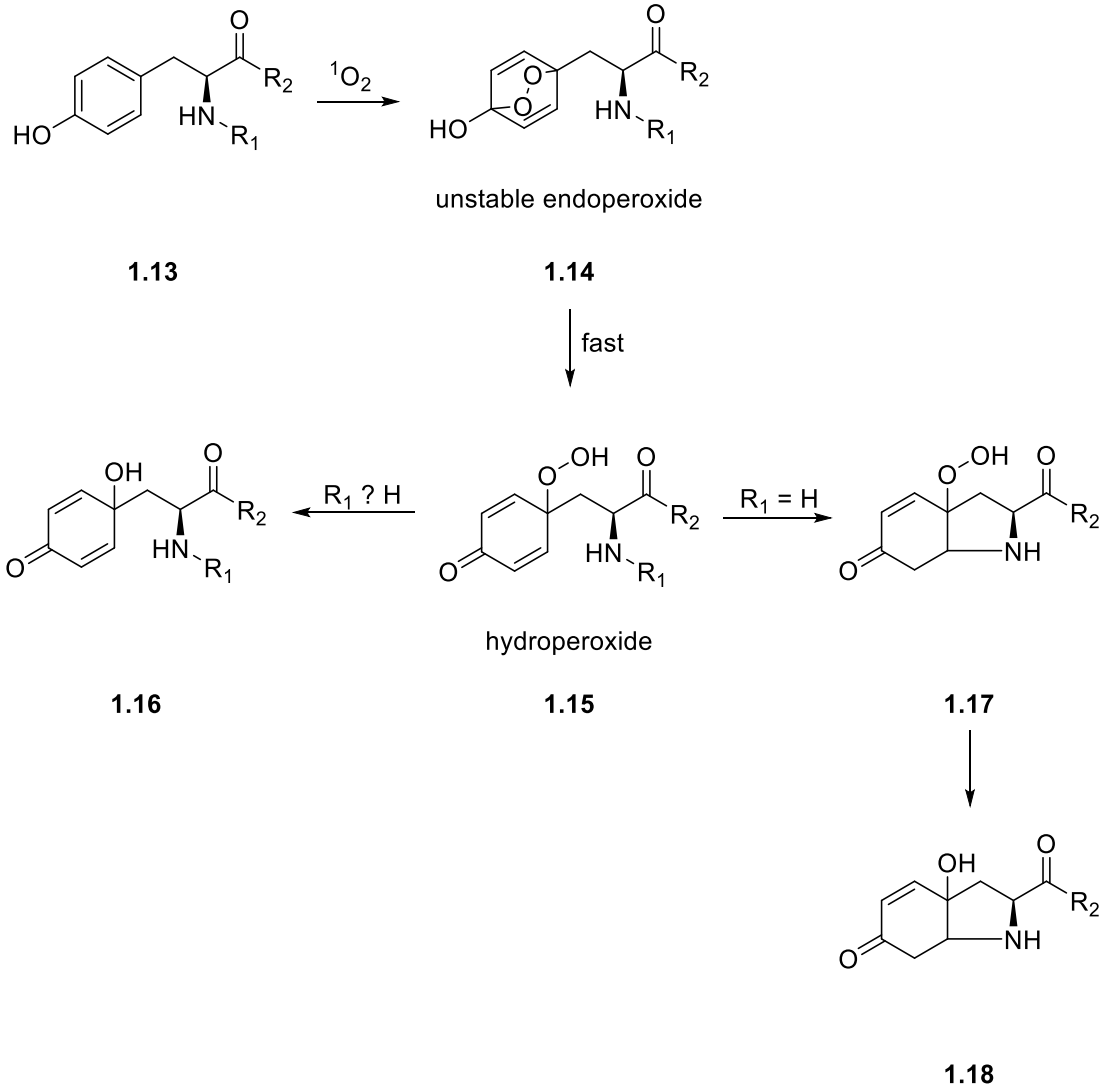

Scheme 9. Reaction of Tyr with singlet oxygen yielding an unstable endoperoxide, that upon ring opening is converted either to a stable alcohol or undergoes intra-molecular nucleophilic addition.

In the case of free Tyr, nucleophilic addition of the α-amino group occurs, to yield the indolic cyclised product **1.17**. Decomposition of the peroxide **1.17** formed yields eventually an alcohol **1.18**, and this process is accelerated in presence of metal ions or UV light. When Tyr is incorporated in peptides or proteins, the cyclisation is disfavoured, and Tyr-associated alcohol **1.16** is obtained. However, other nucleophiles present in the system can attack leading to cross links between proteins.[68]

1.7.2 Superoxide radical anion

The superoxide radical anion ($O_2^{\bullet-}$) can be generated by addition of one electron to the ground state molecular oxygen (Scheme 10; Eq. 1).[71] Superoxide radical anion co-exists in equilibrium with its conjugate acid, hydroperoxyl radical ($HO_2^{\bullet}$) (Scheme 10; Eq. 2).[72]

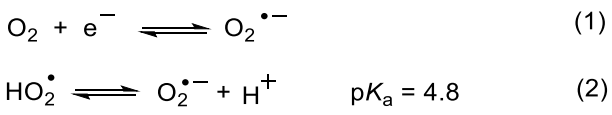

Scheme 10. Generation and acid-base equilibrium for superoxide radical anion and its conjugate acid.

The 4.8 value for the pK_a means that at physiological pH the equilibrium is dramatically shifted towards the left, with the concentration of $O_2^{\bullet-}$ being ~ 500 times more than the concentration of $HO_2^{\bullet}$.[73] As such, the reaction of $O_2^{\bullet-}$ with biological targets has attracted more attention than its acidic counterpart. Despite being a radical, $O_2^{\bullet-}$ is relatively unreactive towards biological targets with typical *k* values < 1 M^{-1} s^{-1}.[74] However, two molecules of $O_2^{\bullet-}$ dismutate readily to form H_2O_2, which in turn, can be cleaved either photolytically or *via* Fenton-type chemistry yielding the significantly more reactive $HO^{\bullet}$ (*vide infra*) (scheme 11).[75]

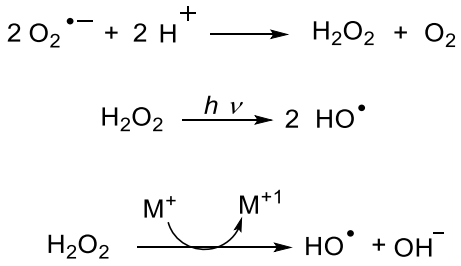

Scheme 11. Generation of H_2O_2 from $O_2^{\bullet-}$ and its reduction to generate transient $HO^{\bullet}$.

On the contrary, the pH of hair is more acidic, with the reported pH for the scalp being 5.5 and the hair shaft 3.67.[76] At this pH the equilibrium is shifted towards the existence of $HO_2^{\bullet}$. Hydroperoxyl

radical is more reactive than its conjugated base and reacts with organic molecules *via* HAA to produce a carbon-centred radical and H_2O_2 (Scheme 12).

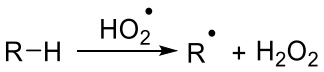

Scheme 12. Hydrogen atom abstraction by $HO_2^\bullet$ from organic molecules to generate a carbon-centred radical and H_2O_2.

The rate constants for the HAA reaction of $HO_2^\bullet$ with aqueous solutions of free amino acids at low pH have been critically reviewed in the literature, and typical values of $k \sim 10^2$ M^{-1} s^{-1} have been determined.[74]

1.7.3 Ozone

One important ROS for the hair chemistry is O_3 (a greenhouse gas) as it is one of the most important atmospheric pollutants, can be present at high concentrations both indoors and outdoors,[77,78] and has been reported to have a negative effect on the human body.[79] Ozone can be generated by various nitrogen oxides (NO_x) and volatile organic compounds (VOCs) that are released in the atmosphere (with the aid of solar radiation), or by the reaction of $^1O_2$ with O_2.[80] Unlike $HO^\bullet$ which is a short-lived and non-selective oxidant (*vide infra*), O_3 is very selective and reacts with organic molecules *via* well-defined mechanisms involving aromatic compounds and double bonds.[81]

The kinetics for the O_3-mediated oxidation of aqueous solutions of free amino acids have been determined experimentally and range from second order rate constants of $k_{O3} \sim 10^3$ M^{-1} s^{-1} (for aliphatic amino acids) to $k_{O3} \sim 10^6$ M^{-1} s^{-1} (for aromatic amino acids).[82] The highest rate constants were obtained for Phe, Tyr, Cys and Trp. Ozonolysis of Tyr leads to the incorporation of 1 or 3 O atoms to the amino acid, and two possible reaction pathways have been proposed, that are, hydroxylation and bond cleavage (Scheme 13).[83]

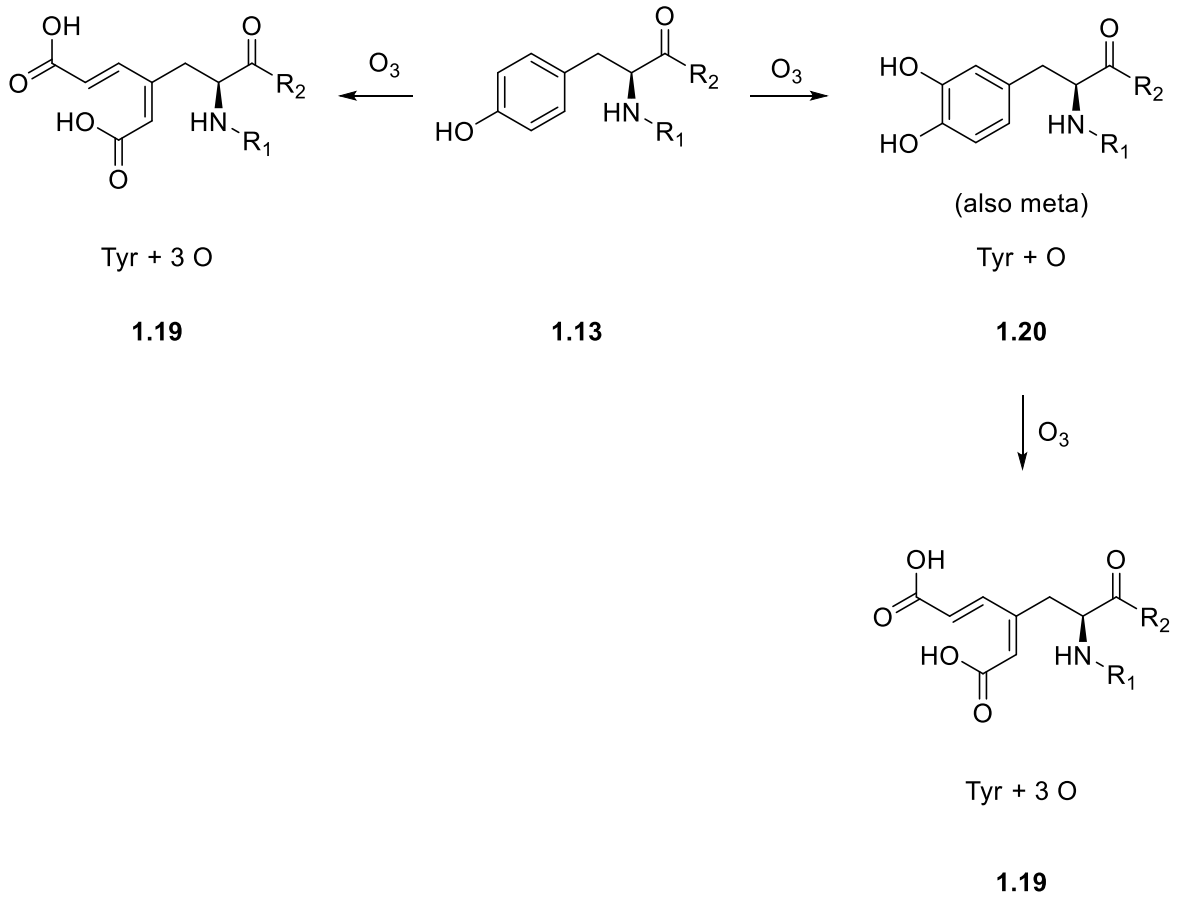

Scheme 13. Reaction of O_3 with Tyr resulting in bond cleavage and modification of Tyr.

The proposed products shown in Scheme 13 have been suggested based on the mechanism of O_3 with phenols,[84] and were further confirmed by MS analysis.[83,85] Hydroxylation of Tyr leads to the formation of catechols **1.20** and hydroquinones (depending on the positional hydroxylation in respect to the phenol of Tyr). However, these molecules have been only detected to low abundance as they are reactive towards O_3 leading to a similar bond cleavage and the observed incorporation of 3 O on Tyr **1.19**.

1.7.4 Hydroxyl radical

Hydroxyl radical is a salient biological oxidant, and has the highest one-electron reduction potential of all the species that can be generated by living organisms.[86,87] Effectively, this means that it is capable of oxidising all of the reduced species that are listed below it in the hierarchy of the free radical electron transfer reactions.[87,88] The most probable source for $HO^{\bullet}$ in the hair environment is Fenton-type chemistry of transition metals with residual H_2O_2 (*vide supra*).

Hydroxyl radicals are capable of removing a hydrogen or an electron from all biological targets in their surrounding *loci* with near diffusion-controlled rate constants (typical $k \sim 10^8 - 10^{10}$ M^{-1} s^{-1}).[67,89] Due to the high rate constants, and the high availability of targets, $HO^{\bullet}$ are short-lived, show little selectivity, and diffuse near the site of generation.[59,90] Two main reaction pathways exist for the reaction between $HO^{\bullet}$ and amino acids; that are HAA and addition to aromatic rings.[91–93] Although, more recently the possibility of $HO^{\bullet}$ to react with aromatic compounds *via* electron transfer has been established.[94] In any case, the immediate products are transient radicals, that undergo rapid subsequent reactions, and will be discussed in detail in the next Sections.

1.7.4.1 Hydrogen atom abstraction

Most of the amino acids that are found in proteins react *via* HAA with $HO^{\bullet}$ yielding a carbon-centred radical on the protein with typical second order rate constants $k \sim 10^8 - 10^9$ M^{-1} s^{-1} in aqueous solutions and physiological pH (Scheme 14).[89,95]

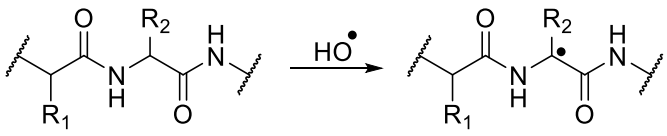

Scheme 14. Hydrogen atom abstraction by $HO^{\bullet}$ from the α-carbon of the peptide generating a carbon-centred radical on the peptide.

The controlling factors for the $HO^{\bullet}$ positional attack are mainly i) the BDE of the C-H bond, ii) the steric hindrance of the C-H bond and iii) the electronic properties of the substituents in the attacked carbon, that can further stabilise the resulting radical.[96] Initial abstraction of hydrogen from **1.21** can occur in two positions, that are the $^{\alpha}$C-H (backbone) and the $^{\beta}$C-H (side-chain), leading to radicals **1.22** or **1.23**, respectively (Scheme 15).

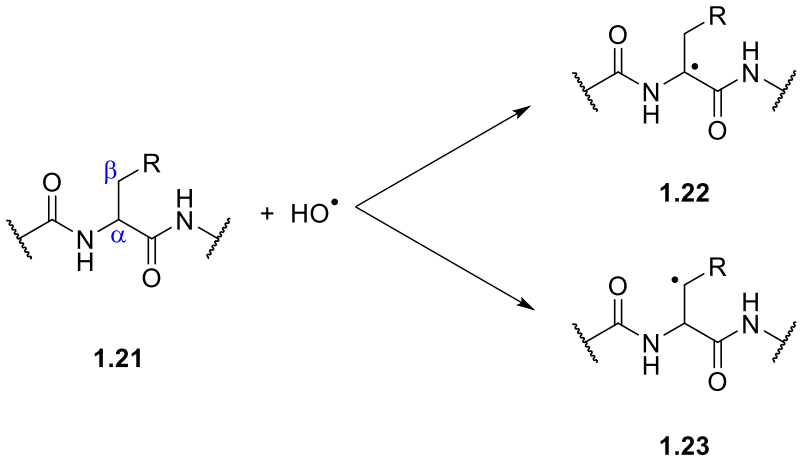

Scheme 15. Reaction mechanism for the two possible positions that hydroxyl radicals can abstract a proton from the amino acid ($^{\alpha}$C-H vs $^{\beta}$C-H).

The HAA is well-understood for free amino acids, and it is expected to take place primarily on the $^{\alpha}$C-H of the backbone, as the resulting tertiary radical is further stabilised due to delocalisation of the unpaired electron in the nearby amide and carbonyl functionalities (Figure 4).[45,59,65,97–99]

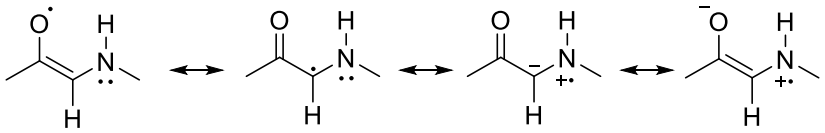

Figure 4. Stabilisation of the α-carbon radical on the neighbouring functionalities.

This stabilisation of the intermediate radical, that requires the presence of both an electron withdrawing (or captor) group and an electron donating (or dative) group (carbonyl and amino in this case, respectively), is termed the captodative effect.[100] Advanced theoretical studies have shown that for the majority of the free amino acids (Scheme 15; R=H), hydrogen atom abstraction from the $^{\alpha}$C-H is considerably more favourable.[101] This result is explained by the fact that HAA from the $^{\beta}$C-H would generate an intermediate radical that is further away from the captor and dative groups, and thus, the stabilisation effect is reduced. Interestingly, in the case of amino acids with aromatic side chains (i.e., Phe, Tyr, His), abstraction from the $^{\beta}$C-H is predicted to effectively compete with the $^{\alpha}$C-H (Scheme 15; R=Ar).[101] Indeed, it is proposed that aromatic side chains partially delocalise the unpaired electron, thus enhancing the stability of the intermediate radical. Finally, the HO$^{\bullet}$-mediated HAA from the $^{\alpha}$C-H shows negligible dependence on the conformation of the amino acid (α-helix vs β-sheet).[101]

In more realistic scenarios (i.e., polypeptides and proteins), the magnitude of this stabilization depends on the protein and peptide structure due to steric and electronic interactions.[98,102,103] Statistical factors can further influence the initial positional attack of the HO•, and in long peptides with high aliphatic side chains and sterically bulky substituents, damage is skewed along the side chain, and product prediction becomes cumbersome.[104,105]

1.7.4.2 Addition to aromatic ring

The reaction of HO• with aromatic-containing amino acids (i.e., Phe, Tyr, Trp), is of particular importance as they are present in various proteins, and it is now well-documented in the literature.[106–110] Reaction between HO• and Trp or Phe can be neglected since only traces of the two amino acids can be found in hair keratins. On the contrary, reaction with Tyr is pertinent to hair chemistry and attention should be drawn to it.

By 1970 the products of the reaction of HO• with Tyr in aqueous solutions and various pH were already established, and phenoxyl radical had been identified as the major intermediate product.[111] However, the exact mechanism that gives rise to the phenoxyl radical remained unclear until 1984. Getoff and co-workers, employed pulse radiolysis and computational tools, to investigate in-depth the mechanism of the HO•-initiated oxidation of Tyr, and determine the kinetics of build-up and disappearance of the transient species.[112]

Addition of HO• to aromatic rings is typically faster than HAA ($k \sim 10^{10}$ M^{-1} s^{-1};). For Tyr, formation of a phenoxyl radical, has been identified as the thermodynamically favoured product, however, it is only formed to a very small extent directly *via* HAA from the hydroxyl group (~ 5%) (Scheme 16A).[112,113] Indeed, reaction of HO• with Tyr results almost invariably in addition of the HO• to the *ortho*- and *meta*-position of the aromatic ring, that yields a transient cyclohexadienyl adduct **1.24** (Scheme 16B).[106,114]

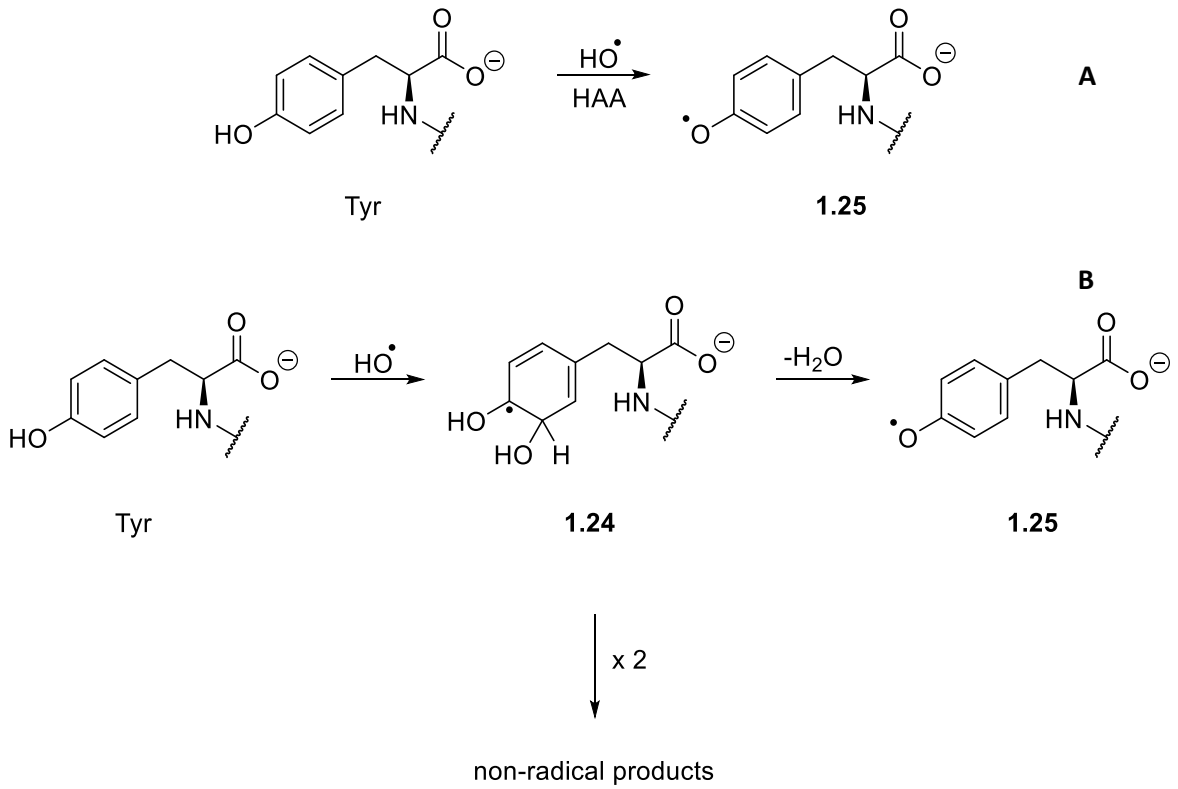

Scheme 16. Different pathways for the reaction of HO •with Tyr. A) Direct HAA from the phenolic O-H, generating a phenoxyl radical. B) Direct addition to the aromatic ring of Tyr generating an unstable cyclohexadienyl radical. Two cyclohexadienyl radicals can decay to produce non-radical products or can eliminate H_2O to produce a phenoxyl radical.

By monitoring the UV spectroscopic properties of the transient adducts, the authors were able to estimate rate constants for both the formation and the decay of these species. Interestingly, it was shown that HO• addition to the *ortho*-position of Tyr proceeds with a near diffusion-controlled rate constant of $k \sim 7 \times 10^9$ M^{-1} s^{-1}, while the *meta*-adduct is formed with a $k \sim 5 \times 10^9$ M^{-1} s^{-1}. On the contrary, the phenoxyl radical *via* HAA is formed with a $k \sim 5 \times 10^8$ M^{-1} s^{-1}. The *ortho*-adduct undergoes spontaneous bimolecular dimerisation or disproportionation reactions with a $2k \sim 3 \times 10^8$ M^{-1} s^{-1} leading to non-radical products, and dehydration with a $k \sim 2 \times 10^4$ s^{-1} to afford the more stable phenoxyl radical **1.25**. Therefore, even if initial HAA to yield a phenoxyl radical **1.25** accounts for only ~ 5% of the total HO• + Tyr reactivity, its formation as a major product can be justified by the decay of the transient *ortho*-cyclohexadienyl adduct **1.24**. Phenoxyl radicals can follow three different reaction pathways that are in competition between them (Scheme 17).

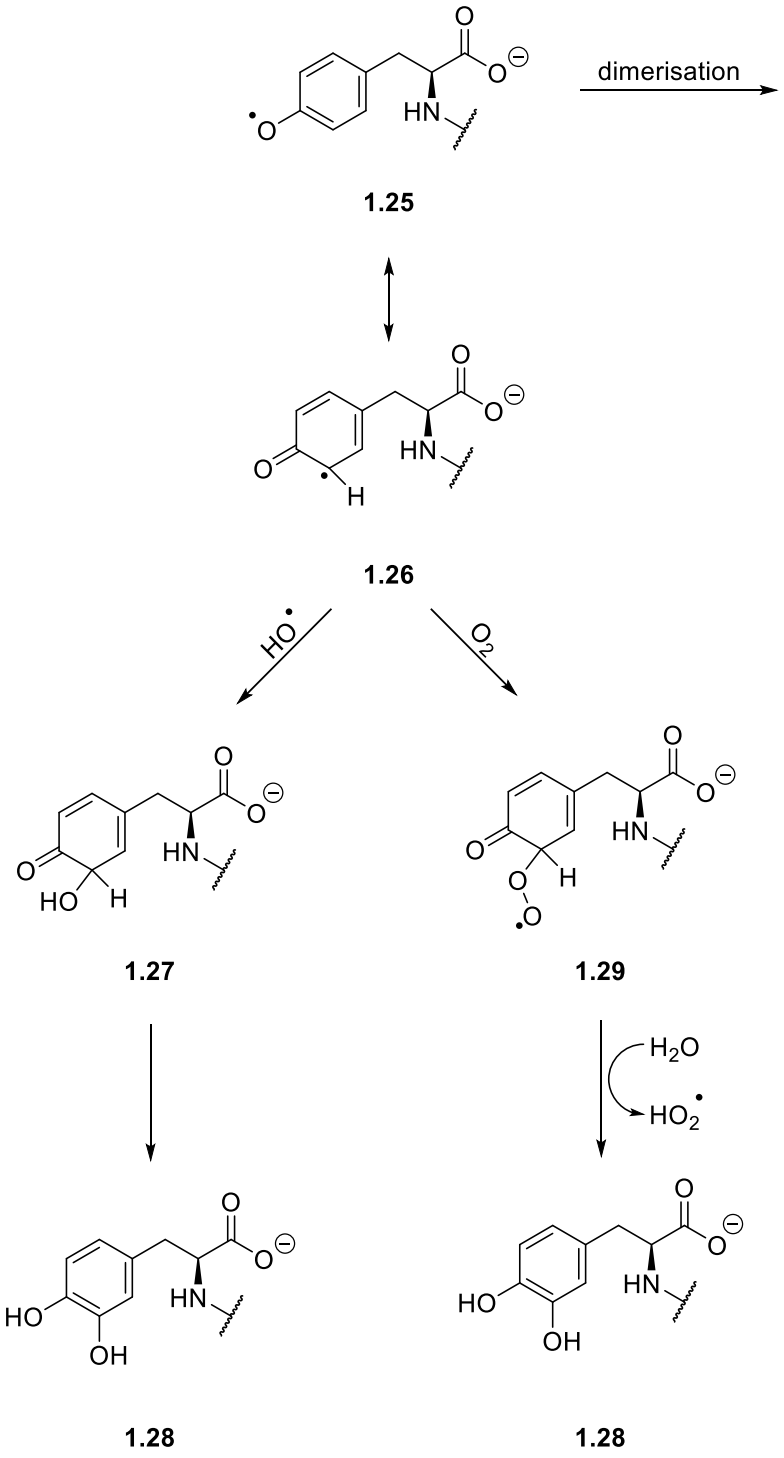

Scheme 17. Possible pathways for phenoxyl radical. Two phenoxyl radicals can participate in radical-radical dimerisation reactions. Alternatively, reaction with another molecule of HO• or O_2 is possible to eventually afford stable dihydroxyphenylalanine derivatives.

The first path (dimerisation) has already been covered in Section 1.6 and involves linkages by both C-C and C-O bond formation. The unpaired electron is delocalised in the aromatic ring **1.26**. In systems where there is a high flux of $HO^{\bullet}$, a second attack can occur, quenching the tyrosyl radical and *via* keto-enol tautomerization, afford a stable dihydroxyphenylalanine **1.28** (DOPA). Dihydroxyphenylalanine has been identified as the main product of the aerobic $HO^{\bullet}$-mediated oxidation of Tyr, and it is utilised as marker of Tyr oxidation.[112] Although the phenoxyl radical is stabilised and long-lived, an irreversible reaction with dissolved O_2 can take place affording an unstable peroxyl radical **1.29**. The peroxyl radical undergoes H_2O-assisted hydroperoxyl radical ($HO_2^{\bullet}$) elimination with a $k \sim 10^5$ s^{-1}, and ultimately produces DOPA **1.28** via keto-enol tautomerisation.[113,115]

It is well-established that for the $HO^{\bullet}$-induced oxidation of Tyr (or of Tyr-containing peptides and proteins) in aerated solutions, the only products generated to a noticeable degree is DOPA and dimeric species.[107,116,117] Reaction of $HO^{\bullet}$ with Phe is similar as with Tyr, and predominantly affords a hydroxylated product on the benzene ring of Phe (the mechanism of $HO^{\bullet}$ addition to Phe will be discussed in more detail in Chapter 2).

1.7.4.3 Electron transfer

Certain radicals, (e.g., sulfate radical anion ($SO_4^{\bullet-}$)), have a documented propensity to react with aromatic compounds *via* single electron transfer mechanism,.[118,119] Indeed, $SO_4^{\bullet-}$ is well-known to oxidise aromatic compounds to the corresponding radical cation, with typical second order rate constants of $k_{ET} \sim 10^8$ - 10^9 M^{-1} s^{-1}.[120] More recent studies have shown that $HO^{\bullet}$ are capable of participating in the same chemistry with aromatic compounds (including tyrosine and phenylalanine).[94,118] In general, the electron transfer component of the $HO^{\bullet}$ reactivity with aromatic compounds depends on the ionisation potential of the substrate, and usually electron transfer and addition occur simultaneously.[94]

In the case of tyrosine, the electron transfer pathway leads to the formation of tyrosyl (phenoxyl) radical (similar to the O_2 addition/ H_2O-elimination pathway of Section 1.7.4.2). On the other hand, the electron transfer component in the $HO^{\bullet}$ reaction with phenylalanine **1.30** yields a transient radical cation **1.31** (Scheme 18).

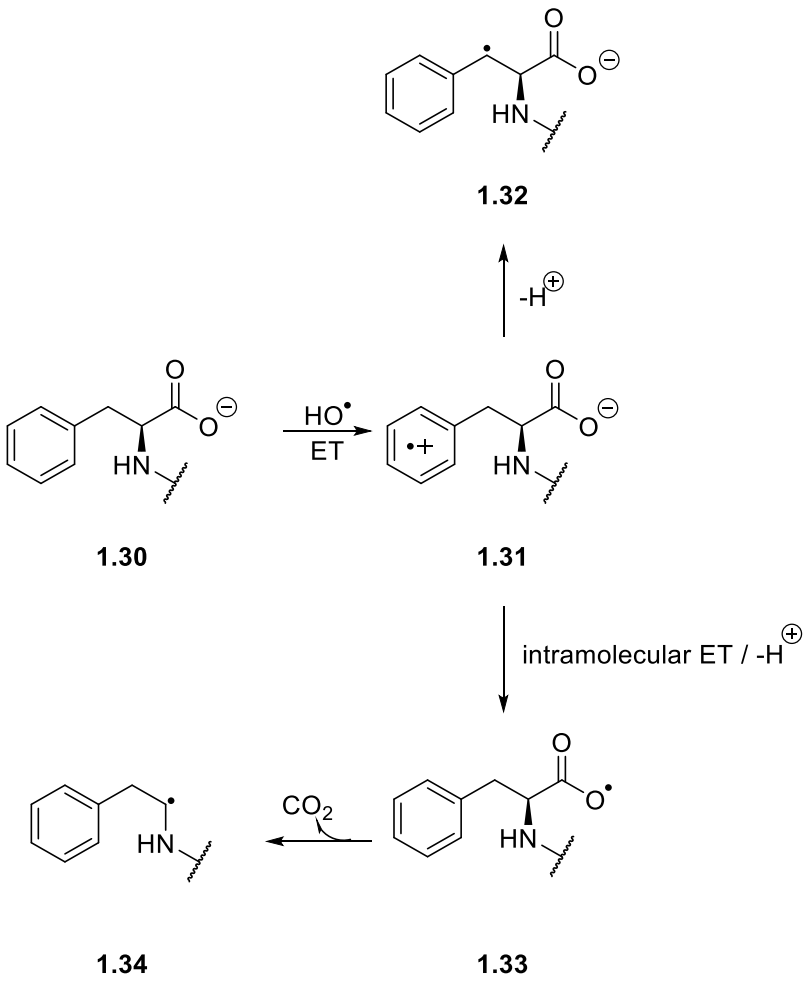

Scheme 18. Possible electron transfer mechanism between phenylalanine and HO•, yielding a transient radical cation. Depending on the pH of the reaction medium, two pathways have been proposed. At low pH an irreversible proton loss takes place yielding a benzylic radical, while at high pH a second intramolecular electron transfer can take place, followed by deprotonation, producing a carboxylate radical that spontaneously decays.

The phenylalanine-derived radical cation has been documented to follow two different pathways that are pH-dependent.[121] At low pH where phenylalanine is present as the carboxylic acid, irreversible proton loss can take place, to produce the benzylic radical **1.32** as shown in Scheme 17. It is noted that the same benzylic radical can also be formed *via* direct HAA by HO• from the -CH_2 of phenylalanine. Thus, the generation of the benzylic radical is not unique to the electron transfer mechanism.

At higher pH, that phenylalanine is present as the carboxylate anion, a rapid intramolecular electron transfer ($k \sim 10^4$ - 10^5 s^{-1}) can take place, followed by deprotonation. This process gives rise to a carboxylate radical **1.33** which has been proposed to undergo spontaneous radical decarboxylation releasing CO_2 and a carbon-centred radical **1.34**.[121]

The reactivity of $HO^{\bullet}$ with amino acids and peptides results in the formation of various transient radicals that have complex reactivity and can follow different reaction pathways. In the following Section the chemistry and mechanisms of these biological radicals will be explored in-depth. A particular emphasis is given to the formation of hydroperoxides (a mechanism known as peroxidation), and their role in protein modification.

1.8 Reactivity of biological radicals

1.8.1 Reactions of peroxyl radicals

In aerobic environments, carbon-centred radicals react with diffusion-controlled rate constant with molecular O_2 ($k \sim 10^9$ -10^{10} M^{-1} s^{-1}) to yield peroxyl radicals ($ROO^{\bullet}$; Scheme 19).[59]

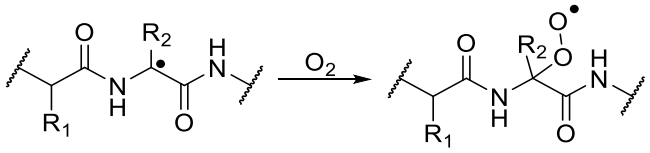

Scheme 19. Reaction of carbon-centred radicals with O_2 to produce peroxyl radicals.

1.8.1.1 Radical-radical reactions

Peroxyl radicals can participate in many different reaction pathways. In general, radical-radical termination reactions can occur between two peroxyl radicals. Two main reactions have been identified in the literature (Scheme 20).

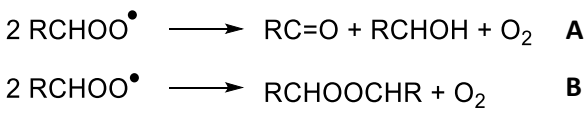

Scheme 20. Possible radical-radical reactions of peroxyl radicals. A) Disproportionation reaction to produce stable carbonyls, alcohols, and release O_2. B) Radical-radical reaction to release O_2 and generate a new peroxide bond.

For primary and secondary peroxyl radicals, disproportionation reaction (Scheme 19A) is a major pathway yielding an alcohol and a ketone/aldehyde.[122] In 1970 Bennett and co-workers, studied the reactions of many primary and secondary peroxyl radicals **1.35** in O_2-saturated solutions, and a rate constant of $2k \sim 10^7$ M^{-1} s^{-1} was determined.[122] The proposed mechanism for this reaction is believed to go *via* a tetroxide intermediate **1.36** that spontaneously decays to release O_2 and produce the more stable alcohol and carbonyl (Scheme 21).[66]

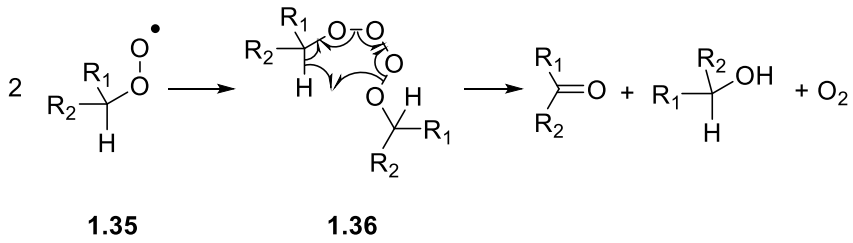

Scheme 21. Proposed mechanism for the dismutation of peroxyl radicals to afford stable carbonyls and alcohols via an unstable tetroxide intermediate.

On the contrary, disproportionation reactions are not possible for tertiary radicals. As such, radical-radical termination reactions more likely occur *via* reaction shown in Scheme 19B that yields a new peroxide and releases O_2. In 1990 Bennet and co-workers further advanced their work on the studies of peroxyl radicals. Using photolysis experiments and EPR analysis, a comprehensive kinetic and mechanistic study was performed for the reactivity of *t*-butyl peroxyl radicals in aqueous solutions.[123] This investigation revealed that radical-radical reaction (Scheme 20B), is a much slower process and proceeds with a rate constant of $2k \sim 10^3$ M^{-1} s^{-1}.

In addition to unimolecular reactions, radical-radical reactions leading to radical products can also occur. Indeed, two tertiary peroxyl radicals can combine to yield two alkoxyl radicals ($RO^{\bullet}$) and release O_2, *via* a tetroxide intermediate (Scheme 22).

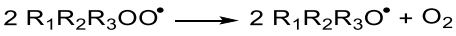

Scheme 22. Reaction between two peroxyl radical generating two reactive alkoxyl radicals and molecular O_2.

This reaction was determined to be faster by one order of the magnitude ($2k \sim 10^4$ M^{-1} s^{-1}) compared to reaction of Scheme 18B,[123] indicating that for tertiary radicals, formation of RO$^\bullet$ is noteworthy, and their chemistry will be discussed in Section 1.9.

1.8.1.2 $HO_2^\bullet$ elimination and HAA

Apart from radical-radical reactions, two main reaction pathways exist for ROO$^\bullet$. Tertiary ROO$^\bullet$, that contain an α-heteroatom (e.g., α-amino radicals generated on peptides and proteins; **1.37**), undergo facile unimolecular $O_2^{\bullet-}$-elimination, to yield acyl imines **1.38** (Scheme 23).[59,124,125]

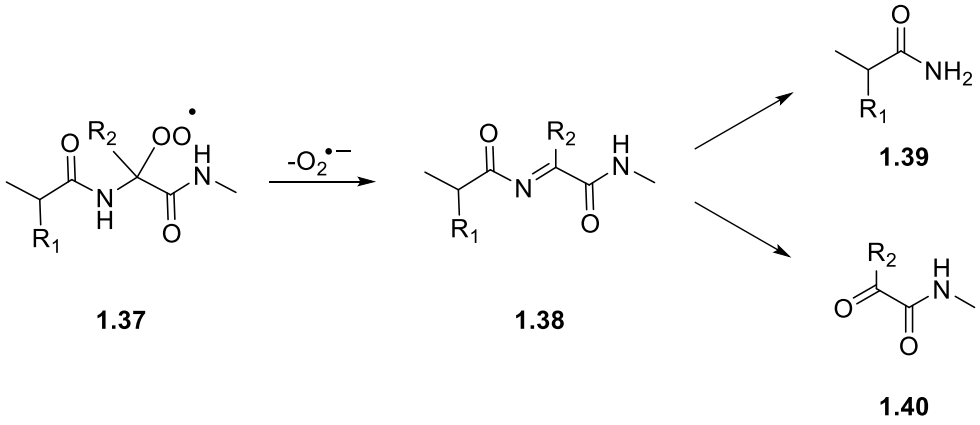

Scheme 23. A major pathway for the unimolecular decay of tertiary peroxyl radicals. Elimination of $HO_2^\bullet$, followed by imine hydrolysis that results in the peptide bond cleavage. The process produces free amines and carbonyls.

The rate for the spontaneous decay of the peroxyl radical has been reported to be base-catalysed, and $O_2^{\bullet-}$-elimination occurs with $k \sim 10^5$ s^{-1} at alkaline pH for peroxyl radicals generated on glycine.[124] Conversely, neutral and acidic pH reduce the rate of $O_2^{\bullet-}$-elimination (typical $k \sim 10^2$ s^{-1} for many α-hydroxy peroxyl radicals).[126,127] Hydrolysis of the imine occurs readily to afford a free amine **1.39** and a diketone **1.40**.[49] The elimination of $O_2^{\bullet-}$, may be of high quantitative significance, as it results in cleavage of the peptide bond with concomitant release of a new radical that can extend the initially inflicted damage.

ROO$^\bullet$ participate in HAA reaction (either intra-molecularly or with nearby available C-H bonds) to yield hydroperoxides (ROOH), with typical rate constant of $k \sim 10^3$ M^{-1} s^{-1} (Scheme 24).[128]

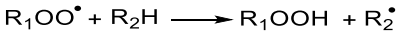

Scheme 24. Hydrogen atom abstraction by peroxyl radicals from organic molecules generating hydroperoxides and carbon-centred radicals.

The product distribution therefore is markedly dependent on the conditions. In systems where the radical flux is high, radical-radical reactions become more important. Conversely, when the radical flux remains low, and there is a high abundance of nearby C-H bonds (e.g., biological systems and the hair environment), HAA to yield ROOH becomes the prevailing pathway. Hydroperoxides have evoked high attention over the past 20 years, and they have been identified as the main intermediaries of the aerobic protein oxidation.[60–62,129] Section 1.10 is focused on the chemistry of hydroperoxides.

1.9 Reactivity of alkoxyl radicals

Similarly to $HO^{\bullet}$ and $ROO^{\bullet}$, alkoxyl radicals ($RO^{\bullet}$) exhibit rich chemistry that can enhance protein damage and should be examined carefully. Alkoxyl radicals have been well-characterised, and their reactivity has drawn considerable attention as they are the main intermediate product in the photolysis and pyrolysis of organic peroxides.[130] Two alkoxyl radicals can participate in a disproportionation reaction to produce an alcohol and the corresponding carbonyl (Scheme 25), with a nearly diffusion-controlled rate (k ~ 10^{10} M^{-1} s^{-1}, determined for aqueous solutions of methoxyl radical).[131]

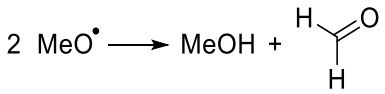

Scheme 25. Diffusion-controlled radical-radical reaction between two transient methoxy radicals to generate methanol and formaldehyde.

A major and critical reaction pathway is rapid intra- or inter-molecular HAA reactions yielding stable alcohols and new carbon-centred radicals in the substrate (k ~ 10^{6} M^{-1} s^{-1}), thus accelerating the damage (Scheme 26).[131]

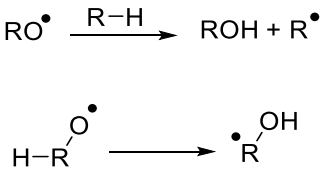

Scheme 26. Examples of intra- and inter-molecular hydrogen transfer by alkoxyl radicals, generating carbon-centred radicals.

Hydrogen atom abstraction reaction can take place from ROOH (resulting in alcohols and ROO$^{\bullet}$), however the concentration of the peroxides is usually low, and this pathway is neglected.[123] For primary and secondary RO$^{\bullet}$, HAA is in competition with hydrogen shifts to yield the corresponding α-hydroxyalkyl radicals with typical $k \sim 10^6 - 10^7$ M^{-1} s^{-1} in neutral aqueous solutions.[132]

Tertiary RO$^{\bullet}$ **1.41**/**1.42** have a documented propensity to undergo facile fragmentation reactions to afford stable carbonyls and nascent carbon-centred radicals ($k \sim 10^7$ M^{-1} s^{-1} for *t*-BuO$^{\bullet}$ in aqueous solutions).[133] Depending on the site of generation for the initial hydroperoxide (side chain vs backbone), different fragmentation reactions can take place (Scheme 27).

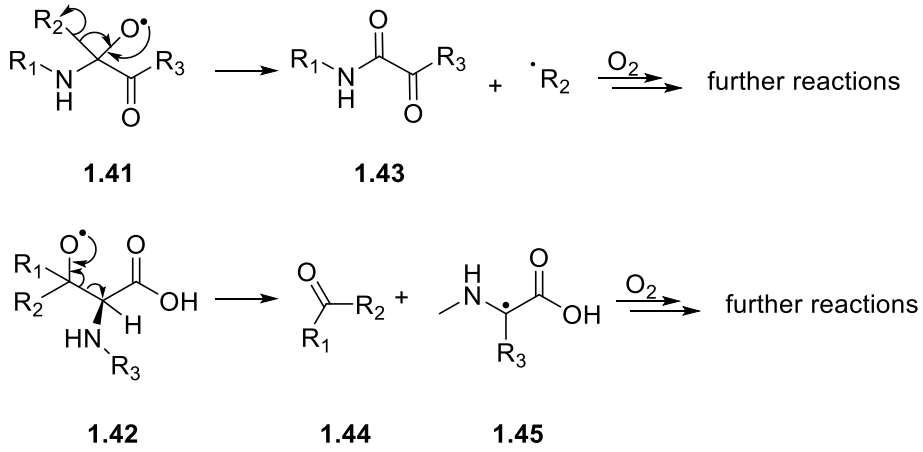

1.41 **1.43** **1.42** **1.44** **1.45**

Scheme 27. Possible fragmentation reactions of alkoxyl radical resulting in bond cleavage on the peptide. The bond cleavage results in the formation of carbonyls and carbon-centred radicals that participate in further reactions.

As such, α-amino alkoxyl radicals **1.41** fragment to yield amides **1.43** and new carbon-centred radicals,[134] while β-alkoxyl radicals **1.42** undergo scission reactions to yield carbonyls **1.44** and α-amino radicals **1.45**.[133] In both cases, new carbon-centred radicals are released that are likely to undergo rapid O_2 addition, and ultimately convert to hydroperoxides.

Fragmentation reactions are particularly important as i) they lead to protein modification and ii) they release new radicals. It is evident that RO$^{\bullet}$ generated as a result of ROOH decomposition can further propagate the protein damage. Indeed, in 1993 Stocker and co-workers attempted a quantitative examination of initial radicals formed on free amino acids and concomitant amino acid loss.[135] It was highlighted for the first time that the total amino acid loss exceeded the number of radicals formed, thus proving that chain reactions (propagation) take place to deliver higher damage to the biological substrate.

1.10 Chemistry of protein hydroperoxides

The first report of hydroperoxides formed on proteins can be traced as back as 1942 (for a historic overview see reference 58).[59,60] Only sporadic reports appeared until the 1990's, when the first systematic studies emerged in the scene of protein oxidation by ROS. Hydroperoxides are organic compounds with a generic formula of ROOH that are characterised by a labile -O-O- bond with a typical BDE ~ 45 kcal mol^{-1} (e.g., 45.3 kcal mol^{-1} for *t*-BuOOH).[136,137]

Despite recognition of hydroperoxides as the main intermediates of the aerobic protein oxidation, their true meaning was not appreciated until recent years. The reason for this is mainly associated with their instability under endogenous and exogenous catalysts (e.g., elevated temperatures, metal ions), that facilitate their rapid decay to give a range of different products, therefore making their detection (or product identification), challenging.

1.10.1 Hydroperoxide formation

Formation of hydroperoxides on free amino acids, peptides and proteins are dependent on the conditions (e.g., sufficient availability of O_2, availability of nearby C-H bonds). Multiple research groups around the world have studied the $HO^{\bullet}$-induced formation of hydroperoxides on free amino acids, and their findings demonstrate that high concentrations of hydroperoxides can be achieved.[138–142] In 1993 Gebicki and co-workers investigated the $HO^{\bullet}$-derived evolution of hydroperoxides for all free amino acids.[141] The authors were able to illustrate that the peroxidation efficiency increases in line with the number of aliphatic C-H bonds. The highest peroxide yields were obtained for valine, leucine, proline, and lysine, while aromatic and sulfur containing amino acids were less susceptible to peroxidation. This is readily rationalised for aromatic amino acids as $HO^{\bullet}$ react *via* addition rather than HAA. For the sulfur-containing amino acids HAA takes place preferentially in the sulfur centre, and formation of hydroperoxides is less favoured (as O_2 addition is readily reversed to recover the thiyl radical; see Section 1.5.1).

For short peptides a similar pattern has been observed, that is, peptides with high aliphatic content appear to be more susceptible to peroxidation. In 1996 Davies and co-workers exposed Ala and some related short peptides to γ-irradiation and the results showed that the total hydroperoxide content increased in line with the increase of the aliphatic C-H bonds.[139] More recent studies from the same group further corroborate that short peptides follow the same pattern, i.e., short Val peptides gave considerably higher peroxide yields compared to Ala peptides, and in turn, Ala peptides produced higher yields compared to Gly peptides.[64,66]

1.10.2 Hydroperoxide quantification and detection

As hydroperoxides are reactive and unstable intermediates, direct evidence for their existence has been elusive, and their quantification problematic. Two main assays have been developed for their indirect measurement: each one possessing its own advantages as well as limitations and drawbacks.

The first and most reliable method developed is the iodometric assay.[143] In this method the hydroperoxide under examination reacts with iodide under acidic conditions and generates triiodide (I_3^-) which is then measured spectroscopically at 358 nm. The major advantage of this method is that it is a quantitative reaction with a known 1:1 stoichiometry between the organic hydroperoxide and the moles of iodide. However, iodide can be oxidised by H_2O_2 that is often present in the system. To avoid this, solutions are treated (before the assay) with catalase, an enzyme that has been shown to selectively decompose H_2O_2 and is unreactive to organic peroxides.[140,144] Even if catalase is used to remove H_2O_2, the major drawback of the technique is that it must be carried out under strictly anaerobic conditions due to the oxygen sensitivity of iodine.

In order to overcome the oxygen sensitivity of the iodometric assay, a new method has been developed more recently. The new technique is called the Ferrous Oxidation - Xylenol Orange (henceforth to be abbreviated as FOX) and it was first reported in 1994 by Wolff.[145–148]

This method utilizes the hydroperoxide-mediated oxidation of Fe(II) to Fe(III) that binds strongly to xylenol orange (XO), with spectrophotometric quantification of the latter at 560 nm (Figure 5). As Fe(II) can react with H_2O_2 in the same way as with organic peroxides, solutions are again treated with catalase prior to the analysis. The FOX assay has the advantage that shows minimal sensitivity to O_2. However, the organic hydroperoxides react in an unknown stoichiometry with Fe(II), depending on the system under study.

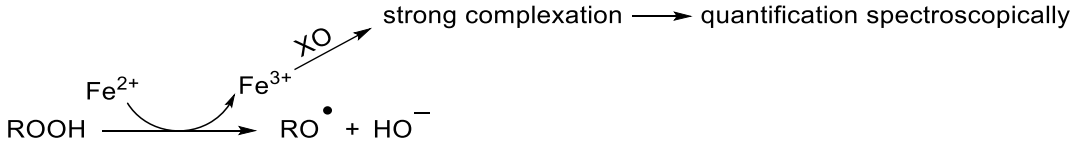

Figure 5. Basic principle of the FOX-assay. Oxidation of Fe^{2+} by the hydroperoxide, yields Fe^{3+} that binds to xylenol orange, and the resulting complex is quantified spectroscopically.

Due to the unknown stoichiometry of the reaction, the assay is usually used as a semi-quantitative method and the peroxide levels are reported as H_2O_2 equivalents rather than actual ROOH concentrations.[149] A H_2O_2 solution is used to construct a calibration standard curve using various concentrations of H_2O_2.[149]

Hydroperoxides can be conveniently detected by MS, as they yield distinct $[M + 32]^+$ peaks.[150,151] In practice however, their MS detection is not trivial. The high temperatures required for the electron spray ionisation (ESI) may induce thermal decay of peroxides thus suppressing their detection. Nonetheless, MS has been reported to be the most reliable analytical technique in our toolbox for their detection.[152] Furthermore, MS coupled to other analytical techniques can be valuable in gaining a deeper understanding of the peroxides formed. Liquid chromatography – mass spectrometry (LC-MS) is a powerful tool that enables separation of hydroperoxides with the same mono-isotopic mass. Tandem MS (MS/MS) can provide further information about the identity of the peroxides by fragmenting the molecules.[64,66,153,154]

1.10.3 Hydroperoxide reactivity

Detection and structural identification of hydroperoxides is challenging due to their decay during analysis and/or sample handling. Hydroperoxides are generally considered moderately stable at RT and in the dark / absence of reducing agents or transition metal ions.[67,68]

The effect of temperature on peroxide decay has been investigated in detail, and it has been shown that at RT and in the dark, protein hydroperoxides exhibit half-lives of days or weeks, and alteration of the temperature further enhances or decreases their lifetime.[140,141] In the 2000's Davies and co-workers, investigated the kinetics of thermal decay for both Tyr- and Trp-derived hydroperoxides, generated *via* reaction with $^1O_2$.[58,150] It was demonstrated that at 37 °C within 24 h, *ca*. 80% of the initial peroxide content had been lost, while when incubated at 4 °C for the same duration hydroperoxides remained intact.

Ultraviolet irradiation can induce homolysis of the peroxide bond (Scheme 28A). For instance, *t*-BuOOH has been reported to absorb UV light over the wavelength of 210-300 nm with a calculated quantum yield of 1 at 248 nm.[155] In addition, peroxides undergo rapid one-electron reduction in presence of transition metal ions (Fenton-type chemistry; Scheme 28B).[140,142,156]

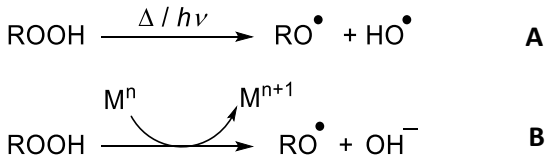

Scheme 28. Possible H_2O_2 decomposition conditions. A) Strong irradiation can induce homolytic cleavage of the peroxide bond, B) Reductive decomposition of the peroxide bond induced by transition metal ions.

These processes generate reactive RO• and HO• radicals (or hydroxyl anions). These radicals are capable of extending the initial damage to the proteins. The chemistry of both HO• and RO• in relation to amino acids and peptides has been explored in detail.

1.11 Project outline and aims

Proteins in biological systems are susceptible to oxidation by ROS that can result in major alterations including modification, fragmentation, cross-links and more.[97,105,135] The reaction mechanisms for these processes are complex and have been discussed in this Chapter (though the list is unlikely to be exhaustive). Similar chemical reactions are likely responsible for the hair damage.[9,157–161] Despite the fact that hair cosmetic products are widely available and used worldwide, scientific literature and research is scarce.[162] Understanding the chemistry and the interactions behind hair damage is critical, as this can enable the development of new formulations that can be incorporated in hair cosmetics products (e.g., shampoos, conditioners), and the development of new treatments to reduce the damage. It was discussed that hydroperoxides have been identified as the major intermediate product of protein oxidation. However, there are not many convincing literature data on their effect on protein damage. Our primary aim is to evaluate the effect of hydroperoxides on protein degradation, and whether increased protein damage is associated with accumulation of hydroperoxides.

As hair is a very complex material, it is necessary to develop a simplified model system. The first Chapter explores the HO•-mediated aerobic oxidation of short model peptides that are used as protein mimics. A particular emphasis is given in the detection and chemistry of hydroperoxides. We attempt to see if peptide-derived hydroperoxides, can act as prooxidants to trigger enhanced damage to the peptides. Important considerations for the model system were the ability to identify the formation of hydroperoxides, and to monitor the degradation of peptides. Upon confirming the prooxidant effect of hydroperoxides on the peptide decomposition, we attempt to link our findings with experiments in real human hair.

In living organisms, the harmful effects of ROS are attenuated, at least to an extent, by defensive mechanisms within cells and organisms.[59] Such defensive systems include radical scavengers (e.g. ascorbic acid), enzymes that have the ability to remove oxidants directly (e.g. superoxide dismutase for the $O_2^{\bullet-}$) and more.[59] Hair is an example of dead biological tissue, and so is prone to damage that cannot be repaired. As such, researching ways to prevent or reduce hair damage is of great importance to the cosmetic industry. The second Chapter focuses on the chemistry of polyphenolic compounds, and their antioxidant capacity on peptide oxidation. Polyphenolic compounds (flavonoids) have been utilised as antioxidants for many years in various industries (e.g., food, pharmaceutical), owing to their ability to break the propagation steps of autoxidation processes.[73,163,164] Polyphenolic compounds derived from natural extracts, have been recently investigated as potential antioxidants for hair cosmetics products. The second Chapter investigates the $HO^{\bullet}$-mediated aerobic oxidation of *N*-acetylated amino acids in the absence and presence of four catechol-based compounds as potential antioxidants. We monitor the decomposition of the starting amino acids by analytical techniques, and we identify oxidation products formed on the antioxidants. The aim of this Chapter is to explore whether the oxidation of amino acids is reduced in the presence of antioxidants, and to propose mechanistic pathways for their antioxidant activity.

As protein oxidation is governed by radical chain reactions, product identification is challenging. The final Chapter aims to elucidate the reaction mechanisms by detection of intermediate radicals in the aerobic oxidation of short *N*-acetylated peptides. Recently, a new method for trapping and characterising short-lived radical intermediates has been developed in our group.[165–167] The trapping results in the conversion of the radical intermediate to a stable non-radical product which can be analysed by MS and LC-MS. The method is used to capture and detect transient radicals formed during the aerobic oxidation of biological targets and is explained in detail in the third Chapter.

Chapter 2: Ultraviolet light and heat synergism hypothesis

2.1 Introduction

In biological systems, proteins are prime targets for damage by a wide range of different oxidants (both one- and two-electron), due to their high abundance and fast rate constants.[65] The ensuing reactivity and the formation of oxidation products is complex and depends on the oxidant.[168] Despite the highly variable resulting damage to the biological targets, under typical availability of O_2, hydroperoxides (ROOH) are usually the main intermediate product.[59] The mechanisms for the generation of amino acid-, peptide- and protein-hydroperoxides are reasonably well-understood (some of them have been covered in the Introduction), and many studies have been published in the field over the past 20 years.[61,138,141,169,170]

Despite the high protein content of the hair fibre (90 – 95% by dry weight),[171] literature data on the generation of keratin hydroperoxides is scarce. By comparison, the % of lipids on human hair is considerably lower (1 – 9% by dry weight)[171]. Nonetheless, most of the attention has been drawn to the formation of lipid peroxides, and the development of methods to control and reduce their damaging effect on hair.[28,157,172–174] The reason for this is likely two-fold; i) lipids can be easily extracted from hair, thus making it easier to study them, and ii) lipid peroxidation is a more efficient process compared to protein peroxidation. Since human hair is exposed to sunlight on a daily basis, it is reasonable to postulate that apart from photogeneration of lipid peroxides, keratin peroxides are also formed.

However, human hair is often exposed to different oxidation sources, for instance sunlight exposure followed by flat ironing, and hydroperoxides can be formed and degraded during both. In these cases, hydroperoxides accumulated during the first insult (e.g., photochemical exposure) could be hypothesized to lead to enhanced keratin degradation during the second insult (e.g., thermal treatment), resulting in the synergistic action of light and heat (Scheme 29).

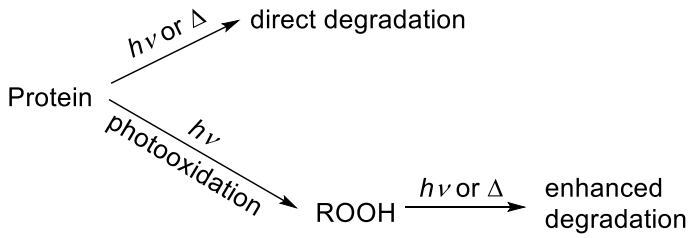

Scheme 29. Oxidation of proteins leads to relatively long-lived hydroperoxides. Elevated temperatures break the peroxide bond (-O-O-) yielding reactive short-lived alkoxyl and hydroxyl radicals.

Formation and accumulation of hydroperoxides in photochemical and thermal autoxidation processes (e.g., in environmental degradation) is well documented, with this leading to additional damage and an autocatalytic behaviour.[175–177] There is some anecdotal evidence to support this hypothesis, e.g., P&G noticed higher level of hair damage in customers who use both chemical (e.g., bleaching/colouring) and thermal (e.g., flat iron) treatments than would be expected from a simple combination of the two. We propose that the reason for the observed enhanced degradation is the generation of transient alkoxyl radicals ($RO^{\bullet}$) and $HO^{\bullet}$ (from the decomposition of hydroperoxides) that are capable of reacting with fast rate constants with the initial protein.

2.2 Kinetic modelling

2.2.1 Kinetic modelling - introduction

Most of the reaction mechanisms leading to protein degradation have been discussed in the introduction. Acquiring experimental data to determine protein damage, and deciphering the role of hydroperoxides in the process are not trivial. Indeed, assessing protein damage is challenging as most of the techniques used offer only qualitative or semi-quantitative (and therefore direct comparison between different studies is not an option) results.[149] Moreover, detection and quantification of protein peroxides is, on its own, a complicated and challenging task and only semi-quantitative data can be obtained (see Introduction Section 1.10).

For this reason, we believe the construction of a theoretical kinetic model can be a useful tool to obtain an insight into protein oxidation. Kinetic models have been used recently in chemistry to model complex processes where experimental quantitative or qualitative data are not readily available.[178–182] Kinetic modelling in chemistry is a discipline that describes the progress of reactions, from simple molecules to complex reaction networks.[179,183] Our main aim was to build a simplistic yet reliable prediction tool that would allow us to test the extent and boundaries of the synergism hypothesis.

2.2.2 Kinetic modelling - design

The design of a kinetic model is not trivial. First, all reactions that take place in the system need to be considered. Furthermore, designing kinetic models that are governed by chain reactions are hard to model, as small differences in rate constants can give significant errors in the results. Choosing appropriate rate constants is further confounded by the reaction medium. For instance, it has been reported that the rate of HAA reaction is solvent-dependet.[184] Indeed, it is well-established that HAA reactions are significantly slower in polar solvents compared to non-polar hydrocarbon solvents.[185] In view of this, it was advised to use reaction rate constants in the same solvent for every reaction incorporated in the model. It was decided to assume reactions in aqueous solutions, as protein oxidation in biological systems is delineated, and most reaction rate constants have been previously critically evaluated.

To test the scope and feasibility of the proposed synergism, a kinetic model of protein autoxidation based on Scheme 30 with some additional reactions (can be found in the Experimental Chapter) was constructed.

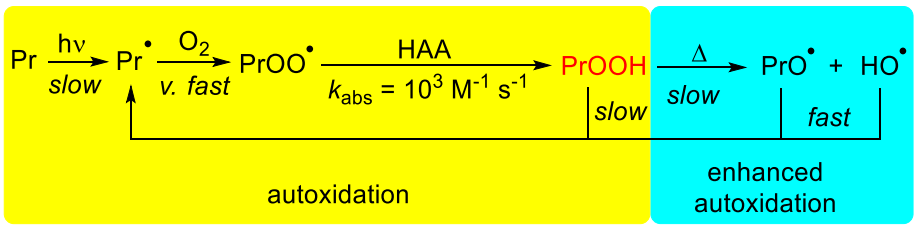

Scheme 30. Fate of initial carbon-centred radical generated on hair proteins in high abundance of O_2 to yield unstable peroxyl radicals (PrOO•), ultimately leading to the formation of transient alkoxyl (PrO•) and hydroxyl radicals.

Scheme 29 shows a simplified depiction of the preliminary protein oxidation, aimed to highlight the formation, decay and role of hydroperoxides in the synergism hypothesis. Protein (Pr) oxidation starts with the formation of a carbon-centred radicals that react with O_2 to yield peroxyl radicals (PrOO•).[59] In biological systems, where availability of nearby C-H bonds is high, the majority of PrOO• participate in HAA to yield hydroperoxides (PrOOH; typical k_{abs} = 10^3 M^{-1} s^{-1}).[128] Some hydroperoxides decompose resulting in an autocatalytic behaviour, but a significant amount accumulates in the system. Subsequent elevated temperatures and sunlight can induce rapid homolytic decay to hydroperoxides yielding alkoxyl radicals (PrO•) and HO•. These radicals are capable of further reacting with the starting protein or a different protein present in the system, thus extending the initially photo- or thermally-inflicted damage to the protein.

Due to lack of reliable kinetic data on protein hydroperoxide decomposition in the literature, a rate constant for the decay of hydroperoxides formed in aqueous solutions of *N*-Ac-Gly-Gly-OH (5 mM) upon exposure to a lamp that simulates sunlight, was experimentally determined(see Section 2.5.3), and this rate constant (10^{-4} s^{-1}) was used in the model (discussed in detail in Section 2.5.3).

2.2.3 Kinetic modelling - results

The model was used to estimate accumulation of hydroperoxides in a protein upon exposure to UV light. Initially, the rate of photoinitiation was adjusted to achieve *ca.* 10% decomposition of the protein (at 1 mM concentration) over a 30 min simulation period (Figure 6A; left Y axis). The rate constants used in this model were all literature values for reactions in aqueous solutions. The results show continuous growth of hydroperoxides (PrOOH) (Figure 6A; right Y axis).

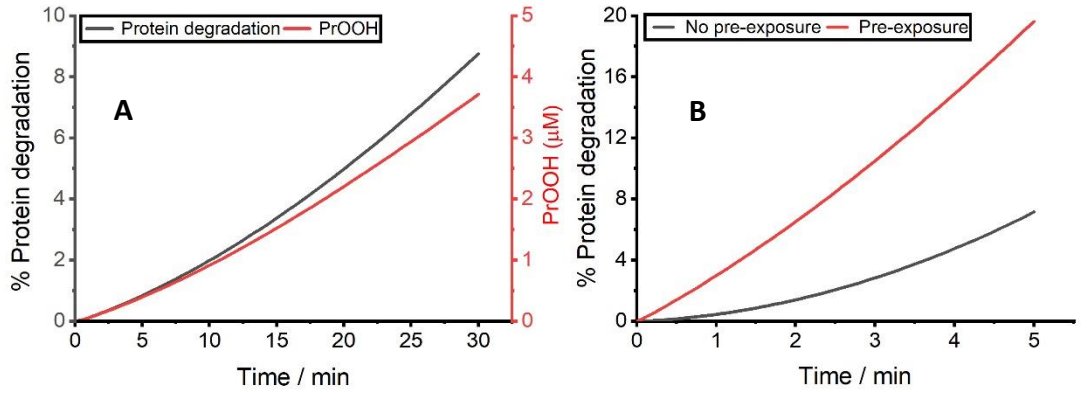

Figure 6. Kinetic model output. A) Hair protein decomposition and protein peroxides evolution. The concentration of the parent protein was set at 1 mM, and the initiation was adjusted to achieve a 10% decomposition of the starting protein after 30 min of sunlight exposure. B) Evaluation of the synergistic action using 3.7 µM as initial concentration of protein hydroperoxides.

The concentration of hydroperoxides would plateau and then decay at much longer exposure times. The outcome of this simulation is in a reasonable agreement with our experimental data on $HO^{\bullet}$-mediated decomposition of 3 model substrates (*vide infra*).

In order to test the synergistic action hypothesis, further kinetic modelling runs were performed. Specifically, the system without and with accumulated hydroperoxides (at the end of simulation in Figure 6A) was exposed to elevated temperature (100 °C) for 5 min (Figure 6B). The results in Figure 6B show enhanced thermal degradation of protein which was pre-exposed to UV light (*ca*. 20% vs 7% of the initial protein has been degraded), thus suggesting the hypothesis of the synergism of UV and thermal treatments.

The effect was also tested at a much slower initiation rate (*ca*. 2% protein degradation after 8 h light exposure; Figure 7) that would be much closer to a real-life scenario. The reaction rates of other photochemical steps were reduced accordingly.

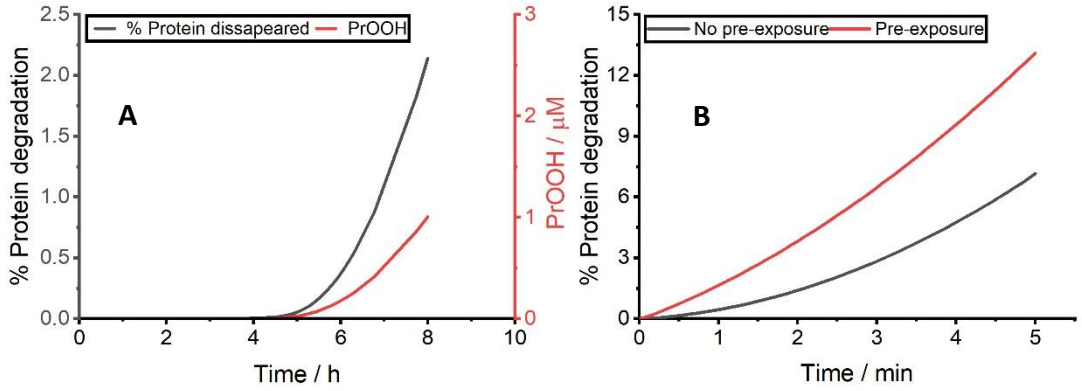

Figure 7. Kinetic model output. A) A prediction of a more realistic scenario where 8 h of sunlight exposure led to 2% protein decomposition. Second axis shows the protein peroxides evolution. The concentration of the parent protein was again set at 1 mM. B) Evaluation of the synergistic action using 1 µM as initial concentration of protein hydroperoxides.

The model predicted a considerably slower accumulation of hydroperoxides with nearly 1 µM at the end of the 8 h simulation (Figure 7A; right Y axis). Importantly, the sample pre-exposed to UV light also showed enhanced degradation (*ca*. 12%) compared to the untreated control (*ca*. 6%) (Figure 7B).

It is worth noting that the effect is strongest at the beginning of the protein degradation (within the first 3.5 min). After this time, the two systems appear to follow a similar rate of protein decay. This can be easily explained by the fact that hydroperoxides are formed in any autoxidation, and so, as the thermal degradation in Figure 6B is progressing, the amount of hydroperoxides formed reaches similar level to the sample which was pre-treated with UV, and the two samples would then degrade at similar rates.

It is important to state that a critical assumption was made for this model. While the major reaction pathways are probably those incorporated in the model; the reaction rate constants will be significantly slower in hair, compared to aqueous solutions. The restricted environment in hair was considered, however, rate constants for these reactions in the solid phase are not known. Importantly, when certain reaction rate constants were varied (e.g., the initiation rate, the reactions of PrOO$^{\bullet}$) the general trends of the model remained the same. So, even though absolute rate constants are different, it is likely that the general behaviour will be similar.

2.3 Choice of model system

Hair fibre is comprised primarily of keratin proteins that can undergo multiple chemical changes. Chromophores present in hair are capable of absorbing sunlight which leads to a series of different reactions. Moreover, keratin proteins are susceptible to oxidation by a range of oxidants that can be generated in the hair environment. As such, investigating keratin photochemistry or the reactivity of keratin proteins with one-electron oxidants is not trivial. Similarly, generation and detection of organic peroxides formed on hair keratins is not straightforward. In order to test the synergism hypothesis and assess the role of hydroperoxides in it, hydroperoxides have to be detected and quantified reliably. To enable a thorough investigation of the synergism postulate and to acquire experimental evidence for the role of hydroperoxides in the process, a simplified model system is required.

The mechanisms giving rise to hydroperoxides in biological systems have already been discussed in Section 1.10.1, and the same mechanisms should occur in the hair fibre. Considering the rich literature data on the formation of hydroperoxides in aqueous solutions of individual amino acids or short peptides, attention was turned to similar systems. Since keratin proteins are the major component of dry hair, we believe that short peptides can be used as reliable protein mimics. Initial work was carried out using *N*-Ac-Gly-Gly-OH **2.1** (Figure 8).

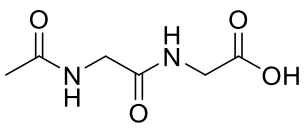

2.1

Figure 8. Chemical structure of N-Ac-Gly-Gly-OH, the peptide that was chosen for preliminary studies.

The peptide shown in Figure 8 was chosen for our studies as it is comprised of the simplest amino acid (glycine) that contains no side chain. As such, the reactivity will be limited to the backbone of the peptide and identification of hydroperoxides and/or oxidation products should be less complicated. In 1993 Gebicki and co-workers exposed aqueous solutions of free amino acids (20 mM) to $HO^{\bullet}$ to measure their ability to form hydroperoxides, and their work revealed that glycine is one of the least efficient amino acids for peroxidation (see also Section 1.10.1).[141] The outcome was rationalised by the lack of available C-H from where HAA by $HO^{\bullet}$ can take place. Indeed, free glycine contains only one secondary carbon centre, and therefore, peroxidation is not expected to occur readily. Nonetheless, we believe that *N*-Ac-Gly-Gly-OH can be used as a suitable starting point for our studies. We decided to use an *N*-protected dipeptide to reduce formation of $RNH_2^{\bullet}$ and the following reactions. The acetyl group was chosen as a protection group for the free amine, as it resembles the peptide bond that occurs in peptides and proteins.

2.4 Photogeneration of $HO^{\bullet}$

Following the decision over the model system, attention was turned to the generation of hydroperoxides. As discussed in the Introduction Section 1.10 hydroperoxides are the main intermediates in the reaction of free amino acids, peptides, and proteins with many reactive oxidants (e.g., $HO^{\bullet}$, $^1O_2$ etc.). There is rich literature research on the reaction of $HO^{\bullet}$ with amino acids, peptides, and proteins in aerobic solutions, indicating formation of a range of different products, including hydroperoxides, carbonyls, alcohols and molecular fragments.[49,92,98,106,186] As such, it was opted to use $HO^{\bullet}$ as an oxidant for the generation of hydroperoxides with *N*-Ac-Gly-Gly-OH.

Some of the possible ways for the formation of $HO^{\bullet}$ have been covered in Introduction Section 1.7. We believe that photolysis of aqueous H_2O_2 is a well-established and "clean" method for the generation of $HO^{\bullet}$. This is usually achieved by employing a light source with strong emission between 230-255 nm; wavelengths where H_2O_2 has a relatively high molecular absorption coefficient (ε).[187] Most commonly, low pressure-Hg lamps have been used, that emit light at 253.7 nm where H_2O_2 has an $\varepsilon = 18.6\ M^{-1}\ cm^{-1}$. Photolysis of H_2O_2 is a wavelength-depended, relatively efficient process (quantum yield of 0.5 mol Ein^{-1}) that results in the formation of two highly reactive $HO^{\bullet}$ (Scheme 31; Eq. 1).[180,188]

Equation #	Reaction	k (M^{-1} s^{-1})	Reference
1	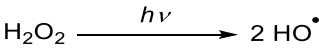	Φ = 0.5 mol Ein^{-1}	189,190
2	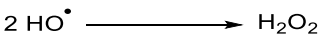	5×10^9	89
3	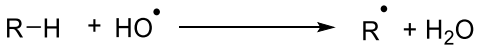	10^8 - 10^{10}	67,89
4	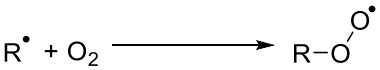	diffusion controlled	74
5	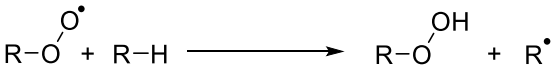	10^3	128

Scheme 31. Production of HO• utilising the UV/H_2O_2 system and subsequent main reaction pathways for the irradiated-generated HO•, ultimately yielding hydroperoxides (ROOH).

Two main reaction pathways exist for the photolytically generated HO•; that are, diffusion-controlled recombination inside the cage to reform H_2O_2 (Scheme 31; Eq. 2) or reaction with an organic molecule to yield a carbon-centred radical (R•) and H_2O (Scheme 31; Eq. 3). The newly formed R• reacts with O_2, to afford peroxyl radicals (ROO•), that are converted to hydroperoxides (ROOH) in presence of nearby C-H bonds (Scheme 31; Eq. 4 and 5 respectively). Alternatively, ROO• can participate in radical-radical termination reactions to afford non-radical products. Scheme 31 is a simplified representation of the reactions taking place to highlight the HO•-mediated formation of ROOH in aqueous solutions. In actuality, HO• are involved in many more reactions, including reaction with H_2O_2 (reactions can be found in the Appendix).

2.5 *N*-Ac-Gly-Gly-OH

2.5.1 FOX-assay quantification of *N*-Ac-Gly-Gly-OH-derived hydroperoxides

Upon establishing the model system and the HO•-generation method, experiments to form and detect hydroperoxides were carried out. After optimisation of reaction conditions (i.e., peptide and H_2O_2 concentration and irradiation time), an appreciable concentration of hydroperoxides was obtained when aqueous solutions of *N*-Ac-Gly-Gly-OH (5 mM) were exposed to UV light for 60 min in the presence of H_2O_2 (100 mM). To minimize artefactual oxidation of the peptide, all aqueous solutions were prepared using high-purity water (Milli-Q), as it contains virtually no transition metals that can catalyse oxidation (e.g., Fenton chemistry).[149] It was considered that peptides could be photoexcited by absorbing UV radiation. To test this, aqueous solutions of the peptide was exposed to the same UV light, and its decomposition was monitored by UV-Vis spectroscopy. This

resulted in no loss of the peptide (data not shown). The formation of hydroperoxides was determined by the FOX-assay (Figure 9).

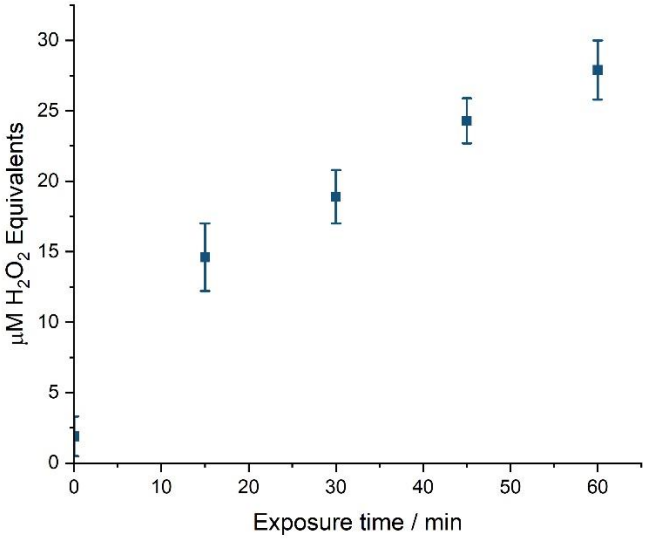

Figure 9. Quantification of the total HO•-mediated hydroperoxide content on aq. solutions of N-Ac-Gly-Gly-OH (5 mM) in presence of aq. H_2O_2 (100 mM) upon exposure to UV light for 60 min. Aliquots were taken at the indicated timestamps and were frozen immediately until analysis Results are the mean ± SE of three independent experiments, analysed the same day with the FOX-assay.

Aliquots were taken prior to irradiation and then every 15 min until the end of the exposure. Upon collecting, all aliquots were treated with catalase (3150 U mL^{-1}; aq. solution), an enzyme that has been shown to selectively decompose H_2O_2 but is unreactive towards organic peroxides (more information can be found in the Experimental Chapter).[191] Figure 9 demonstrates an accumulation of hydroperoxides in-line with irradiation time (triplicate experiments).

The evolution is faster in the first 15 min (*ca*. 15 µM), and the rate of formation appears to be reduced thereafter, with *ca*. 25 µM at the end of the irradiation. This outcome is not surprising. It has been discussed in Introduction Section 1.10.3 that hydroperoxides are unstable under strong UV light, and homolytic decay, to yield RO• and HO• takes place. Therefore, after an initial period of evolution, hydroperoxides are formed and decomposed simultaneously, thus the total peroxide content increases at a slower rate. To confirm that hydroperoxides measured in Figure 9 are HO•-derived and are formed on *N*-Ac-Gly-Gly-OH, control experiments were run firstly in the absence of H_2O_2, and secondly in the absence of *N*-Ac-Gly-Gly-OH. Both experiments resulted in no formation of hydroperoxides (data not shown).

2.5.2 LC-MS Identification of *N*-Ac-Gly-Gly-OH-derived hydroperoxides

While Figure 8 suggests the formation of hydroperoxides on *N*-Ac-Gly-Gly-OH, no information about the chemical composition of the peroxides can be obtained from the FOX assay which only detects the total ROOH content. In order to acquire evidence for the formation of specific *N*-Ac-Gly-Gly-OH-associated hydroperoxides, reactions were analysed by direct-injection mass spectrometry (DI-MS) and liquid chromatography mass spectrometry (LC-MS). Since *N*-Ac-Gly-Gly-OH is a simple dipeptide with no side chain, hydroperoxides **2.2** are expected to form on the backbone (Scheme 32).

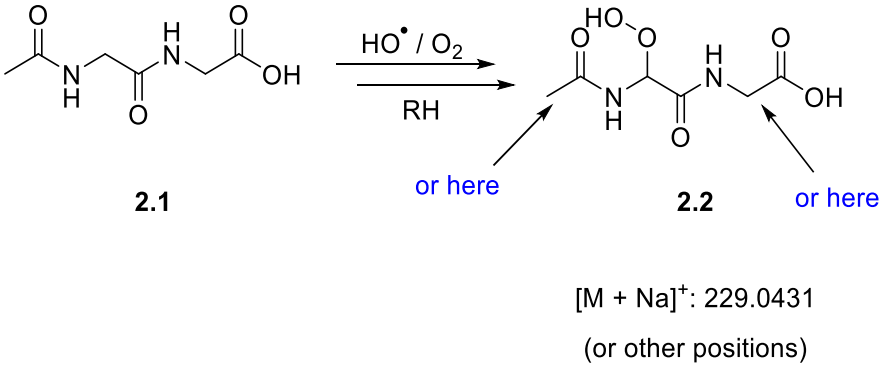

Scheme 32. Aerobic HO•-induced oxidation of N-Ac-Gly-Gly-OH ultimately generating hydroperoxides, via initial HAA reaction.

The structure of the hydroperoxide shown in Scheme 32 is representative and peroxidation could occur at other positions as shown in the scheme. Analysis by DI-MS returned no results (we found that *N*-Ac-Gly-Gly-OH generally ionises very poorly in DI-MS). LC-MS chromatograms were scanned for the potential hydroperoxides shown in Scheme 31, and the extracted ion chromatogram (EIC) is presented in Figure 10.

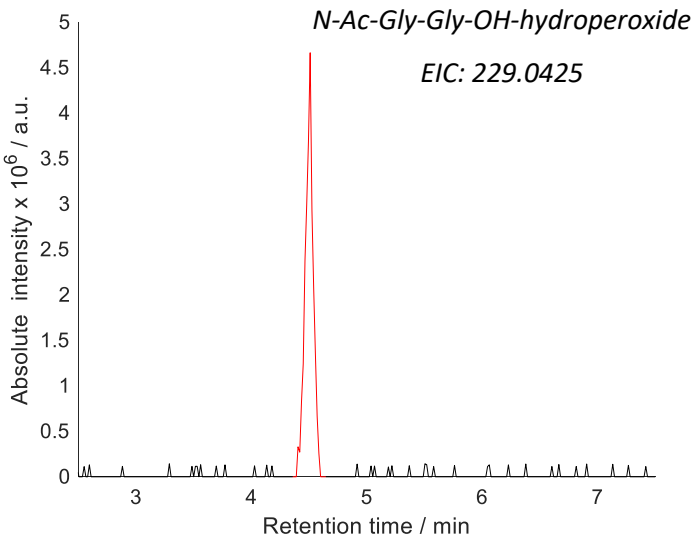

Figure 10. Extracted ion chromatogram (EIC) of 229.0425 (potential N-Ac-Gly-Gly-OH-derived hydroperoxide). Hydroperoxides were generated by exposure of aqueous solutions of N-Ac-Gly-Gly-OH (5 mM) to UV light in presence of aqueous H_2O_2 (100 mM). Aliquots were diluted and analysed by LC-MS.

The EIC of the LC-MS analysis shows evidence for the formation of a hydroperoxide formed on *N*-Ac-Gly-Gly-OH (highlighted in red as the sodiated ion). It is noted that in all cases were MS was used for the detection of degradation products or trapped radicals (Chapter 4), the acquired *m*/*z* was in excellent agreement with the calculated *m*/*z* (error was < 0.0010 *m*/*z*; more information under the Experimental Chapter)

Control reactions, that were incubated in the dark, showed no evidence for formation of hydroperoxide thus confirming that the peak eluting at 4.5 min is due to $HO^{\bullet}$ oxidation (data can be found in the Appendix). The emergence of only one peak, suggests that peroxidation selectively occurs in one of the three available positions of *N*-Ac-Gly-Gly-OH, although it is possible that peroxidation takes place at different carbons, but the abundance of the molecules is too low to detect, or the peaks could not be separated in the LC. It is important to note that the compound responsible for the peak with an *m*/*z* of 229.0425 could be a dihydroxy derivative (diol) formed on *N*-Ac-Gly-Gly-OH (Scheme 33), as a result of second oxidation by a $HO^{\bullet}$. No data were obtained to distinguish between *N*-Ac-Gly-Gly-OH-derived hydroperoxides or diols, however hydroperoxide assignment would be consistent with the fact that the FOX-assay detected hydroperoxides.

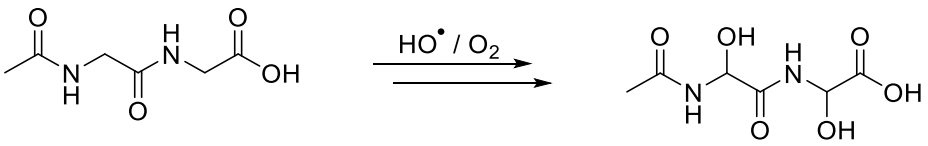

2.1 **2.3**

Identical *m*/*z* with the hydroperoxide

Scheme 33. Formation of a dihydroxy derivative as a result of a 2nd HAA by HO•. The dihydroxy derivative shares identical m/z with potential hydroperoxides.

It was discussed in the introduction how exogenous catalysts (e.g., strong irradiation, high temperatures and more) can induce reductive homolysis on the peroxide bond. Our main goal is to evaluate the hydroperoxide role in peptide degradation with an emphasis on their relevance to hair damage. Therefore, it was decided to test the hydroperoxide decay under exogenous conditions that keratin hydroperoxides could be exposed to. The next two Sections are focused on the decay of *N*-Ac-Gly-Gly-OH hydroperoxides under sunlight (Section 2.5.3), and elevated temperatures (Section 2.5.4).

2.5.3 Sunlight-induced decay of *N*-Ac-Gly-Gly-OH-derived hydroperoxides

Hydroperoxides formed on hair keratins will be likely exposed to sunlight. Since it is well-established that solar radiation leads to significant damage to hair in various forms, it is reasonable to investigate the effect of sunlight on hydroperoxides, as their photo-induced decay can accelerate keratin damage *via* mechanisms outlined in Scheme 30. The sunlight-induced decay of *N*-Ac-Gly-Gly-OH hydroperoxides was investigated by employing a lamp that simulates sunlight. The irradiance of the sunlight simulated lamp was 100 W cm^{-2}, and the output spectrum was AM1.5G which refers to the standard spectrum of the solar output at Earth's surface. The output is from 290 to 1250 nm, with a maximum at 500 nm.

Initially, hydroperoxides were generated in aqueous solutions of *N*-Ac-Gly-Gly-OH (5 mM) as in Section 2.4. At the end of the irradiation, solutions were treated with catalase (3150 U mL^{-1}; aq. solution) to destroy any leftover H_2O_2. Aliquots were taken and frozen immediately to determine the total peroxide content at the end of the UV exposure. The remainder of the solutions, after degradation of H_2O_2, were exposed to a lamp that simulates sunlight for 2 h with aliquots taken every 30 min (Figure 11).

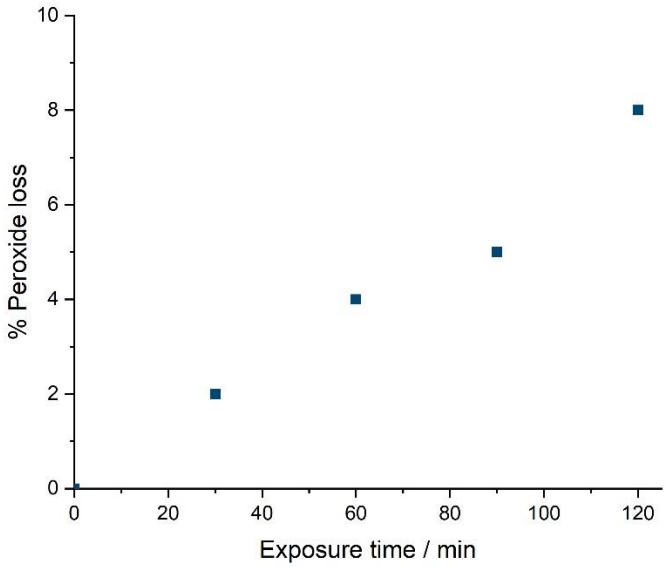

Figure 11. Sunlight-induced decay of HO•-mediated peroxides. Hydroperoxides were generated on N-Ac-Gly-Gly-OH (5 mM aq. solutions) in presence of 100 mM aq. H_2O_2. Data are the results of a single experiment analysed by the FOX-assay.

Figure 11 suggests a minor loss of peroxides upon exposure to sunlight. At the end of the exposure *ca*. 9% of the initial peroxide has been decomposed. The kinetics of amino acid-, peptide- and protein-hydroperoxides decay upon exposure to visible light or sunlight are generally less researched, and therefore it is hard to compare our experimental findings with previous literature. Nonetheless, some research has been carried out on the visible-light induced decay of amino acid-derived hydroperoxide.[58,150] In 2002 Davies and co-workers studied the photochemical stability of Tyr-derived hydroperoxides, and their results showed that visible light (250 W lamp, with a cut-off filter at 345 nm) has a small, but noticeable effect on the peroxide concentration.[58] More specifically, within 2 h of exposure to visible light *ca*. 15% of the initial peroxide content was lost, indicating that visible-light hydroperoxide decay is indeed a slow process.

The sunlight-induced decay of peroxides, albeit slow, is important for the hair chemistry, since in many real-life scenarios our hair is exposed to sunlight for long periods of time. The peroxide decay shown in Figure 6, appears to follow pseudo-first order kinetics, with an estimated $k_{decay} \sim 10^{-4}$ s^{-1} (the fitting of the data to first order kinetics can be found in the Appendix). However, it is reported that the kinetics of peptide- and protein-derived hydroperoxide decay are much more complex, and do not follow first or second order kinetics.[60] This is likely a result of multiple competing reactions in the system. For instance, photolysis of hydroperoxides yields new transient radicals (Scheme 34; Eq. 6).

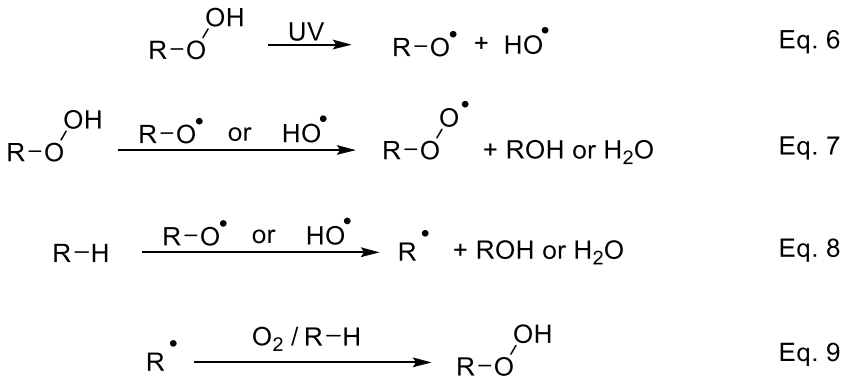

Scheme 34. Initial photolysis of organic peroxides yielding transient radicals, and their ensuing reactivity that can either react with hydroperoxides or react with starting substrate to generate more hydroperoxides.

The RO$^{\bullet}$ and HO$^{\bullet}$ can participate in HAA reactions with hydroperoxides to yield ROO$^{\bullet}$ (Scheme 34; Eq. 7). However, considering that usually the concentration of RH exceeds the concentration of ROOH in the system, this reaction can be discounted. A more likely pathway for the newly generated RO$^{\bullet}$ and HO$^{\bullet}$ is HAA from the starting substrate RH (Scheme 34; Eq. 8) to produce R$^{\bullet}$, that can be quickly converted to ROOH (Scheme 34; Eq. 9). Reactions 6-9 portray a simplistic view of competing reactions that can affect the concentrations of ROOH in the system when considering simple peptide-derived hydroperoxides. When dealing with protein-derived hydroperoxides, more competing reactions can take place, thus making the decay kinetics more complex.

2.5.4 Thermal decay of *N*-Ac-Gly-Gly-OH-derived hydroperoxides

Apart from exposure to sunlight, human hair is frequently exposed to elevated temperatures (e.g., flat-ironing of hair *etc*.). As such, it is instructive to consider the thermal decay of hydroperoxides, as their homolysis can extent hair keratin damage. The thermolysis of amino acid-, peptide-, and protein-hydroperoxides has been measured by different research groups at various temperatures, ranging from -20 to 37 °C.[58,61,150,153]. However, hair is exposed to considerably higher temperatures than that (for example temperature for blow-drying hair is ~ 60 °C, while for flat-ironing hair is over 200 °C). Considering this, it was decided to test the kinetics of thermal decay of *N*-Ac-Gly-Gly-OH-derived hydroperoxides, in various temperatures.

To examine the effect of temperature, aqueous solutions of *N*-Ac-Gly-Gly-OH (5 mM) were again exposed to UV light to generate hydroperoxides, after which, solutions were treated with catalase (3150 U mL^{-1}; aq. solution). At the end of the exposure, aliquots were taken and frozen immediately to determine the total peroxide content. The remainder of the solutions, after H_2O_2 decomposition, were incubated at various temperatures for 2 h with aliquots taken at the indicated timestamps (Figure 12).

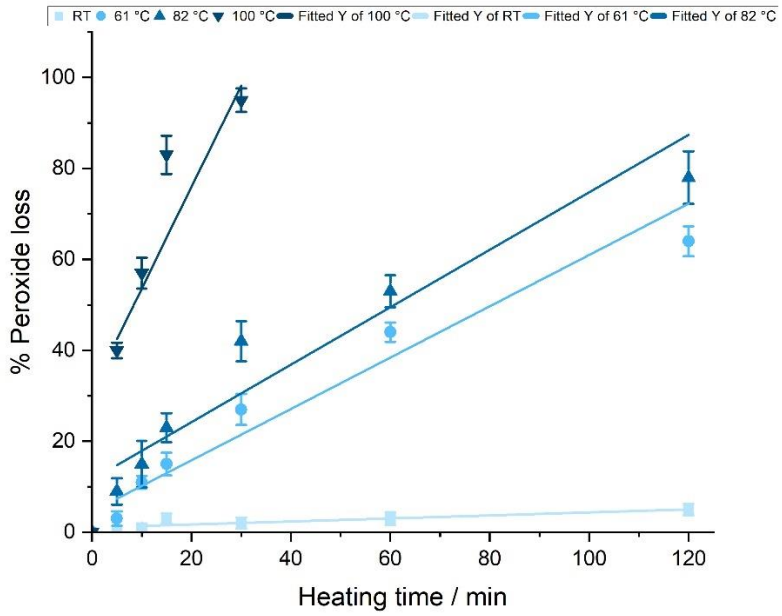

Figure 12. Thermal decay of photogenerated hydroperoxides formed on N-Ac-Gly-Gly-OH (5 mM; aq. solutions) upon exposure to UV light in presence of H_2O_2 (100 mM). Solutions were incubated at various temperatures, and aliquots were taken at the indicated timestamps. Results are the mean ± SE of three independent experiments analysed in the same day by the FOX-assay. First order kinetics were fitted in all cases.

Figure 12 demonstrates that elevated temperatures induce rapid decay to hydroperoxides. Incubation at RT resulted in nearly no loss, while the rate of decay increased at higher temperatures, consistent with thermal breakdown. Interestingly, the rate of decay appears to follow first order kinetics in all cases, with calculated decomposition rate constants of $k_{61} \sim 10^{-4}\ s^{-1}$, $k_{82} \sim 2 \times 10^{-4}\ s^{-1}$, and $k_{100} \sim 10^{-3}\ s^{-1}$. It is noted that the hydroperoxide decay at 100 °C is very rapid (nearly 100 times faster than in 82°C), and this might be due to experimental error (this was not investigated further).

The kinetics of hydroperoxide thermolysis are quite interesting and important for the hair chemistry. As we have stated in the kinetic modelling design Section, it is usual for our hair to alternate between exposure to sunlight and elevated temperatures. In both scenarios, it is likely that hydroperoxides are formed and decomposed simultaneously. Consequently, keratin-associated hydroperoxides that have been pre-accumulated during exposure to sunlight, will be rapidly decomposed if a heat-source is applied to hair. Depending on the heat-source applied, this temperature can be as high as 230 °C (flat-ironing). Such temperature will probably induce rapid decay of peroxides irrespective of the duration of the heat (flat ironing is usually applied for seconds, not minutes). Indeed, hydroperoxides will be thermally decomposed to $RO^{\bullet}$ and $HO^{\bullet}$ radicals, with an ensuing reactivity similarly to Scheme 30. Therefore, pre-accumulated hydroperoxides can act as prooxidants to deliver extended damage to the hair fibre.

2.6 New model system

The reasoning for choosing *N*-Ac-Gly-Gly-OH was to ensure relatively simple reactivity (by avoiding side chains), so we could develop the appropriate methods and assays to quantify and identify hydroperoxides. However, glycine peroxidation is an inefficient process as was demonstrated by Gebicki and co-workers.[141] Indeed, in order to produce hydroperoxides at a level shown in Figure 8, highly concentrated solutions of *N*-Ac-Gly-Gly-OH (5 mM) had to be employed, as when reactions were run in more dilute solutions (1 mM), no appreciable concentration of hydroperoxides could be detected (data not shown). To investigate the synergism hypothesis in a system pertaining to the hair care industry, three N-acetylated dipeptides/amino acids were chosen as model substrates (Figure 13).

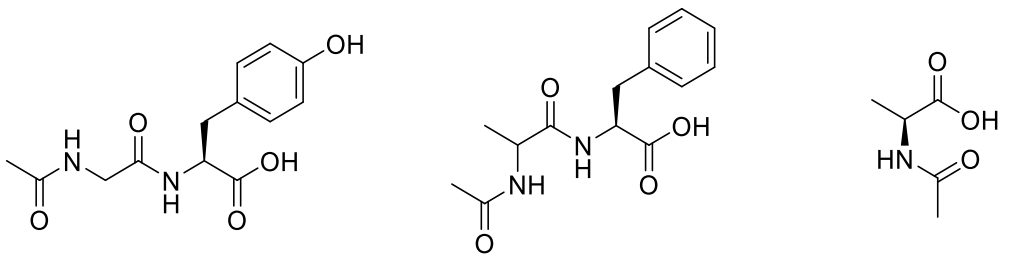

N-Ac-Gly-Tyr-OH **2.4**

N-Ac-Ala-Phe-OH **2.5**

N-Ac-Ala-OH **2.6**

Figure 13. Chemical structures of the three biological substrates used in this work.

The constituent amino acids (Tyr, Gly, Ala, Phe) form low to moderate amount of hydroperoxides on reaction with HO$^{\bullet}$ radicals, and they are all found in hair keratins. Tyrosine is one of the main chromophores responsible for photodamage of hair (see introduction for more information). Alanine and Gly were chosen to probe different types of HO$^{\bullet}$ reactivity: aromatic amino acids (e.g., Tyr, Phe) predominantly react by direct addition of the HO$^{\bullet}$ to the ring (and peroxidation is less efficient), whereas Ala and Gly react *via* HAA that primarily leads to formation of hydroperoxides. A combination of analytical techniques to assess the parent peptide decomposition and detect and quantify hydroperoxides accumulated during photochemically-triggered oxidation of the model substrates by the HO$^{\bullet}$ radical were utilised.

2.6.1 FOX-assay quantification of HO$^{\bullet}$-mediated hydroperoxides

The same method that was used for *N*-Ac-Gly-Gly-OH was employed again, however more dilute solutions of peptides were now exposed to UV light. The reason for this is that Ala, Tyr, and Phe are all more efficient amino acids for peroxidation reactions, and therefore, highly concentrated solutions (and prolonged irradiation times) were not necessary. Hydroperoxides were generated by exposing aqueous solutions of the three substrates (1 mM) to UV light in presence of H_2O_2 (100 mM) for 2 min. Reactions were run in a 100-fold excess of H_2O_2 in order to reduce the likelihood of direct absorption of UV light by the protected peptides or their hydroperoxides.

Unless otherwise stated, all reactions were carried out in unbuffered solutions. Therefore, prior to any analysis and interpretation of data, the pH of the reactions needs to be considered, as this can significantly alter the stability of the intermediate radicals (*vide infra*). The first pKa value (carboxy group) for all the amino acids is similar, and for the three amino acids used here the calculated values are 2.20, 1.83, and 2.34 for Tyr, Phe, and Ala, respectively. Considering the concentration of the starting substrates in our reactions (all 1 mM), then the pH of the reactions can be easily calculated, and it was found to be ~ 3. Effectively, this means that in every reaction the % of protonated and deprotonated dipeptide is different. Indeed, further calculations, show that in our reactions the three substrates are mostly present in their anionic form (% of presence as the carboxylate anion: *N*-Ac-Gly-Tyr-OH ~ 86%, *N*-Ac-Ala-Phe-OH is 94%, and *N*-Ac-Ala-OH is 82%).

It is important to highlight that the high degree of deprotonation of the substrates will likely affect the formation of intermediate radicals. Indeed, as it has been discussed in the introduction, the most probable positional attack for the HO$^{\bullet}$-mediated HAA is the $^{\alpha}$C-H, as the resulting radical is stabilised by the captodative effect (see Section 1.7.4.1). However, this stabilising effect will be

highly reduced since the majority of the substrates are present as the carboxylate anions (significantly weaker EWG). Therefore, the initial HAA reaction by HO$^{\bullet}$ can likely take place in other positions of the three substrates (e.g., the benzylic position for *N*-Ac-Gly-Tyr-OH, and *N*-Ac-Ala-Phe-OH, as the aromatic rings will stabilise the intermediate radical).

Aliquots were collected at the indicated timestamps and were analysed by the FOX-assay for the total peroxide content (Figure 14).

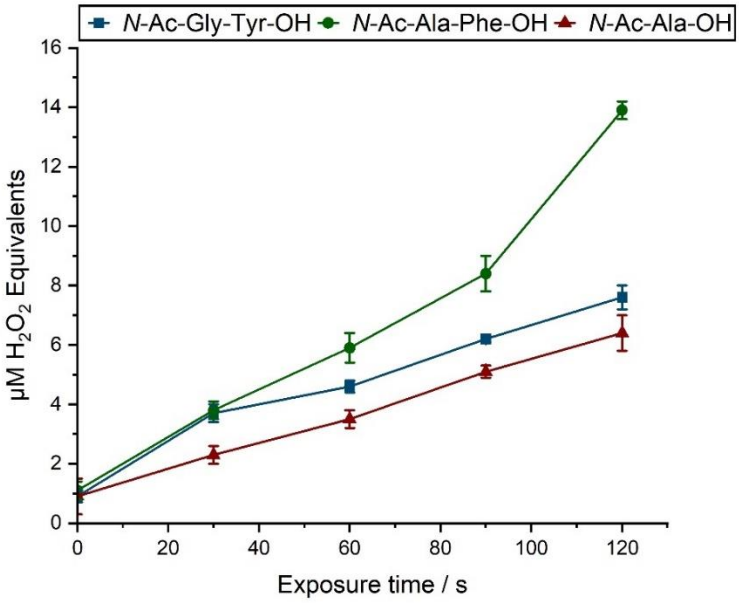

Figure 14. Quantification of the total HO$^{\bullet}$-mediated hydroperoxide content on aq. solutions of the three substrates (all 1 mM) in presence of aq. H_2O_2 (100 mM) upon exposure to UV light. Aliquots were taken at the indicated timestamps and were frozen immediately until analysis. Results are the mean ± SE of three independent experiments, analysed the same day by the FOX-assay.

Figure 14 illustrates that photolysis of the three substrates resulted in formation of hydroperoxides as determined by the FOX-assay. The total peroxide content increased with irradiation time. In the case of *N*-Ac-Ala-Phe-OH the highest peroxide yields were detected, with *ca*. 15 µM after 2 min of UV exposure. On the contrary, *N*-Ac-Gly-Tyr-OH and *N*-Ac-Ala-OH provided intermediate yields of *ca*. 7 µM of hydroperoxides in both cases.

The higher peroxide yields detected for *N*-Ac-Ala-Phe-OH over *N*-Ac-Gly-Tyr-OH are consistent with literature reports where it was demonstrated that HO$^{\bullet}$-induced peroxidation of Phe is slightly more efficient than Tyr. [141] Furthermore, Ala contains a secondary C-H, which is inherently more reactive than the primary C-H position of Gly. Thus, the higher detected peroxide levels, can be attributed to the more reactive C-H positions from where HO$^{\bullet}$-HAA can occur.

2.7 Ultraviolet light-induced decay of peroxides

In Section 2.5 hydroperoxides formed on *N*-Ac-Gly-Gly-OH were quantified, and their decay under sunlight and elevated temperatures was studied. However, strong UV radiation is also capable of inducing homolytic decay to hydroperoxides. Indeed, in 1998 Griffiths and co-workers exposed aqueous solutions of various amino acids (including tyrosine) to γ-radiation and reported that high doses resulted in a plateau of the hydroperoxide formation.[142] The observation was rationalised by progressive degradation of the intermediate hydroperoxides that occurs in a similar rate to their formation (therefore resulting in a net zero outcome). It is possible that the UV source we have used for the H_2O_2 photolysis, apart from generation of hydroperoxides, causes concomitant degradation.

In order to test the UV-induced decay of hydroperoxides, aqueous solutions (1 mM) of all three substrates were irradiated in presence of H_2O_2 (100 mM). At the end of the exposure (2 min) the solutions were treated with catalase (3150 U mL^{-1}; aq. solution) to destroy the H_2O_2 excess. After this, aliquots were taken to determine the total peroxide content at the end of the irradiation. The remainder of the solutions were re-submitted to the same experimental conditions for another 2 min, with aliquots taken every 30 s. The total peroxide content was determined by the FOX-assay, and the results (depicted as the % of the total peroxide content lost) can be seen in Figure 15.

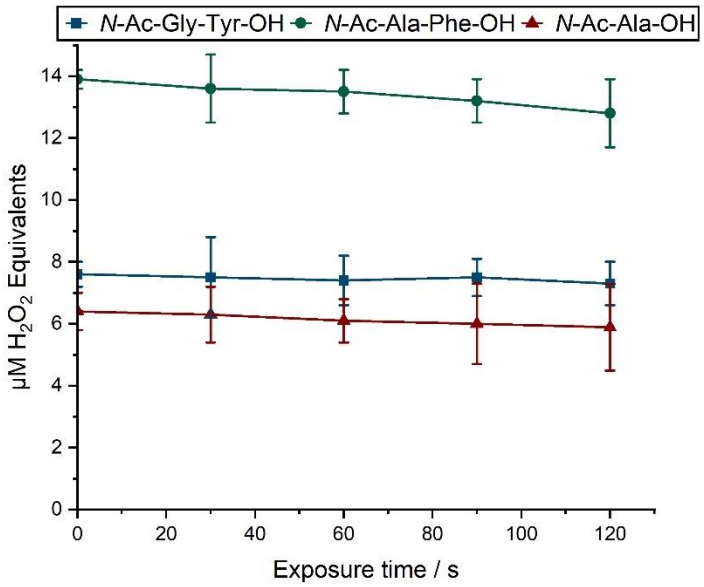

Figure 15. UV-induced decay of hydroperoxides generated on the three substrates (1 mM; aq. solutions) upon exposure to UV light in presence of H_2O_2 (100 mM). Solutions were liberated from H_2O_2 and re-submitted to UV light, and aliquots were taken at the indicated timestamps, and were frozen immediately until the day of analysis. Results are the mean ± SE of three independent experiments analysed the same day by the FOX-assay.

The results suggest that hydroperoxides formed on the parent substrates are reasonably stable under irradiation, with only a very small loss at the end of the 2 min exposure. This is consistent with the continuous increase of hydroperoxide content in Figure 14, as significant hydroperoxide degradation would have led to its plateauing. It is noteworthy that the concentration of the unreacted starting substrates remains intact upon exposure to UV light (see Section 2.9.1). Therefore, the possibility of light being absorbed by the starting substrates and not hydroperoxides can be discounted.

2.8 MS Identification of hydroperoxides

In Section 2.4 it was shown how LC-MS was used to detect potential hydroperoxides formed on *N*-Ac-Gly-Gly-OH. Similarly, DI-MS and LC-MS were utilised to detect potential hydroperoxides for all three substrates. Firstly, DI-MS analyses were scanned for the detection of potential hydroperoxides on *N*-Ac-Ala-OH.

2.8.1 *N*-Ac-Ala-OH

2.8.1.1 Peroxidation mechanism

Reaction of *N*-Ac-Ala-OH with HO$^{\bullet}$ produces a transient carbon-centred radical **2.7**, that after reaction with O_2 and a HAA by nearby available C-H produces *N*-Ac-Ala-OH-derived hydroperoxides **2.8** (Scheme 35; hydroperoxide is shown as the sodiated adduct).

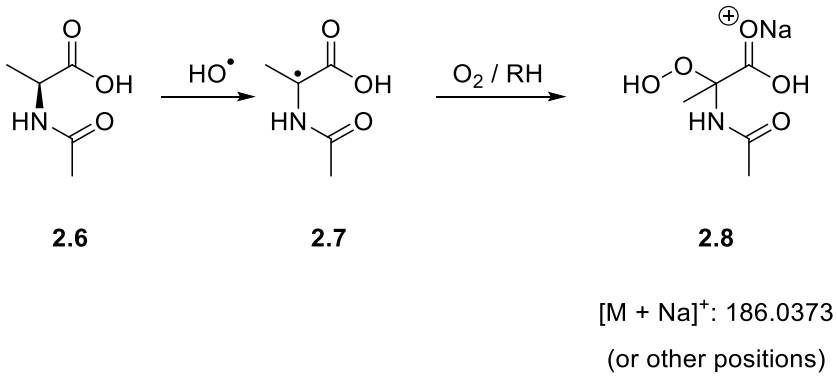

Scheme 35. Generation of N-Ac-Ala-OH-derived hydroperoxides via initial HAA reaction, followed by O_2 addition and HAA. Scheme shows only one possible hydroperoxide, and peroxidation could occur in other available positions.

2.8.1.2 DI-MS Identification of *N*-Ac-Ala-OH-derived hydroperoxides

The hydroperoxide structure of Scheme 35 is one possibility, and peroxidation can occur in other available positions of the molecule. Figure 16 shows a DI-MS analysis, highlighting (in red) a peak corresponding to a potential *N*-Ac-Ala-OH-derived hydroperoxide.

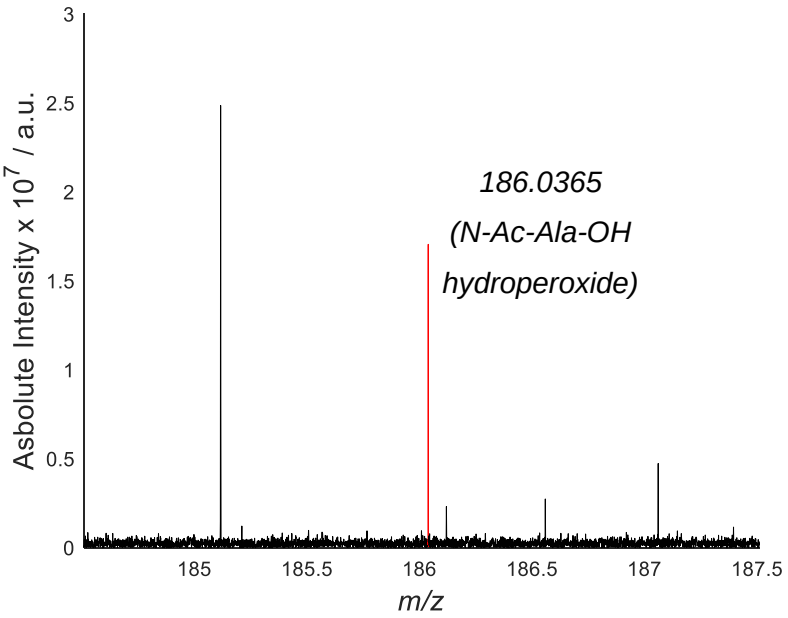

Figure 16. DI-MS spectra of the HO•-induced oxidation of N-Ac-Ala-OH. Highlighted in red is the acquired [M + Na]⁺ of potential N-Ac-Ala-OH-derived hydroperoxide. Hydroperoxides were generated by exposure of aqueous solutions of N-Ac-Ala-OH (1 mM) to UV light in presence of aqueous H_2O_2 (100 mM).

The peak is not present in the non-irradiated solutions (MS data in Appendix), thus proving that the compound with the 186.0365 *m*/*z* is a product of the HO•-oxidation of the parent substrate. However, assigning the observed *m*/*z* to a hydroperoxide is not trivial. Indeed, in these reactions it is possible for different molecules to share the same mono-isotopic mass with others. For instance, a potential hydroperoxide **2.8** will have an identical *m*/*z* with a potential diol **2.9** (Figure 17).

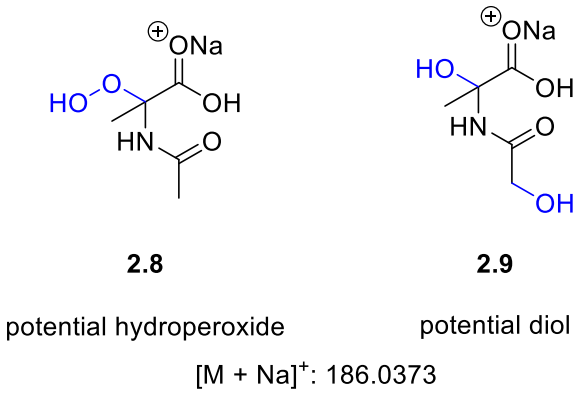

2.8 **2.9**

potential hydroperoxide potential diol

$[M + Na]^+$: 186.0373

Figure 17. Chemical structures and [M + Na]⁺ of potential N-Ac-Ala-OH-derived hydroperoxides and diols. Only one possible isomer is depicted in the Figure.

Traditional mass spectrometry cannot differentiate between these two products. Liquid chromatography coupled to MS could potentially separate different isomers with the same *m*/*z*, but still, no information can be gained on whether the products are doubly hydroxylated or

hydroperoxides. Therefore, acquiring conclusive data for the formation of specific hydroperoxides is complicated.

2.8.1.3 Deuterium exchange studies

In order to distinguish between the two products shown in Figure 16, isotope exchange experiments were carried out (more information in the Experimental Chapter), as the two compounds possess a different number of exchangeable protons (3 and 4 for hydroperoxides and diols respectively). Therefore, irradiations were repeated in D_2O (instead of H_2O; all other reaction parameters were maintained the same), and were analysed again by DI-MS. If all of the labile protons are exchanged with deuterons, then the two products **2.10** and **2.11** should now have a different *m/z* (Figure 18A).

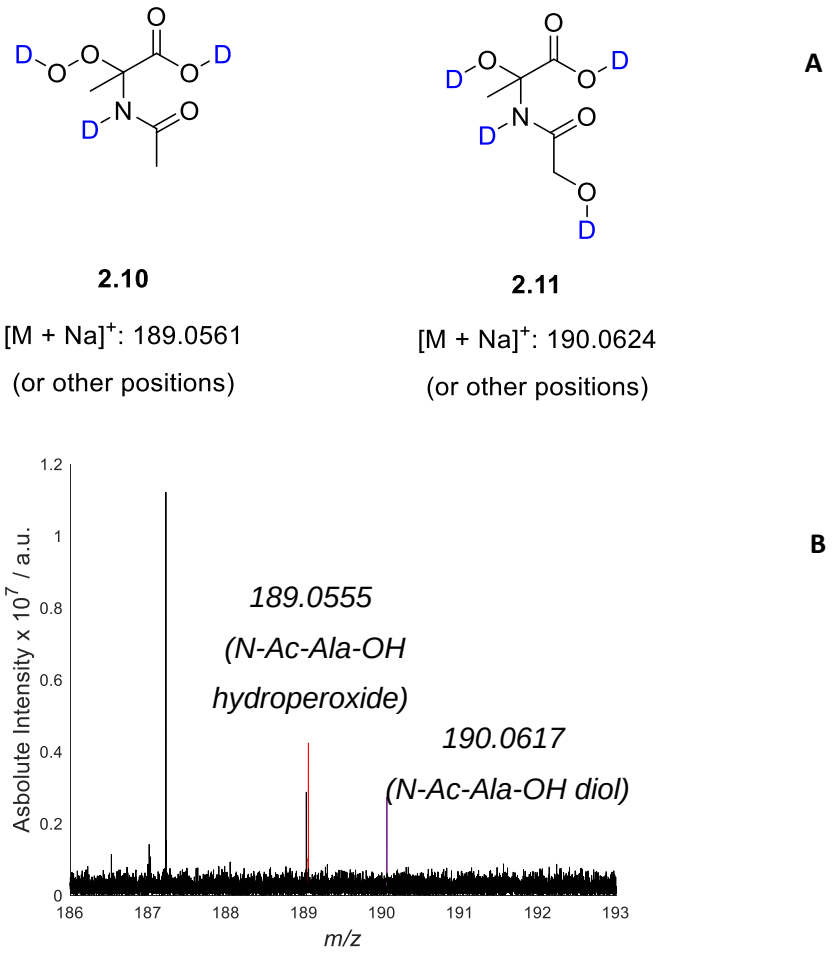

Figure 18. A) Chemical structures and the [M + Na]⁺ of the two fully deuterated products. B) A representative MS spectrum of the HO•-induced oxidation of N-Ac-Ala-OH. Reactions were run in D_2O (more details under the Experimental Chapter). Highlighted in red is the [M + Na]⁺ corresponding to potential hydroperoxides (i.e., 3 D shift in the m/z) and highlighted in purple is the [M + Na]⁺ corresponding to potential dihydroxylated species (i.e., 4 D shift in the m/z).

Analysis of the DI-MS spectra revealed that both a hydroperoxide (Figure 18B; highlighted in red), and a diol (Figure 18B; highlighted in purple) are generated during the irradiations. The peaks are not present in the non-deuterated (but irradiated) solutions (data in Appendix). Furthermore, no *m*/*z* corresponding to 0, 1 or 2 D exchange could be detected, indicating that the products are fully deuterated. It is highlighted that the MS instrument used for these studies offers high resolution analysis, and differentiation of compounds with very close $[M + H]^+$. As such, the $[M + Na]^+$ (Figure 18B; highlighted in purple) can confidently be assigned to the diol, and not the ^{13}C satellite of the hydroperoxide signal. Indeed, the ^{13}C satellite of the hydroperoxide peak is predicted to have an $[M + Na]^+$ of 190.0600, which in this instrument is significantly different from the 190.0617 that we have obtained. For clarity, a similar justification for the differentiation of peaks corresponding to genuine products or ^{13}C satellites is avoided in the remainder of the thesis. For every isotope-exchange experiment, the same logic as here was followed throughout this thesis and the fully deuterated species could be separated from the ^{13}C satellite peaks (see also Experimental Chapter; Section 5.5.2). In the event where a ^{13}C satellite peak cannot be conclusively separated from a fully deuterated peak, then this will be fully acknowledged and discussed appropriately.

In addition to hydroperoxides, the $[M + Na]^+$ of potential *N*-Ac-Ala-OH-derived alcohols was detected in the MS of the oxidation mixture (MS data in the Appendix). The alcohol product is likely produced *via* hydroperoxide decomposition, and its observation indirectly supports formation of intermediate hydroperoxides. Although, alcohols can also be generated *via* the dismutation of two peroxyl radicals (Russel mechanism),[66] the latter mechanism is only applicable to primary or secondary peroxyl radicals (and not peroxyl radicals formed on the α-carbon of *N*-Ac-Ala-OH).

2.8.2 *N*-Ac-Gly-Tyr-OH

2.8.2.1 Peroxidation mechanism

The $HO^\bullet$ reaction with *N*-Ac-Gly-Tyr-OH differs significantly compared to *N*-Ac-Ala-OH and involves predominantly addition to the aromatic ring to produce DOPA (see Introduction; Section 1.7.4). The photogenerated hydroperoxides on *N*-Ac-Gly-Tyr-OH (as confirmed by the FOX-assay; Figure 14) is more likely a result of the HAA reaction by $HO^\bullet$ from either the backbone of the peptide or the $-CH_2$ of the tyrosine side chain (Scheme 36; peroxidation mechanism is shown *via* initial HAA from the benzylic position of Tyr).

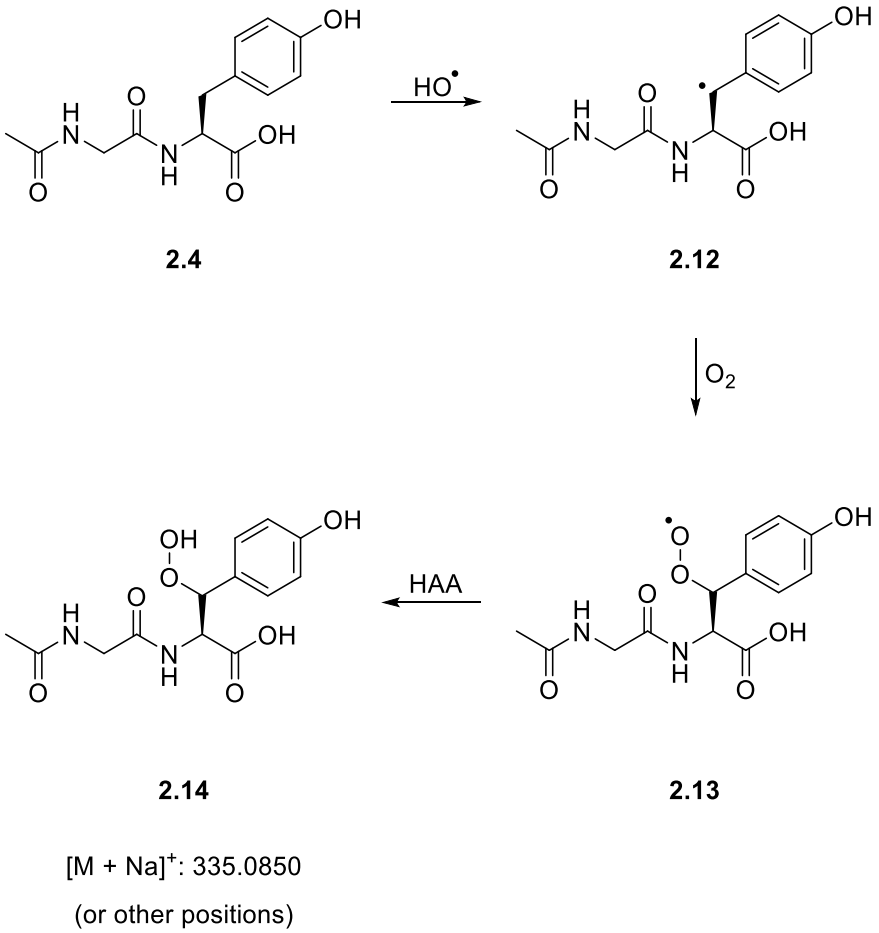

Scheme 36. Proposed peroxidation mechanism involving a HAA reaction by HO• from the backbone of N-Ac-Gly-Tyr-OH yielding hydroperoxides.

The HAA reaction of HO• with Ala and Gly occurs with a similar rate ($k \sim 10^7$ M^{-1} s^{-1}) and is at least 2 orders of magnitude slower compared to addition to the aromatic ring of Tyr and Phe. [141] Thus the HO•-mediated peroxidation of *N*-Ac-Gly-Tyr-OH is less favoured compared to formation of DOPA (which has been established as the major HO•-induced oxidation product of Tyr).[107,116,117]

2.8.2.2 DI-MS Identification of *N*-Ac-Gly-Tyr-OH-derived hydroperoxides

The hydroperoxide structure of Scheme 36 is one possible isomer, and peroxidation can occur in other available positions of the molecule. Figure 19 shows a DI-MS analysis, highlighting (in red) a peak corresponding to a potential *N*-Ac-Gly-Tyr-OH-derived hydroperoxide.

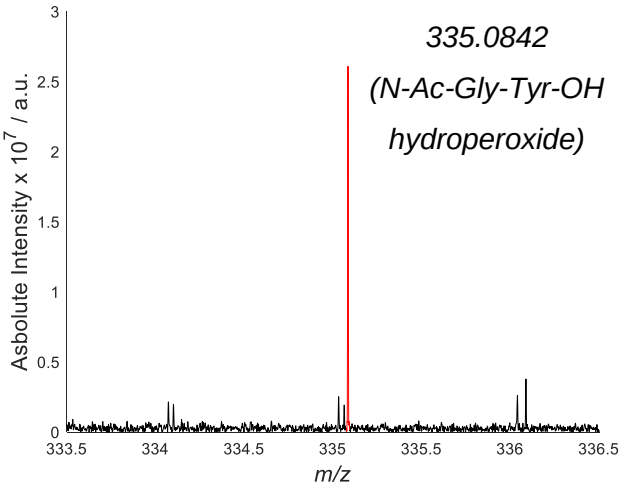

Figure 19. DI-MS spectra of the HO•-induced oxidation of N-Ac-Gly-Tyr-OH. Highlighted in red is the acquired [M + Na]⁺ of potential N-Ac-Gly-Tyr-OH-derived hydroperoxide. Hydroperoxides were generated by exposure of aqueous solutions of N-Ac-Gly-Tyr-OH (1 mM) to UV light in presence of aqueous H_2O_2 (100 mM).

Figure 19 demonstrates that the *m*/*z* corresponding to a potential hydroperoxide is present, with the peak being completely absent when non-irradiated samples were analysed (MS data can be found in the Appendix). Similarly to the case of *N*-Ac-Ala-OH, hydroperoxides **2.14** and dihydroxy products **2.15** will have the same *m*/*z* (Figure 20). Considering the documented tendency of HO• to undergo addition to the aromatic ring of Tyr,[106,111,114] generation of dihydroxy products is likely to occur.

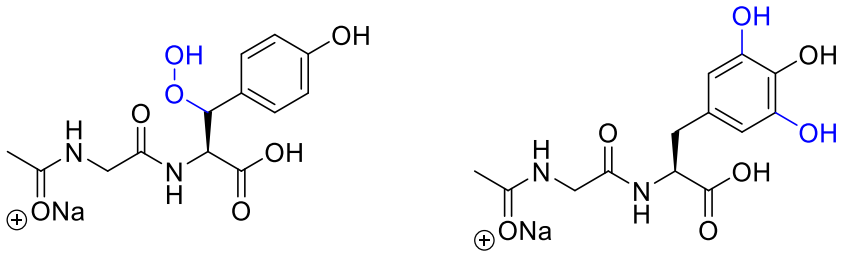

2.14

potential hydroperoxide

2.15

potential diol

[M + Na]+: 335.0850

Figure 20. Chemical structure and [M + Na]⁺ of potential hydroperoxides and diols on N-Ac-Gly-Tyr-OH. Only one potential hydroperoxide is depicted in the Figure.

2.8.2.3 Deuterium exchange studies

In order to get a better understanding of the oxidation mechanism and confirm the formation of hydroperoxides, reactions were repeated in D_2O (instead of H_2O) while all other reaction conditions remained the same. As the two products have a different number of exchangeable protons (5 and 6 respectively), differentiation in MS should now be possible.

After analysis by DI-MS it was revealed that no *m/z* associated with a possible 0, 1, 2, 3 and 4 D shifts was detected in the MS spectra. However, the *m/z* corresponding to 5 (potential hydroperoxides; highlighted in red) and 6 (potential double hydroxy adduct; highlighted in purple) D shifts were evident (Figure 21).

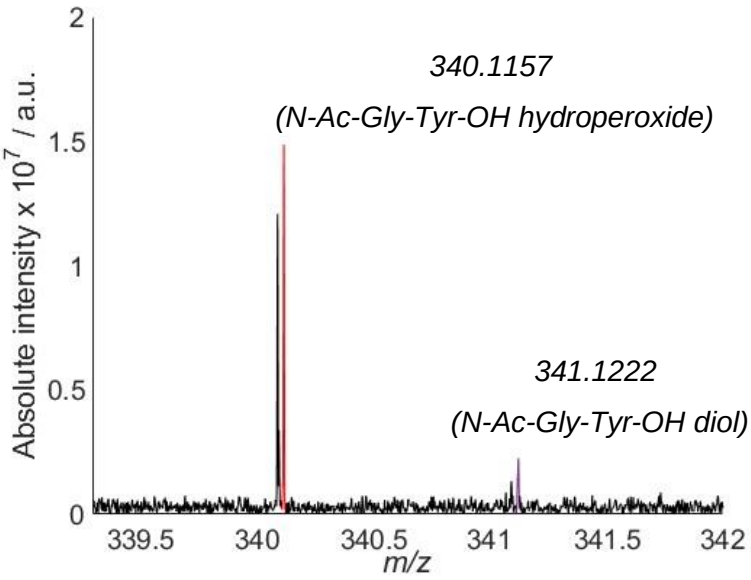

Figure 21. DI-MS spectrum of the HO•-induced oxidation of N-Ac-Gly-Tyr-OH. Reactions were run in D_2O (more details under the Experimental Chapter). Highlighted in red is the $[M + Na]^+$ corresponding to a hydroperoxide (i.e., 5 D shift in the m/z) and highlighted in purple is the $[M + Na]^+$ corresponding to a dihydroxylated species (i.e., 6 D shift in the m/z).

These data strongly suggest both hydroperoxide and diol formation for *N*-Ac-Gly-Tyr-OH. The two peaks highlighted in Figure 21 were not present when irradiations were carried out in H_2O instead of D_2O (MS data can be found in the Appendix).

2.8.3 *N*-Ac-Ala-Phe-OH

2.8.3.1 Peroxidation mechanism

N-Ac- Ala- Phe-OH is expected to react with HO• in a similar way to *N*-Ac-Gly-Tyr-OH. The reactivity of Phe with HO• has been investigated carefully and in-depth by Solar in 1985, and it results principally in addition of HO• to the benzene ring of Phe.[109] Based on literature experimental and theoretical data, formation of Phe-derived hydroperoxides *via* addition of the HO• to the benzene ring can be discounted.

Hydroperoxides **2.18** are more likely generated *via* HAA from the side chain *N*-Ac-Ala-Phe-OH (benzylic position; Scheme 37). Indeed, Solar experimentally confirmed that a small amount of the initial HO• concentration (~ 6%) reacts with the alanine moiety of phenylalanine *via* a HAA reaction with a $k \sim 10^9$ M^{-1} s^{-1} to yield a carbon-centred radical **2.16** that similarly to *N*-Ac-Gly-Tyr-OH can be converted to a hydroperoxide.

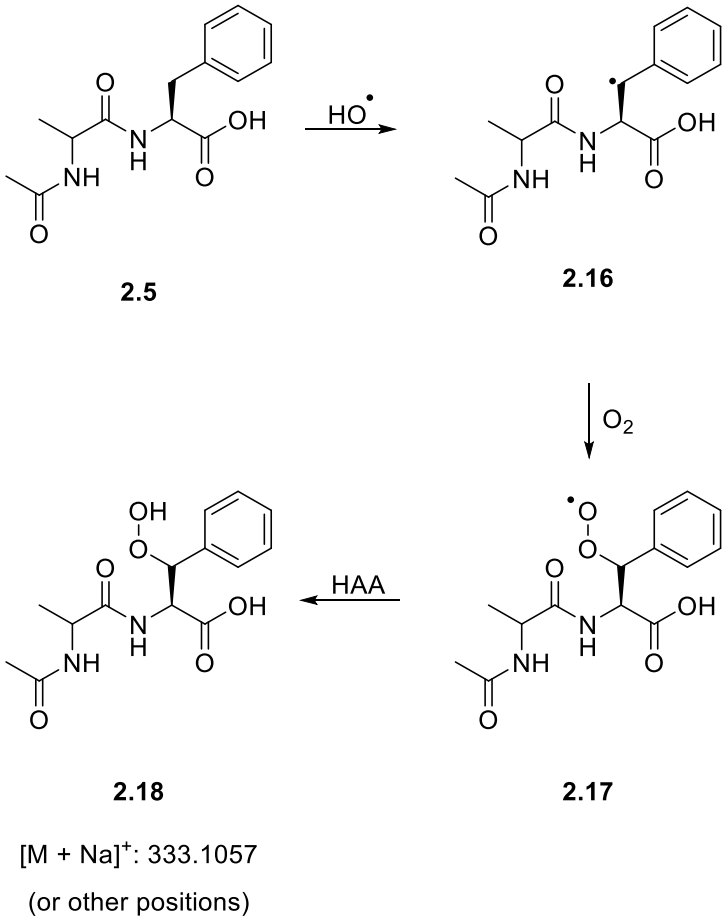

Scheme 37. The HAA component of the reaction of HO• with Phe, resulting in formation of hydroperoxides. Scheme 36 shows only one possible hydroperoxide, and peroxidation can occur in different positions.

2.8.3.2 DI-MS Identification of *N*-Ac-Ala-Phe-OH-derived hydroperoxides

The hydroperoxide shown in Scheme 37 is just one possible isomer, and equally, peroxidation can occur in other available positions. Next, DI-MS and LC-MS analyses of irradiated *N*-Ac-Ala-Phe-OH solutions were investigated for the detection of potential hydroperoxides (Figure 22).

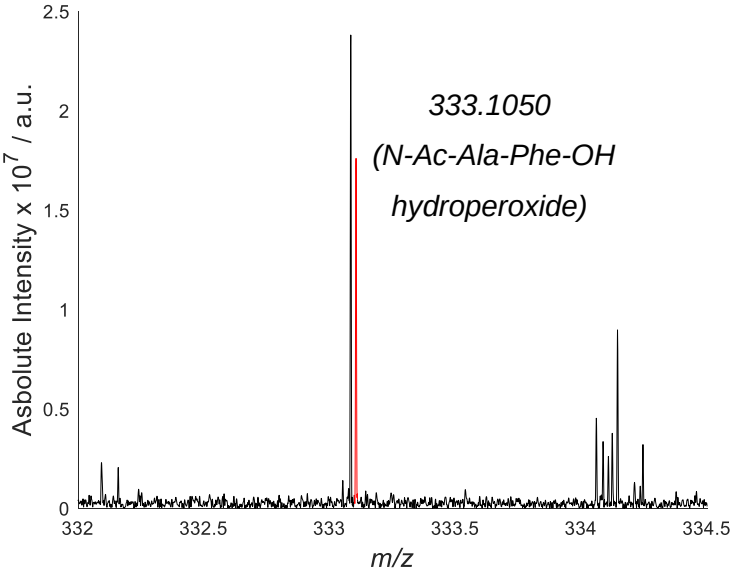

Figure 22. Representative MS spectra of the HO•-induced oxidation of N-Ac-Ala-Phe-OH. Highlighted in red is the found [M + Na]+ of potential N-Ac-Gly-Tyr-derived hydroperoxides. Hydroperoxides were generated by exposure of aqueous solutions of N-Ac-Ala-Phe-OH (1 mM) to UV light in presence of aqueous H_2O_2 (100 mM).

The $[M + Na]^+$ of potential *N*-Ac-Ala-Phe-OH-derived hydroperoxides was present in the DI-MS spectrum (Figure 22; highlighted in red), with the peak being absent in the non-irradiated samples (data can be found in the Appendix). However, as HO• have the propensity to undergo addition to aromatic rings, the formation of doubly hydroxylated products has a high probability in the case of *N*-Ac-Ala-Phe-OH too.

2.8.3.3 Deuterium exchange experiments

In an attempt to distinguish between doubly hydroxylated and hydroperoxides formed on *N*-Ac-Ala-Phe-OH, irradiated solutions were diluted x 100 times in D_2O, as the two compounds possess a different number of exchangeable protons (Figure 23).

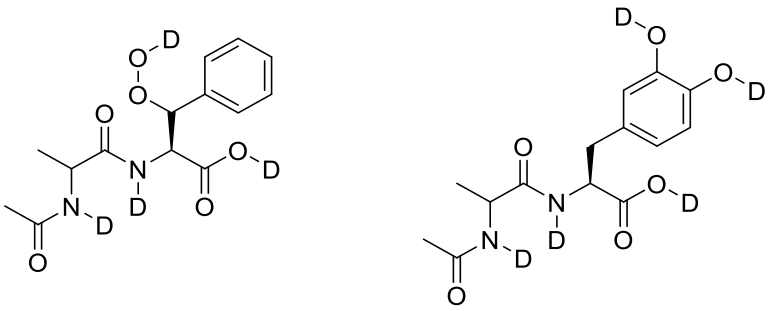

2.19

$[M + Na]^+$: 337.1308

(or other positions)

2.20

$[M + Na]^+$: 338.1371

(or other sites of the ring)

Figure 23. Chemical structure and the $[M + Na]^+$ of potential N-Ac-Ala-Phe-OH-derived hydroperoxides and dihydroxylated products where all labile protons have been exchanged with deuteriums.

Therefore, the MS data were scanned for the mono-isotopic masses corresponding to 0, 1, 2, 3, 4 and 5 D shifts. Pleasingly, the signal for the 4 and 5 D shift this time was present (Figure 23), while no peaks corresponding to 0-3 D shifts was observed.

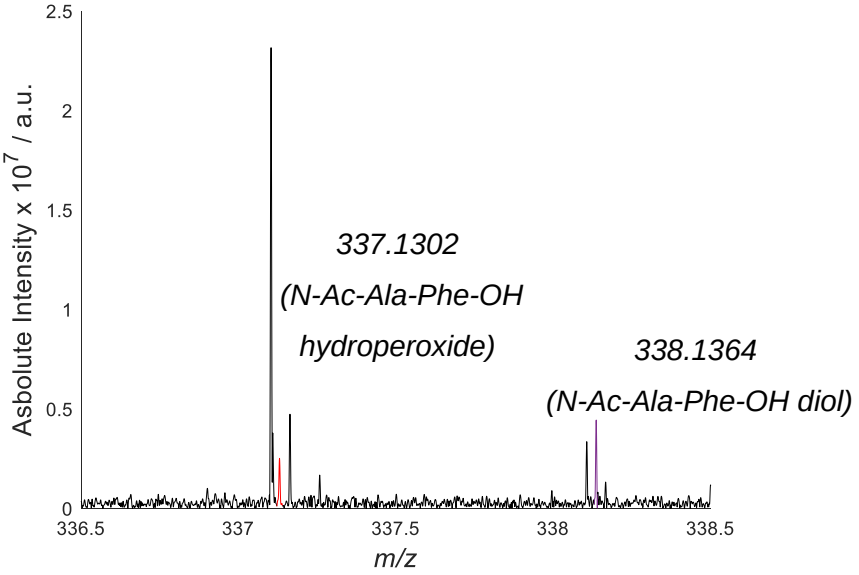

Figure 24. A representative MS spectrum of the $HO^{\bullet}$-induced oxidation of N-Ac-Ala-Phe-OH. Aliquots were diluted x 100 in D_2O (more details under the Experimental Chapter). Highlighted in red is the [M + Na]+ corresponding to potential hydroperoxides (i.e., 4 D shift in the m/z) and highlighted in purple is the $[M + Na]^+$ corresponding to potential dihydroxylated species (i.e., 5 D shift in the m/z).

Deuterium experiments revealed that the reaction mixtures contain both doubly hydroxylated and hydroperoxides formed on *N*-Ac-Ala-Phe-OH (the peaks were absent when solutions were not diluted in D_2O – MS data in Appendix). It is noteworthy that no *m*/*z* associated with possible 0, 1, 2 and 3 D shift was detected. The D_2O experiments strongly suggest the formation of specific *N*-Ac-Ala-Phe-OH-derived hydroperoxides.

2.9 Substrate oxidation

Exposure of aqueous H_2O_2 to UV light in the presence of the three substrates was shown to lead to the formation of organic peroxides that are stable at RT and in the dark. Furthermore, it was verified experimentally, that the rate of thermal peroxide decay was increased at higher temperatures, and the decay was most rapid at 100 °C, while decay under sunlight was slower. We were able to identify potential hydroperoxides associated with all three substrates, and their formation was further reinforced by isotope exchange experiments.

However, the goal of this project was to evaluate whether two insults act in synergy to deliver higher peptide damage, to confirm our kinetic modelling results of Section 2.2.3. To achieve this, a method needs to be developed that would allow an accurate determination of the peptide concentration, prior and after the application of each insult (UV light and heat). More importantly, experimental data that elucidate the role of peroxides in this process need to be acquired.

For the purpose of the synergism postulate, quantification of oxidation products is not necessary, but accurate quantification of the parent substrates is required. To address that, careful LC-MS quantification can be used. Liquid chromatography coupled to mass spectrometry offers the advantage of separation between different peaks. As such, if the compound of interest is separated from other compounds, then its ionisation will not be affected by other competing molecules in the system.

Calibration curves using standard solutions for all substrates were built. In all cases, the parent substrates eluted cleanly, and the calibration curves showed an excellent correlation between concentration and peak intensity ($R^2 > 0.997$ for all cases; all calibration curves can be found in the Appendix). For *N*-Ac-Gly-Tyr-OH and *N*-Ac-Ala-Phe-OH the UV chromatogram was used (the detector was set at 280 and 260 nm respectively), and the calibration curves were constructed based on the integration of the peak area of the peak for each standard solution. For *N*-Ac-Ala-OH, the total ion count of the extracted ion chromatogram was used (this was done as *N*-Ac-Ala-OH only

exhibits significant light absorption at very low wavelengths, and therefore not a clean UV detection could be achieved) . More details, including the calibration curves and how the daily- and the weekly- variation of them was assessed, can be found in the Experimental Chapter. The quantification assumed constant ionisation efficiency in ESI-MS. While this is not normally a safe assumption, at low conversions the composition of the reaction mixtures is almost constant, and big changes in ionisation efficiency over reaction time would not be expected.

2.9.1 Hydroxyl radical mediated decomposition

To assess the extent of the HO•-induced oxidation of the substrates, aqueous solutions (1 mM) were exposed to UV light in presence of H_2O_2 (100 mM) for 2 min with aliquots taken prior to the exposure and then every 30 s until the end of the irradiation. All aliquots were analysed by LC-MS to determine the parent substrate loss (Figure 25).

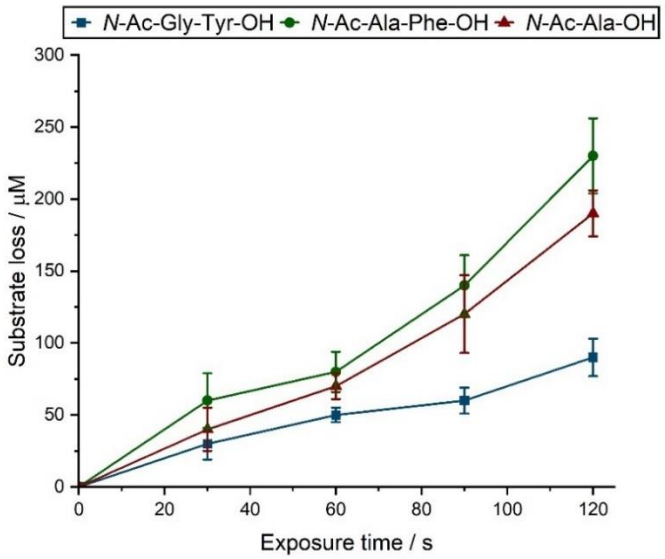

Figure 25. Decomposition of the three substrates upon exposure of aq. solutions (all 1 mM) to UV light for 2 min in presence of aq. H_2O_2 (100 mM). Aliquots were taken at the indicated timestamps, and were frozen immediately until analysis by LC-MS. The extent of decomposition was calculated by integration of the peak area of the LC-MS peak corresponding to the starting peptide (the TIC of the EIC for N-Ac-Ala-OH). Reactions were carried out in triplicate (6 times for N-Ac-Ala-OH) and the results are the mean ± SE of the experiments.

Figure 25 demonstrates that reaction of substrates with HO• resulted in their partial degradation. To ensure reproducibility and reliability of the experimental setup and the quantification method, reactions of *N*-Ac-Gly-Tyr-OH and *N*-Ac-Ala-Phe-OH were carried out in triplicate, while reactions of *N*-Ac-Ala-OH were carried out 6 times, as quantification using the total ion count (TIC) showed higher variations.

It is evident that *N*-Ac-Gly-Tyr-OH is more resistant to the HO$^{\bullet}$-induced oxidation with a nearly 100 µM loss of the parent substrate at the end of the irradiation. In contrast, exposure of *N*-Ac-Ala-Phe-OH and *N*-Ac-Ala-OH to HO$^{\bullet}$ resulted in *ca*. 200 µM decomposition. The reason for this could be related to the reactivity of HO$^{\bullet}$ with the respective substrates.

Reaction of HO$^{\bullet}$ with Tyr affords the thermodynamically stable phenoxyl radical (see Introduction Section 1.7.4). Phenoxyl radicals have been proposed to react slowly with O_2, with a rate constant of $k < 10^3$ M^{-1} s^{-1} estimated for tyrosyl phenoxyl radicals.[192] As such, tyrosyl radicals are unlikely to propagate peptide damage (as the formation of peroxyl radicals is a very minor pathway). When solutions of the substrates were exposed to UV light in the absence of H_2O_2, no appreciable decomposition was detected (data not shown), thus confirming that the observed substrate loss is indeed HO$^{\bullet}$-induced.

2.9.2 Thermal decomposition

To evaluate the proposed synergistic action, a second insult (heat treatment) was applied to the solutions. Since the two insults applied here are used to provide evidence for a proof of concept, the exact temperature of the heat treatment becomes less important. In Section 2.5.4 we have shown the kinetics of thermal decay for the *N*-Ac-Gly-Gly-OH-derived hydroperoxides. The temperature and the duration of the treatment were chosen to afford *ca*. 50% decomposition of the photo-generated peroxides (i.e., incubation at 82 °C for 30 min),

Prior to investigating the effect of temperature on partially-oxidised substrates, control experiments where solutions of the starting substrates were incubated at 82 °C (without pre-exposure to UV light) in the absence of H_2O_2 were carried out (Figure 26).

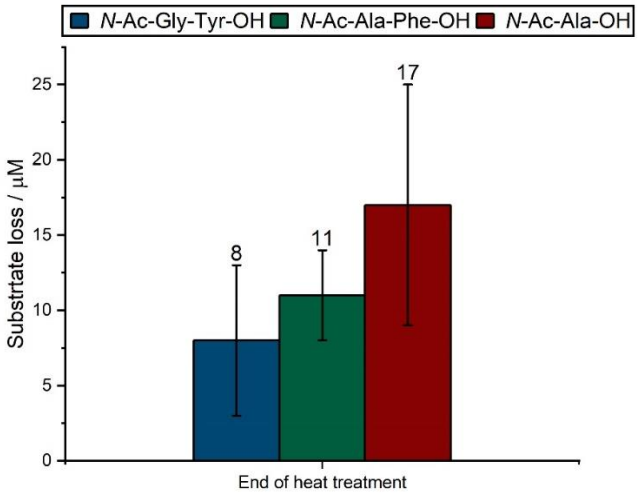

Figure 26. Substrate loss for the parent substrates upon incubation at 82 °C for 30 min. The substrate loss was determined by LC-MS analysis. Graph highlights the loss in the concentration and data are expressed as the means ± SE of 3 independent experiments (6 for N-Ac-Ala-OH).

The three substrates appear to be thermally stable at 82 °C with only a small loss (< 20 µM) of their initial concentration after 30 min of incubation. Next, our focus was turned to the investigation of the synergy between UV light and heat treatment.

2.9.4. Investigation of the synergistic action

Incubation of isolated substrates at 82 °C resulted in less than 2% loss of their starting concentration. This outcome means that if substrates that have been previously exposed to UV light and are incubated at 82 °C, show a peptide loss that is higher than the sum of the individual treatments (Figure 25 and 26), then the two insults act in synergy. To investigate that, oxidised substrate solutions were incubated at 82 °C for 30 min. Solutions were analysed by LC-MS to determine the concentration of the parent substrate at the end of the UV exposure and at the end of the heat treatment (Figure 27).

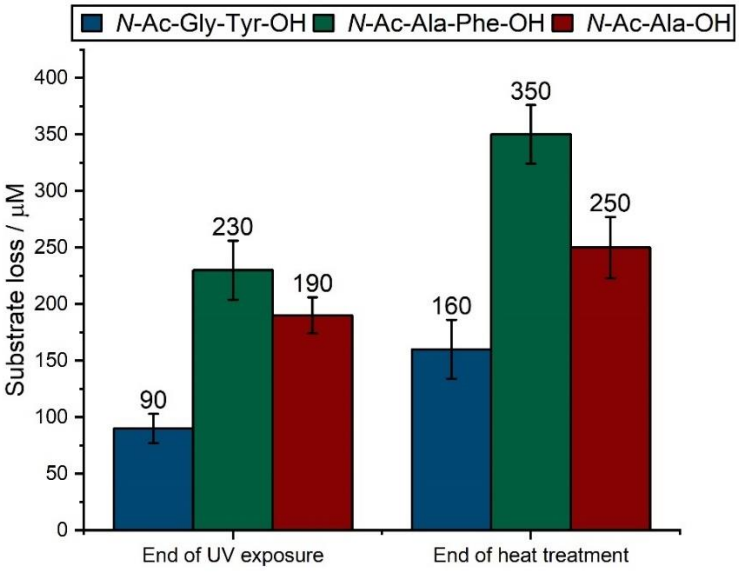

Figure 27. Comparison between the parent substrate concentration at the end of the UV irradiation and the end of the thermal treatment. Graph highlights the loss in the concentration on incubation of irradiated parent substrates at 82 °C for 30 min. Data are expressed as the means ± SE of 3 separate experiments (6 for N-Ac-Ala-OH) analysed by LC-MS.

Figure 27 illustrates that thermal treatment resulted in further damage to the light-exposed substrates, thus providing strong evidence for our proposed hypothesis. More specifically, *N*-Ac-Gly-Tyr-OH and *N*-Ac-Ala-OH suffer a similar extended damage of *ca*. 60 µM, while the concentration of *N*-Ac-Ala-Phe-OH is reduced by *ca*. 120 µM at the end of the heat treatment. The decomposition occurring upon heat-treatment, is consistent with thermal breakdown of species generated during the UV exposure (such as hydroperoxides). The thermal stability of the peptide at 82 °C (Figure 26), suggests that exposure to UV light leads to the formation of semi-stable species that upon heating decay and facilitate modifications to the parent peptide.

Data reported on Figures 25-27 corroborate that the two insults act in synergy and exacerbate the initially inflicted (UV light) damage to the parent substrates. However, the role of hydroperoxides in the process remains unclear. To obtain more information about the concentration of the photo-generated hydroperoxides at the end of the UV exposure and at the end of the heat treatment, solutions were analysed by the FOX-assay (Figure 28).

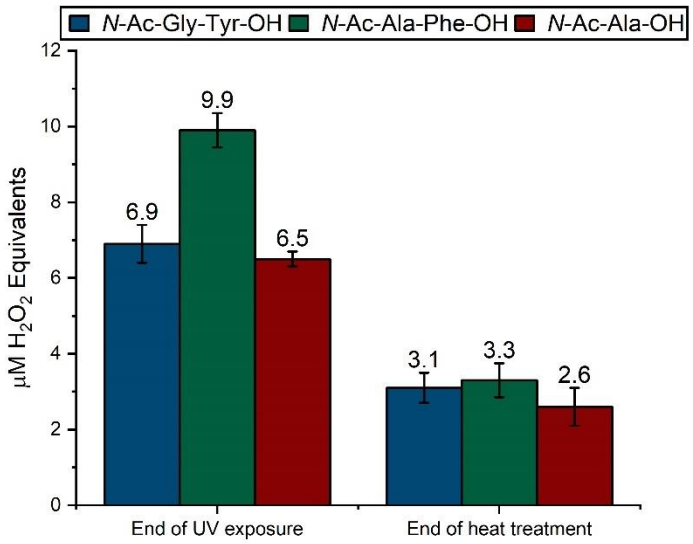

Figure 28. Comparison between hydroperoxides at the end of the UV irradiation and the end of the thermal treatment. Graph highlights the loss in the hydroperoxide concentration on incubation of irradiated parent substrates at 82 °C for 30 min. Results are the mean ± SE of three (six for N-Ac-Ala-OH) separated experiments analysed by the FOX-assay the same day.

As predicted, incubation at 82 °C resulted in a substantial peroxide decomposition. Specifically, *N*-Ac-Ala-Phe-OH-derived hydroperoxides suffered a loss greater than 60%, while *N*-Ac-Gly-Tyr-OH- and *N*-Ac-Ala-OH-derived hydroperoxides were decomposed with a *ca*. 50% loss of the initial total hydroperoxide content. The greater peroxide decomposition of *N*-Ac-Ala-Phe-OH might provide an explanation for the higher substrate loss (Figure 25). Indeed, a rough approximation of the data shown in Figure 22 and 23 shows that a loss of 1 μM of peroxide results in 18 μM loss of the parent substrates (this is if peroxide decay is the only reason for the observed synergism). This result is consistent with homolysis of the peroxide bond to yield transient RO$^{\bullet}$ and HO$^{\bullet}$, that initiate chain radical reactions to accentuate the substrate decomposition.

2.10 Sodium borohydride reduction of hydroperoxides

In order to further confirm the role of accumulated hydroperoxides in the extended peptide damage, we sought to selectively destroy the hydroperoxides *via* a non-radical pathway. Control experiments where solutions of the parent substrates were incubated at 82 °C without prior exposure to UV light proved that only a small peptide degradation occurs (< 2%) at this temperature. Therefore, if all the HO$^{\bullet}$-formed hydroperoxides were destroyed *via* non-radical pathways, then thermal treatment of the irradiated solutions should result in only marginal decomposition of the parent substrates.

This can be done by a number of reducing agents.[141] In particular, $NaBH_4$ decomposes hydroperoxides to the corresponding alcohols *via* a non-radical pathway under mild conditions (e.g., 1 h incubation at room temperature). Many studies have utilised $NaBH_4$ to reduce protein and peptide hydroperoxides to alcohols in order to indirectly quantify the hydroperoxides.[58,63,150] Based on literature precedent, we considered $NaBH_4$ to be a suitable reductant for our work. The total hydroperoxide content (post-UV exposure) could be reduced to alcohols without generating any reactive radical species. If this was successful, then thermal treatment of the substrates should, similarly to controls, result in no appreciable decomposition of the starting substrates. The advantage of $NaBH_4$ is that it is a mild reducing agent which can only reduce hydroperoxides and carbonyls but should be unreactive towards any other functional groups in the system. Indeed, potential carbonyls (oxidation products) can be reduced to the corresponding alcohols, but i) this should not result in any further damage to the parent substrate, and ii) our quantification method does not rely on the existence of oxidation products. Finally, at the end of the treatment any remaining $NaBH_4$ can be cleanly converted to inert $NaBO_2$ by lowering the pH of the solution (before re-adjusting the pH back to the initial value of the solutions).

In order to test the efficiency of the method, aqueous solutions of the starting substrates were exposed to UV light as earlier. At the end of the irradiation, the solutions were treated with catalase (as per the Experimental Chapter) to remove any leftover H_2O_2. After 15 min, aliquots were taken, diluted and frozen in liquid N_2. These aliquots were analysed both by the FOX-assay and LC-MS, in order to determine the total hydroperoxide content and the starting substrate concentration. The remainder of the solutions was treated with $NaBH_4$ (1 mg per mL of solution) for 1 h to reduce any UV-generated hydroperoxides to alcohols (more information under the Experimental Chapter). At the end of the 1 h a few drops of aqueous HCl (2 M) were added to reduce the pH of the solution (in order to convert any remaining $NaBH_4$ to $NaBO_2$), before re-adjusting the pH to the initial value with a few drops of aqueous NaOH (2 M). Following this, aliquots were taken, diluted and frozen in liquid N_2 until analysis. These aliquots were analysed by the FOX-assay, to evaluate whether $NaBH_4$ treatment results in the reduction of the total hydroperoxide content (Figure 29).

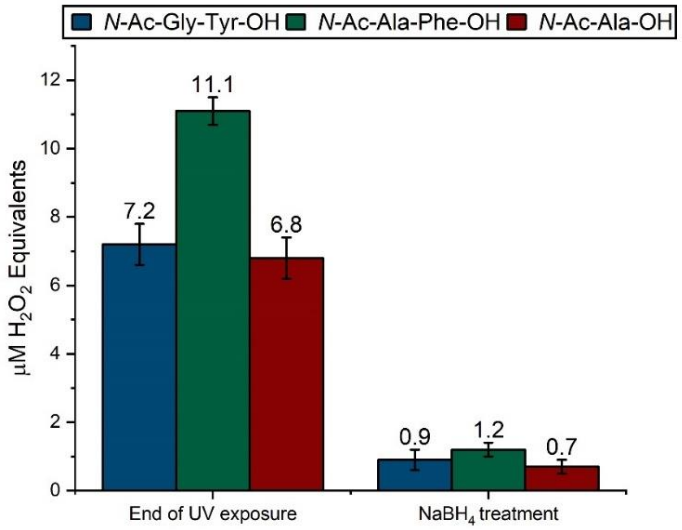

Figure 29. Decomposition of HO•-mediated peroxides in the three substrates under study after UV exposure. Aliquots were treated with NaBH4 (1 mg per mL of aliquot) and were incubated in the dark for 1 h (more details in the experimental). Results are the mean ± SE of three separated experiments analysed by the FOX-assay the same day.

Figure 29 reports the total hydroperoxide content before and after the $NaBH_4$ treatment. In harmony with literature precedent, FOX-assay confirmed a nearly complete reduction of the peroxide groups in all substrates. At this stage, the possibility that the acidic environment after $NaBH_4$ treatment, would result in the decomposition of organic peroxides was considered. To understand if the destruction of peroxides is due to $NaBH_4$ treatment or a result of the acidic pH, a control experiment was conducted. The total peroxide content was assessed (FOX-assay) after $NaBH_4$ treatment, but without lowering the pH, which resulted in the complete disappearance of the total peroxide content. This revealed that any organic peroxides are destroyed during the $NaBH_4$ treatment and not when the pH of the solutions is lowered.

Encouraged by the effectiveness of $NaBH_4$ to decompose peroxides, the thermal stability of starting substrates was then investigated.

After the $NaBH_4$ treatment, all solutions were subjected to heat-treatment as earlier (82 °C; 30 min). At the end of the thermal treatment, aliquots were again collected, diluted and frozen in liquid N_2 until analysis by LC-MS (Figure 30).

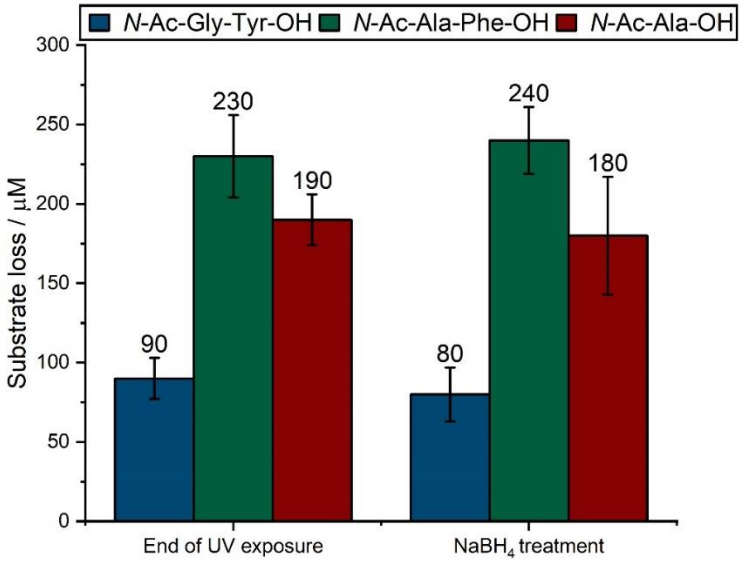

Figure 30. Stability of the three starting substrates at 82 °C. Solutions were initially exposed to UV light for 2 min as outlined in the Experimental Chapter. After the cessation of irradiation, samples were treated with NaBH4 (1 mg per mL of solution) to reduce any photo-generated hydroperoxides to alcohols. Following that, samples were incubated at 82 °C for 30 min. Results are the mean ± SE of three separated experiments determined by LC-MS.

Figure 30 demonstrates that all three starting substrates remained intact upon thermal treatment. The observed thermal stability of the peptides strongly reinforces our original hypothesis and peptide degradation upon thermal treatment in Figure 27 is at least partially due to the accumulation of hydroperoxides during the preceding UV exposure.

2.11 Evaluation of the synergistic action on human hair

Encouraged by our recent work and the evidence to support the synergism between two insults on the model peptides, it was sought to investigate whether this effect could be detected on human hair. As such, natural white hair samples (that contain little or no melanin) were exposed to UV light for 20 and 40 h, before applying heat-treatment (more information under the Experimental Chapter). Figure 31 shows the evolution of a known UV marker.

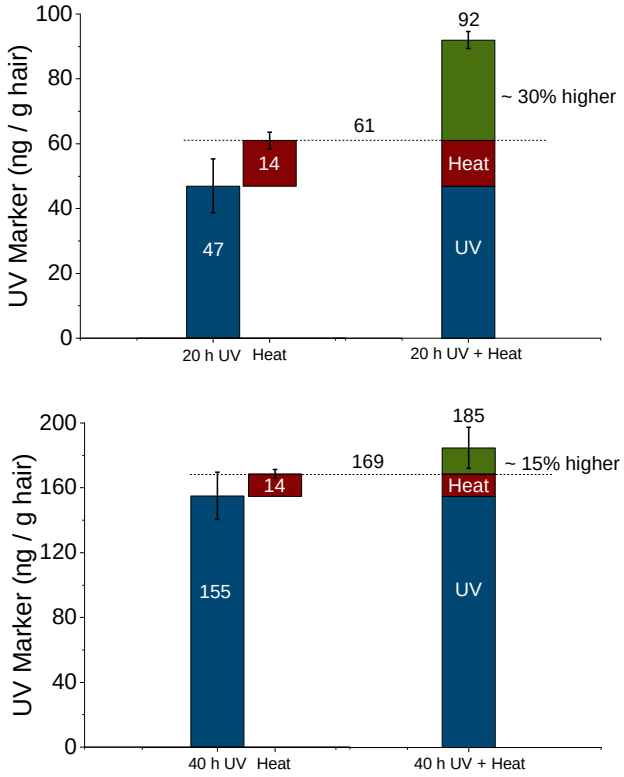

Figure 31. Evolution of UV marker upon exposure of hair to UV light for 20 or 40 h and further heat-treatment. Results are the mean ± SE of 12 different experiments. The measurement of the UV marker correlates to UV protein damage and total protein loss. Experiments of human hair, and analysis of the data was carried out by P&G (see Experimental Chapter).

Protein degradation was assessed by monitoring a UV marker with m/z 1278.7 which originates from the calcium-binding protein S100A3.[159] Procter and Gamble have previously reported a linear correlation between UV exposure of hair and generation of this marker.[193] It is likely formed via peptide bond cleavage which involves intermediate formation of a hydroperoxide.[159] It is assumed that some copper ions (which catalyse decomposition of hydroperoxides) can exchange with calcium at S100A3 binding site, which explains selective cleavage of this fragment. The evolution of the UV marker is thus associated with the oxidation of hair protein.

Interestingly, Figure 31 suggests that evolution of the UV marker upon 20 h of UV exposure followed by heat-treatment (20 h UV + Heat) is greater than when the combined effect of the two insults (Heat and 20 h UV). This result is consistent with our work on short model peptides and indicates that exposure of hair to UV light generates thermally unstable hydroperoxides that decay at elevated temperatures to yield transient radicals, which in turn accelerate protein damage.

The effect at 40 h of UV exposure is less clear and the errors are higher. This is however not surprising. Our kinetic model has shown a similar trend, where at longer irradiation timeframes the prooxidant effect of hydroperoxides is attenuated. We believe that after an initial period hydroperoxide accumulation, a steady state concentration is reached. The reason for this is that in autoxidation processes hydroperoxides are formed and decomposed simultaneously. This is in good agreement with our kinetic modelling results. Figure 5B demonstrates that after an initial period, the decomposition rate of the protein is the same for the two simulations as the hydroperoxide concentration remains the same. As such, it is likely that the total peroxide content at the end of the 40 h exposure is similar to that at the end of the 20 h exposure.

2.12 Chapter 2: Conclusions

Exposure of *N*-Ac-Gly-Tyr-OH, *N*-Ac-Ala-Phe-OH, and *N*-Ac-Ala-OH to $HO^{\bullet}$ in presence of O_2 resulted in accumulation of hydroperoxides, and the total peroxide content was quantified by the FOX-assay. Evidence for the identification of specific hydroperoxides was obtained for all three substrates by DI-MS. Importantly, robust isotope exchange studies further supported our findings for the detection of hydroperoxides.

Following accumulation of hydroperoxides, incubation of the three substrates at elevated temperatures resulted in accelerated oxidative damage as confirmed by the quantification of their concentration by LC-MS. Our experimental results demonstrate that the combined damage of the two insults is greater than the sum of the two, thus confirming that the two insults act in synergy. The extent of the accelerated peptide damage appears to increase in line with the hydroperoxide formation/decay. Indeed, the highest thermal hydroperoxide loss was observed for *N*-Ac-Ala-Phe-OH (*ca*. 6 µM), and this resulted in the highest parent substrate thermal loss (*ca*. 120 µM). In all three cases, a 1 µM hydroperoxide loss during thermal treatment, resulted in *ca*. 18 µM thermal substrate loss. These data suggest that exposure to UV light followed by thermal treatment of the substrates extends the initial photo-induced decomposition. It is proposed that the reason for this is hydroperoxide thermolysis which triggers radical chain reactions based on Scheme 38.

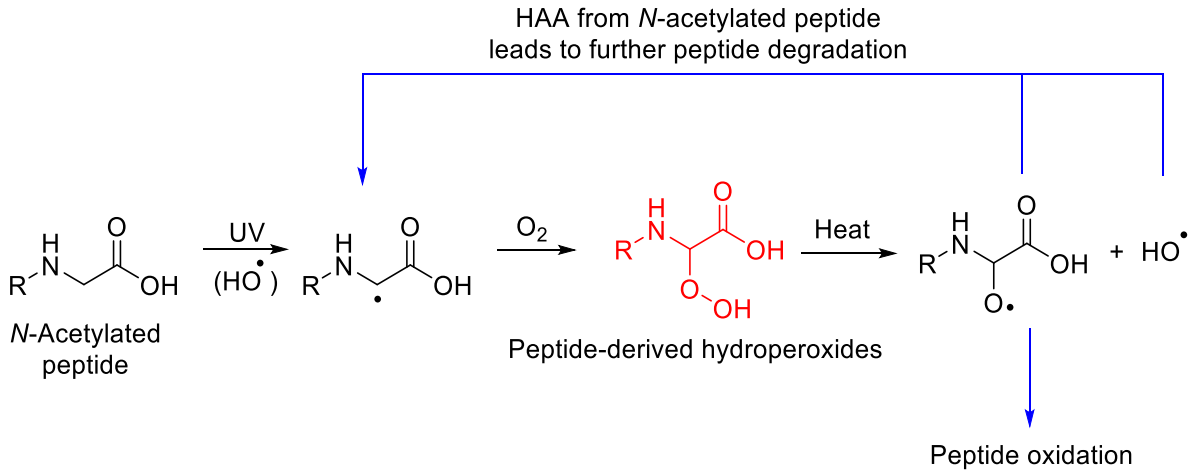

Scheme 38. Proposed mechanistic pathway to highlight the prooxidant effect of the hydroperoxides. Secondary free radicals arising from their homolysis are capable of further reacting with the parent substrate thus extending the initially inflicted damage.

The prooxidant effect of the hydroperoxides is further confirmed by $NaBH_4$ experiments, which resulted in no further decomposition of the peptides. We believe this chemistry leading to enhanced damage is relevant to oxidation of other dead biological tissue (where no self-repair mechanisms are in place) including hair. Experimental data on human hair degradation are consistent with the conclusion that UV light and heat-treatment act together in synergy to accelerate damage on hair proteins. Our findings here can be used as an insight to develop new technologies in order to reduce the hydroperoxide-mediated keratin damage.

Chapter 3: Effect of catechol-based antioxidants on the $HO^{\bullet}$-mediated oxidation of biological substrates

3.1 Introduction

Humans are constantly exposed to a large number and variety of biological and environmental oxidants, such as reactive free radicals. These oxidants are known as ROS (e.g., $HO^{\bullet}$, $O_2^{\bullet-}$, O_3; whose reactivity with amino acids and peptides has been covered in the introduction). The propensity of ROS to undergo rapid reactions with biomolecules, results in cell damage and initiates (or accelerates) many chronic diseases, such as cardiovascular diseases, cancer, Parkinson's disease, different types of diabetes and more.[194–197] Over the past decades, there has been an upsurge of chronic diseases, which has been linked to inadequate diets, that is, diets insufficient in fruits and vegetables.[198] Indeed, today there are multiple studies that have reported the potential and benefits of diets rich in fruit and vegetables to exert protection against such diseases.[199–205]

The comprehensive research on the effect of fruits and vegetables led to the realisation that the presence of specific active compounds inside fruits and vegetables is associated with a protective effect against the diseases. These compounds are called antioxidants.[164,206] However, in living organisms, the biological activity of the antioxidants appears to be complicated by other mechanisms. Indeed, the potential of the antioxidants to negatively influence health is often overlooked, and today there are multiple reports demonstrating that unnecessary antioxidant supplementation has been linked with damage to biomolecules.[198,207–210] However, on dead tissue, such as food, fabric and hair, the role of antioxidants is less confounded by such mechanisms. Indeed, antioxidants (especially natural) have found great success as food preservatives, and have been shown to increase the shelf-life of high-fat content food.[211–213] More recently, natural antioxidants have attracted high attention in the textile industry.[214] There are now documented examples where that treatment of fabric (cotton and wool) with natural antioxidants significantly enhanced both the antibacterial and antioxidant properties of the fabric.[215] The next Sections will discuss the role of antioxidants in autooxidation processes and their antioxidant mechanisms.

3.2. Mechanism of autoxidation

Different definitions have been used to explain the activity of antioxidants.[163,216,217] Generally, antioxidants can be viewed as compounds (natural or synthetic) that are capable of preventing or retarding an autoxidation process, that is, the radical chain reactions between organic molecules and molecular oxygen.[163] To reduce the damage on the organic compounds and delay the rate of autoxidation, the use of antioxidants has evoked high attention, especially in the pharmacology and food industry.[213,218–221]

3.3 Antioxidants in oxidation processes

Depending on their mode of action, antioxidants (AH) can be essentially divided into two categories, preventive and chain-breaking.[73] Preventive antioxidants are those that eliminate the initiating oxidant, such as compounds that decompose H_2O_2, metal ion chelators, ROS scavengers and $^1O_2$ quenchers, thereby converting these oxidants to stable molecules and reducing the initiation rate. The second category (chain-breaking) involves antioxidants that act as free radical terminators (mainly for peroxyl but also alkoxyl radicals), thus retarding the propagation steps (Scheme 39; Eq. 2).

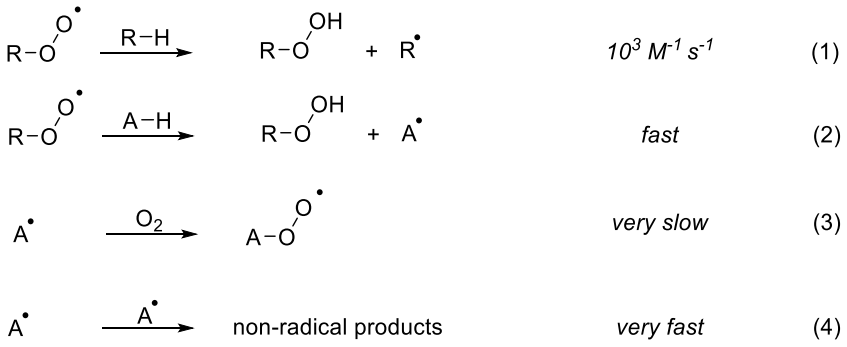

Scheme 39. An inhibited oxidation process. An antioxidant (AH) acts as a chain-breaking antioxidant by quenching peroxyl radicals (mainly; equation 2) and other radicals, thus slowing down the propagation steps.

The actual oxidation process can be quite complex and reactions 1-4 (Scheme 39) as written are not intended to convey the detailed mechanism, but rather highlight the inhibition of the peroxyl radicals by the antioxidant. The main purpose of a chain-breaking antioxidant is to donate a hydrogen atom to the peroxyl radical formed during the autoxidation and generate a ROOH and a radical on the antioxidant ($A^{\bullet}$; Scheme 39; reaction 2). The power of a chain-breaking antioxidant is dictated by three factors. Firstly, for an antioxidant to be efficient, it should react with propagating radicals ($ROO^{\bullet}$ and $RO^{\bullet}$) faster than polyunsaturated lipids and proteins do, as the latter reaction generates C-centred radicals that undergo diffusion-controlled addition of O_2 (propagation).

Secondly, radical-radical termination reactions between two A$^{\bullet}$ are desired since they lead to stable non-radical products and break the propagation cycle. Finally, it is important that A$^{\bullet}$ is unreactive towards other common C-H bonds in the system (so that new C-centred radicals aren't generated).

In principle, the competition between any two given reactions is controlled by two factors. Firstly, the concentrations of the reactants, and secondly the activation energy of the reactions. However, when AH are employed in autoxidation systems, their concentration is typically lower than that of the RH, and therefore, if the rates of the HAA reactions 1 and 2 (Scheme 41) were similar, then the former would predominate. As such, to discover (natural) or design (synthetic) antioxidants, the focus was drawn to the rate of reaction 2, which, ideally should be higher than that of 1 (i.e., higher than 10^2-10^3 M^{-1} s^{-1}).[128]

The rate of reactions 1 and 2 are determined by the thermochemistry of the reactions, that is the BDE of the R-H and A-H, and the relative concentrations of R-H and A-H. Generally, the efficiency of the antioxidant increases with decreasing A-H bond strength. Therefore, for a thermodynamically favourable donation of hydrogen from an antioxidant to a ROO$^{\bullet}$, the BDE of the A-H must be below that of the R-H.

The typical BDEs of the backbone C-H of simple amino acids have been calculated theoretically and determined experimentally, and were found to be ~ 85 kcal mol^{-1}.[222] For instance, for the C-H of the backbone of Tyr a BDE of ~ 83.4 kcal mol^{-1} was estimated, while for the C-H of the side chain and the phenolic O-H the BDEs were determined to be ~ 88.2 and 93.1 kcal mol^{-1} respectively (Figure 32).

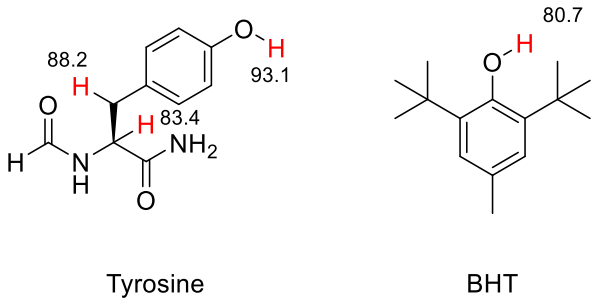

Figure 32. Calculated BDEs for the phenolic O-H, the backbone, and the side chain C-H of Tyr, and the phenolic O-H of BHT. Values are expressed in kcal mol^{-1}.

For simple amino acids accessibility of the oxidant to the substrate is considered unrestricted, and as such, HAA by a ROO$^{\bullet}$ is expected to give rise to R$^{\bullet}$ where the lowest C-H BDE is found (i.e., on the α-carbon). On the contrary, for long peptides or proteins, HAA is more challenging to predict, and it is accepted that damage is skewed to the remote side chains of the amino acid residue that are less sterically hindered.[104,105]

Therefore, for an effective antioxidant, the BDE of the A-H, must be lower than that of the $^{\alpha}$C-H of the biomolecule, in this case tyrosine (i.e., < 83.4 kcal mol^{-1}). For example, 2,6-Di-*tert*-butyl-4-methylphenol (BHT) is one of the most widely used synthetic antioxidants, and the BDE of the phenolic O-H has been calculated experimentally and a value of 80.7 kcal mol^{-1} (Figure 32) has been determined.[223] This value is considerably lower than the 83.4 kcal mol^{-1} of the $^{\alpha}$C-H of tyrosine, and as such, BHT could potentially be an effective antioxidant at reducing the rate of tyrosine oxidation (although BHT is not water soluble, and therefore delivery into biological systems is challenging).

3.4. Phenolic antioxidants

It was stated earlier that the beneficial effects of diets rich in vegetables and fruits were largely attributed to the high polyphenolic content that can act as antioxidants. As such, it is not surprising that investigation of various substituted phenols, catechols (benzene-1,2-diols), and hydroquinones (benzene-1,4-diols; Figure 33) moieties, as potential antioxidants has received great attention over the past 20 years.[73,163,164,212,224–226]

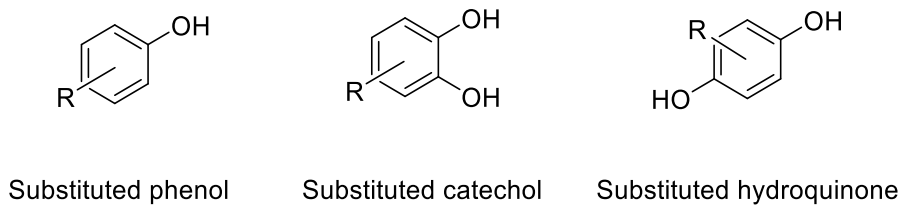

Figure 33. Structures of the most common substituted phenolic antioxidants.

The reported BDEs values for the O-H of unsubstituted phenols and catechols are ~ 87.6 and ~ 81.2 kcal mol^{-1} respectively, while the value for the unsubstituted hydroquinone lies in-between (~ 84.9 kcal mol^{-1}).[227–230] These values show that catechol can be a potent antioxidant, as its O-H BDE is considerably lower than that of the $^{\alpha}$C-H in amino acids, but phenols and hydroquinones are likely to be less efficient. However, the introduction of substituents can exert strong steric and electronic effects, thus altering the BDE of the O-H bond significantly. Indeed, electron donating substituents in phenol, have been shown to significantly lower the BDE of the phenolic O-H (e.g., BDE value of 82.1 kcal mol^{-1} for 4-methoxyphenol **3.1** has been calculated; Figure 34),[231] while electron withdrawing substituents increase the phenolic BDE (e.g., BDE value of 95.1 kcal mol^{-1} for 4-hydroxybenzaldehyde **3.2** has been calculated; Figure 34).[232] Similarly, sterically crowded substituted phenols (e.g., BHT; Figure 32) have lower phenolic BDE thus enhancing their antioxidant properties.

Figure 34. Structure of 4-methoxyphenol and 4-hydroxybenzaldehyde, highlighting the phenolic O-H BDE.

Flavonoids are polyphenolic compounds encountered often in plants and vegetables (some representative structures are given in Figure 35),[233] that can act both as preventive (by intercepting the initiation source), and chain-breaking antioxidants (by rapid donation of a hydrogen atom to another propagating radical yielding relatively stable radicals).

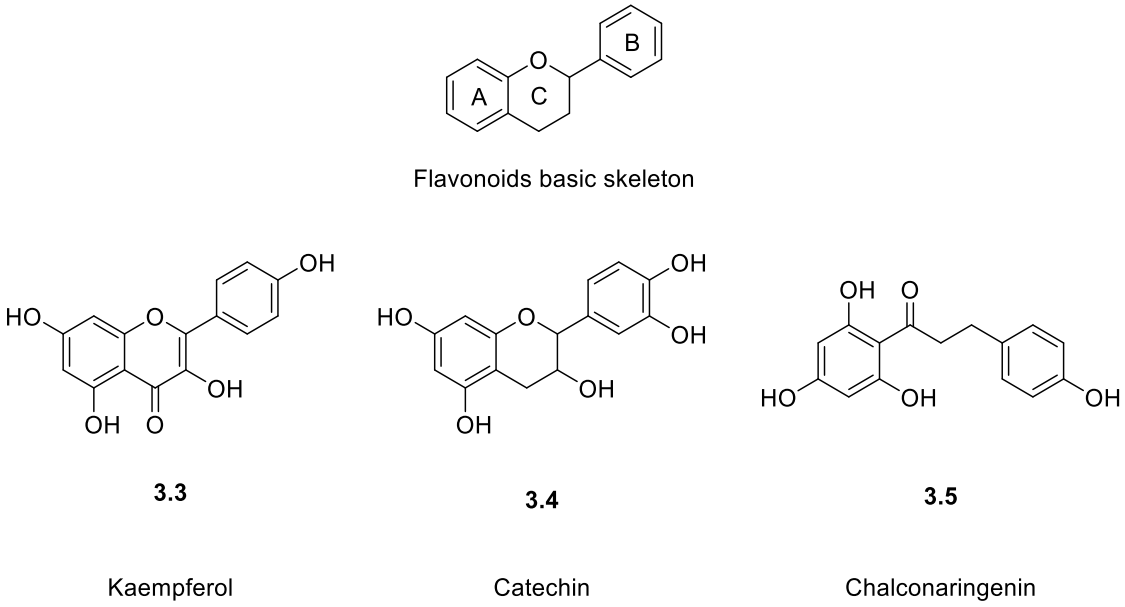

Figure 35. The generic structure of flavonoids, and some examples of naturally occurring flavonoids. Flavonoids are encountered in plants, fruits, or vegetables.

The former reaction depends on the initiation source, while the latter generates phenoxyl, and semiquinone radicals on the antioxidants. These compounds are excellent antioxidants, as their radical intermediates are stabilised due to resonance delocalisation in the aromatic ring, and O_2 addition is an inefficient process.[234] For instance, tyrosine phenoxyl radical reacts with molecular O_2 with a rate constant that has been estimated to be $< 10^3$ M^{-1} s^{-1}.[53,55,113] For 1,4-semiquinone radicals O_2 addition takes place with a $k \sim 10^5$ M^{-1} s^{-1} followed by facile elimination of $HO_2^{\bullet}$ to afford a quinone,[235] while 1,2-semiquinone radicals are generally accepted to show little reactivity towards O_2 ($k << 10^5$ M^{-1} s^{-1}).[236]

The low reactivity for 1,2-semiquinone radicals towards O_2 was attributed to the development of an intramolecular hydrogen bond framework between the oxygen-centred radical and the neighbouring O-H group of catechol, that further enhances the stability of the radical intermediate (Figure 36).[229]

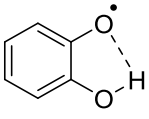

Figure 36. Development of an intramolecular H-bond framework providing further stability to the 1,2-semiquinone radical.

The HAA reaction between ROO• (the main propagating species in an autoxidation process) and simple phenols, catechols and hydroquinones in neutral aqueous solutions, has been extensively researched in the past, and rate constants in the order of $k \sim 10^5$ - 10^6 M^{-1} s^{-1} have been experimentally measured.[73,237–240] These values are at least two orders of magnitude higher compared to the HAA reaction between ROO• and proteins or peptides. The subsequent chemistry of phenoxyl radicals has been discussed in the Introduction. The focus of the next Section will be in the chemistry of semiquinone radicals.

3.5 Reaction pathways of semiquinone radicals

Hydrogen atom abstraction reaction by ROO• from catechols and hydroquinones produces semiquinone radicals. Since semiquinone radicals **3.6** are highly stabilised, they react slowly with O_2 and are unreactive towards other C-H bonds in the system, they can accumulate in relatively high concentrations and participate in bimolecular termination reactions (Scheme 40).

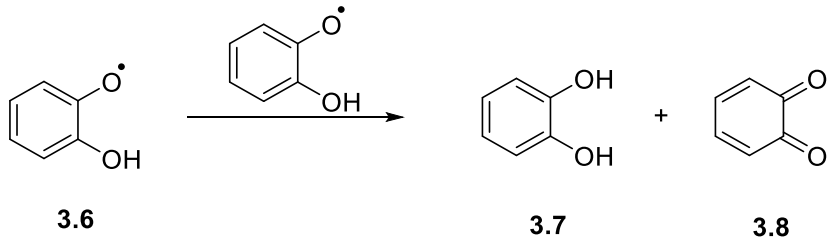

Scheme 40. Bimolecular reaction between two stable 1,2-semiquinone radicals, producing a stable quinone and regenerating the initial catechol.

It is widely accepted that for semiquinone radicals in neutral aqueous solutions, the most favourable pathway is decay *via* a (reversible) disproportionation reaction to yield a stable quinone **3.8** and recover the starting substrate **3.7** (Scheme 42). Such bimolecular reactions proceed with fast rate constants near the diffusion limit ($2k \sim 10^9$ M^{-1} s^{-1}).[235,241,242] Self-dimerisation of semiquinone radicals to form dimeric species is possible, although this reaction is reported to be a minor pathway for these.[243] Another important reaction pathway for semiquinone radicals is a radical-radical reaction with another ROO• (Scheme 41).

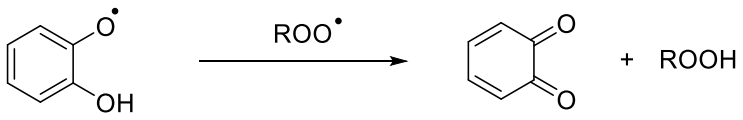

3.6 **3.8**

Scheme 41. Reaction between a 1,2-semiquinone radical and a propagating peroxyl radical, yielding a stable quinone and a hydroperoxide.

The reaction of Scheme 43 is accepted as major pathway for 1,2-semiquinone radical decay but is less probable for 1,4-semiquinone radicals.[244] For 1,2-semiquinone radicals, reaction with $ROO^{\bullet}$ has been proposed to proceed *via* a formal proton coupled electron transfer to give rise to a quinone and a hydrocarbon-derived hydroperoxide.

Whether reaction of semiquinone radicals with O_2 proceeds *via* an electron transfer mechanism to afford a hydroquinone and $HO_2^{\bullet}$,[245] or involves addition of O_2 to the aromatic ring, followed by facile $HO_2^{\bullet}$-elimination is unclear, with conflicting reports.[235] More recent theoretical studies have calculated that the activation energy for electron transfer from the semiquinone radical to O_2 is too high for the reaction to occur. However, electron transfer from the corresponding semiquinone radical anion to O_2 is thermodynamically favoured.[246] Thus, electron transfer becomes prominent at neutral to high pH where the semiquinone radical exists predominantly as the semiquinone radical anion ($pK_a \sim 4.4$),[247] but is less favoured at low pH. Substituents can strongly influence the electron density of the semiquinone radical, and thus dramatically change the autoxidation of semiquinone radicals. Indeed, it has been experimentally confirmed that electron withdrawing substituents in the parent hydroquinone result in more stable semiquinone radicals, that are less reactive towards O_2.[248] Conversely, electron donating substituents produce more reactive semiquinone radicals that react readily with O_2 to produce $HO_2^{\bullet}$.[248]

Catechols and hydroquinones are probably the most well-research antioxidants. However, natural polyphenolic compounds usually contain other moieties in their rings that have the potential to act as antioxidants. Two typical examples are resorcinol (benzene-1,3-diols), and pyrogallol (benzene-1,2,3-triols; Figure 37) moieties.[249–251] For instance kaempferol and catechin shown in Figure 35, both contain a resorcinol moiety in their aromatic ring. The next Section will briefly discuss the use of resorcinol and pyrogallol as antioxidants.

Substituted resorcinol Substituted pyrogallol

Figure 37. Structures of some common substituted phenolic antioxidants.

3.6 Resorcinol and pyrogallol

The antioxidant activity of resorcinols and pyrogallols is similar to that of catechols and hydroquinones. Indeed, there are documented examples where they act both as preventive and chain-breaking antioxidants.[252–254] Both resorcinol and pyrogallol are potent antioxidants as the resulting radicals are stabilised due to electron delocalisation in the aromatic ring (similarly to phenols, catechols and hydroquinones).

The estimated phenolic O-H BDE for resorcinol (~ 86.7 kcal mol^{-1}),[255] is in fact, very close to the BDE value for the unsubstituted phenol (~ 87.6 kcal mol^{-1}; Section 3.4). Even though for both resorcinol and hydroquinone there is no development of hydrogen bond framework to stabilise the resulting radical (as in the case of catechol), the BDE of the O-H in resorcinol is considerably higher compared to the O-H of hydroquinone (~ 84.9 kcal mol^{-1}; Section 3.4). The discrepancy in the phenolic O-H BDEs between resorcinol and hydroquinone can be readily explained by the fact that in hydroquinone the radical is further stabilised in the -OH group in the *para*-position.

On the contrary, the estimated BDE for the phenolic O-H of pyrogallol is significantly lower (~ 75.3 kcal mol^{-1}).[255] This is not surprising as pyrogallol is a highly conjugated system. It is noted that for pyrogallol this BDE value refers to the O-H in the middle position of the ring. These values further support that the position of the -OH groups in the aromatic ring is critical for the antioxidant properties of polyphenols. The lower BDE for pyrogallols (compared to catechols) can be readily explained by the development of a strong intramolecular hydrogen bond framework, where the O-centred radical is stabilised by both neighbouring O-H (Figure 38).

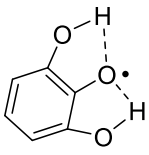

Figure 38. Development of an intramolecular H-bond framework from two neighbouring O-H groups providing further stability to the 1,2-semiquinone radical.

Apart from acting as chain-breaking antioxidants by donation of a hydrogen, polyphenolic antioxidants can act *via* scavenging the initiation radical. This reactivity depends on the oxidant. Hydroxyl radical, is a powerful oxidant and one of the most common initiators of radical chain reactions. The next Section will explore the reactivity of polyphenolic compounds with $HO^{\bullet}$.

3.7 Reaction between polyphenols and hydroxyl radical

Hydroxyl radicals can be generated in various systems, including *via* the reduction of H_2O_2 by redox active metals present in hair. Hydroxyl radicals can undergo rapid addition to polyphenolic compounds, generating transient cyclohexadienyl radicals **3.9** (Scheme 42).[256]

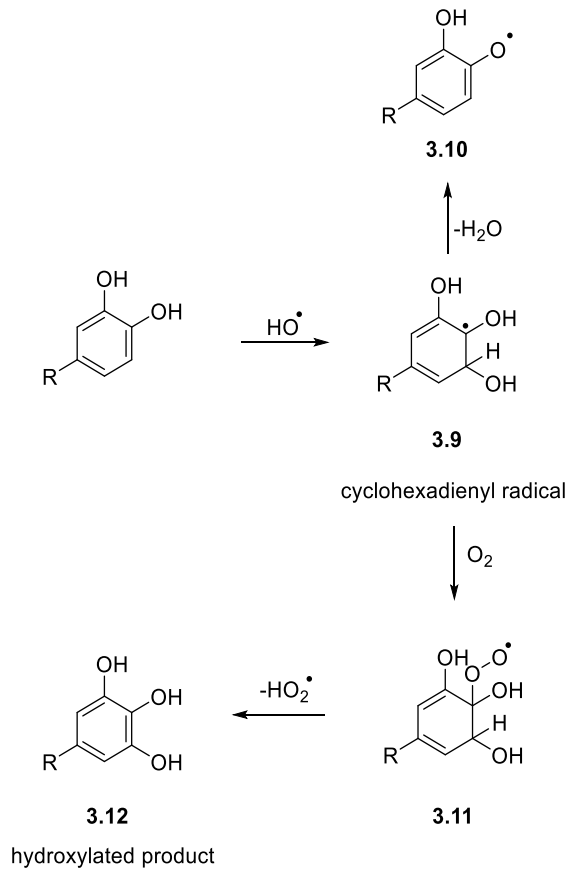

Scheme 42. Reaction between a catechol and $HO^{\bullet}$ yielding a transient cyclohexadienyl radical, that can either eliminate -H_2O or add to O_2. Subsequent $HO_2^{\bullet}$ elimination affords a stable hydroxylated product.

This reaction is near the diffusion-control ($k \sim 10^{10}$ M^{-1} s^{-1} for unsubstituted catechol).[189] The transient cyclohexadienyl adduct **3.9** can now follow two different pathways; that are facile H_2O-elimination ($k \sim 10^5$ s^{-1}) to generate a highly delocalised semiquinone radical **3.10**,[257]or near diffusion-controlled O_2 addition ($k \sim 10^9$ M^{-1} s^{-1}),[113] followed by $HO_2^{\bullet}$-elimination ($k \sim 10^5$ M^{-1} s^{-1}) to afford a stable hydroxylated product **3.12**.[113] The same process can occur successively to generate multi-hydroxylated products on the parent polyphenol.[256] In this way the antioxidant (and the newly generated hydroxy derivatives) act as a preventive antioxidant, since it intercepts the initiation radical (i.e., $HO^{\bullet}$).

More recently, botanical extracts that have been traditionally employed for food protection, have been used in the hair industry. There are now documented examples where botanical extracts offer colour, protein and hair growth protection on human hair, and this protection is driven by their high polyphenolic material.[258–261] Botanical extracts are ideal candidates for antioxidants for two reasons. Firstly, they have a rich polyphenolic content which is essential for an efficient antioxidant (*vide supra*). Secondly, they are natural, and consumers show a preference for health and cosmetic products that contain compounds derived directly from nature, as opposed to synthetic antioxidants that create a negative perception in consumers. Some representative antioxidants that are often encountered in botanical mixtures are given in Figure 39.

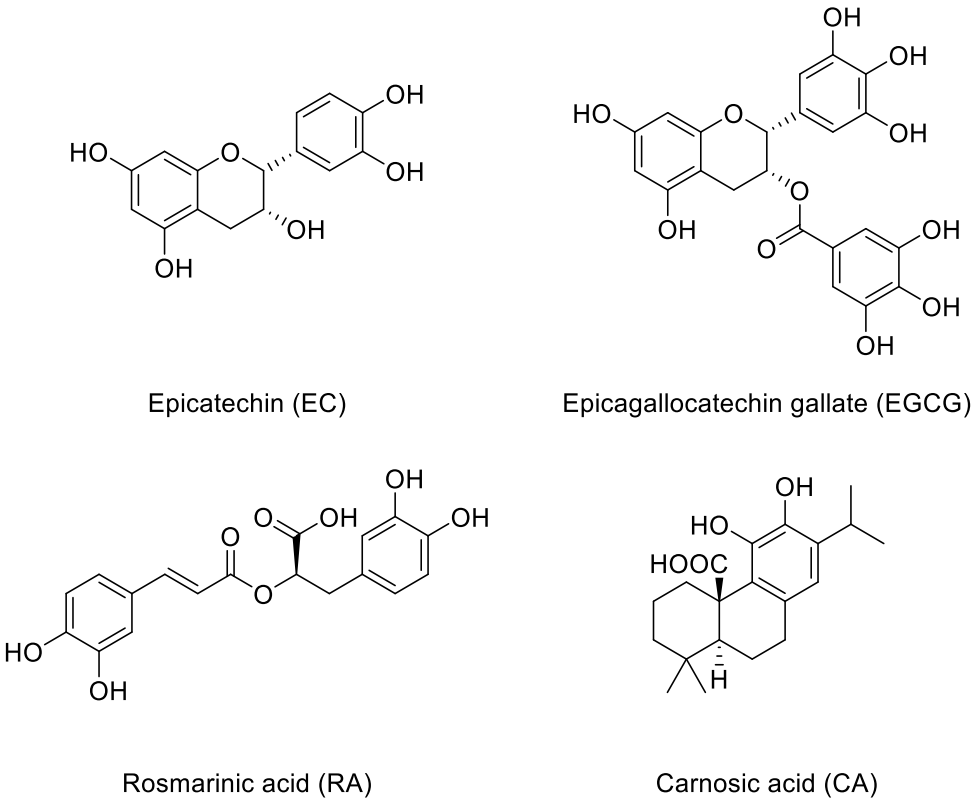

Figure 39. Chemical structures and abbreviations for the four catechol-based compounds investigated as potential antioxidants in this work.

The antioxidant mechanisms of these compounds are more often explored by their ability to inhibit lipid peroxidation and quench ROO$^{\bullet}$ that are generated by thermally unstable azocompounds (e.g., AAPH or AIBN).[240,262–264] Hydrogen atom abstraction reaction from the thermally generated ROO$^{\bullet}$ is predicted to give rise to highly delocalised 1,2-semiquinone radicals (for all four antioxidants), that in time convert to the corresponding quinones. Indeed, quinones have been identified as the main degradation product of the ROO$^{\bullet}$-mediated oxidation of flavonoids,[265–269] although not as many reported examples exist for the compounds of Figure 39. This is probably because reaction pathways are further complicated by the system, and for instance, some studies have reported the characterisation of adducts between semiquinone radicals and AIBN/AAPH-derived radicals.[269,270] Autoxidation of these compounds (Figure 39) is well-defined in the literature, and also leads to the corresponding quinones,[267,271,272] while quinone formation can also occur in presence of transition metals (e.g., Cu^{2+}).[209] For EC and EGCG there is some evidence to support the formation of dimeric species as a result of radical-radical reactions between two highly stabilised semiquinone radicals.[270]

Reaction of these antioxidants with HO$^{\bullet}$ is less explored, although it is predicted to follow similar trends as reaction between HO$^{\bullet}$ and catechols, as shown in Scheme 42. Nonetheless, it is well-documented that flavonoids are powerful HO$^{\bullet}$ scavengers,[273] and some literature precedent exists to support that the aerobic HO$^{\bullet}$-induced oxidation of the four antioxidants leads to the formation of hydroxylated products.[257,274] The ability of antioxidants to scavenge HO$^{\bullet}$ is probably beneficial, as it can lead to the generation of hydroxylated products (Scheme 44), that in turn act as antioxidants. This is because the hydroxylated degradation products, can react with HO$^{\bullet}$ or ROO$^{\bullet}$ to further reduce the oxidation of biomolecules.

3.8 Project outline and aims

In this Chapter we investigate the protective effect of four catechol-based compounds (Figure 39; EC, EGCG, RA and CA) isolated from natural sources (tea and rosemary) on the aerobic $HO^{\bullet}$-mediated peptide oxidation, with a particular interest on hair damage. It is well-documented that both protein damage and colour fade in human hair are caused by radical based chemistry.[29,157,159,275,276] To prevent or at least reduce the extent of this damage, one approach is to quench the oxidants that are responsible for the initiation and the propagation of these processes. As such, it is anticipated that these four catechol-based compounds can offer protection against hair damage. Our ultimate objective is to determine the factors that affect the antioxidant efficiency of these compounds.

One of our aims it to take advantage of the existing literature in this area and understand their antioxidant mechanism. While mechanistic pathways, and product formation is well-understood for generic polyphenols, research in these specific compounds (EC, EGCG, RA and CA) is underexplored. A possible reason for this is that their antioxidant capacity is usually investigated by their ability to quench ROS in complex systems,[262–264,277–284] and thus product analysis and mechanism proposal are challenging. We aim to use advanced analytical techniques to detect the formation of products, and experimentally confirm reaction pathways for their antioxidant mechanism.

Next, we attempt to assess their antioxidant potency by monitoring the aerobic $HO^{\bullet}$-induced oxidation of two protected amino acids in their presence and absence. Procter and Gamble has been studying these four compounds as potential antioxidants, and their antioxidant power has been measured by well-established tests, principally the oxygen radical absorbance capacity (ORAC) assay (Section 3.11.2).[285–287] Our objective is to compare our experimental data against well-established techniques and see if there is an agreement for their antioxidant power. Lastly, we explore the protective effect of rosemary extracts (and not isolated compounds) in the aerobic $HO^{\bullet}$-mediated oxidation of peptides. Procter and Gamble has supplied as with rosemary extracts that contain a range of different compounds, but the main active compounds are either RA or CA. This is key for the hair industry as P&G has previously shown reduced protein damage and colour loss in the presence of these four antioxidants, and the rosemary extracts (unpublished data).

3.9 Hydroxyl radical-induced oxidation

The aerobic HO•-induced oxidation of *N*-Ac-Ala-OH in the presence of the four catechol-based antioxidants (EC, EGCG, RA and CA) was examined. Hydroxyl radicals were generated *via* H_2O_2 photolysis (Scheme 43). Since our goal is to contextualise the protective effect of the four compounds on hair proteins, *N*-Ac-Ala-OH is used a protein mimic (similarly to Chapter 2; more details in Section 3.11).

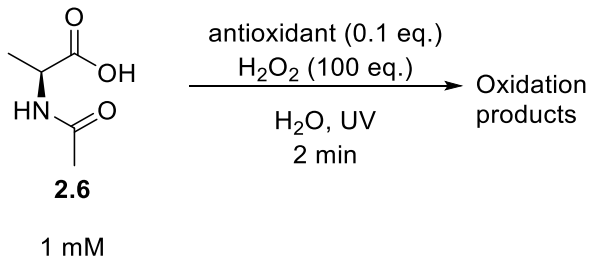

Scheme 43. Experimental conditions for the investigation of the antioxidant mechanism of the four catechol-based antioxidants.

It was decided to explore the antioxidant potency of the four compounds in a system that produces both HO• and ROO•. Hydroxyl radicals are generated directly from H_2O_2 photolysis and can either react with the antioxidant or abstract a hydrogen from *N*-Ac-Ala-OH to ultimately produce ROO•. Therefore, this system allows the study of both the preventive and chain-breaking properties of the compounds based on the analysis of the degradation products. All of the reactions were carried out in open air, to ensure formation of ROO• takes place. The antioxidant equivalents used in our reactions are relatively high (0.1 eq.). Usually, when antioxidants are used in oxidation systems smaller concentrations are used (< 0.01 eq.). However, the antioxidants investigated here ionise very poorly in the MS (see Section 3.11), and as such, high concentrations were required to obtain consistent and reliable signals.

It should be noted that all four compounds here possess aromatic rings and are likely to absorb UV light. The lamp used for the photolysis of H_2O_2 in this work provides broad-band UV light. It is therefore essential to know if the detection of degradation products is HO•-facilitated or due to direct excitation of the antioxidants. To study this, aqueous solutions (0.1 mM) of the antioxidants were exposed to UV light in the absence of the protected amino acids and H_2O_2, and their degradation was assessed spectroscopically by UV-Vis. No decomposition of the four antioxidants, and no degradation products were detected upon a 10 min irradiation (data not shown). In the next

Sections advanced analytical techniques are used to characterise degradation products generated from the antioxidants, and it is attempted to differentiate between $HO^{\bullet}$- and $ROO^{\bullet}$-induced paths.

3.10 Product analysis

Based on the reaction pathways proposed above for flavonoids, two main oxidation products are predicted for the four antioxidants; that are, hydroxylation of the aromatic ring and generation of a quinone (representative structures for the catechol-derived degradation products are given in Figure 40).

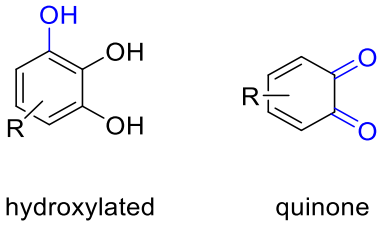

Figure 40. Representative chemical structures for the formation of a hydroxylated product and a quinone in this work, highlighting the formation of the new functional groups.

Irradiated reaction mixtures were initially analysed by DI-MS using positive ion mode. However, investigation of DI-MS spectra for the $[M + H]^+$ and the $[M + Na]^+$ of potential hydroxylated products or quinones returned no results. This is likely due to the poor ionisation efficiency of the molecules, combined with the low abundance of the oxidation products in the reactions and the pre-injection dilution of the samples (samples are diluted at least x 10 to avoid contamination of the instrument). Indeed, it should be noted that the four antioxidants showed very poor ionisation efficiency, and often very high concentrations (~ 0.1 mM) were required to detect even pure samples. Analysis using negative ion mode was attempted as the compounds would be expected to ionise more efficiently. However, negative ion mode produced inconsistent data, and was therefore, dismissed.

On the contrary LC-MS proved more efficient, possibly owing to the separation of the different compounds (no competition for ionisation). Therefore, all reactions were analysed by LC-MS (more information in the experimental Section). It is necessary to highlight that since the four antioxidants used did not ionise efficiently, a comprehensive analysis of every possible mechanism and product was not possible. Indeed, the LC-MS chromatograms prior to, and after irradiation, looked nearly identical. As such, our analysis is limited to the products that based on the mechanisms of the introduction and previous literature, are proposed to be formed in the highest abundance.

Predictably, analysis of the LC-MS chromatograms revealed that hydroxylation of the aromatic ring and quinone formation were evident in all four antioxidants (Figures 41; reported as the EIC $[M + H]^+$). It is noted that the same products (i.e., hydroxylation and quinone) can be formed *via* reactions of $HO^\bullet$ with the antioxidants (c.f., Schemes 42 and 44), and the initial formation of a peptide radical might not be necessary. Differentiating between products formed as a result of direct oxidation of the antioxidants from $HO^\bullet$ or as a result *N*-Ac-Ala-OH-derived $ROO^\bullet$, is not trivial since the same products are expected. Nonetheless, the following control reactions were carried out. Firstly, reactions were repeated as in Scheme 45, but without H_2O_2. Analysis of these reactions revealed no oxidation products on the antioxidant or the peptide, thus proving that the formation of products is $HO^\bullet$-facilitated. Secondly, reactions were repeated as in Scheme 45, however *N*-Ac-Ala-OH was omitted. Interestingly, in this case hydroxylation of the antioxidants was again evident, but no formation of quinone appeared to take place, further supporting that quinone generation is a result of reactions between semiquinone radicals on the antioxidant and peroxyl radical on *N*-Ac-Ala-OH. The next two Sections will discuss the product formation on the four antioxidants.

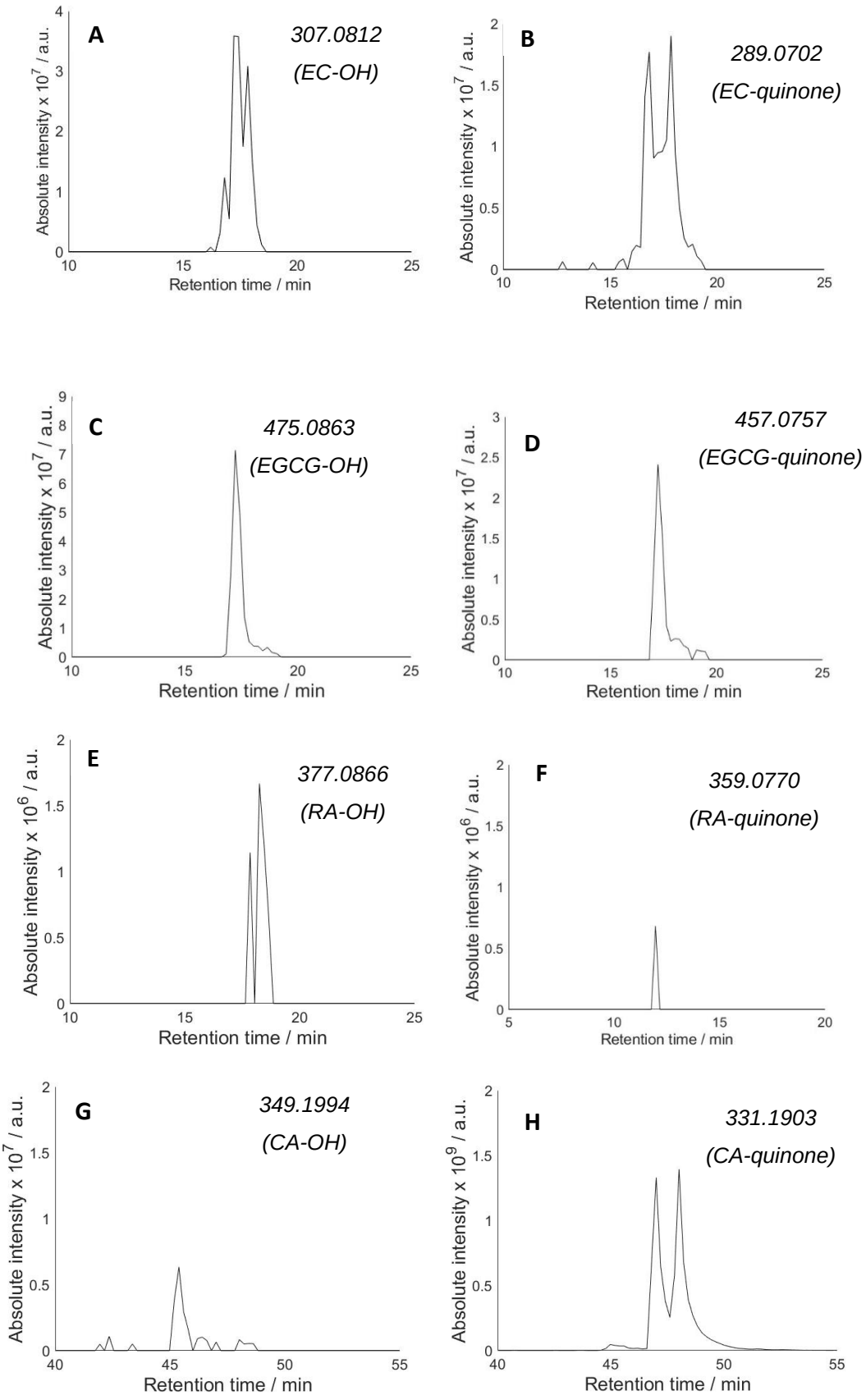

Figure 41. EIC of the $[M + H]^+$ for A) EC-hydroxylation, B) EC-quinone), C) EGCG-hydroxylation, D) EGCG-quinone, E) RA-hydroxylation, F) RA-quinone, G) CA-hydroxylation, and H) CA-quinone. Products were generated by exposure of aqueous solutions of N-Ac-Ala-OH (1 mM) to UV light (open to air) in presence of aqueous solutions of the antioxidants (1 mM) and H_2O_2 (100 mM) for 2 min.

3.10.1 Hydroxylation

It is noted that $HO^{\bullet}$ addition to catechols is diffusion-controlled ($k \sim 10^{10}$ M^{-1} s^{-1}),[189] while HAA from *N*-Ac-Ala-OH is 2 orders of magnitude slower ($k \sim 10^{8}$ M^{-1} s^{-1}), and therefore hydroxylation is predicted to be more efficient than the formation of quinones.[95] Nonetheless, such a conclusion cannot be made based on the data here, as the assumption that different molecules ionise equally should not be made. Hydroxylation of EC, EGCG and RA is expected to occur preferentially in the positions that are activated by the -OH groups. As such, 4, 6 and 4 hydroxylated derivatives are predicted for EC, EGCG and RA, respectively. While literature data on the hydroxylation of these four flavonoids could not be found, previous studies that investigated the $HO^{\bullet}$-induced oxidation of various dihydroxy benzenes, observed selective hydroxylation patterns.[274] For EC (Figure 41A) and RA (Figure 41E) 3 and 2 peaks with similar intensity are revealed indicating that hydroxylation occurs at more than one sites of the aromatic rings. On the contrary, EGCG undergoes selective hydroxylation to one position (Figure 41C). Based on our data here, it is unclear if another hydroxylation occurs. The peak is relatively big and tailing (likely due to high concentration of the sample/peak), and other peaks with the same $[M + H]^{+}$ could be hidden underneath, but it cannot be confirmed. However, these conclusions assume that the isomeric products are well-separated in the LC, which of course might be incorrect. Lastly, CA offers one position for hydroxylation, and that is evident in Figure 39G (low background noise could not be avoided in the analysis).[274]

3.10.2 Quinone formation

Formation of a quinone, which is the result of the reaction between 1,2-semiquinone radical and $ROO^{\bullet}$ formed on *N*-Ac-Ala-OH, or of a disproportionation reaction between two 1,2-semiquinone radicals was evident in all four cases.

3.10.2.1 Epicatechin

For EC the most reactive site from which the $ROO^{\bullet}$ can abstract a hydrogen from is documented to be the "B" ring (i.e., lowest phenolic O-H BDE; Figure 42).[288,289] This is because the resulting 1,2-semiquinone radical formed is stabilised by resonance distribution in the aromatic ring, as well as an intramolecular H-bond framework (*vide supra*).[288,290]

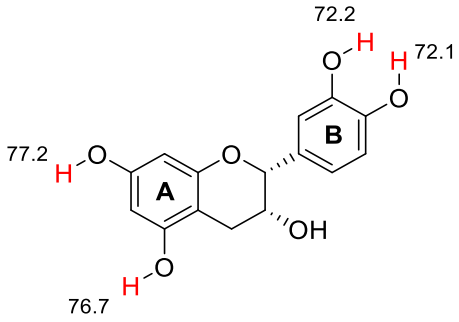

Figure 42. Chemical structure of EC denoting the two different aromatic groups as "A" and "B" and highlighting the BDEs of every phenolic O-H. BDEs are given in kcal mol^{-1}.

For EC the EIC of a potential quinone revealed two peaks (Figure 41B). This was not expected as formation of a quinone can only occur on the "B" ring of EC. This finding suggests that a second oxidation product, sharing the same $[M + H]^+$ as EC-quinone must exist in the system. Indeed, it is documented in the literature that the EC-quinone rapidly interconverts to its tautomeric form compound **3.13** (Figure 43).[289]

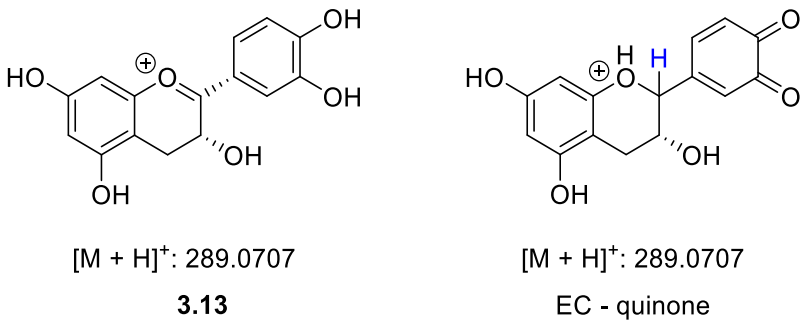

*Figure 43. Chemical structures and $[M + H]^+$ for **3.13** and EC-quinone, highlighting their identical $[M + H]^+$.*

Traditional DI-MS and LC-MS analysis could not differentiate between the two compounds. To gain an insight into the structure of the products with an $[M + H]^+$ of 289.0707 isotope exchange experiments were carried out. Specifically, if **3.13** and the EC-quinone are responsible for the two peaks observed in the EIC of Figure 41B, then deuterium exchange experiments should enable their differentiation, as they possess a different number of exchangeable protons, and upon full deuteration the $[M + D]^+$ will be different (Figure 44).

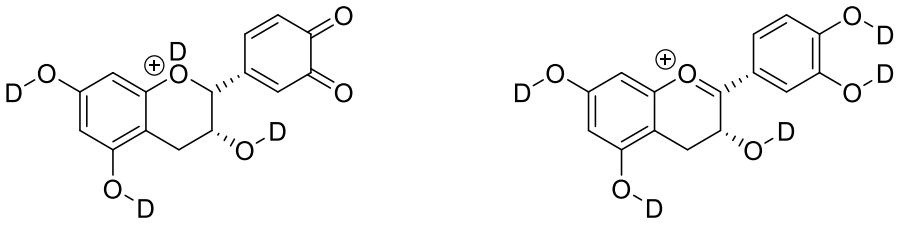

*Figure 44. Chemical structures of the fully deuterated quinone and **3.13** highlighting their different [M + D]⁺. Since the two compounds now have a different m/z, their separation by MS becomes possible.*

Therefore, reactions were repeated as earlier but in D_2O instead of H_2O (all other reaction parameters were maintained the same). Aliquots were then analysed by LC-MS using D_2O as the mobile phase. Representative LC-MS chromatograms are shown in Figure 45.

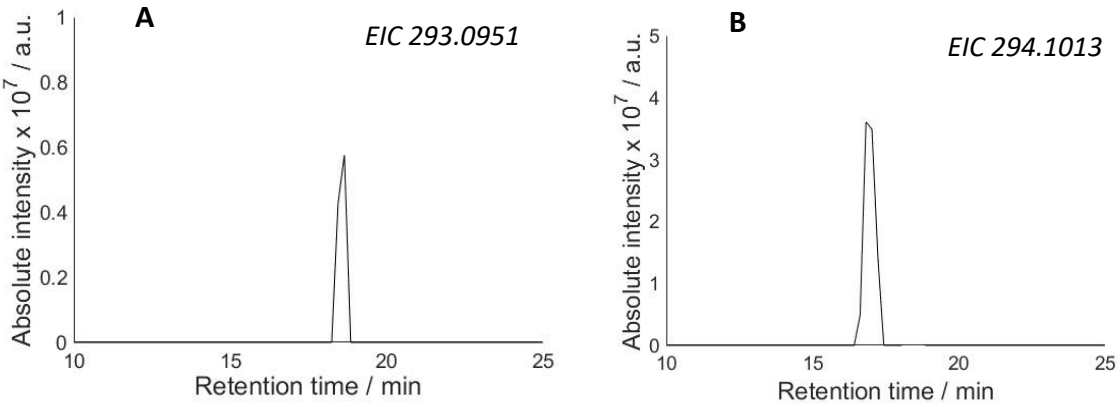

*Figure 45. EIC of the [M + D]⁺ for the completely deuterated A) EC-quinone and B) **3.13**. Products were generated by exposure of solutions of N-Ac-Ala-OH (1 mM) to UV light (open to air) in presence of solutions of the antioxidants (1 mM) and H_2O_2 (100 mM) for 2 min. All stock solutions were prepared in D_2O (instead of H_2O), and reactions were run in D_2O.*

Isotope-exchange and LC-MS analysis further corroborates that the second peak was due to the tautomer of EC-quinone. Indeed, Figures 45A and 45B illustrate that the two previously indiscernible peaks of Figure 41B, are due to two compounds with the same molecular formula, but different number of labile -H.

3.10.2.2 Epigallocatechin gallate

In the case of EGCG, ROO• are predicted to selectively abstract a hydrogen from the "B" or "C" site of the molecule, and more specifically, from the phenolic O-H on the 4'-position (lowest BDE; Figure 46A).[277]

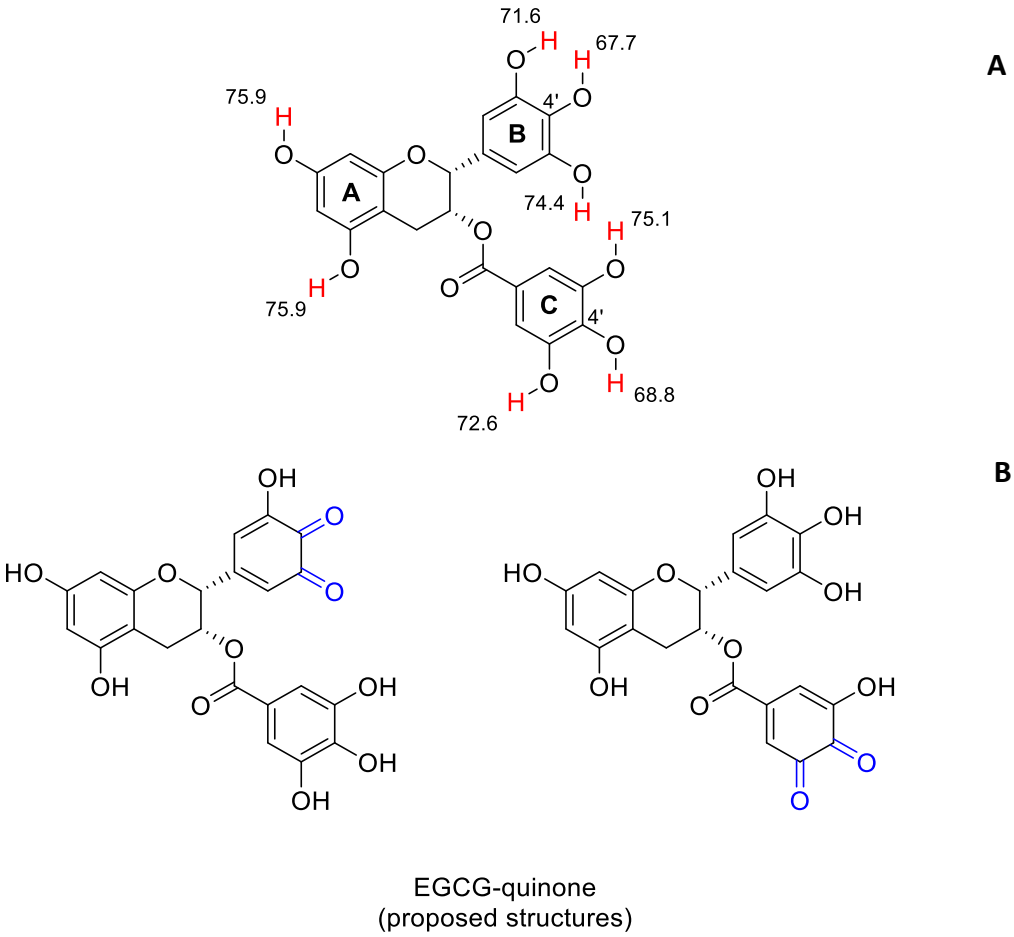

Figure 46. A) Chemical structure of EGCG denoting the three different aromatic groups as "A", "B" and "C", and highlighting the BDEs of every phenolic O-H. BDEs are given in kcal mol^{-1}. B) Chemical structure of the two predicted main EGCG-quinones.

The considerably lower BDE of the two phenolic O-H on the 4'-position of the "B" and "C" ring have been attributed to an intramolecular hydrogen-bond framework that is developed between both neighbouring O-H thus enhancing the stability of the 1,2-semiquinone radical. Based on the above data, the formation of two quinones in similar amounts would be expected for EGCG (Figure 46B). Our experimental data demonstrated that reactions where EGCG was used as the antioxidant produced one EGCG-quinone in high abundance (Figure 41D), and the peak is tailing (similarly to the hydroxylated derivative; Figure 41C). Therefore, it is likely that more than one quinones exist but could not be separated in LC.

3.10.2.3 Rosmarinic acid

Theoretical calculations on the oxidation of RA have determined that the two aromatic sites show almost identical reactivity, and the four phenolic O-H have very similar BDEs (Figure 47A).[291] Therefore, hydrogen abstraction by ROO• should be indiscriminate, and the formation of two quinones are expected (Figure 47B).

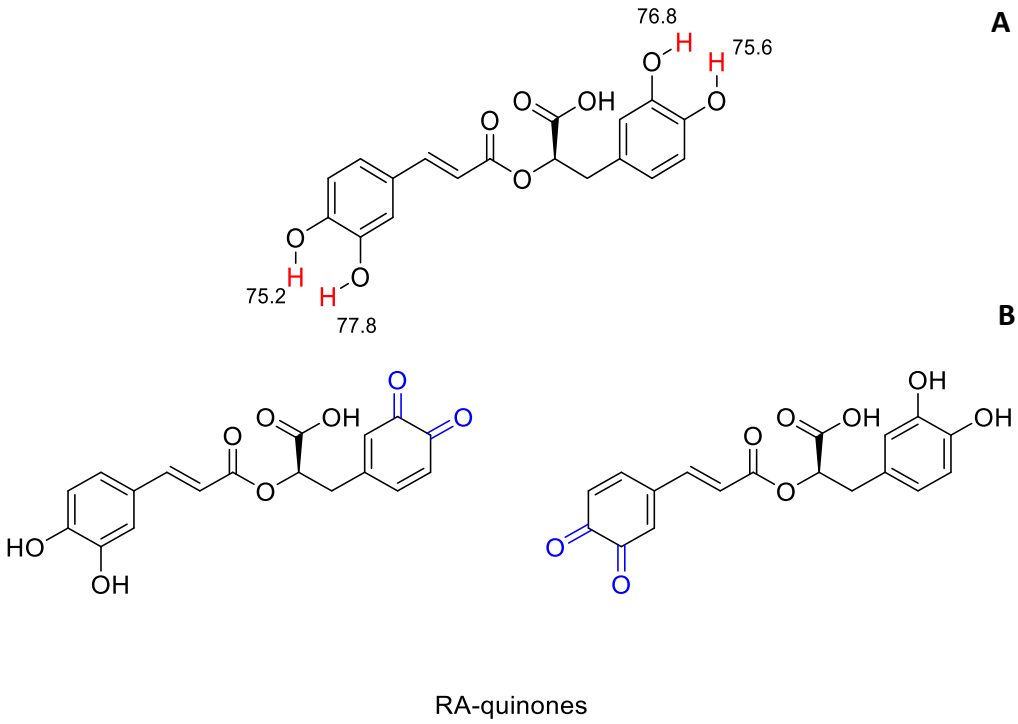

Figure 47. A) Chemical structure of RA highlighting the BDEs of every phenolic O-H. BDEs are given in kcal mol^{-1}. B) Chemical structure of the two predicted main RA-quinones. As the phenolic O-H have similar BDEs, quinone formation is predicted to be non-selective, and the two quinones of the Figure should form in equal amounts.

Oxidation of RA resulted in the formation of only one quinone (as opposed to the predicted two), and even this was present in low abundance (Figure 41F; low 10^6 intensity) . Generally, RA ionised very inefficiently in the MS (the hydroxylated products are also detected in low abundance; Figure 41E), therefore, it is possible that the second predicted quinone was formed but the concentration was too low to allow detection. Equally, the potential quinones that can be formed (for both EGCG and RA) are structurally very similar, and so separation in the LC might not be possible.

3.10.2.4 Carnosic acid

Finally, the case of CA is more straightforward as there is only one available ring, and therefore, only one quinone is predicted. Theoretical studies on the ROO•-scavenging capacity of CA have revealed that the two phenolic O-H have similar BDEs (75.5 and 76.1 kcal mol^{-1}, Figure 48).[282]

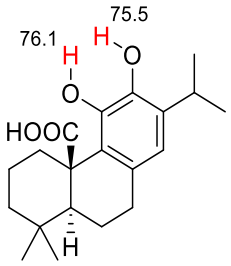

Figure 48. Chemical structure of CA highlighting the BDEs of every phenolic O-H. BDEs are given in kcal mol^{-1}.

Scanning of the LC-MS chromatograms for the HO•-mediated oxidation of CA returned some interesting results (Figure 41H). Firstly, the EIC of the potential CA-quinone revealed two peaks of similar intensities (both present in very high abundance; 10^9 intensity). At first, this is surprising as CA can only form one quinone, indicating that another oxidation product with the same $[M + H]^+$ is present in the oxidation mixture. Secondly, CA is the only antioxidant studied here that afforded the quinone in higher relative abundance over the hydroxylated product. While no definitive conclusions can be drawn, this might suggest that HO• react *via* HAA with either CA or *N*-Ac-Ala-OH rather than addition with CA.

To understand what the second oxidation product is, we sought to find literature precedent on the antioxidant mechanisms of CA. The antioxidant activity of various rosemary extracts (including RA and CA) have been well-researched in the literature by various groups, both in terms of their antioxidant potency, but also product analysis.[266–268,280,281,283,292] It is well-understood that quinone (Figure 49) is one of the major degradation products of the ROO•-facilitated oxidation of CA.[266] Moreover, there is an agreement that CA under aerobic conditions spontaneously converts to carnosol (Figure 49).

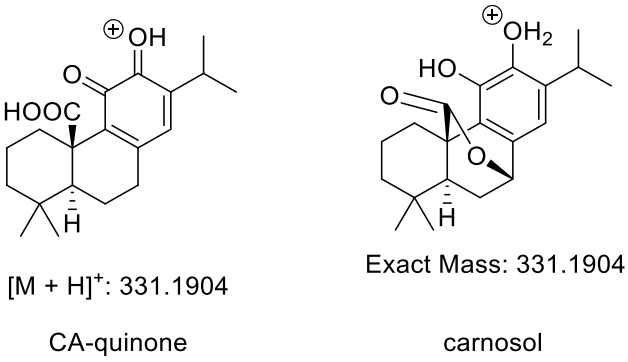

[M + H]$^+$: 331.1904

Exact Mass: 331.1904

CA-quinone

carnosol

Figure 49. Chemical structures and [M + H]$^+$ of the CA-quinone and the primary degradation product of CA, carnosol.

Figure 49 shows the CA-associated quinone and carnosol (both as protonated adducts). These two products share identical mono-isotopic mass, and as such cannot be differentiated by MS. However, similarly to the EC-quinone and **5**, the two products differ in the number of exchangeable protons. Upon complete deuteration the [M + D]$^+$ of the two compounds will now be different (Figure 50). As such, reactions were repeated in D_2O, and a representative EIC of the LC-MS chromatograms are shown in Figure 51.

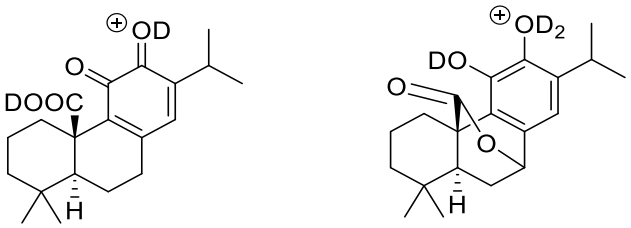

[M + D]$^+$: 333.2029

[M + D]$^+$: 334.2092

CA-quinone

carnosol

Figure 50. Chemical structure and the [M + D]$^+$ of CA-quinone and carnosol where all labile protons have been exchanged with deuteriums. The two proposed products can now be separated in MS.

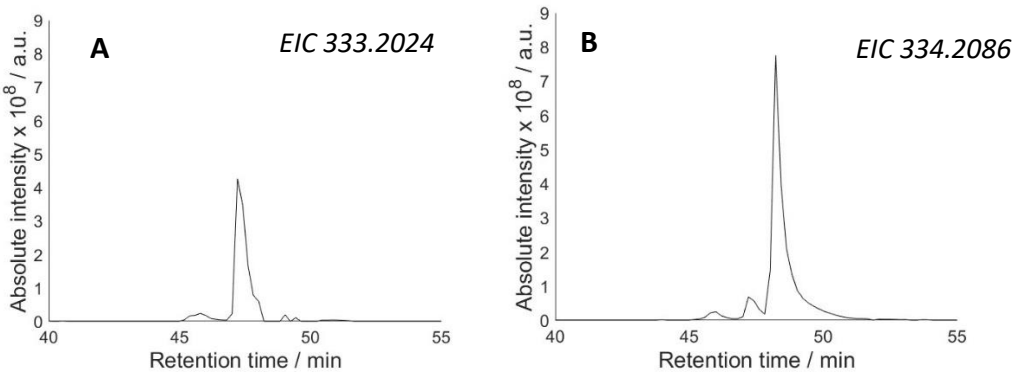

Figure 51. EIC of the $[M + D]^+$ for the fully deuterated A) CA-quinone and B) carnosol. Products were generated by exposure of solutions of N-Ac-Ala-OH (1 mM) to UV light (open to air) in presence of solutions of the antioxidants (1 mM) and H_2O_2 (100 mM) for 2 min. All stock solutions were prepared in D_2O (instead of H_2O), and reactions were run in D_2O.

Isotope exchange experiments verified that the second peak in Figure 41H was indeed due to the formation of carnosol. The retention times for the fully deuterated CA-quinone and carnosol match perfectly the two peaks detected in the non-deuterated sample (Figure 41H). Apart from formation of quinones and hydroxylation of the compounds, overoxidised quinones (i.e., quinone + an -OH group) were evident in all cases (all at lower intensities compared to the quinones; Figures can be found in the Appendix), while dimerised species were not detected.

The relative intensities of the hydroxylated products and the quinones, may indicate that three of the antioxidants (EC, EGCG and RA) act primarily by intercepting the initiation source (i.e., preventive antioxidants). For CA, the major antioxidant mechanistic pathway appears to be scavenging of the propagation radicals ($ROO^{\bullet}$), therefore CA acts as a chain-breaking antioxidant. Although MS is fundamentally not a quantitative technique and care should be taken when interpreting experimental data.

3.10.3 Peroxidation

It was discussed in the introduction of this Chapter that most of the research that has been carried out on the antioxidant properties of these compounds has been on their ability to scavenge ROO• radicals. However, in our system, we explore their antioxidant mechanisms in the presence of a biological target, which can potentially affect their reactivity. For instance, if initial HAA by ROO• from the antioxidant takes place in the aliphatic C-H (and not the phenolic O-H), a C-centred radical is generated (representative example given for EC; Scheme 44).

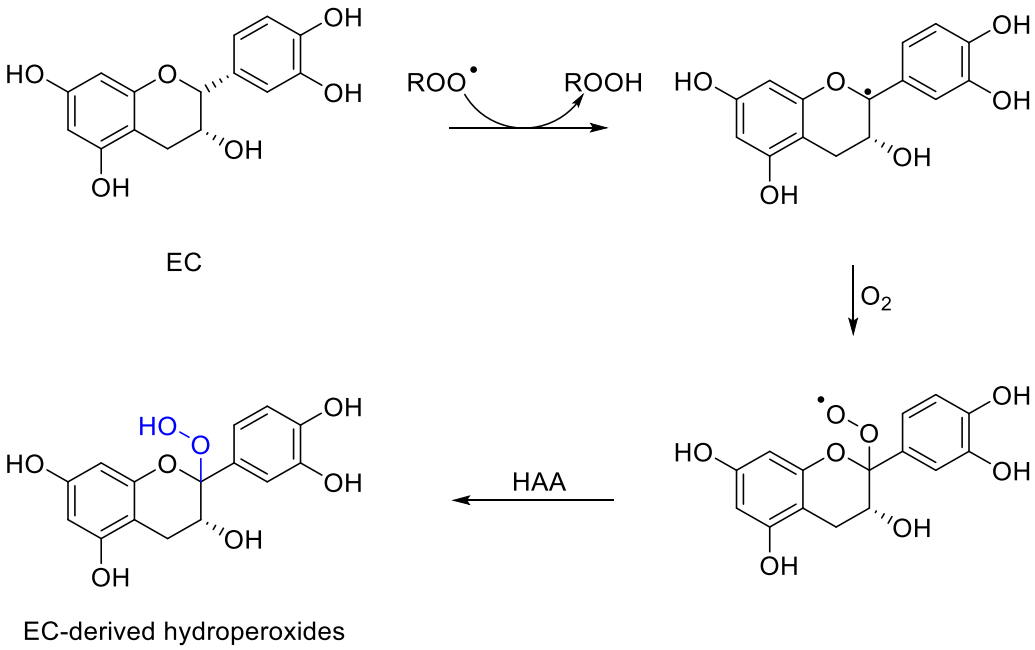

Scheme 44. Peroxidation mechanism of EC. Initial HAA from the benzylic C-H yields a carbon-centred radical that after O_2 addition and HAA converts to a hydroperoxide.

Subsequent O_2 addition followed by another HAA from available C-H bonds (i.e., *N*-Ac-Ala-OH) in close proximity yields antioxidant-derived hydroperoxides. It is noted that the possibility of EC and EGCG to act as antioxidants by donating the benzylic C-H to AAPH-derived peroxyl radicals is established in the literature.[277,289] Scheme 46 shows hydroperoxide formation on the benzylic position of EC, but this is suggestive, and peroxidation can occur in other aliphatic positions (for all four antioxidants). Therefore, LC-MS chromatograms were this time scanned for the formation of potential hydroperoxides on all four antioxidants (Figure 52).

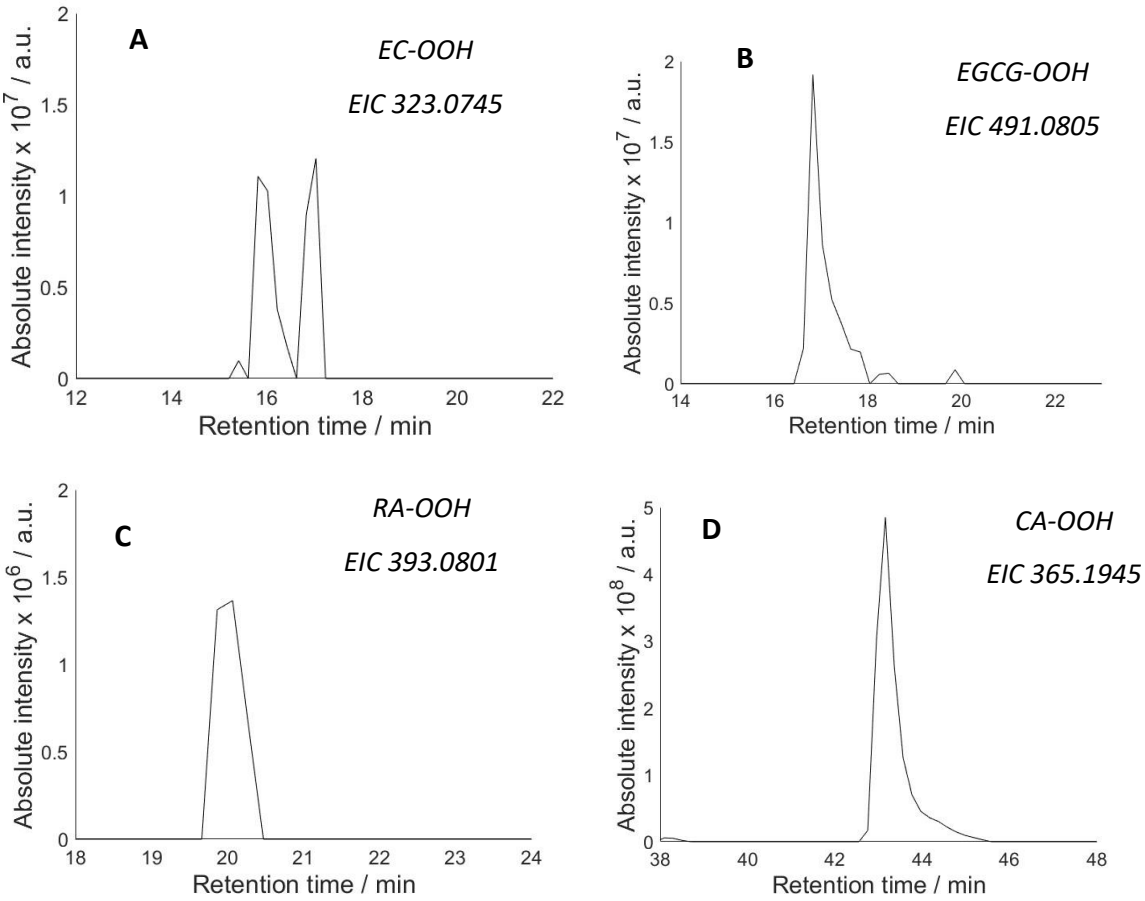

Figure 52. EIC of the $[M + H]^+$ of A) EC-hydroperoxide, B) EGCG-hydroperoxide, C) RA-hydroperoxide, and D) CA-hydroperoxide. Hydroperoxides were generated by exposure of aqueous solutions of N-Ac-Ala-OH (1 mM) to UV light (open to air) in presence of aqueous solutions of the antioxidants (1 mM) and H_2O_2 (100 mM) for 2 min.

Figure 52 shows the EICs of the $[M + H]^+$ for potential hydroperoxides generated on EC (Figure 52A), EGCG (Figure 52B), RA (Figure 52C) and CA (Figure 52D). It is evident that hydroperoxide formation is more prominent on CA, followed by EC and EGCG and lastly by RA (though as it was stated earlier RA suffers generally from poor ionisation). This is in good agreement with our previous MS data (c.f. Figures 41A-H). Indeed, it was discussed earlier that CA may react mostly by scavenging $ROO^{\bullet}$, thus generating C-centred radicals. Aliphatic C-centred radicals can be converted to hydroperoxides based on the mechanism of Scheme 46.

Another interesting point is that Figure 52A shows two peaks suggesting two different compounds with the same *m*/*z* exist in the reaction. This could either be due to the formation of two different hydroperoxides on EC, or the formation of dihydroxylated products. Indeed, as it was discussed in detail in Chapter 2, identification of hydroperoxides in these systems is not trivial, as they share the same *m*/*z* with doubly hydroxylated products (Figure 53; representative example given for EC).

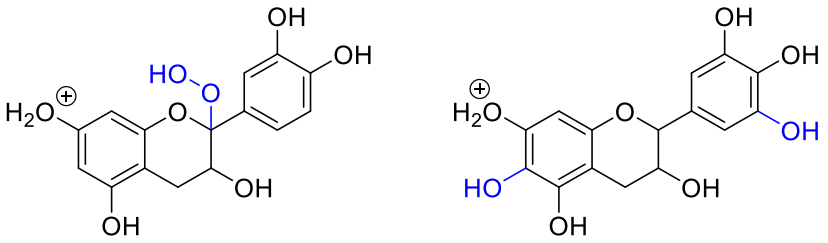

EC-hydroperoxide
(suggested structure)

$[M + H]^+$: 323.0761

EC-diol
(suggested structure)

$[M + H]^+$: 323.0761

Figure 53. Chemical structure and the $[M + H]^+$ of the EC-hydroperoxide and EC-double hydroxylation where all labile protons have been exchanged with deuteriums.

To elucidate whether peaks reported on Figure 52 are due to hydroperoxides or doubly hydroxylated products, and to distinguish between them, two different experiments were carried out. Firstly, irradiated solutions of the antioxidants were treated with $NaBH_4$ (see also Chapter 2). In presence of $NaBH_4$ any generated hydroperoxides should be decomposed *via* non-radical pathways, while doubly hydroxylated products should remain intact. Secondly, reactions were repeated in D_2O instead of H_2O and were then analysed by LC-MS using D_2O as the mobile phase (more information in the Experimental Chapter). Since hydroperoxides and doubly hydroxylated products have a different number of labile -H, this should enable their differentiation by LC-MS. The EICs of the $[M + H]^+$ of potential hydroperoxides for the four antioxidants, after $NaBH_4$ treatment are given in Figure 54.

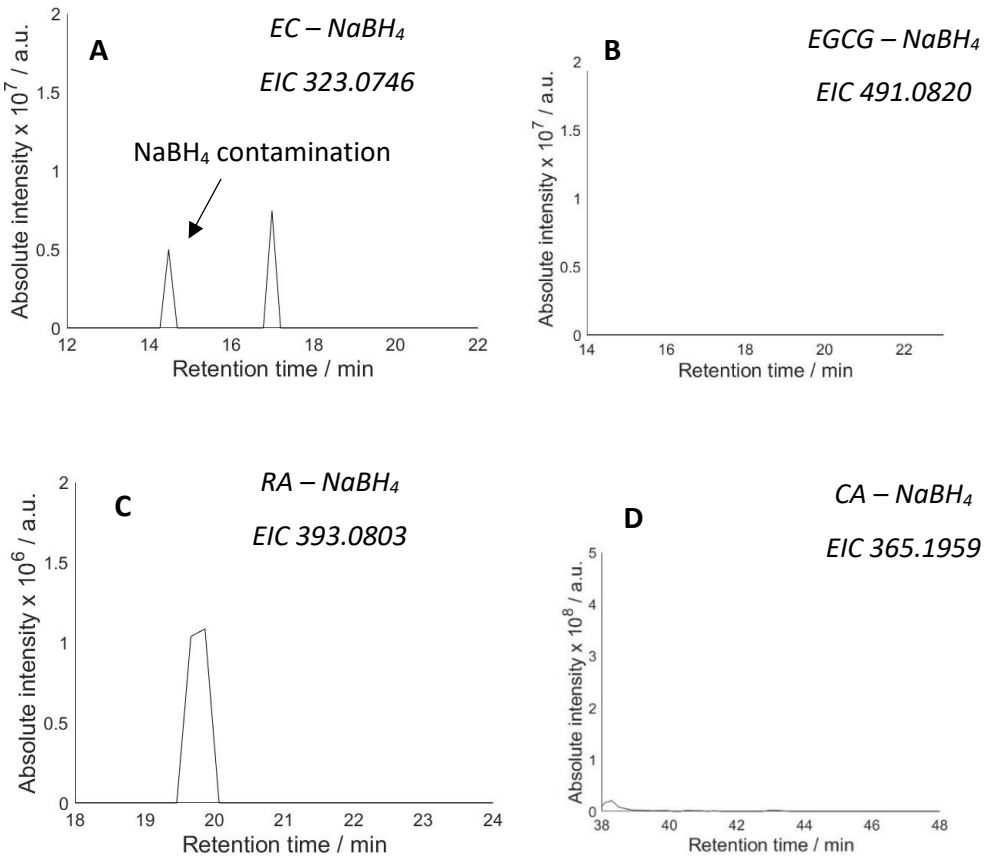

Figure 54. EICs of the $[M + H]^+$ of A) EC-hydroperoxide, B) EGCG-hydroperoxide, C) RA-hydroperoxide, and D) CA-hydroperoxide. Products were generated by exposure of aqueous solutions of N-Ac-Ala-OH (1 mM) to UV light (open to air) in presence of aqueous solutions of the antioxidants (1 mM) and H_2O_2 (100 mM) for 2 min. All EIC are after irradiated solutions were treated with $NaBH_4$ (1 mg per mL of solution; 1 h treatment).

The $NaBH_4$ experiments corroborate that for EC, EGCG and CA the aerobic $HO^{\bullet}$-mediated oxidation leads to the formation of organic hydroperoxides. Our data illustrate that for EC, $NaBH_4$ resulted in the disappearance of the first peak of Figure 54A (t = 16 min), while the second peak remained intact (t = 17 min). This is a strong indication that the peak eluting at 16 min is due to an EC-derived hydroperoxide, while the peak eluting at 17 min is likely a result of a double-hydroxylation on EC. For EGCG and CA (Figure 54B and 54D respectively), there is a complete disappearance of the peaks, confirming that they are indeed due to hydroperoxide formation. Conversely, the peak eluting at 19.5 min in the RA samples remained intact (Figure 54C), showing that is probably due to dihydroxy product and not a hydroperoxide.

To acquire more data to confirm the formation of hydroperoxides, reactions were now repeated in D_2O and analysed by LC-MS using D_2O (instead of H_2O) in the mobile phase. The EICs for the fully deuterated hydroperoxides and dihydroxy products (for all four antioxidants) are given in Figure 55.

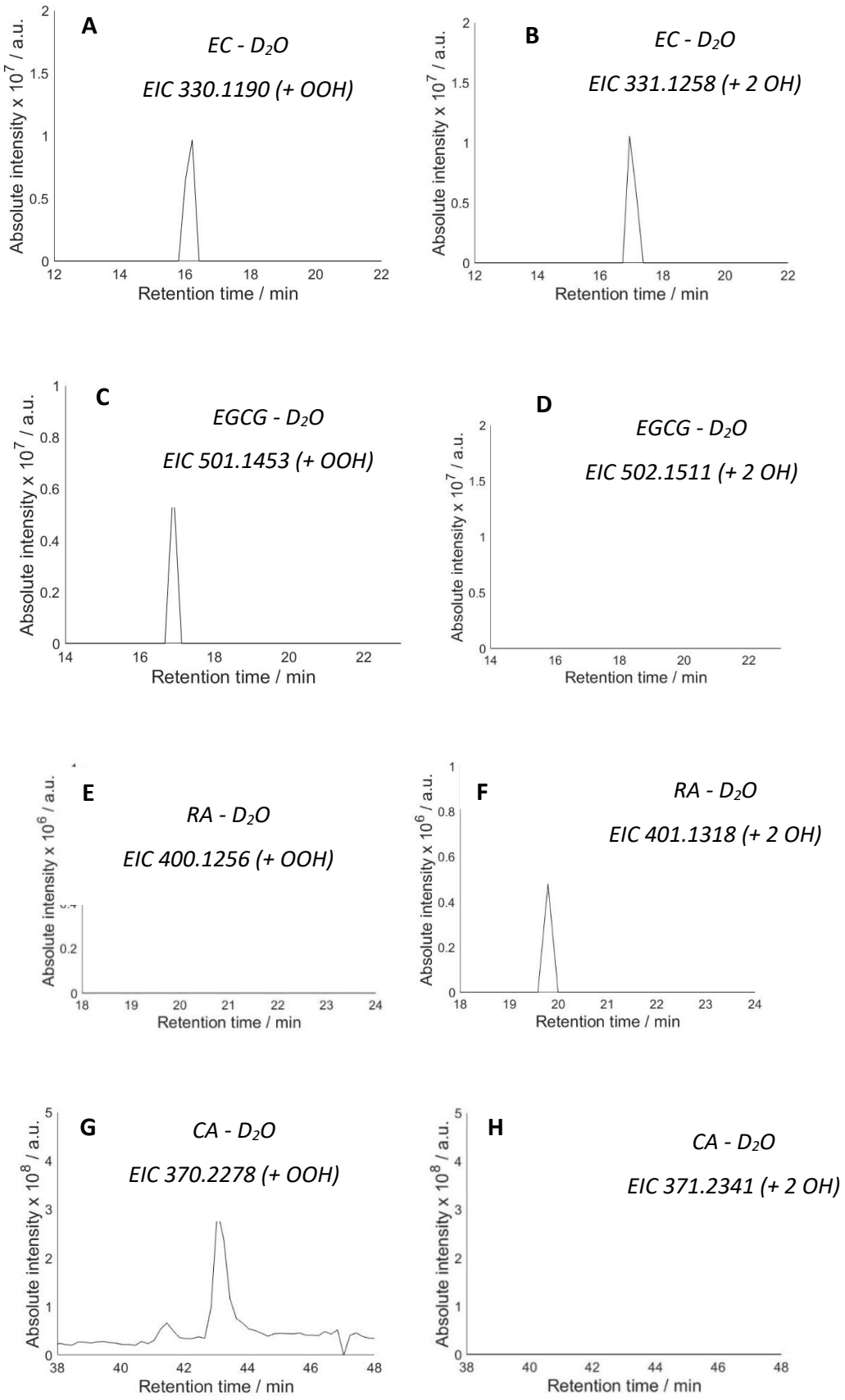

Figure 55. EICs of the $[M + D]^+$ of A) EC-hydroperoxide, B) EC-dihydroxy, C) EGCG-hydroperoxide, D) EGCG-dihydroxy, E) RA-hydroperoxide, F) RA-dihydroxy, G) CA-hydroperoxide, and H) CA-dihydroxy. Irradiations were carried out in D_2O. Products were generated by exposure of deuterated solutions of N-Ac-Ala-OH (1 mM) to UV light (open to air) in presence of deuterated solutions of the antioxidants (1 mM) and H_2O_2 (100 mM) for 2 min

In all four cases, the D_2O experiments confirmed the $NaBH_4$ treatment. Figure 55A and 55B show the EICs of the $[M + D]^+$ for the fully deuterated EC-derived hydroperoxides and doubly hydroxylated products. As predicted, the two compounds have a different number of exchangeable H, and can now be separated by LC-MS. These data are in excellent agreement with the $NaBH_4$ experiments, and further corroborate that the peak eluting at 16 min is due to hydroperoxides, while the peak eluting at 17 min is due to doubly hydroxylated product. Furthermore, in agreement with the $NaBH_4$, EGCG and CA appear to only generate hydroperoxides and no dihydroxy products (Figures 55C-D and 55G-H respectively), while oxidation of RA results in the formation of dihydroxy products but no hydroperoxides (Figure 55E and 55F).

Our analytical data here corroborate the formation of hydroperoxides in three of these antioxidants. These findings were further reinforced by $NaBH_4$ and isotope exchange experiments. It is important to note that formation of antioxidant-associated hydroperoxides, could lead to higher damage to biomolecules. As stated in Chapter 1, hydroperoxides can undergo one-electron reduction in presence of transition metals (Fenton-type reaction), releasing reactive free radicals that can accelerate the damage to biomolecules. Finally, we note that when irradiations were carried out in the presence of the antioxidants, no oxidation products on *N*-Ac-Ala-OH were identified. This highlights the efficiency of the antioxidant at reducing the oxidation of the biological target (although we have observed that *N*-Ac-Ala-OH does not ionise very efficiently in the MS, and thus, at low decomposition, oxidation products are usually not detected) .

3.11 Antioxidant capacity

Thus far, the antioxidant mechanisms of the four compounds were investigated, and degradation products were successfully identified using LC-MS. One of the main objectives of this project, was to explore the protective effect of these compounds against the oxidation of proteins. Even though the antioxidant capacity of these compounds has been investigated in the past, it is not clear how efficient they are at retarding (or preventing) the oxidation of biological targets. The ability to protect biological matter from various oxidants (e.g., $HO^{\bullet}$, $ROO^{\bullet}$) is of great importance to the haircare and cosmetic market. If these compounds are proven to be effective at reducing oxidative damage to proteins, then it can be sought to develop technologies to utilise this insight into commercial products. The next Section is focused on the oxidation of two simple amino acids induced by $HO^{\bullet}$, firstly in the presence of the four catechol-based antioxidants, and then in the presence of the rosemary extracts. We aim to monitor the degradation of the amino acids and determine whether the presence of the antioxidants reduces the rate of decomposition.

3.11.1 Isolated compounds

Here we explore the aerobic $HO^{\bullet}$-induced oxidation of two protected amino acids (Figure 56) in the presence and absence of the antioxidants. However, unlike earlier, we now focus on the degradation of the parent amino acids, rather than trying to characterise antioxidant-derived degradation products. Irradiation conditions were optimised to achieve ca. 10% decomposition of the biological targets in the absence of antioxidants (*vide infra*).

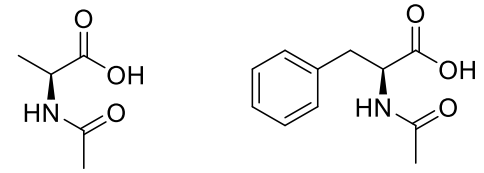

N-Ac-Ala-OH **2.6**

N-Ac-Phe-OH **3.14**

Figure 56. Chemical structures and names of the two protected amino acids used for the measurement of the antioxidant power of the four catechol-based compounds.

The two protected amino acids were exposed to HO$^{\bullet}$ for 2 min, and aliquots were taken prior to the exposure and at the end. All other experimental conditions were maintained the same as our previous studies (Scheme 45)

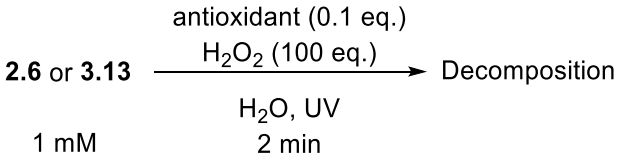

Scheme 45. Experimental conditions for the irradiations.

The concentration of the antioxidant was again set to 0.1 eq. This was done to allow a direct comparison between the decomposition of the starting substrates, and the mechanistic pathways of the antioxidant activity (based on our previous experimental findings). The concentration of the two parent substrates was determined by LC-MS analysis (similarly to the Chapter 2). Figure 57A and 57B report the % of substrate loss for the two protected amino acids.

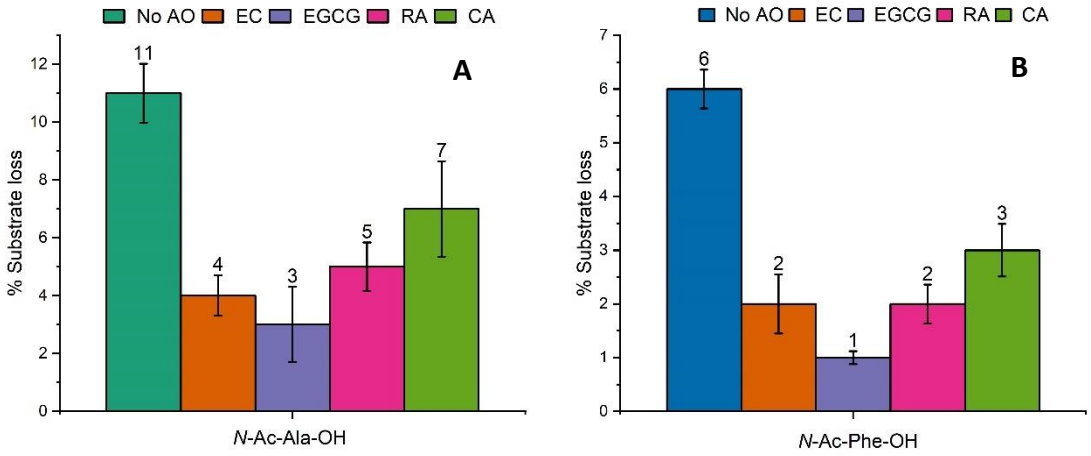

Figure 57. The % decomposition of the two substrates upon exposure of aq. solutions (all 1 mM) to UV light (open to air) for 2 min in presence of aq. H_2O_2 (100 mM), and the antioxidant (0.1 mM). Aliquots were taken before, and at the end of the irradiation, and were analysed by LC-MS. The extent of decomposition was calculated by integration of the peak area of the LC-MS peak corresponding to the starting peptide (the TIC of the EIC for N-Ac-Ala-OH). Reactions were carried out in triplicate and the results are the mean ± SE of the experiments.

The first bar in Figure 57A and 57B illustrates the % of parent substrate loss in the absence of an antioxidant (triplicate experiments). Irradiation conditions were optimised to achieve a *ca*. 10% decomposition for the parent substrates. The decomposition needs to be high enough to ensure that the effect of the antioxidants is noticeable. However, if the substrate decomposition is too high, this means that reactivity induced by secondary species can influence the overall chemistry. As such, it would be complicated to correlate the protective effect of the antioxidants with the identified oxidation products.

Two main conclusions can be drawn based on the data shown on Figure 57A and 57B. The first conclusion from the two Figures is the % decomposition of the starting substrates, with *N*-Ac-Ala-OH suffering a *ca*. 11% loss while *N*-Ac-Phe-OH almost half of that (*ca*. 6%). This outcome can be readily explained from the reactivities of the two compounds with HO$^{\bullet}$. *N*-Ac-Ala-OH is expected to react *via* HAA that ultimately leads to generation of peroxyl radicals that are known propagation species (i.e., they accelerate the damage to the starting substrate). On the contrary, it is estimated that the majority of the photogenerated HO$^{\bullet}$ react *via* addition with *N*-Ac-Phe-OH, forming stable hydroxylated products, and avoiding the formation of peroxyl radicals.[109] Hydrogen atom abstraction by HO$^{\bullet}$ from *N*-Ac-Phe-OH to generate peroxyl radical and propagate the radical chain reactions, takes place but to a smaller extent, thus explaining the smaller damage.

The second conclusion is that both amino acids suffered significantly less damage in the presence of the antioxidants (triplicate experiments). More importantly, there is a good agreement in the antioxidant activity of the compounds between the two graphs. In both cases, tea extracts (EC and EGCG) appear to, overall, be more efficient antioxidants than the rosemary extracts (RA and CA). Our work here demonstrates that in this system EGCG is the most potent antioxidant of the four, followed closely by EC and RA and lastly C, although the difference in their activity is low.

The reason for the discrepancy in the antioxidant efficiency might be related to their reaction with HO$^{\bullet}$. Our experimental data indicate that EGCG, EC and RA intercept the initiation source (HO$^{\bullet}$ scavengers) and the propagation of the chain-reactions is smaller (preventive antioxidants). This is consistent with our product analysis, where oxidation of EGCG, EC and RA afforded the hydroxylated products in higher abundance. Conversely, CA acts as a chain-breaking antioxidant (i.e., quenching the propagating radicals ROO$^{\bullet}$) thus showing lower antioxidant capacity. It is important to clarify that the conclusion that preventive antioxidants outperform chain-breaking

antioxidants can only be made for this system. In other systems where the flux of the propagating ROO• may be higher, chain-breaking antioxidants might prove to be more effective.

3.11.2 Comparison with literature redox assays

Our next goal was to see how the performance of the four antioxidants compares with previous literature, and with well-established methods. The ORAC assay was first introduced in 1993, and has since become one of the most reliable protocols for the measurement of the antioxidant capacity of a compound.[293] The assay measures the ability of the antioxidant to donate a hydrogen to a ROS (usually ROO•, generated by thermal decomposition of azocompounds such as AAPH; Scheme 46), and the results are reported as ORAC units, where 1 ORAC unit equals the net protection produced by 1 µM of Trolox (a water soluble analogue of vitamin E).

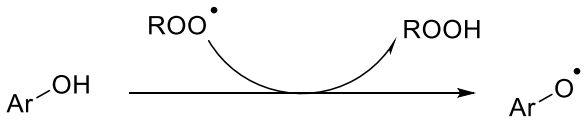

Scheme 46. Basic principle of the ORAC assay. Reaction between an antioxidant and a transient radical. The antioxidant donates a hydrogen to peroxyl (or other) radicals, generating a hydroperoxide and a stable antioxidant-derived radical. A more facile hydrogen transfer equates a higher ORAC score, which in turns, equates a more potent antioxidant.

High ORAC score equates a more facile hydrogen donation, and the higher the ORAC score the more efficient is the antioxidant (although antioxidants can also act *via* other mechanisms such as electron transfer and metal chelators which are measured by other assays). Procter and Gamble has already tested these four compounds with the ORAC assay, and their findings are reported in Figure 58 (unpublished data).

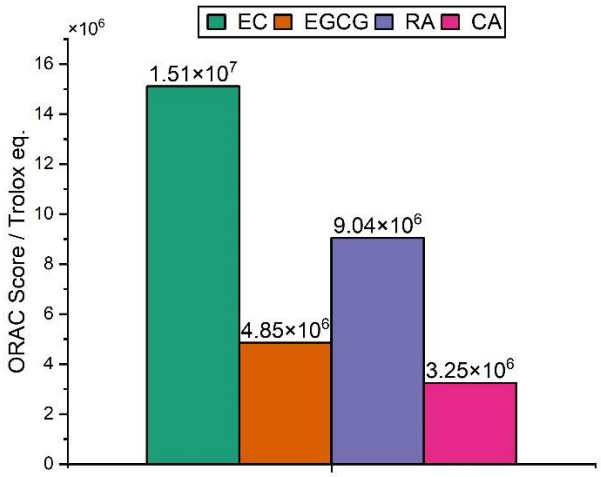

Figure 58. ORAC Score of the four antioxidants used in this work. Data were obtained (with permission) from P&G and are the results of single experiments. Unpublished data.

Data on Figure 58 support the conclusion that EC is the most efficient antioxidant in the ORAC assay, followed by RA, then EGCG and lastly CA. These data are in reasonable agreement with our findings as EC outperforms RA which in turn, outperforms CA. The biggest discrepancy between the two methods is seen for EC and EGCG. In our method EGCG proved to be the most efficient of the four antioxidants, whereas in the ORAC assay EC scored 3 times higher. This is however not surprising, as the methods measure different antioxidant mechanisms ($ROO^{\bullet}$-mediated HAA vs $HO^{\bullet}$ addition to the aromatic rings). More literature research further confirms that EC is more efficient antioxidant than EGCG in the ORAC assay,[285,294] however, there are documented examples where results from ORAC assays do not agree with other $HO^{\bullet}$-scavenging assays.[273]

Our experimental findings on the $HO^{\bullet}$-induced oxidation of two protected amino acids, demonstrate that oxidative damage is reduced significantly in the presence of the antioxidants. However, consumer products usually contain extracts (not isolated compounds), and therefore, it is instructive to study how extracts behave as antioxidants. Not surprisingly, research in this field is rich, with multiple examples where botanical extracts have been categorised based on different assays.[295–298]

3.11.3 Rosemary extracts

Tea and rosemary extracts contain a large variety of compounds, and have been linked with skin, scalp, and hair benefits from UV exposure.[296,299–301] Procter and Gamble has supplied us with 6 different rosemary extracts. Each extract contains a large variety of compounds, but the main active compound is either RA or CA (in different concentrations).

Mechanistic investigation of the extracts is not trivial, as there are too many compounds, and product analysis becomes challenging. Therefore, this study is limited to determining how the rosemary extracts reduce the HO•-mediated oxidation of *N*-Ac-Ala-OH and *N*-Ac-Phe-OH. Aqueous solutions of the two protected amino acids were exposed to UV light in the presence and absence of the 6 rosemary extracts (experimental conditions identical to Scheme 47). Irradiations lasted for 2 min, and the % decomposition of the starting substrate at the end of the irradiation is given in Figure 59.

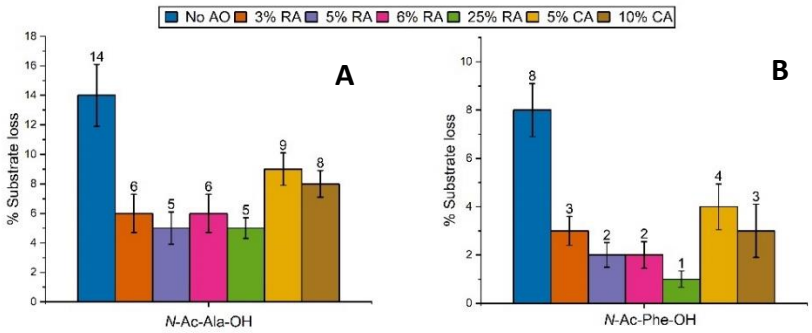

Figure 59. The % decomposition of the two substrates upon exposure of aq. solutions (all 1 mM) to UV light (open to air) for 2 min in presence of aq. H_2O_2 (100 mM), and the antioxidant. Aliquots were taken before, and at the end of the irradiation, and were analysed by LC-MS. The extent of decomposition was calculated by integration of the peak area of the LC-MS peak corresponding to the starting peptide (the TIC of the EIC for N-Ac-Ala-OH). Reactions were carried out in triplicate and the results are the mean ± SE of the experiments.

In good agreement with the isolated RA and CA, all 6 of the extracts exert a protective effect on the aerobic oxidation of the two starting substrates (triplicate experiments). We note that the extracts contain different concentrations of the two active compounds (RA and CA). In order to enable a direct comparison between the isolated compounds and the extracts, it was ensured that in each case the RA and CA content was the same as our previous reactions (Section 3.11.1).

As expected, the decomposition of *N*-Ac-Ala-OH is higher than *N*-Ac-Phe-OH (*vide supra*). The botanical extracts containing RA appear to be more efficient than the ones containing CA, consistent with RA being a better antioxidant than CA as demonstrated for the two isolated compounds in Section 3.11.1 (although the differences are small). It is important to reiterate that while the main active compounds of these extracts is RA or CA, each extract contains a range of different compounds that could act as antioxidants and reduce the oxidative damage of biomolecules. Two representative flavonoids that were identified by LC-MS to be present in the extracts in high abundance and have known antioxidant properties are presented in Figure 60.[302,303]

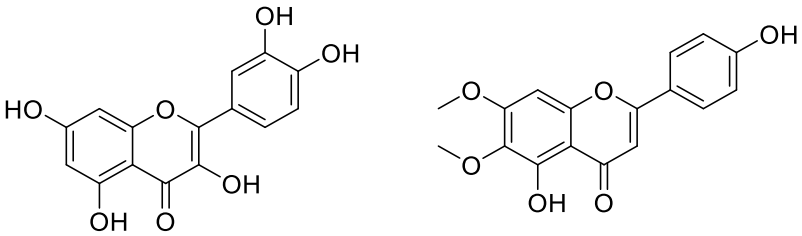

Quercetin Cirsimaritin

Figure 60. Chemical structures of quercetin and cirsimaritin. Both of these compounds have received attention for their antioxidant properties and are found in the rosemary extracts used in this study.

Therefore, the results shown on Figure 59A and 59B might be due to varied concentrations of the active compounds, or even different active compounds acting synergistically to enhance their individual action. Indeed, there are documented examples where two antioxidants act together to reduce the consumption of lipids or proteins.[73] The knowledge we obtained here can be furthered by P&G by performing more tests and assays in these extracts in order to determine whether they can be useful on protein protection, and how they can be implemented in consumer products.

3.12 Chapter 3: Conclusions

The beneficial effects of botanical extracts in simplified systems, have been well-researched in the literature. Flavonoids show promising antioxidants properties. Here we were able to explore the antioxidant potency of four catechol-based compounds found in tea and rosemary extracts, in a model system that mimics the hair environment. The mechanisms of action were investigated by studying the $HO^{\bullet}$-mediated oxidation of *N*-Ac-Ala-OH. In agreement with literature precedent, the major predicted degradation products were, in all cases, a hydroxylated derivative, and a quinone. Whether hydroxylation or formation of quinone prevails, was discussed and it was tentatively linked to the antioxidant mode of action (preventive vs chain-breaking).

Furthermore, MS data suggest that peroxidation of EC, EGCG and CA occurs. A peroxidation mechanism was proposed that proceeds *via* the HAA by either $HO^{\bullet}$ or $ROO^{\bullet}$ from the aliphatic fragment of EC, EGCG and CA. Hydroperoxide formation was further reinforced by $NaBH_4$ and isotope exchange experiments. To our knowledge, this is the first documented example of hydroperoxide formation in these compounds.

The antioxidant capacity of the four antioxidants was determined by following the aerobic $HO^{\bullet}$-induced oxidation of two protected amino acids by LC-MS. All antioxidants provided significant reduction of the starting substrate decomposition, with EC and EGCG performing better than RA and CA (and our data are in good agreement with previous literature studies). This outcome was attributed to their respective reactivity with $HO^{\bullet}$ (*vide supra*). It was also demonstrated that rosemary extracts (as opposed to isolated compounds) are capable of significantly reducing the rate of biological substrate degradation. This result was particularly important as it can be followed up by more detailed analysis by P&G, to discover new extracts that can be implemented in products to deliver higher consumer benefits. It was already discussed, and it is worth reiterating, that while antioxidants show promising results in this system, in real-life scenarios (e.g., use in shampoos and conditioners) it is complicated to predict their effect., and more research is required to draw reliable conclusions.

Chapter 4: Detection of biological radical intermediates by mass spectrometry

4.1 Introduction

Protein oxidation, which was covered in detail in the previous Chapters, is governed by radical chain reactions. This involves protein oxidation in biological systems,[59,90,135] but also in the hair environment.[9,28,304] However, the characterisation of intermediate biological radicals remains elusive for one main reason, that is their high reactivity. Due to their reactive nature, high steady state concentrations are usually not possible, and therefore their detection becomes challenging. In order to confirm their role in a system, often chemists have to rely on the end-products or by-products of the reactions that are thought to be radical-derived.[305] In turn, this helps them draw sensible reaction pathways that involve radical chain reactions. Therefore, detection of free radicals is important as it can provide valuable mechanistic and kinetic information on different chemical systems.

In general, two main radical detection techniques have found significant success in the characterisation of biological radicals; these are electron paramagnetic resonance (EPR) spectroscopy (also known as electron spin resonance, ESR),[306,307] and the spin-trapping method.[308] The next two Sections will briefly discuss the principles, advantages, and limitations of these two techniques in the detection of biological radicals.

4.2 Main detection methods for biological radicals

4.2.1 Electron paramagnetic resonance

EPR is a powerful technique that allows direct detection of free radicals in complex systems. The underlying principles of the technique have been covered in detail in a range of different textbooks and reviews.[306,307,309,310] Radicals generated in biological systems are usually short-lived, and do not accumulate to high concentrations. Since EPR has a relatively poor sensitivity in (μM) in the respect to the steady-state concentration of biological radicals, not many species can be successfully characterised by EPR. Thus, direct detection of biological radicals by EPR is only really possible for long-lived radicals that can accumulate to high concentrations, such as tyrosyl radicals, semiquinone radicals and such.[306]

One technique that has found considerable success in the detection of biological radical is the detection using freeze quenching EPR.[311] In this method, reactions are frozen in liquid nitrogen, and are analysed by EPR. The immediate freezing of the samples results in the slower decay of radicals, thus multiple EPR spectra can be recorded to obtain information about the radicals in the system. Indeed, the mechanisms of many enzymatic reactions, that involve the generation of radicals, have been successfully elucidated by freeze-quenching EPR.[311] However, data obtained by this technique can be limited in the sense that radicals should still have a reasonably high lifetime, and transient intermediates might not survive the freeze-quenching process.

The detection of transient radicals by EPR, has become possible with the development of continuous flow systems. In this technique solutions are mixed in the continuous flow system, and radical species are generated continuously. This enables their detection by EPR at ambient temperature. This method has been used for the detection of radicals generated in proteins.[312,313] Continuous flow EPR is a very costly technique, as often large volumes and high concentrations of reagents are needed.

The most important disadvantage of EPR however remains. That is the low detection limit, that usually prohibits the characterisation of radicals in real biological systems (as radical concentration is low). To overcome this limitation, the chemical community has developed over the years other techniques to allow detection of radicals in biological systems. The most popular and specific tool for the detection of radicals in biological systems today, is the spin trapping method,[308] and is discussed in the following Section.

4.2.2 Spin trapping

Spin trapping is an indirect detection method in which the reactive free radical (R•) is trapped *via* an addition reaction (Scheme 48) and is converted to a more stable radical that is detectable by EPR.[308] Ideally, the information gained from the new radical, should allow identification of the initial radical. The most often used spin traps in biological systems are nitrone spin traps, and the initial radical is converted to a long-lived nitroxide (Scheme 47).

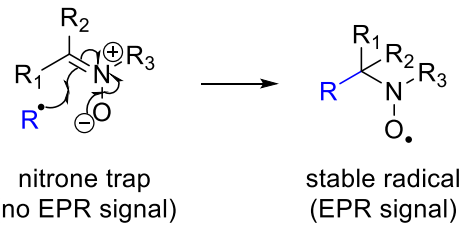

Scheme 47. Reaction of a short-lived radical (R•) with a nitrone spin trap, forming longer-lived nitroxyl radical adduct. The nitroxyl adduct is detectable by EPR spectroscopy. As the initial nitrone trap does not produce an EPR signal, very high concentrations can be used.

Since the initial spin trap (nitrone trap) does not produce an EPR signal, very high concentrations (mM – M) are usually used to ensure a sufficient number of radicals are captured (in order to produce a strong EPR spectrum).[314] This is particularly important as it essentially overcomes the sensitivity issues the EPR technique is facing. Spin trapping is probably the most popular method for detection of radicals in biological systems and has been used with reasonable success for the detection of radicals during the oxidation of aqueous solutions of peptides, proteins, and DNA in both isolated but also complex systems.[132,133,139,314]

However, spin trapping has its limitations. Probably the most important issue with the spin trapping technique is the unwanted side reactions. For instance, nucleophiles present in the system can attack the double bond of the spin trap (the Forrester-Hepburn mechanism), producing a hydroxylamine.[315] Subsequent one-electron oxidation of the hydroxylamine can produce the same nitroxide as the initial radical reaction with the spin trap, therefore leading to false positive results.

In addition, EPR and spin trapping both suffer from one important drawback; that they offer limited structural information for the initial radical.[309] This is because information can only be gained about the chemical environment in close proximity to the unpaired electron. As such, full characterisation of unknown radical species with complex structures is dramatically more challenging. Continuous research in the spin trapping method led to the discovery of a new method for radical trapping in biological systems, called the immuno-spin trapping.[316,317]

Immuno-spin trapping combines the selectivity of the spin trapping with the sensitivity of the analytical techniques (e.g., MS). It was observed that the biological radical nitroxide adduct overtime converts to a a stable nitrone adduct, which can now detected as a stable molecule using anti-bodies.[313,314]

Since the discovery of the immuno-spin trapping there have been multiple documented examples where the technique has been used to identify radicals generated in proteins, DNA, lipids, and other macromolecules.[316–320] Today immuno-spin trapping has been described as the principal technique to detect biological radicals.[316,317]

However, immuno-spin trapping faces its own challenges. The spin trap that is used has been reported to react with other reactive species in the system (e.g., ONOOH), and this can significantly affect the concentration of the spin trap, and by extension its ability to react with protein radicals.[321] Finally, while immuno-spin trapping has been used with reasonable success in the detection of protein radicals in models and purified proteins, the detection of protein radicals *in vivo* remains a challenge.[316,319]

A need exists for readily applicable methods of detecting and identifying low concentrations of free radicals (below the EPR detection threshold), and for methods that are applicable to a wide range of chemical reactions and can more effectively characterise heteroatom-centred radicals. A new trapping technique designed to solve many of the existing issues of these techniques, was recently developed within our group.[165,166] The method has already been successfully applied to different areas of chemistry (synthetic, biological, and atmospheric).[167] The next Section will briefly describe the concept of the new technique, and preliminary results for trapping biological radicals.

4.3 New concept of radical trapping

A new indirect approach for capturing and characterising short-lived radical intermediates was developed in the past years in our group (Scheme 48).[165,166] In a way, this method builds upon the spin trapping method.

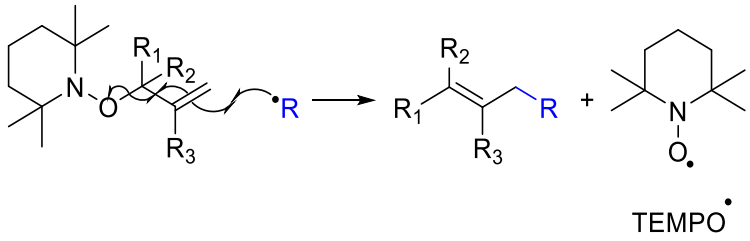

Scheme 48. Reaction between a short-lived radical (R•) and an alkene-based radical trap containing TEMPO• as a leaving group, forming a persistent radical and non-radical product. This non-radical product can then be characterised by analytical techniques (e.g., NMR, MS) allowing R• to be identified. R_1, R_2 and R_3 can be functionalised to suit the radical system being studied.

In this method a new class of alkene-based radical traps is used, possessing a good radical leaving group (usually TEMPO•). This approach aims to utilise the unparalleled reactivity of most short-lived radical intermediates with alkenes (typical k_{add} ~ 10^6 – 10^7 M^{-1} s^{-1}),[322,323] similarly to the addition of radicals to nitrone spin traps.[308,309] The radical leaving group is present in the allylic position, which enables a rearrangement and is released as a persistent radical. The trapping results in the generation of a stable non-radical product (containing the initial radical) that can be studied by highly sensitive techniques such as DI-MS and LC-MS (similarly to the immuno-spin trapping method). All alkene-based traps that were synthesised by previous PhD students working in the Chechik group used TEMPO• as their leaving group.[165–167] The alkene trap **4.1** that was used for trapping and detection of biological radicals in our work here is given in Figure 61.

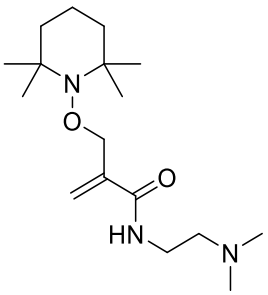

4.1

*Figure 61. Molecular structure of the radical trap **4.1** used for the trapping and detection of biological radicals.*

The alkene trap **4.1** used was designed to suit reactions in aqueous media.[166] The trap was easily accessed after a 3-step robust synthesis (reported yields > 70% for all individual steps), starting from relatively cheap commercially available starting materials which enabled its large scale (> 2 g) synthesis (more information under the Experimental Chapter). Furthermore, the amino group (which upon reaction is present in the trapped adduct) ionises well in the positive ion mass spectrometry and can offer high sensitivity even when trapped adducts are present in very low concentrations.

4.4 Project outline and aims

In this work we attempt to use the new trapping method that was developed in the Chechik group (Section 4.3) to characterise transient biological radicals. A previous PhD student (Peter Williams) in the Chechik group employed radical trap **4.1** to study the oxidation of simple dipeptides for the first time.[166] His work was focused on the detection of radical intermediates formed during the HO•-induced oxidation of aqueous solutions of *N*-Ac-Gly-Gly-OH and *N*-Boc-Gly-Gly-OH (Scheme 49).

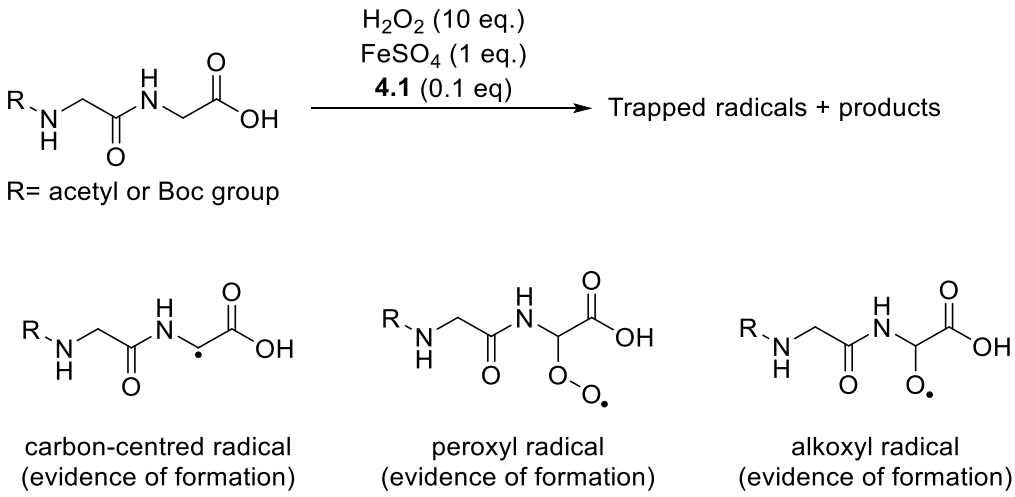

Scheme 49. Reaction conditions for the trapping and detection of HO•-derived radicals on simple dipeptides. Oxidation products and trapped adducts were detected by MS. The structures that are shown are suggestive, and no further elucidation of their structure was possible.

Hydroxyl radicals were generated *via* Fenton chemistry, and data were analysed by DI-MS. For both dipeptides, the *m*/*z* corresponding to potential carbon-centred, peroxyl and alkoxyl radicals were detected in the MS spectra.[166,167] Scheme 49 shows the initial radicals predicted to be formed following a HAA by HO• from the $^{\alpha}$C-H of glycine. In addition, more trapped radicals were identified, resulting from RO• fragmentation on the parent substrate (Figure 62).

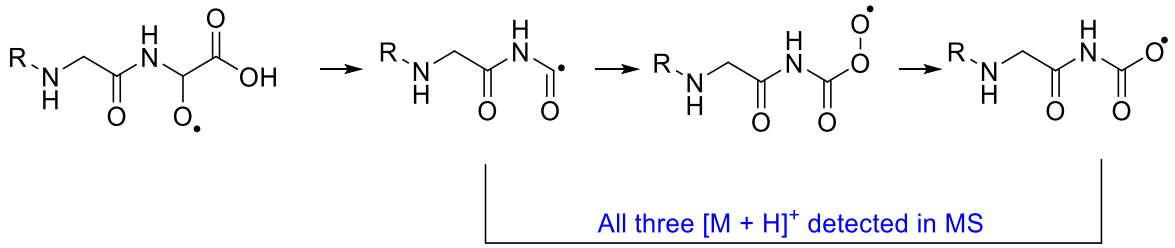

Figure 62. RO• fragmentation gives rise to a transient C-centred radical. Subsequent O_2 addition produces a peroxyl radical, and eventually an alkoxyl radical (via hydroperoxide decomposition). Evidence for the formation of all radicals shown were obtained by MS. The structure that are shown are suggested, and the initial HAA could take place from a different C-H.

This system was used as a simplified oxidation system to explore whether the trapping of biological radicals with **4.1** is feasible, and the two dipeptides were used as protein mimics. The detection of radicals that could only be formed following an initial HAA from the glycine $^{\alpha}$C-H, demonstrated that biological radicals can indeed be trapped by this new method. However, Peter's research focus was to develop this methodology further, and investigate its scope of application in different chemical systems. As such, the detection of biological radicals was not examined further. For instance, some of the predicted radical adducts can have the same $[M + H]^+$ (e.g., a ROO• and a RO• + HO), and advanced techniques would be required to differentiate between the two species.

Our principal aim was to build on Peter's work, and further explore this new approach of radical trapping in peptide oxidation. Oxidation of peptides and proteins in biological systems can occur *via* different mechanisms (e.g., HAA, ET) depending on the oxidant. By trapping and characterising biological intermediate radicals, we believe we can obtain important mechanistic information, and provide further evidence for literature proposed reaction pathways. One of our most important goals was to differentiate trapped adduct with the same $[M + H]^+$, but different chemical structures. Three different oxidation systems were explored.

Our investigation begins with the well-established peroxynitrite-mediated oxidation of *N*-Ac-Gly-Tyr-OH (Section 4.5). This system was used to test the sensitivity of our detection method in a system where the generated radicals are only predicted to be present in very low steady state concentrations (*vide infra*). Next, we studied the HO•-induced oxidation of three biological targets (Section 4.6). Unlike previous work carried out by Peter Williams, here HO radicals were generated *via* H_2O_2 photolysis, in order to explore the metal-free HO•-mediated oxidation of peptides.

Moreover, in Peter's work the HO radicals participated exclusively in HAA reactions with the chosen peptides (Scheme 50). Here, we employed biological targets to probe different reaction pathways with HO radicals; i.e., hydrogen atom abstraction, addition, and electron transfer, that lead to the generation of different intermediate radicals. Finally, we investigate the oxidation of peptides facilitated by transient radicals arising from the decomposition of terpene-derived hydroperoxides (Section 4.7). This system was chosen in order to investigate whether our new radical trapping technique can be used to systems that are closer to real-life scenarios.

4.5. Peroxynitrite-induced oxidation

4.5.1 Peroxynitrite introduction

The reactivity of selected amino acids (e.g., tyrosine) with selected oxidants (e.g., $O_2^{\bullet-}$, $HO^{\bullet}$) has already been discussed (Chapter 1). One of the biologically relevant oxidants that was not discussed, and is generated continuously *in vivo* is peroxynitrite ($ONOO^-$).[324] Peroxynitrite is a weak acid, and at physiological pH is in a rapid acid-base equilibrium with its conjugate acid (ONOOH; pK_a = 6.8).[325] Peroxynitrite is formed readily *in vivo* by the diffusion-controlled recombination of nitric oxide ($^{\bullet}NO$) and $O_2^{\bullet-}$ (Scheme 50).[326]

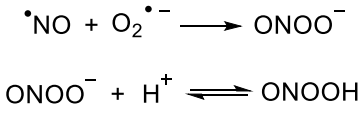

Scheme 50. In vivo formation of peroxynitrite anion ($ONOO^-$), and the acid-base equilibrium between $ONOO^-$ and its conjugate acid (ONOOH).

Peroxynitrous acid (ONOOH) is a powerful oxidising and nitrating agent capable of inducing damage to biomolecules both directly, *via* two-electron oxidation reactions, and indirectly *via* one-electron reactions of radicals ($^{\bullet}NO_2$ and $HO^{\bullet}$), arising from the homolysis of the -O-O- bond (Scheme 51).[327]

Scheme 51. Homolysis of the -O-O- bond in ONOOH, yielding transient radicals that are capable of reacting with biomolecules to inflict protein damage.

Homolytic cleavage of the -O-O- bond is reported to be fast with a reported value of k = 0.9 s^{-1} at 37 °C and pH 7.4.[328] Of the total flux of the transients $^{\bullet}NO_2$ and $HO^{\bullet}$, *ca*. 70% recombines inside the cage, whilst the remaining 30% escapes the cage and undergoes reactions with biomolecules.[329] Peroxynitrite-derived radicals react more readily with sulfur containing amino acids (cysteine and methionine), and aromatic containing amino acids (tryptophan, tyrosine, phenylalanine and histidine). The overall reactivity of ONOOH (including reactions with different amino acids) is complicated and will not be discussed any further here (for a detailed description see ref 325).[325]

An important aspect of its activity is tyrosine nitration, which results in the alteration of protein function.[324] Reaction of ONOOH with tyrosine **4.2** is the most specific and well-understood oxidative modification induced by ONOOH (Scheme 52).[324,325]

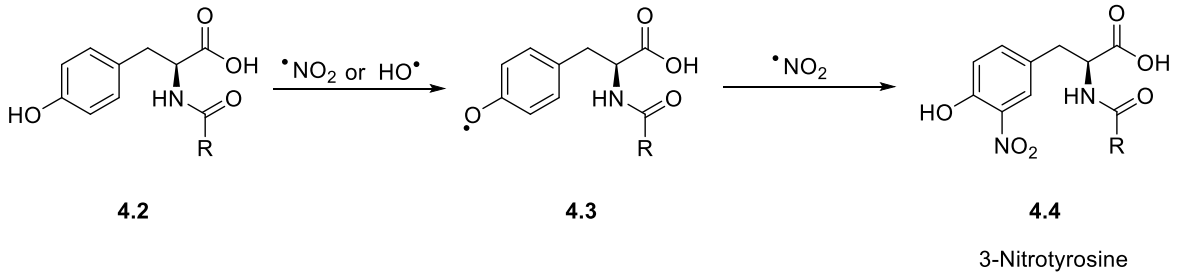

Scheme 52. Free radical oxidation of tyrosine to 3-nitrotyrosine. Tyrosine can be oxidised to the tyrosyl radical by either $^{\bullet}NO_2$ and $HO^{\bullet}$, and subsequent reaction with $^{\bullet}NO_2$ produces the stable non-radical product 3-nitrotyrosine.

Formation of the intermediate tyrosyl radical **4.3** can be either $^{\bullet}NO_2$-assisted (formally an ET; $k \sim 10^5$ M^{-1} s^{-1}), [330] or $HO^{\bullet}$-assisted (*via* addition and subsequent H_2O-elimination; see Section 1.7.4.2). Radical-radical reaction between tyrosyl radical and $^{\bullet}NO_2$ is near the diffusion limit ($k \sim 10^9$ M^{-1} s^{-1}) and yields the stable 3-nitrotyrosine product **4.4**.[329] In general, generation of 3-nitrotyrosine is a fast, selective and high-yielding reaction, and its detection was used as a footprint for the ONOOH-mediated nitration of tyrosine (although more recent studies have shown that it can also form *via* ONOOH-independent pathways).[325]

Perhaps unsurprisingly, other products that are formed to a noticeable extent during the ONOOH-mediated oxidation of tyrosine are dimeric species (dityrosine) and hydroxylated species (DOPA), both from the tyrosyl intermediate radical (see Introduction; Section 1.7.4.2). The dimerisation of two tyrosyl radicals, and the radical-radical reaction of tyrosyl radical with $HO^{\bullet}$ are both near the diffusion limit.[54,56] Lastly, due to the high stabilisation of the tyrosyl radical O_2 addition is supressed even in aerobic systems.[325] Based on the above data, the ONOOH-facilitated oxidation of tyrosine,

initially produces a phenoxyl radical, that can follow three different pathways (all near the diffusion controlled limit). Therefore, we believed that this system can be used as a proof-of-principle study to demonstrate that our radical trap **4.1** can capture radical intermediates even when competing reactions are near the diffusion limit.

4.5.2. Preliminary results and optimisation

Initial experiments were carried out using equimolar concentrations of the radical trap **4.1** and *N*-Ac-Gly-Tyr-OH, while ONOOH was used at a 5-fold excess (Scheme 53). Peroxynitrite was synthesised according to well-established literature protocols using isoamyl nitrite and H_2O_2, with any residual H_2O_2 removed by passing through a column containing MnO_2 (more details under the Experimental Chapter).[331] Stock solutions of ONOOH were stored frozen immediately after synthesis, and used immediately after defrosting, with unused material discarded.

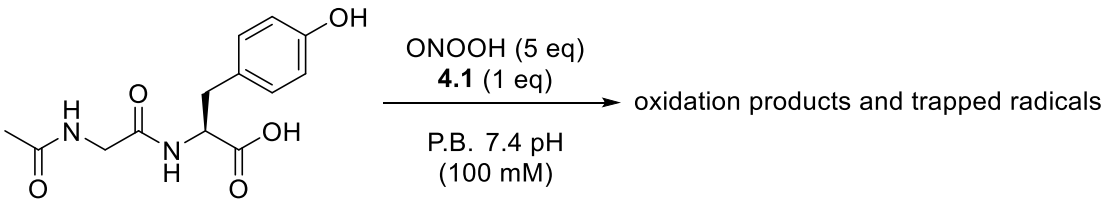

N-Ac-Gly-Tyr-OH

2.4

10 μM

Scheme 53. Initial reaction conditions for the ONOOH-facilitated oxidation of N-Ac-Gly-Tyr-OH. A stock ONOOH solution was thawed the day of the reaction and was used immediately. All reactions were frozen until analysis by LC-MS.

As the concentration of the starting substrate is low (i.e., μM), all reactions were analysed undiluted by LC-MS. DI-MS could not be used in this work for two reasons. Firstly, reactions were run in phosphate buffer, and injections of non-volatile buffers could lead to contamination of the MS instrument. However, LC-MS analysis requires a very small amount to be injected (1 μL in this case), and so the amount of phosphate buffer that is injected to the MS instrument is negligible. Secondly, the radical trap **4.1** ionises very strongly in the MS, and high concentrations (> 1 μM) should be avoided as they can lead to instrument contamination. This can be avoided in LC-MS by introducing a "waste-segment" in the separation method that filters out the unreactive trap (more details under the Experimental Chapter). This LC-MS feature proved to be valuable for our studies, as it enabled high trap concentrations to be injected in order to collect experimental data (*vide infra*).

Investigation of the chromatograms revealed that the major expected products of the reaction (i.e., nitrotyrosine **4.5** and DOPA **4.6**) are present (Figure 63; shows the expected products and the LC-MS chromatograms as the EIC).

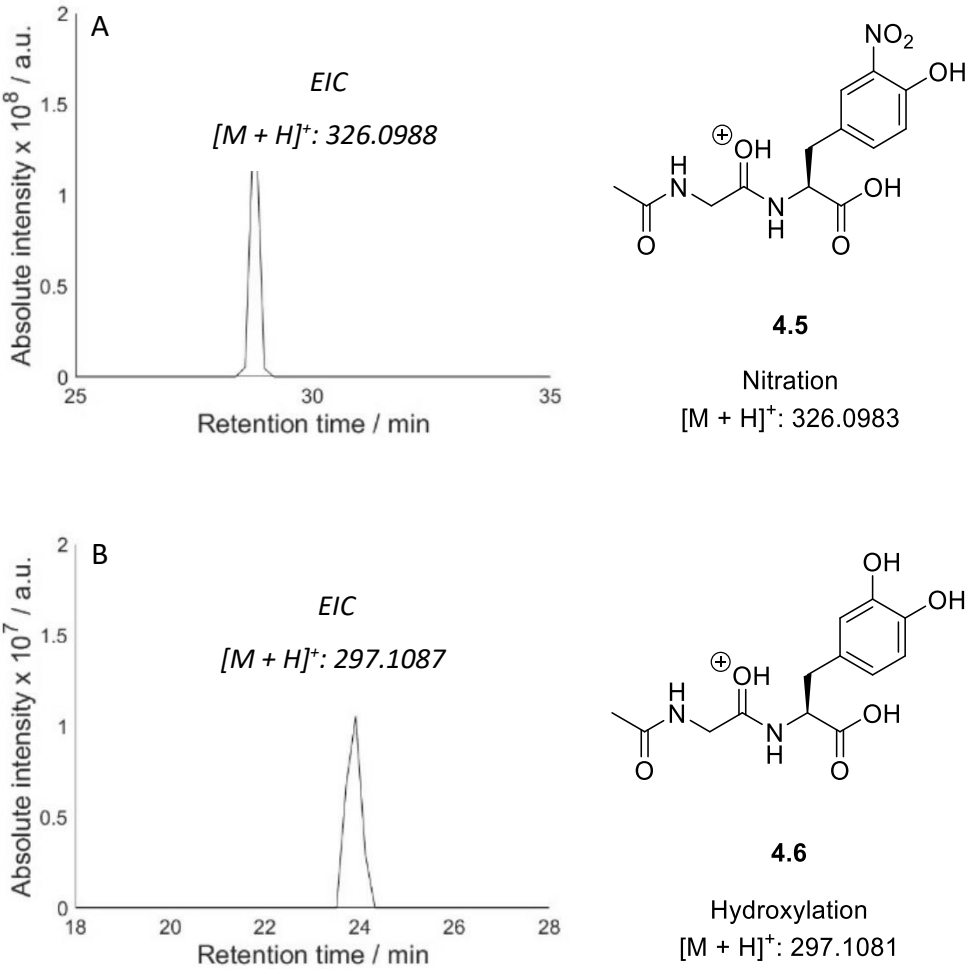

Figure 63. Chemical structures and representative extracted ion chromatograms (EIC) of the main oxidation products. A) m/z of 326.0988 (nitration of N-Ac-Gly-Tyr-OH), and B) m/z 297.1087 (hydroxylation of N-Ac-Gly-Tyr-OH) acquired by MS from the ONOOH-mediated oxidation of N-Ac-Gly-Tyr-OH. Chemical structures are shown as the protonated adducts. Reactions were carried out in open air.

Figure 63 shows the EICs of the $[M + H]^+$ for the nitration (63A) and hydroxylation (63B) products. While intensity in the MS does not necessarily equal higher abundance in the reaction, nitration is expected to be the predominant oxidation product. This is because $^{\bullet}NO_2$ is generally a long-lived radical that in this system primarily reacts with tyrosyl radicals to afford the nitrated product. On the contrary, HO radicals are unstable and can participate in more reactions. As such, overtime $^{\bullet}NO_2$ are expected to accumulate in the system and outcompete $HO^{\bullet}$.

No dimeric species or trapped adducts were identified when reactions were run under these conditions. The absence of trapped adducts is however not so surprising. As tyrosyl radicals react with second order rate constants near the diffusion limit with $^{\bullet}NO_2$, and $^{\bullet}NO_2$ is a stable radical (*vide supra*), it is likely that the majority of the generated tyrosyl radicals are converted to the nitrotyrosine-adduct. Therefore, in order to successfully trap and detect trapped tyrosyl radicals, the concentration of ONOOH must be reduced (to reduce the production of $^{\bullet}NO_2$) and the concentration of trap **4.1** must be increased (to outcompete $^{\bullet}NO_2$). Taking this into account, the relative ratios of *N*-Ac-Gly-Tyr-OH: ONOOH: **4.1** were varied in order to achieve optimised experimental conditions that would allow the detection of a tyrosyl trapped radical.

After a series of experiments screening various ratios between the reactants, optimised results were obtained when *N*-Ac-Gly-Tyr-OH: ONOOH: **4.1** were used in a 1:2:6 ratio. The initial concentration of *N*-Ac-Gly-Tyr-OH was increased from 10 to 50 µM to get higher concentration of oxidation products and trapped radicals, which in turn would allow an easier detection in the MS analysis. Investigation of the LC-MS chromatograms revealed that again the major predicted reaction products (i.e., nitration and hydroxylation) were evident (data not shown). Pleasingly, changing the ratios between the reactants and increasing the concentration of the radical trap resulted in the detection of a trapped tyrosyl radical **4.7** in relatively high abundance (10^7; Figure 64 shows the chemical structure of the trapped adduct and the EIC).

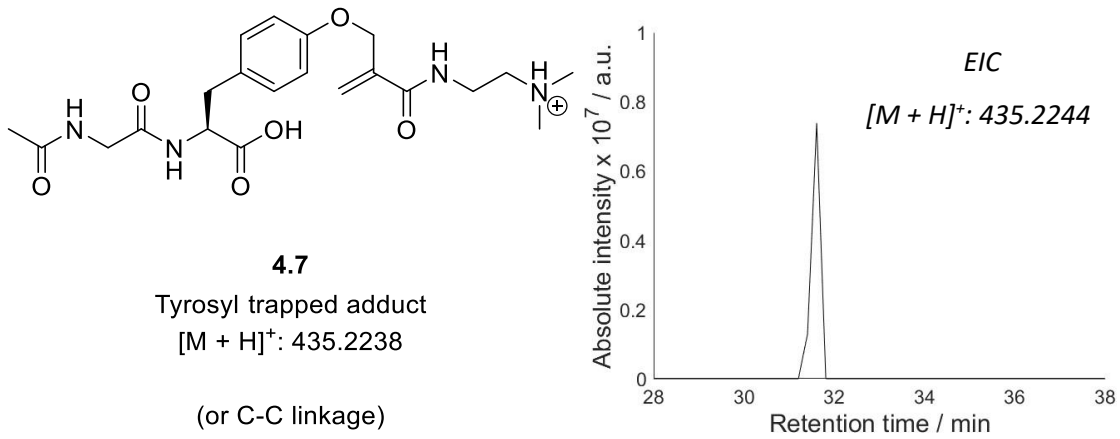

*Figure 64. Chemical structure and extracted ion chromatograms (EIC) for the m/z of 435.2244 acquired by LC-MS from the ONOOH-mediated oxidation of N-Ac-Gly-Tyr-OH. Chemical structure is shown as a protonated adduct. It is noted that the EIC could be due to a C-C bond formation between the tyrosyl radical and **4.1**. Reactions were carried out in open air.*

Figure 64 shows a potential structure for the trapped adduct. It is noted that reaction of the tyrosyl radical with the **4.1** can occur either *via* the phenoxyl radical (leading to a C-O trapped adduct as shown in Figure 64), or *via* the resonance form yielding C-C trapped adduct. Figure 64 reports the EIC of a potential trapped tyrosyl radical, with the $[M + H]^+$. Whether the trapped radical is a C-C or a C-O adduct cannot be verified. However, as it was discussed in the previous Section, a by-product of the trapping reaction is the release of TEMPO$^\bullet$. As TEMPO$^\bullet$ is a persistent radical, it can react rapidly with C-centred radicals (e.g., $k \sim 10^9$ M^{-1} s^{-1} for the reaction with *t*-Bu$^\bullet$),[332] but it does not react with O-centred radicals. This side reaction can be used as an indication of whether the trapped radicals detected are C-C or C-O bonds. For instance, if the same tyrosyl radical can be detected as a TEMPO-adduct, then this would strongly support that it reacts as a C-centred radical. Conversely, if no TEMPO-adduct can be detected, then this could suggest that the tyrosyl radical reacts as a phenoxy radical. To that end, LC-MS chromatograms were scanned for the detection of the tyrosyl radical as a TEMPO-adduct, but no evidence were obtained for the formation of this compound. While this is not definitive proof, it does support the notion that reaction between tyrosyl radical and radical trap **7** occurs *via* the phenoxyl radical.

4.5.3 Side reactions

It is important to address the possibility of reactions between the trap and the oxidising agents. Indeed, HO$^\bullet$ is a well-documented powerful and non-selective oxidising agent. As such, apart from reaction with *N*-Ac-Gly-Tyr-OH, it can undergo facile addition to the radical trap. This reaction leads to the formation of an HO-trapped adduct and shows that trap **4.1** can act as an HO$^\bullet$-scavenger. When LC-MS chromatograms were scanned for the $[M + H]^+$ of the HO-trapped adduct the following EIC was obtained (Figure 65A).

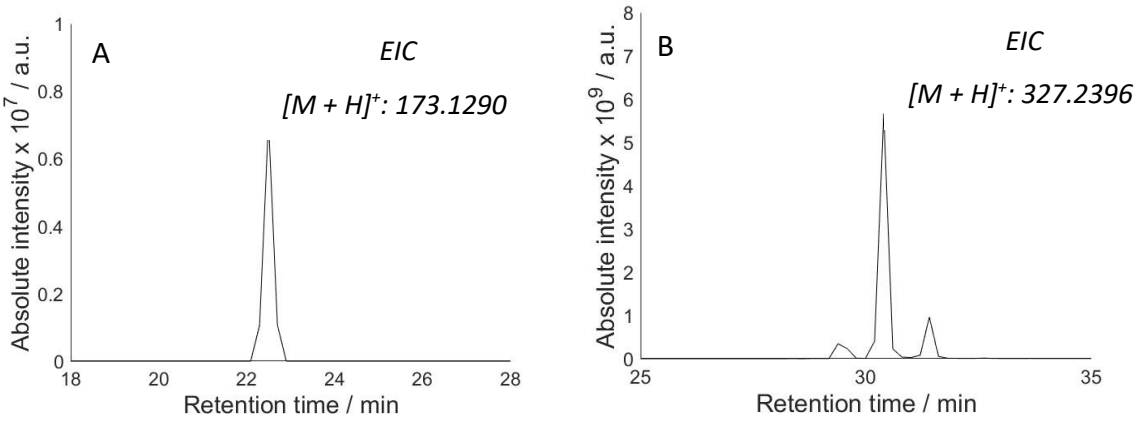

*Figure 65. Extracted ion chromatograms for potential non-radical products arising from the reaction of HO$^\bullet$ with **4.1**. A) EIC for the m/z of 173.1290 (HO-trapped adduct), and B) EIC for the m/z of 327.2396 (trap dimer). Reactions were carried out in open air.*

The $[M + H]^+$ of the trapped $HO^\bullet$ was observed (Figure 65A), and actually was present at similar absolute intensity as the hydroxylated product (10^7). However, the most dominating peak of this reaction was an unidentified compound eluting at *ca.* 31 min with an $[M + H]^+$: 327.2396, whose EIC is provided in Figure 65B. After careful examination it was realised that this is a consequence of using high trap concentration. The species responsible for this peak is a $HO^\bullet$-mediated trap dimer **4**.**10**, and the following structure and mechanism is tentatively proposed (Scheme 54).

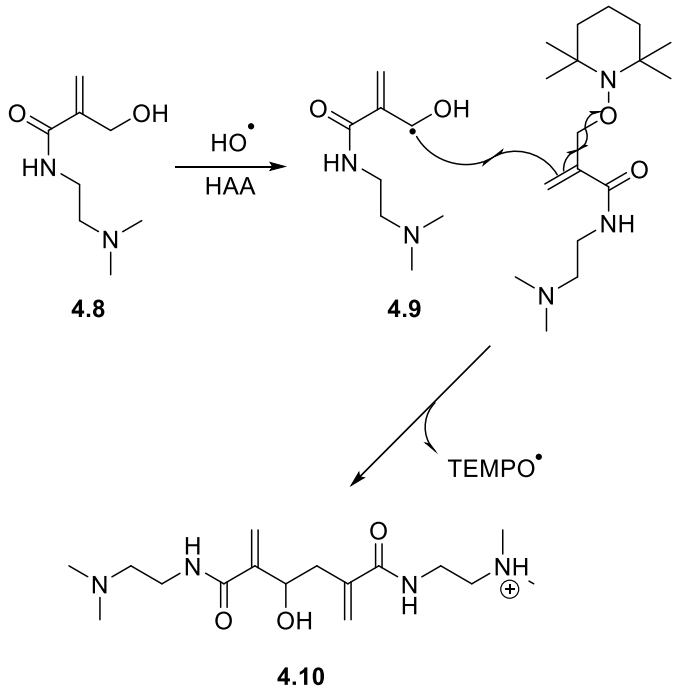

Scheme 54. Proposed mechanism for the formation of the trap dimer with an $[M + H]^+$ of 327.2391, via allylic hydrogen abstraction by $HO^\bullet$ from the HO-trapped adduct.

Initial reaction of $HO^\bullet$ with the trap yields compound **4**.**8** (confirmed by the EIC of Figure 65A). It was then postulated that allylic HAA from 4.**8**, produces a transient allylic radical 4.**9** that upon further reaction with another molecule of trap **4.1**, leads to 4.**10** (the allylic radical was also successfully detected as a TEMPO-adduct; data in Appendix). In order to further corroborate whether the two EICs (Figures 65A and 65B) are a manifestation of the reaction between $HO^\bullet$ and the radical trap **4.1**, two control reactions were carried out. Firstly, reactions were run in the absence of **4.1**, and secondly in the absence ONOOH (all other reaction conditions were maintained the same). In both cases the signals were completely absent, thus verifying that the two products are formed from the reaction between $HO^\bullet$ and the radical trap **4.1**. No adducts as a result of reaction between the allylic radical 4.**9** of Scheme 54 and O_2 could be detected.

Radical trap **4.1** was successfully used in the trapping and characterisation of a tyrosyl radical (the only expected radical intermediate in the ONOOH-induced oxidation of *N*-Ac-Gly-Tyr-OH). Importantly, despite the fast competing reactions, reaction conditions and detection methods were optimised, and strong evidence for the formation of a tyrosyl-trapped adduct were obtained. Our results here can be used as a proof-of-principle to study other less selective systems. Next our attention was turned to other oxidation systems to further explore the scope of this method.

4.6 HO$^{\bullet}$-induced oxidation

In Chapter 2 we investigated the aerobic HO$^{\bullet}$-induced peptide oxidation with a particular emphasis on the formation of peptide-derived hydroperoxides. Hydroxyl radicals are the most powerful oxidising agent, are unselective, and are omnipresent in both biological and atmospheric systems.[333,334] Therefore, it was decided to explore whether our radical trap **4.1** can be used to trap biological radicals produced from photogenerated HO$^{\bullet}$. Moreover, work on the trapping of radical intermediates generated on simple peptides by HO$^{\bullet}$ (generated *via* Fenton chemistry) has already been carried out in our group (see Section 4.4), and this would allow us to compare our experimental results. Since a series of experiments was already carried out utilising the UV/H_2O_2 system in Chapter 2, the same reaction conditions were applied here with the addition of 10% of radical trap **4.1** (Scheme 55).

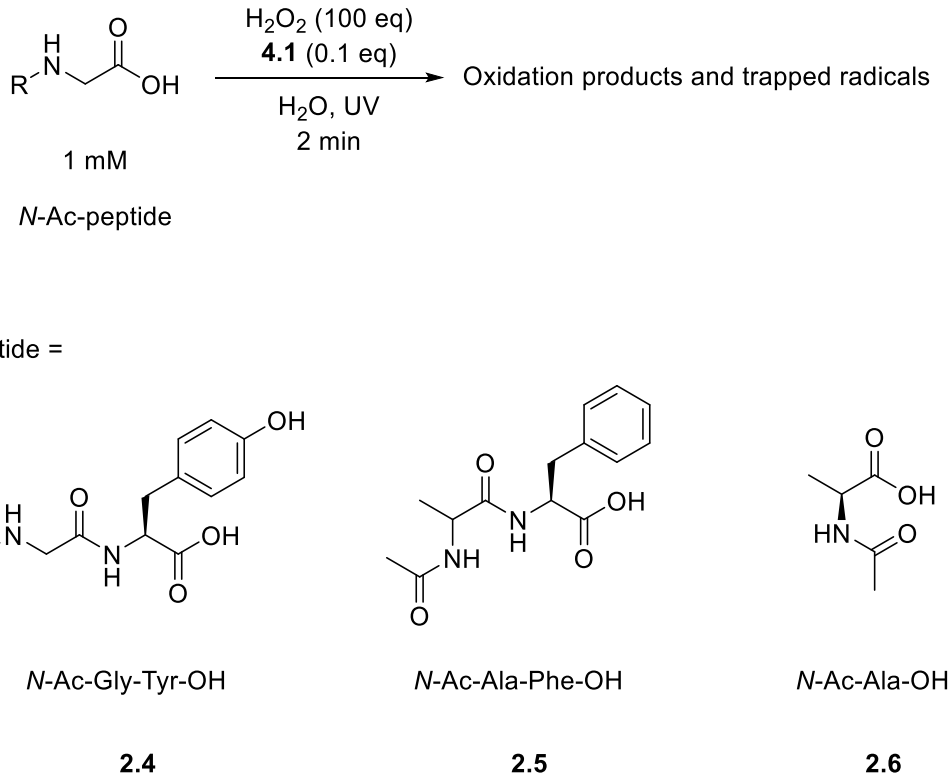

*Scheme 55. Experimental conditions for aerobic HO•-induced oxidation of three biological targets in presence of radical trap **4.1**. All oxidised solutions were frozen immediately after cessation of irradiation until analysis by either DI-MS or LC-MS.*

Unlike the ONOOH system where high concentrations of trap **4.1** were necessary to outcompete the reaction of $^{\bullet}NO_2$ with tyrosyl radicals, here low amounts of trap are preferred. The reason for this is to allow some autoxidation to proceed. Moreover, using only 0.1 eq. of **4.1** has allowed analysis of reactions by both DI-MS and LC-MS (and not only LC-MS as in the ONOOH studies). It is acknowledged that the extremely high concentration of H_2O_2 in respect to the starting substrates is not representative of actual biological systems, however, as photolysis of H_2O_2 is not that efficient with the lamp we have used (*vide infra*), these conditions were used to ensure a substantial HO•-induced oxidation of the substrates (ca. 10%) The H_2O_2 degradation was quantified spectroscopically and was found that under these experimental conditions only 1% of the total H_2O_2 is decomposed (data not shown). To confirm that any detected oxidation products were a result of the hydroxyl radical-mediated oxidation, and not from the direct excitation of the starting substrates, the following control experiment was conducted. Aqueous solutions of the starting substrates (all 1 mM concentration) were exposed to the same UV light source in the absence of H_2O_2. This resulted in no appreciable degradation of the substrates, and no oxidation products / trapped radicals could be identified (data not shown).

The reactivity between $HO^{\bullet}$ and the three *N*-acetyl protected substrates has been explored in Chapter 2, but some product discussion will be held here as we are looking at more than just hydroperoxide formation. Nonetheless, as most of the oxidation products are well-characterised in the literature, the majority of this Section will focus on the trapping and detection of radical intermediates formed in the three substrates upon exposure to $HO^{\bullet}$.

4.6.1. *N*-Ac-Ala- OH

Exposure of *N*-Ac-Ala-OH to $HO^{\bullet}$ resulted in a range of different degradation products that were successfully characterised by DI-MS (i.e., alcohols, hydroperoxides as confirmed by D_2O experiments, dimeric species, and carbonyls from $RO^{\bullet}$ fragmentation; all of the MS data can be found in the Appendix). Reactivity of *N*-Ac-Ala-OH with $HO^{\bullet}$ is well-defined (discussed in detail in Chapter 2), and it involves a HAA mechanism that generates a C-centred radical on the protected amino acid. The C-centred radical can add to dioxygen to afford the corresponding peroxyl radical. In turn, peroxyl radicals yield alkoxyl radicals *via* intermediate formation of hydroperoxides.

4.6.1.1 Primary detected radicals

Based on these mechanisms three main radicals are predicted to be generated in this system, that are; a C-centred (Figure 66A), a peroxyl (Figure 66B) and an alkoxyl radical (Figure 66C). Similarly to the experiments in Chapter 2, these reactions here were also run in unbuffered solutions, and as such, the % of the substrates in their anionic form is high (see section 2.6.1). Identification of peroxyl and alkoxyl radicals is complicated by the presence of different isomeric species having identical $[M + H]^+$. For instance, a peroxyl radical will have the same $[M + H]^+$ as an alkoxyl radical + OH group, or a C-centred radical + 2 OH groups. As such, further experiments (e.g., isotope exchange experiments) are required to conclusively assign the acquired *m*/*z* to specific chemical compounds (*vide infra*). It is noted that *N*-Ac-Ala-OH ionised very poorly in LC-MS, and as such, all irradiated solutions were analysed by DI-MS.

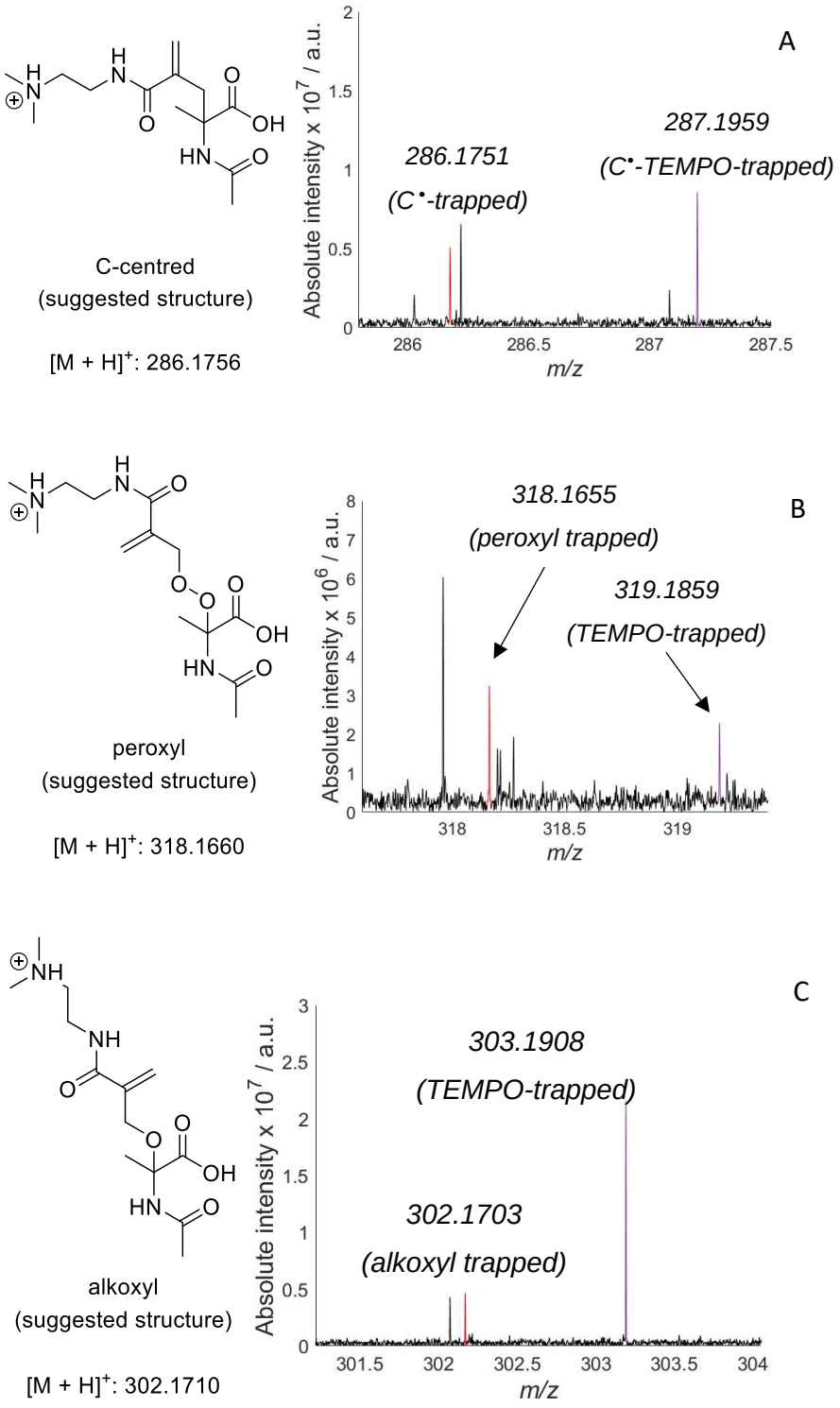

Figure 66. Suggested chemical structures, [M + H]⁺, and DI-MS spectra for A) a trapped C-centred radical, B) a trapped peroxyl radical, and C) a trapped alkoxyl radical. All radicals are generated via initial HAA by HO• from an available C-H on N-Ac-Ala-OH. Reactions were carried out in open air.

Before any discussion can be held, it is instructive to address the possibility of reactions/fragmentations occurring during the DI-MS analysis. While reactions taking place in the gas phase during DI is certainly a possibility, and cannot be ruled out, the ionisation technique we have used throughout our MS analysis (ESI), is generally viewed, and accepted as a "soft" ionisation technique, that allows the detection of intact molecular ions.[335]

Interestingly, investigation of the DI-MS spectra revealed that all three supposed radicals are detected as trapped molecules with our radical trap **4.1** (highlighted in red in Figures 66A, 66B, and 66C), and also as TEMPO-adducts (highlighted in purple in Figures 66A, 66B, and 66C). The detection of a C-centred trapped radical is perhaps unexpected, as most carbon-centred radicals react with electron-deficient alkenes with typical second order rate constants in the range of $k \sim 10^6$ - 10^7 M^{-1} s^{-1},[322] while O_2 addition is at least 100 times faster. Therefore, the existence of C-centred trapped radicals likely indicate that reactions suffered from deoxygenation. Control reactions that were carried out in N_2 revealed that no peaks that could be associated with trapped $ROO^{\bullet}$ or oxygenated products (e.g., hydroperoxides) could be identified (but C-centred radicals were evident).

The fact that the supposed $ROO^{\bullet}$ and $RO^{\bullet}$ adducts are present as TEMPO adducts too, suggest that (at least to an extent) the signals are due to C-centred radicals that have previously underwent one or two hydroxylations. Therefore, while assigning the acquired *m*/*z* to C-centred trapped radicals is straightforward, O-centred ones are more complicated to assign. To better understand whether the acquired signals are due to C-centred or O-centred radicals, isotope exchange experiments (similarly to our hydroperoxide work; see Chapter 2 and Experimental Chapter) were carried out. This is because the supposed radicals have a different number of exchangeable protons. Indeed, isotope exchange can allow the differentiation of $ROO^{\bullet}$, $RO^{\bullet}$ + OH, and $R^{\bullet}$ + 2 OH, as well as $RO^{\bullet}$ and $R^{\bullet}$ + OH. Therefore, irradiations were repeated, but aliquots were now diluted in D_2O instead of H_2O before injection in the MS instrument. Peroxyl and alkoxyl trapped adducts can now be differentiated by C-centred adducts as upon full deuteration the $[M + D]^+$ is different (Figure 67).

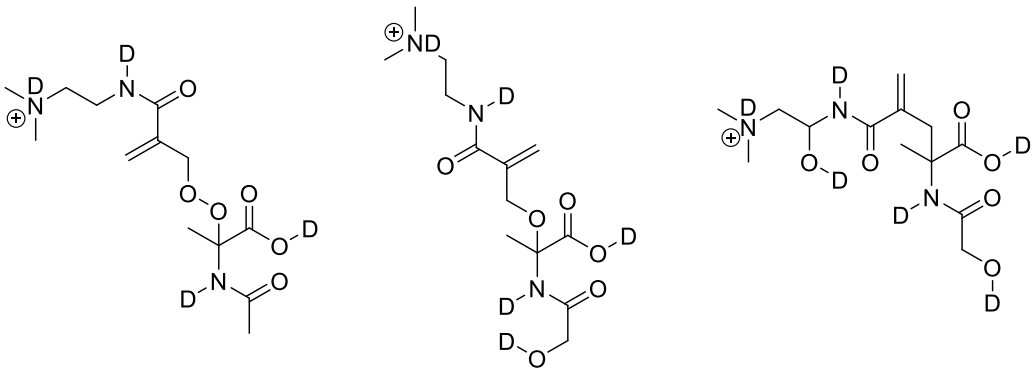

peroxyl
(suggested structure)

$[M + D]^+$: 322.1911

alkoxyl + OH
(suggested structure)

$[M + D]^+$: 323.1973

C-centred + 2 OH
(suggested structure)

$[M + D]^+$: 324.2036

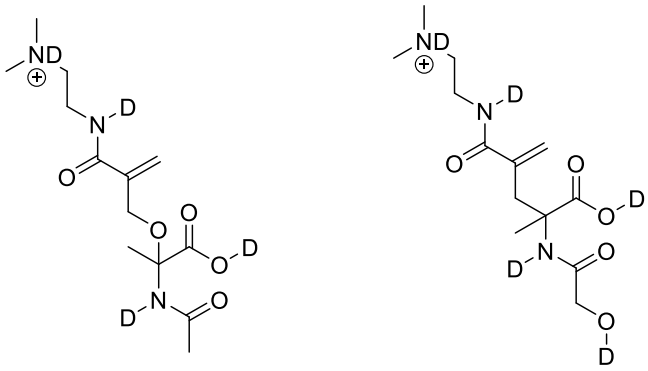

alkoxyl
(suggested structure)

[M + H]+: 306.1962

C-centred + OH
(suggested structure)

$[M + H]^+$: 307.2024

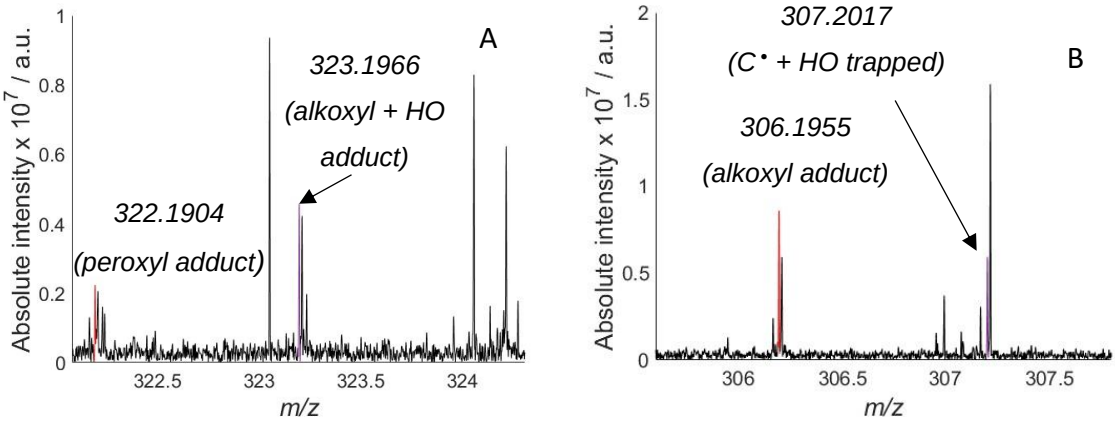

Figure 67. Suggested chemical structures of potential trapped adducts (with identical m/z) that upon isotope-exchange experiments now have a different m/z and can be differentiated by MS. Representative DI-MS spectrum of a reaction that has been diluted in D_2O to allow separation of compounds with same m/z but different number of exchangeable protons. The MS spectra shows the existence of A) trapped peroxyl (highlighted in red), and trapped alkoxyl (highlighted in purple) radicals, while B) shows the existence of trapped alkoxyl (highlighted in red), and trapped C-centred radicals (highlighted in purple). Reactions were carried out in open air.

Figure 67 shows a DI-MS spectrum of an irradiated solution of *N*-Ac-Ala-OH (diluted in D_2O). Isotope exchange experiments were successful and strong evidence for the existence of trapped O-centred radicals were obtained. In Figure 67A, the acquired *m*/*z* of 322.1904 (highlighted in red) supports the existence of a trapped peroxyl radical, while the *m*/*z* of 323.1966 (highlighted in purple) supports the existence of a trapped alkoxyl radical. Our D_2O experiments here further corroborate the generation of intermediate peroxyl and alkoxyl radicals in the aerobic $HO^{\bullet}$-mediated oxidation of *N*-Ac-Ala-OH. Figure 67B suggests that the acquired *m*/*z* of the potential alkoxyl radicals (Figure 66C), is due to both alkoxyl and C-centred radical adducts in the reaction mixture.

No signal for a potential C-centred radical that has been previously dihydroxylated could be obtained in the D_2O analysis. This result is contradicting the data of Figure 66B, as the $[M + H]^+$ of supposed peroxyl radical has been detected as a TEMPO-adduct indicating the presence of a C-centred radical + 2 OH with the same *m*/*z*. This outcome can be explained by the relative abundance of the species in the solutions. While trapped C-centred radicals + 2 OH with the same $[M + H]^+$ as the trapped peroxyl radical might exist, their abundance could be very low, and therefore, when fully deuterated cannot be detected (below the limit of MS detection). However, the peak corresponding to the $[M + H]^+$ of the TEMPO-adduct of Figure 66B (highlighted in purple) is reasonably strong, and upon full deuteration should be still detected. To confirm this hypothesis, DI-MS spectra of the deuterated samples were scanned for the $[M + D]^+$ of the TEMPO-adduct of potential dihydroxylated C-centred radicals. This signal was indeed present in the analysis (data not shown), therefore confirming that three species are contributing to the $[M + H]^+$ of 318.1655 of Figure 66B. Next our focus turned to secondary radicals, arising from further oxidation of the degradation products.

4.6.1.2 Secondary detected radicals

The main degradation product that was identified was an *N*-Ac-Ala-OH-derived carbonyl **4.12** (arising from tertiary RO$^{\bullet}$ fragmentation **4.11**; Scheme 56).

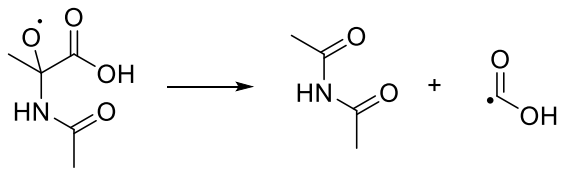

4.11 **4.12** **4.13**

Scheme 56. Formation of N-Ac-Ala-OH-derived carbonyls, as a result of an alkoxyl radical fragmentation. The alkoxyl radical is generated most likely via homolysis of an N-Ac-Ala-OH-derived hydroperoxide.

It was theorised that further HAA from the diacetamide **4.12** shown in Scheme 56 by HO$^{\bullet}$ could occur thus leading to new C-centred radicals (and consequently, peroxyl and alkoxyl radicals). The structures and the corresponding EICs of the $[M + H]^+$ for the three potential trapped adducts are given in Figure 68.

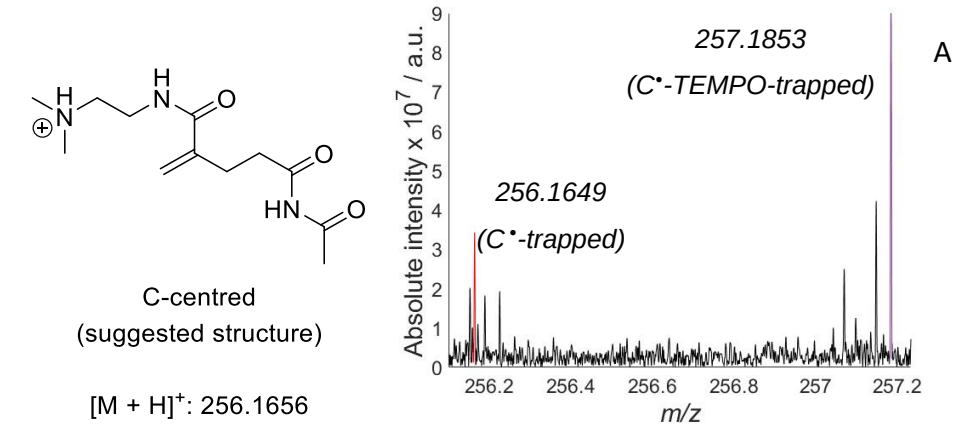

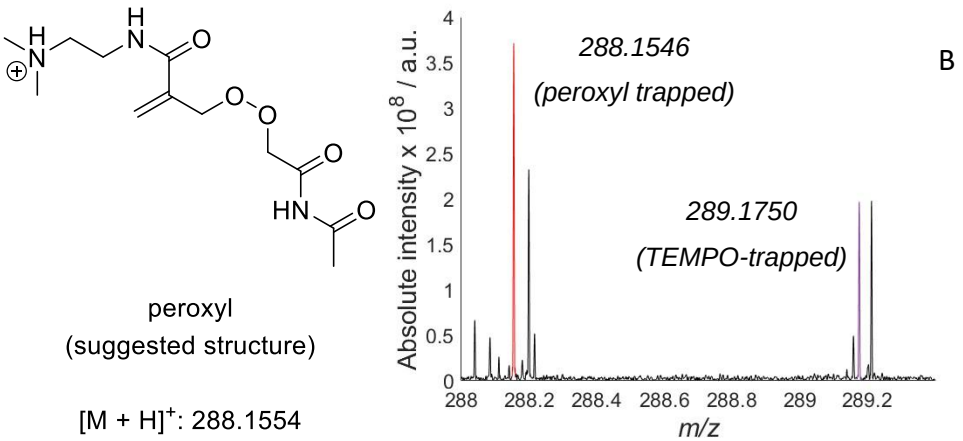

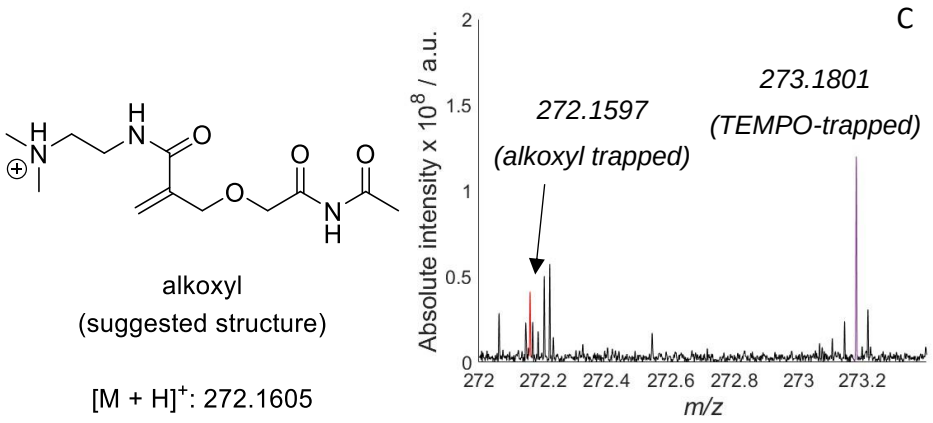

Figure 68. Suggested chemical structures, $[M + H]^+$, and DI-MS spectra for A) a trapped C-centred radical, B) a trapped peroxyl radical, and C) a trapped alkoxyl radical. These radicals arise from HAA by HO• from the N-Ac-Ala-OH carbonyl of Scheme 57. Reactions were carried out in open air.

Consistent with our prediction, the $[M + H]^+$ of all three predicted radicals were present in the DI-MS spectrum (Figure 68; highlighted in red are the trapped adducts, while highlighted in purple are the radicals trapped with TEMPO•). All three supposed radicals are trapped with TEMPO• indicating that the signal could be due to C-centred, and not O-centred radicals. Again, the acquired *m/z* of potential peroxyl radicals (Figure 68B), can be due to ROO•, RO• + OH, or R• + 2 OH. Similarly, the acquired *m/z* of potential alkoxyl radicals (Figure 68C) can be due to either RO•, or R •+ OH. To further elucidate the exact identity of these species, D_2O analysis was carried again (Figure 69).

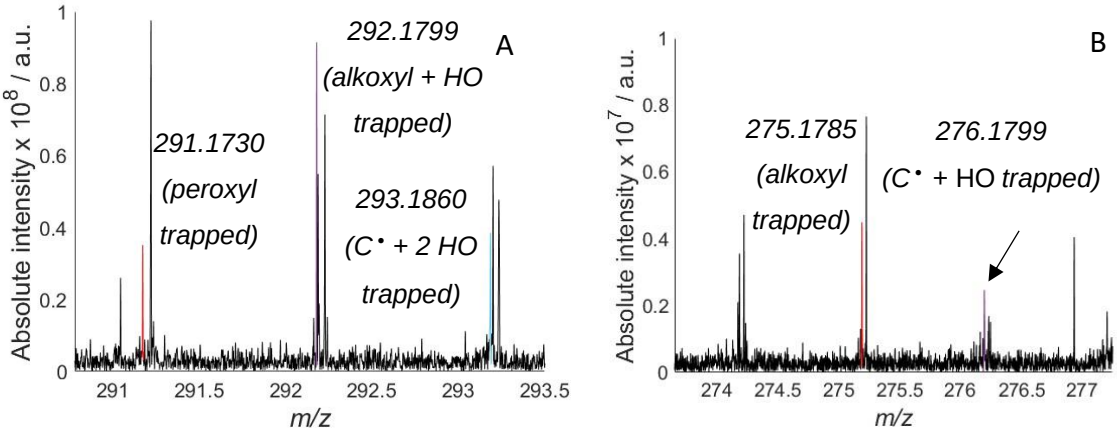

Figure 69. Suggested chemical structures of potential trapped adducts (with identical m/z) that upon isotope-exchange experiments now have a different m/z and can be differentiated by MS. Representative DI-MS spectrum of a reaction that has been diluted in D_2O to allow separation of compounds with same m/z but different number of exchangeable protons. The MS spectra shows the existence of A) trapped peroxyl (highlighted in red), trapped alkoxyl (highlighted in purple), and C-centred (highlighted in teal) radicals, while B) shows the existence of trapped alkoxyl (highlighted in red), and trapped C-centred radicals (highlighted in purple). Reactions were carried out in open air.

Interestingly, our D_2O experiments confirm that the signal for the $[M + H]^+$ of 288.1546 (Figure 68B), is in fact, a contribution of three different species. Indeed, the $[M + D]^+$ for potential trapped peroxyl radicals (Figure 69A; highlighted in red), alkoxyl radicals (Figure 69A; highlighted in purple), and C-centred radicals (Figure 69A; highlighted in teal) were all present when reaction mixtures were diluted in D_2O. The abundance of the potential peroxyl radical adducts is lower than the corresponding alkoxyl, and that could be attributed to the relative trapping rates ($RO^{\bullet}$ are expected to react faster with the radical trap **7**). Similarly, Figure 69B confirms that the acquired *m*/*z* of potential alkoxyl radicals (Figure 68C) is due to both alkoxyl radicals (Figure 69B; highlighted in red) and C-centred radicals that have been previously hydroxylated (Figure 69B; highlighted in purple). We note that the fragmentation mechanism of Scheme 57, also releases $^{\bullet}CO_2H$ and this was detected as a trapped adduct providing further evidence for the mechanism (MS data in the Appendix).

The fragmentation mechanism of Scheme 56 can also follow a different pathway and produce a $N^{\bullet}$ **4.15** and a carbonyl **4.14** (Scheme 57).

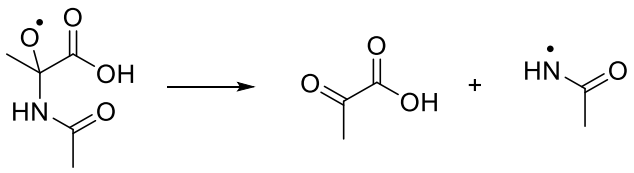

4.11 **4.14** **4.15**

Scheme 57. Fragmentation of a tertiary N-Ac-Ala-OH-derived alkoxyl radical to generate a new carbonyl and an N• radical.

Subsequent HAA by $HO^{\bullet}$ from the new carbonyl can yield transient C-centred, and O-centred radicals (similarly to the case of the acetamide; Figure 68). Therefore, DI-MS spectra were scanned for these trapped adducts (Figure 70).

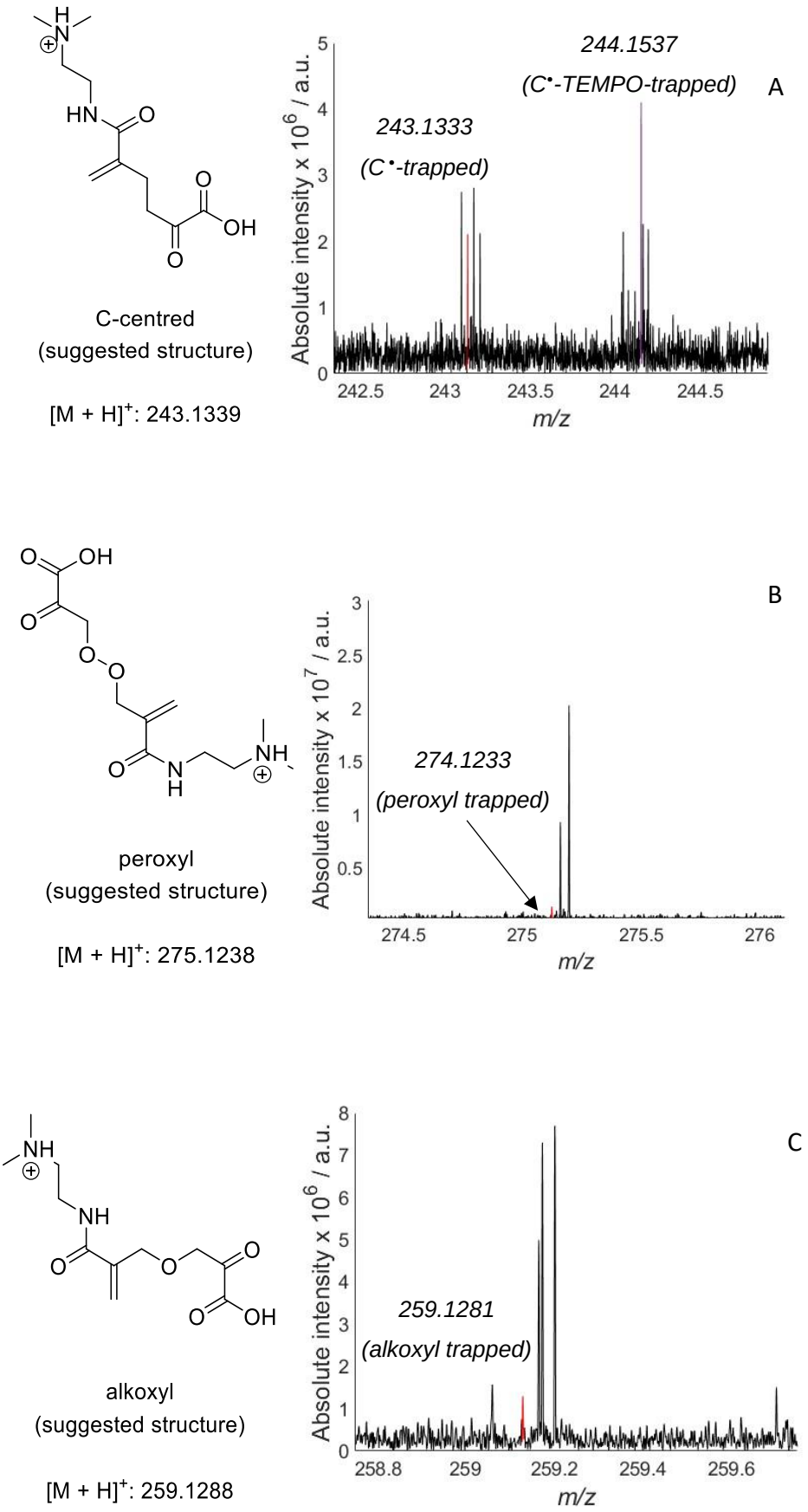

Figure 70. Potential chemical structures, $[M + H]^+$, and DI-MS spectra for A) a trapped C-centred radical, B) a trapped peroxyl radical, and C) a trapped alkoxyl radical. These radicals arise from HAA by HO• from the N-Ac-Ala-OH carbonyl of Scheme 58. Reactions were carried out in open air.

Our analytical data corroborate the formation of both C- and O-centred radical from this mechanistic pathway. Figure 70A shows the *m*/*z* corresponding to possible C-centred trapped adduct (highlighted in red), while the *m*/*z* of the predicted radical as a TEMPO-adduct is also present (highlighted in purple). Moreover, Figure 70B and 70C demonstrate that both peroxyl and alkoxyl trapped adducts are present in the irradiated mixtures (highlighted in red). No TEMPO-adducts were detected for the potential peroxyl and alkoxyl radicals this time, indicating that the MS signals are likely due to O-centred, and not C-centred radicals. Unfortunately, the peaks are too weak in intensity to allow D_2O analysis, and therefore, the exact structures were not further elucidated.

It is noted that the identified trapped adducts of Figure 70, can also result from the HAA reaction between the amidyl radical **4.15** and the carbonyl **4.14** inside the solvent cage (Scheme 58).

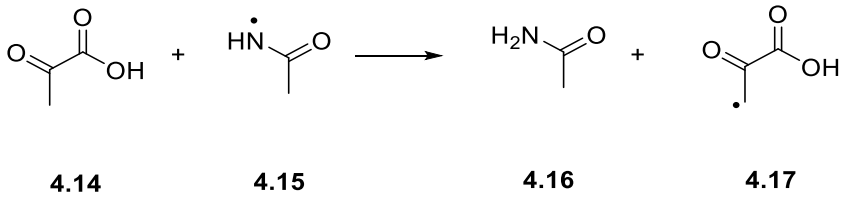

4.14 **4.15** **4.16** **4.17**

Scheme 58. Hydrogen atom abstraction reaction between an amidyl radical and a carbonyl, yielding an amide and a new C-centred radical.

In fact, recent advanced theoretical studies have shown the propensity of amidyl radicals to undergo HAA reactions, as the resulting closed-shell species (the amide; in this case **4.16**) is further stabilised due to the delocalisation of the nitrogen lone pair on the empty π*orbital of the carbonyl moiety.[336] In the amidyl radical **4.14**, this stabilisation effect is reduced as it is the unpaired electron that is delocalised on the nearby carbonyl moiety.

Our experimental data here are consistent with previous work carried out in our group.[166] Indeed, when aqueous solutions of *N*-Ac-Gly-Gly-OH were oxidised by $HO^{\bullet}$ (generated *via* Fenton-chemistry; experimental conditions as outlined in Scheme 50), MS signals corresponding to the same C- and O-centred trapped radicals (as in Figures 66, 68 and 70) were obtained, although their exact identify was not further elucidated as in this case (D_2O experiments; Figures 67 and 69).

It is noted that when $HO^{\bullet}$ were generated by the reductive cleavage of H_2O_2, more trapped radicals were detected. These radicals were likely a result of decomposition of intermediate hydroperoxides formed in *N*-Ac-Gly-Gly-OH. This is not unexpected as Fe^{2+} is known do induce one-electron reduction of hydroperoxides, thus generating more radical species in the system. Furthermore, the

difference in the number of different radicals that were observed in the two systems (i.e., Fe^{2+}/H_2O_2 vs UV/H_2O_2) could be attributed to the relative $HO^{\bullet}$-fluxes. While the extent of H_2O_2 degradation was not assessed in the Fe^{2+} / H_2O_2, the iron-catalysed decomposition of H_2O_2 is a very fast and efficient way of generating $HO^{\bullet}$, and thus the radical flux was likely high. Conversely, in our system only 1% of the total H_2O_2 is decomposed (H_2O_2 concentration was determined spectroscopically).

Having demonstrated that exposure of *N*-Ac-Ala-OH to $HO^{\bullet}$ leads to the generation of transient radicals, it was sought to explore the oxidation of more complex peptides. The next Section will focus on the aerobic $HO^{\bullet}$-induced oxidation of *N*-Ac-Ala-Phe-OH.

4.6.2. *N*-Ac-Ala-Phe-OH

The $HO^{\bullet}$-mediated oxidation of *N*-Ac-Ala-Phe-OH is more complicated compared to *N*-Ac-Ala-OH, as $HO^{\bullet}$ can react *via* three different pathways; that are direct addition to the benzene ring, electron transfer, and HAA. Degradation products from all three reaction mechanisms were identified by MS, and these include hydroxylation and dihydroxylation of the benzene ring, peroxidation, dimeric species, and carbonyls from tertiary alkoxyl radical fragmentation (all MS data can be found in the Appendix).

Addition of $HO^{\bullet}$ to the aromatic ring of *N*-Ac-Ala-Phe-OH is near the diffusion controlled limit and gives rise to an unstable cyclohexadienyl radical. Diffusion controlled oxygen addition followed by facile $HO_2^{\bullet}$-elimination produces a stable hydroxylated adduct.[109,337,338] Therefore, this mechanism is not expected to yield transients that can be captured. On the contrary, both HAA and electron transfer are predicted to afford radical species, and thus, these two mechanisms will be further explored. Unlike *N*-Ac-Ala-OH, *N*-Ac-Ala-Phe-OH ionised very efficiently in the LC-MS, and so oxidised solutions were analysed both by DI-MS and LC-MS.

4.6.2.1. Hydrogen atom abstraction

Hydrogen atom abstraction by $HO^{\bullet}$ can take place (from different C-H positions of the molecule) forming isomeric C-centred radicals, and consequently peroxyl and alkoxyl radicals (similarly to *N*-Ac-Ala-OH). Nonetheless, based on the % of deprotonated *N*-Ac-Ala-Phe-OH, the most likely position from which the $HO^{\bullet}$ can abstract a hydrogen from remains the benzylic position. As such, initially, MS data were scanned for these potential trapped adducts (Figure 71; structures shown for potential HAA from the benzylic position of the molecule).

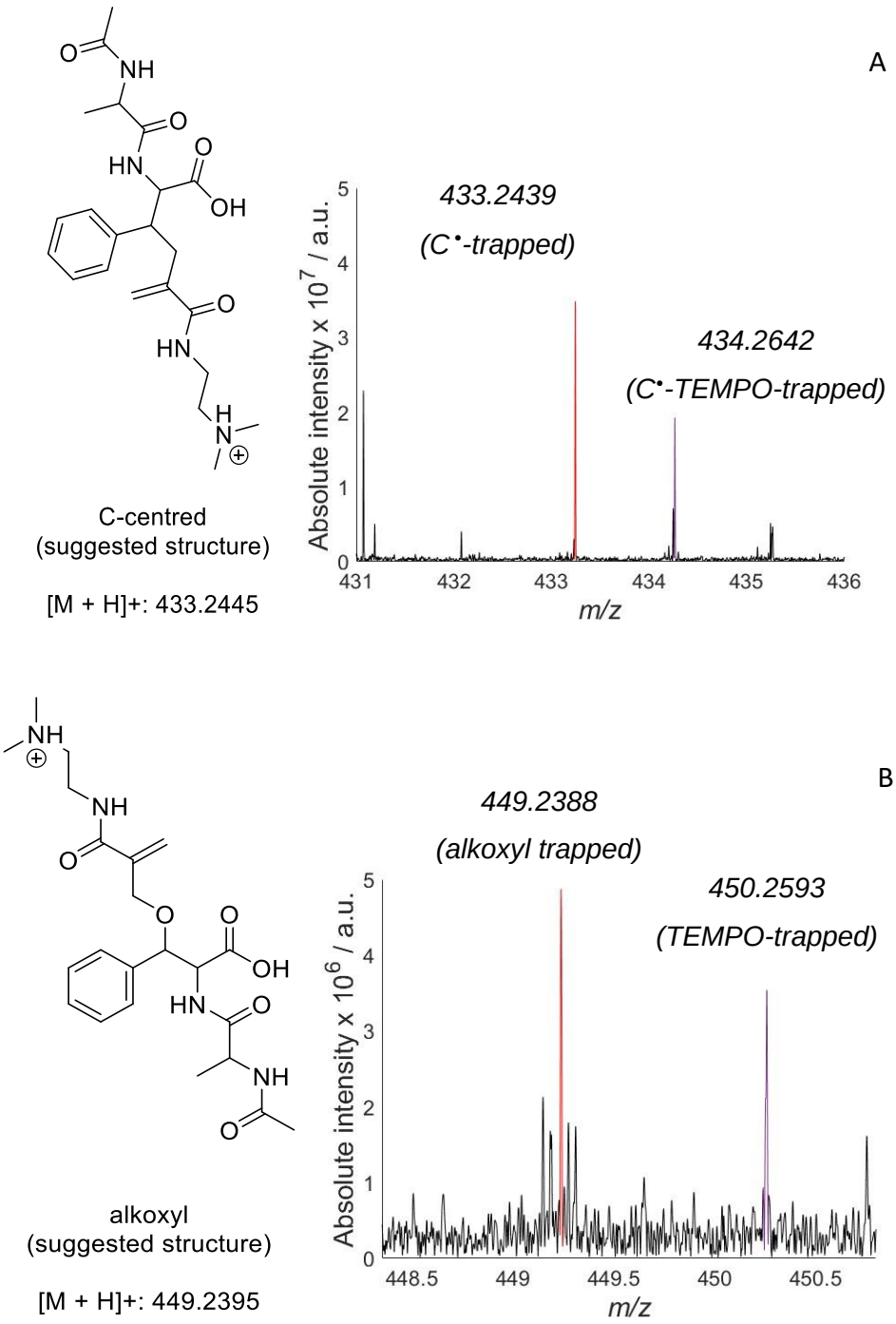

Figure 71. Suggested chemical structures and DI-MS spectra for potential C-centred and alkoxyl radical adducts. A) DI-MS spectrum of potential C-centred radical as a trapped adduct, and as TEMPO-adduct, B) DI-MS spectrum of potential alkoxyl radical as a trapped adduct and as a TEMPO-adduct. Reactions were carried out in open air.

Investigation of the MS spectra revealed that the *m*/*z* corresponding to potential C-centred and alkoxyl radicals trapped were present (Figure 71A and 71B, respectively). Both supposed radicals were also detected as TEMPO-adducts. Unfortunately, the *m*/*z* peak for the trapped alkoxyl radical (Figure 71B; highlighted in red) is too weak to allow D_2O experiments, and therefore, the nature of the trapped radical could not be further elucidated. No *m*/*z* corresponding to potential peroxyl trapped radicals could be obtained. C-centred trapped radicals were also identified by LC-MS (but no trapped alkoxyl adducts). Indeed, the EIC of 433.2445 (potential C-centred trapped radicals) revealed 4 peaks, indicating that HAA by HO$^\bullet$ from *N*-Ac-Ala-Phe-OH is non-selective and yields multiple C-centred radicals (LC-MS data can be found in the Appendix).

Similarly to *N*-Ac-Ala-OH, carbonyls resulting from alkoxyl radical fragmentation (Scheme 57) were identified (albeit in lower relative abundance; MS data in the Appendix). However, no radicals generated on *N*-Ac-Ala-Phe-OH-derived carbonyls could be detected, indicating that this is not a major degradation pathway for *N*-Ac-Ala-Phe-OH.

4.6.2.2 Electron transfer

In Introduction (Section 1.7.4.3) it was discussed how electron transfer between HO$^\bullet$ and phenylalanine is a rapid process ($k \sim 10^9$ M^{-1} s^{-1}),[94] that yields a radical cation **4.18**. Since *N*-Ac-Ala-Phe-OH exists mostly as a carboxylate anion in the solution (see Section 2.6.1), a second intramolecular electron transfer can take place, followed by a deprotonation affording a thermodynamically unstable carboxylate radical **4.19** (Scheme 59).

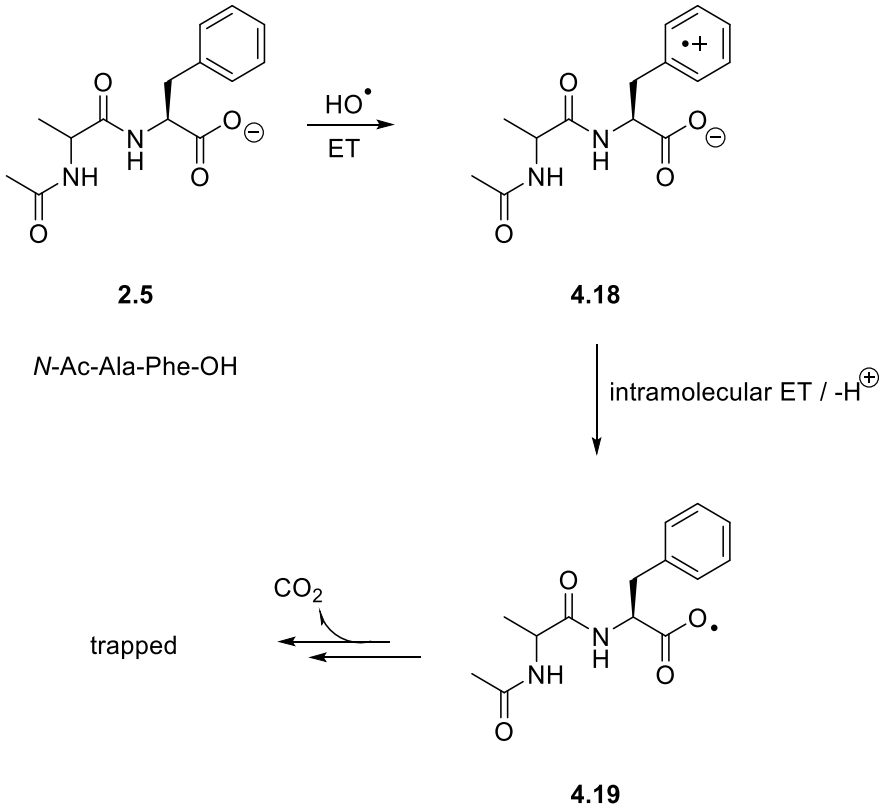

Scheme 59. Radical decarboxylation mechanisms, facilitated by an ET mechanism between HO• and N-Ac-Ala-Phe-OH. The radical cation intermediate undergoes fast intramolecular ET to produce a highly unstable carboxylate anion.

Spontaneous radical decarboxylation releases CO_2 and leads to the formation of a transient C-centred radical,[121,339] which can either be trapped by **7** or react with O_2 to produce peroxyl and alkoxyl radicals. Therefore, DI-MS spectra were investigated for the existence of these trapped species (Figure 72).

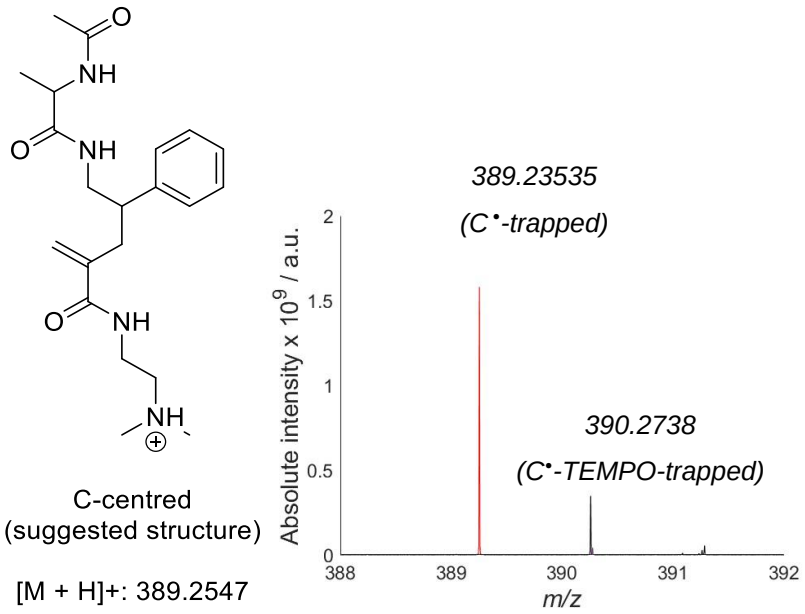

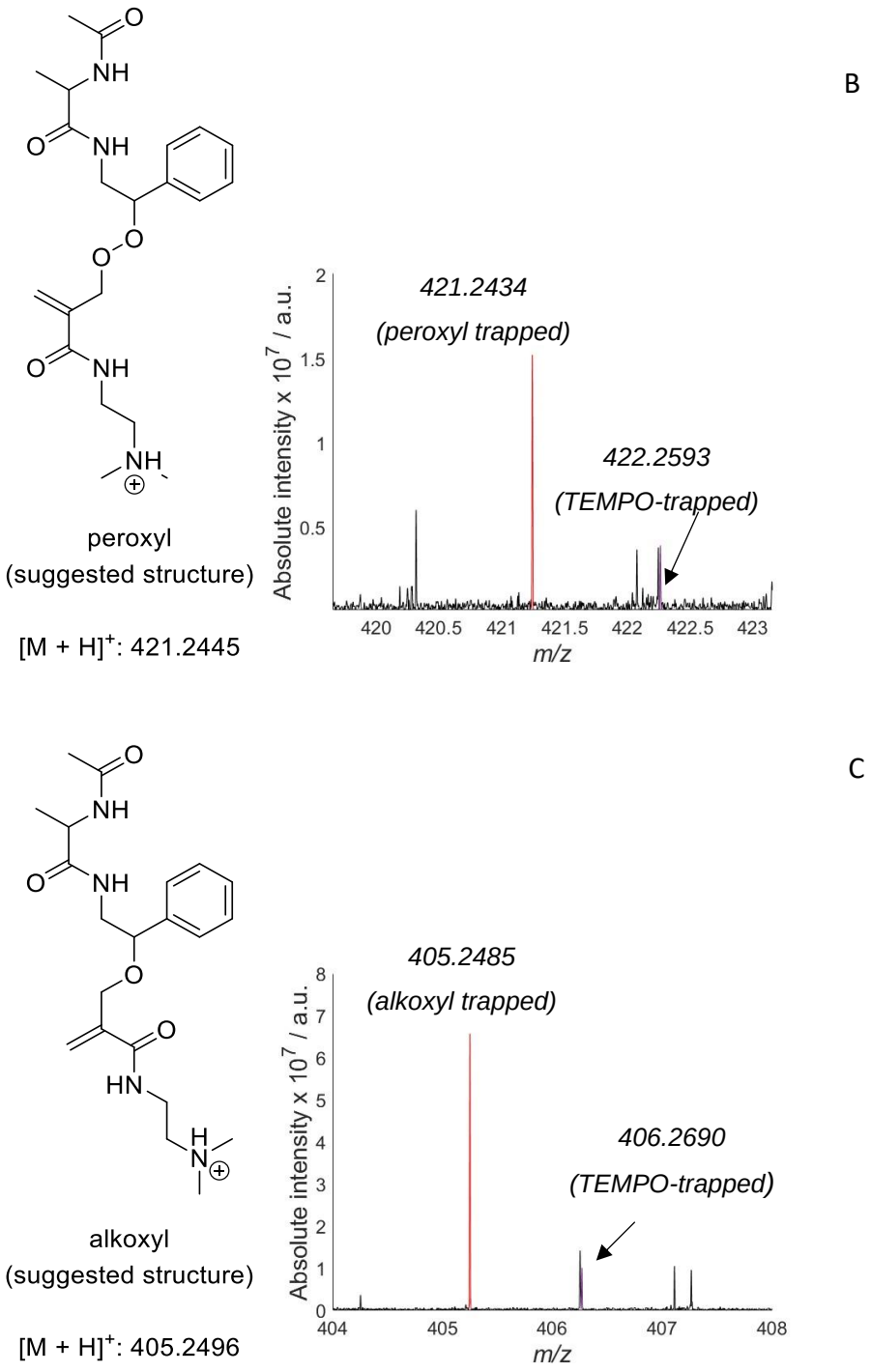

Figure 72. Suggested chemical structure for trapped radicals on N-Ac-Ala-Phe-OH arising from the radical decarboxylation mechanism. A) DI-MS spectrum of the C-centred trapped adduct, B) DI-MS spectrum of the peroxyl trapped adduct, and C) DI-MS spectrum of the alkoxyl trapped adduct. Reactions were carried out in open air.

The $[M + H]^+$ of potential C-centred, peroxyl and alkoxyl radicals as trapped adducts were all identified by DI-MS (Figure 72A, 72B and 72C respectively; highlighted in red). The *m*/*z* of the TEMPO-adducts is also present in all cases (highlighted in purple). It is noted that the C-centred trap adduct (Figure 72A; highlighted in red) was the most dominant peak of the MS spectra (both DI-MS and LC-MS).

Further investigation of LC-MS chromatograms of the oxidised solutions for the $[M + H]^+$ of the potential trapped peroxyl and alkoxyl radicals of Figure 72 revealed that multiple products with the same *m*/*z* exist (LC-MS data in the Appendix). This is not unexpected as peroxyl radicals share the same *m*/*z* with alkoxyl radicals + an OH group, or a C-centred radical + 2 OH groups (similarly to *N*-Ac-Ala-OH). These data further corroborate that $HO^{\bullet}$ reacts primarily *via* ET with *N*-Ac-Ala-Phe-OH.

To further elucidate the MS peaks of Figure 72B and 72C, D_2O analysis was carried. Indeed, different trapped adducts with the same $[M + H]^+$ possess different number of exchangeable protons, and upon full deuteration have a different $[M + D]^+$. As such, peroxyl trapped radicals can now be differentiated by alkoxyl + HO trapped radicals, and C-centred + 2 HO trapped radicals (Figure 73).

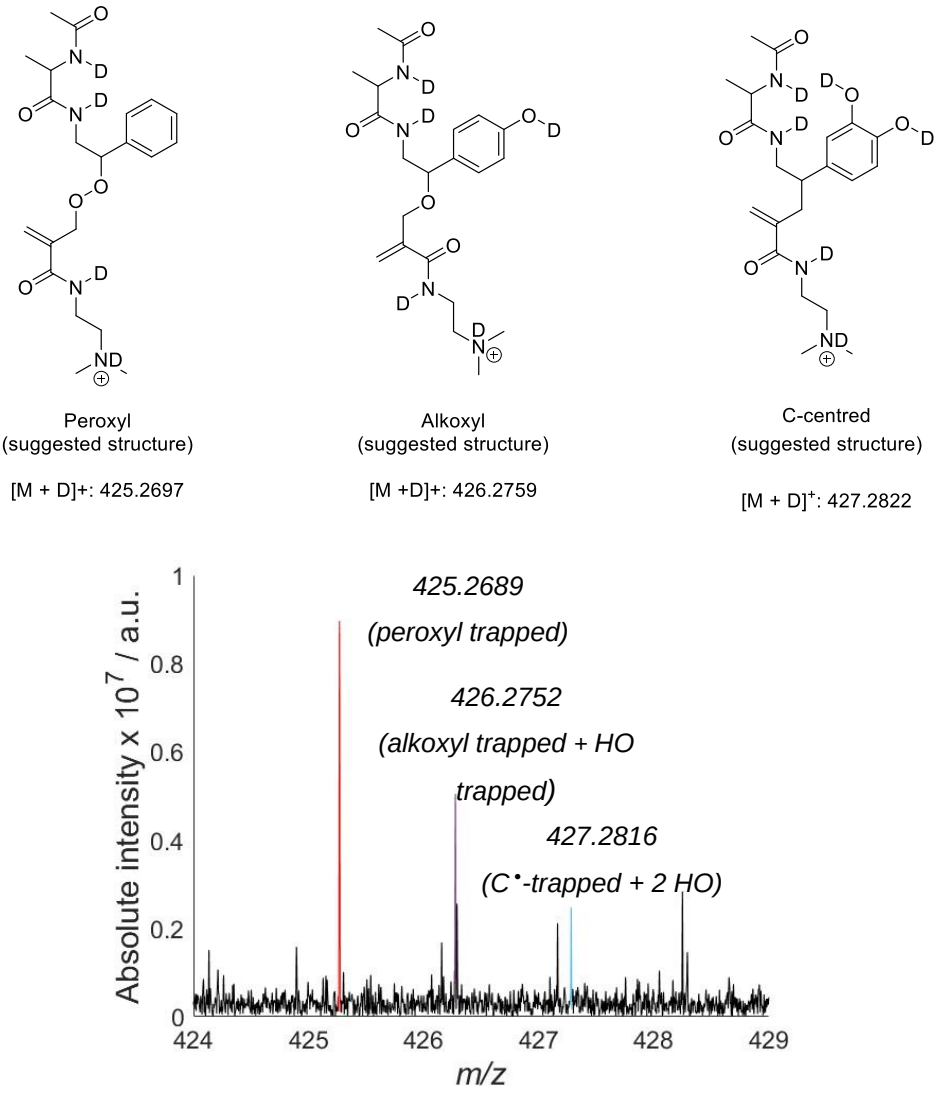

Figure 73. Suggested chemical structures of three potential trapped adduct (with identical m/z) that upon isotope-exchange experiments now have a different m/z and can be differentiated by MS. Representative DI-MS spectrum of a reaction that has been diluted in D_2O to allow separation of compounds with same m/z but different number of exchangeable protons. The MS spectra shows the existence of trapped peroxyl radical (highlighted in red), a trapped alkoxyl radical (highlighted in purple), and a trapped C-adduct (highlighted in teal). Reactions were carried out in open air.

Isotope exchange experiments were successful, and the previously indiscernible structures can now be separated. Indeed, our D_2O data indicate that (at least) three different compounds contribute to the initially acquired $[M + H]^+$ of 421.2434. The most dominating signal is attributed to a peroxyl radical adduct (Figure 73; highlighted in red), followed by the alkoxyl (Figure 73; highlighted in purple), and lastly the C-centred adduct (Figure 73; highlighted in teal). These data strongly support the formation of both peroxyl and alkoxyl radicals in this system.

Similarly to peroxyl radicals, the acquired $[M + H]^+$ of 405.2485 of Figure 72C (potential alkoxyl radical adducts) could be due to a C-centred radical + an OH group, and can be differentiated by deuterium exchange experiments, as the supposed compounds possess different number of labile -H (Figure 74).

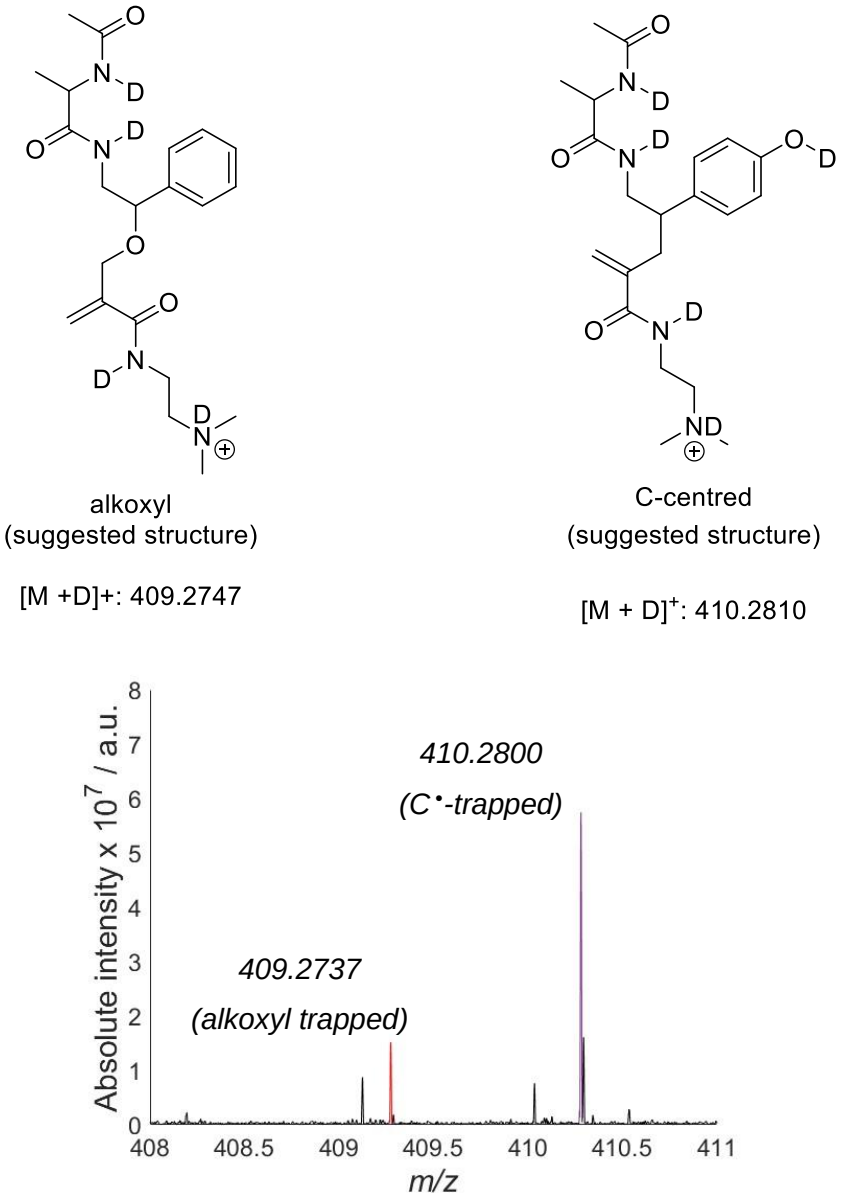

Figure 74. Suggested chemical structures of two potential trapped adduct (with identical m/z) that upon isotope-exchange experiments now have a different m/z and can be differentiated by MS. Representative DI-MS spectrum of a reaction that has been diluted in D_2O to allow separation of compounds with same m/z but different number of exchangeable protons. The MS spectra shows the existence of trapped alkoxyl radical (highlighted in red), and a trapped C-adduct (highlighted in purple). Reactions were carried out in open air.

Predictably, D_2O experiments confirmed the existence of both alkoxyl and C-centred radicals (that have been previously hydroxylated) trapped with **7**. The DI-MS data here indicate that the C-adduct (Figure 74; highlighted in purple) is the most abundant species compared to the alkoxyl adduct (Figure 74; highlighted in red). This is likely a result of the hydroxylation occurring at different positions of *N*-Ac-Ala-Phe-OH (before decarboxylation takes place), thus leading to a range of isomeric products (as confirmed by the multiple peaks for the EIC of the trapped alkoxyl radical of Figure 73B in the LC-MS trace; data in the Appendix). The MS data coupled with well-established isotope-exchange experiments strongly corroborate the characterisation of O-centred (both $ROO^{\bullet}$ and $RO^{\bullet}$) in the aerobic $HO^{\bullet}$-induced oxidation of *N*-Ac-Ala-Phe-OH. It is noted that degradation products (i.e., alcohols and hydroperoxides; confirmed by D_2O analysis) resulting from the radical decarboxylation mechanism were also identified in the MS spectra (MS data in the Appendix).

The relative intensities of the degradation products and trapped adducts suggest that *N*-Ac-Ala-Phe-OH reacts primary *via* addition and electron transfer with $HO^{\bullet}$, and to a lesser extent *via* HAA. This could explain why trapped adducts from the HAA reaction were present in lower abundance (and no trapped peroxyl radicals were detected). Generally, peroxyl radicals are relatively stable radicals, and addition to alkenes is slow (e.g., *t*-$BuOO^{\bullet}$ reacts with an estimated $k \sim 0.1\ M^{-1}\ s^{-1}$ with methyl methacrylate, which has similar electronic properties to **4.1**).[340] Therefore, trapped adducts are mostly detected when high concentrations of $ROO^{\bullet}$ are present in the mixtures. This is probably the case for the electron transfer mechanism.

Our analytical data suggest that the aerobic reaction between $HO^{\bullet}$ and *N*-Ac-Ala-Phe-OH occurs *via* three different mechanisms, that are; addition to the benzene ring, HAA and ET. Importantly, strong evidence for the generation of intermediate radicals as a result of all three mechanisms were obtained. The radical decarboxylation of *N*-Ac-Ala-Phe-OH initiated by $HO^{\bullet}$ (ET mechanism) has been proposed in the literature,[121] but to the best of our knowledge, this is the first reported example of detected intermediate radicals arising from this mechanism by MS.

Having explored the reactivity between $HO^{\bullet}$ and *N*-Ac-Ala-Phe-OH, it was decided to move to a tyrosine-containing peptide to examine how the presence of a hydroxy group in the benzene ring will affect the overall reaction mechanisms.

4.6.3. *N*-Ac-Gly-Tyr-OH

Reaction between HO$^{\bullet}$ and *N*-Ac-Gly-Tyr-OH proceed *via* the same three mechanisms as with *N*-Ac-Ala-Phe-OH. Both addition and electron transfer afford a highly stabilised tyrosyl (phenoxyl) radical (see Introduction; Section 1.7.4.2 and 1.7.4.3), while HAA from the aliphatic C-H yields a C-centred radical. Therefore, in this system the first two mechanisms cannot be differentiated.

4.6.3.1 Addition / electron transfer

The stabilised phenoxyl radical can undergo addition reaction to the radical trap **4.1** and produce a tyrosyl trapped adduct. Therefore, DI-MS analyses were scanned for the $[M + H]^+$ of a potential trapped adduct (Figure 75).

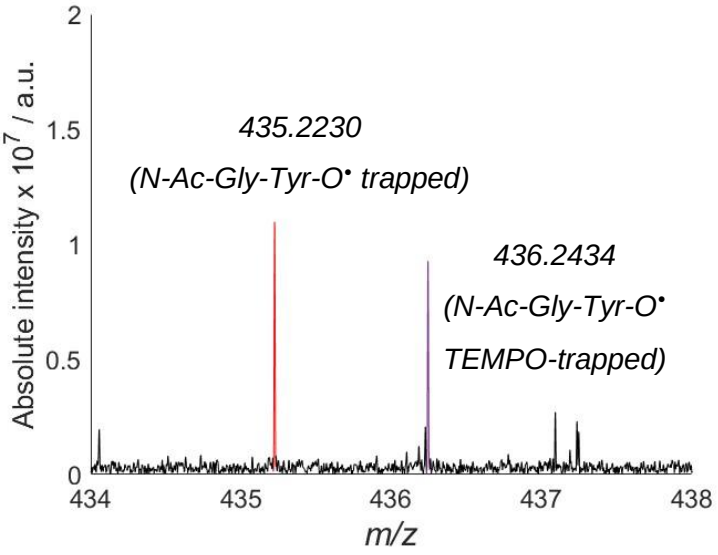

Figure 75. DI-MS spectrum showing the suspected tyrosyl radical as a trapped adduct (highlighted in red), and as a TEMPO-adduct (highlighted in purple). The tyrosyl radical can be formed via addition of HO$^{\bullet}$ to the aromatic ring of N-Ac-Gly-Tyr-OH, via ET, or via HAA by HO$^{\bullet}$ from the phenolic O-H. Reactions were carried out in open air.

Scanning of the MS spectrum revealed that a peak suggesting the formation of a tyrosyl radical trapped is evident (Figure 75; highlighted in red). The *m*/*z* of 435.2230 was also detected by LC-MS as a single peak (data in the Appendix). The same radical trapped with TEMPO$^{\bullet}$ was also identified in the DI-MS spectra (Figure 75; highlighted in purple). These data suggest that a C- and not an O-centred radical is trapped in our reactions (as reaction of TEMPO$^{\bullet}$ with O-centred is less likely), although it is possible that two different compounds contribute for the peak with the 435.2230 *m*/*z*. If the peak is due to a C-centred radical, then this could either be a resonance structure of the phenoxyl radical, or a C-centred radical generated *via* HAA on another part of the molecule (Figure 76; for the HAA mechanism see next Section).

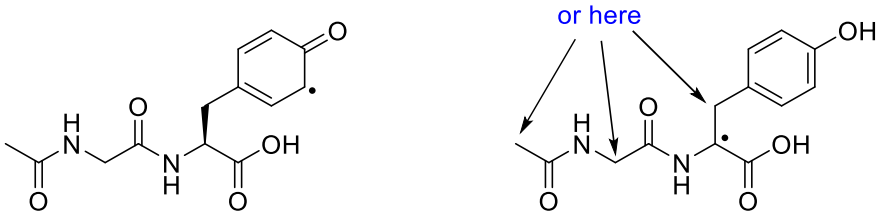

C-centred radical on *N*-Ac-Gly-Tyr-OH

*Figure 76. Possible C-centred radical structures that upon reaction with radical trap **4.1** would produce the DI-MS signal of 435.2230 of Figure 75.*

Unfortunately, due to time constraints a more in-depth investigation was not possible, and no further data were acquired to further elucidate structure responsible for the acquired *m*/*z* of 435.2230.

4.6.3.2. Hydrogen atom abstraction

The hydrogen atom abstraction component of the reactivity between $HO^{\bullet}$ and *N*-Ac-Gly-Tyr-OH can be divided into two parts. Indeed, HAA can take place from the phenolic O-H yields a phenoxyl radical (similarly to the addition/ET mechanism Section 4.6.3.1). Alternatively, HAA from the aliphatic C-H of the molecule generates C-centred radicals (either on the backbone or the side chain of the molecule, however considering the high % of deprotonation, the benzylic position would appear as the most likely position; Figure 76), that in presence of O_2 can be converted to peroxyl and alkoxyl radicals. Therefore, DI-MS were now investigated for peroxyl and alkoxyl trapped radicals (Figure 77).

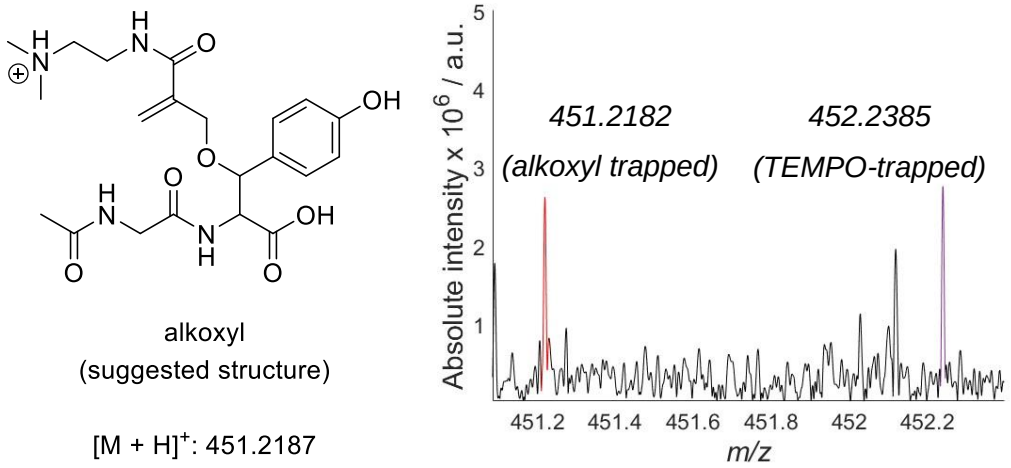

*Figure 77. Suggested chemical structure and representative DI-MS spectrum showing the suspected alkoxyl radical as a trapped adduct with **4.1** (highlighted in red), and as a TEMPO-adduct (highlighted in purple). Reactions were carried out in open air.*

Our analysis showed that the *m/z* of potential alkoxyl radical trapped adducts is present (Figure 77; highlighted in red), while the same is true for the TEMPO-adduct (Figure 77; highlighted in purple). This result indicates that the *m/z* of 451.2182 is (at least to an extent) due to a C-centred radical. This could be the case if the trapped radical is a C-centred radical that has been previously hydroxylated (i.e., a DOPA-trapped radical). Again, due to time constraints this was not investigated further, and the exact chemical structure could not be elucidated any further.

No trapped peroxyl radicals were detected. This was not surprising as the majority of the HO$^{\bullet}$ reacts with tyrosine *via* addition or electron transfer, and not HAA (see Introduction; Section 1.7.4). Therefore, the steady state concentration of peroxyl radicals remains low, and other more favoured reactions (e.g., HAA to form hydroperoxides) are taking place. Conversely, alkoxyl radical are much more reactive, and typical second order rates constants for addition of *t*-BuO$^{\bullet}$ to alkenes are in the range of $k \sim 10^5$ - 10^6 M^{-1} s^{-1}.[341] Finally, similarly to the cases of *N*-Ac-Ala-OH and *N*-Ac-Ala-Phe-OH, a wide range of degradation products were detected (DI-MS and LC-MS data can be found in the Appendix).

4.7. HO•-mediated oxidation - conclusions

We were able to use the new concept of radical trapping, that was previously developed in the Chechik group,[165–167] to characterise elusive O-centred radicals during the aerobic oxidation of biological targets, thus providing strong validation of the literature proposed mechanistic pathways. The radical trap **7** offers significant advantages for the trapping and characterisation of biological intermediate radicals as it is easily accessible, water soluble, and ionises excellently in the MS, thus making the detection of even low µM concentrations of trapped radicals possible. From our work here it becomes clear that **7** is a good compound for the trapping of carbon- centred and alkoxyl radicals but reacts less efficiently with peroxyl radicals. This is not unexpected as peroxyl radicals are generally long-lived species that follow many reaction pathways (e.g., bimolecular dismutation, HAA etc.), and show little reactivity towards electron-deficient alkenes (see Section 4.6.2.2).

Our experimental data are consistent with HO• reacting *via* different mechanisms with aliphatic and aromatic amino acids. Specifically, for *N*-Ac-Ala-OH multiple radicals arising from initial HAA by HO• were identified. The exact nature of these radicals was further elucidated by robust isotope exchange experiments, and it was confirmed that both C- and O-centred radicals were successfully trapped and characterised. Conversely, for *N*-Ac-Ala-Phe-OH and *N*-Ac-Gly-Tyr-OH radicals arising mostly from addition / ET were detected.

For *N*-Ac-Ala-Phe-OH the major reaction pathway appears to be the ET mechanism leading to a radical decarboxylation. The radical decarboxylation of phenylalanine is a well-established reaction mechanism known to proceed *via* an ET mechanism in the presence of strong oxidants (e.g., $SO_4^{\bullet-}$; see Section 1.7.4.3),[121] or by direct photolysis. Indeed, there are documented examples where direct photolysis of aqueous solutions of phenylalanine leads to the radical decarboxylation of the compound, and the ensuing C-centred radical has been characterised by time-resolved spectroscopy.[339,342,343] However, the decarboxylation as a result of direct photolysis of *N*-Ac-Ala-Phe-OH can be discounted in our work, as when aqueous solutions of *N*-Ac-Ala-Phe-OH were irradiated in the absence of H_2O_2 (all other experimental conditions were maintained the same), no radicals or oxidation products were identified. To the best of our knowledge this is the first example that the ensuing alkoxyl and peroxyl intermediate radicals, arising from the radical decarboxylation of phenylalanine are characterised by MS. Furthermore, using well-established isotope-exchange experiments both C- and O-centred radicals were conclusively identified.

We acknowledge that the experimental conditions of this study do not emulate realistic biological scenarios, and this is something that could be addressed in the future. In addition, lower concentrations of H_2O_2 (or $HO^{\bullet}$) could be used in order to resemble oxidation in living organisms more closely. Finally, we have demonstrated that our new trapping concept can be used with different oxidising agents. Indeed, we have shown that our radical trap **7** is capable of trapping intermediate radicals generated during both the ONOOH- and $HO^{\bullet}$-mediated oxidation of biomolecules. However, there are many other oxidants that are capable of reacting with biological targets.[59] It is well-established that hydroperoxides are the major intermediate compounds of protein oxidation, and it was shown that they can accelerate peptide damage, by decomposing to transient radicals.

Terpene hydroperoxides are common compounds in the atmosphere and are formed from terpene emissions. Terpenes are common naturally occurring fragrance compounds that are widely used in cosmetics, perfumes, and household products. Some terpenes have the documented propensity to undergo autoxidation leading to allylic hydroperoxides, that in turn have been linked with skin contact allergy.[344] Recently, studies have proposed that allergic contact dermatitis is a radical process mediated by allylic hydroperoxides, generated from the autoxidation of terpenes.[345,346] The final Section of this Chapter is focused on exploring terpene-derived hydroperoxides as initiators in the peptide oxidation.

4.8. Peptide oxidation by terpene-derived hydroperoxides

The process is believed to be initiated by a homolytic cleavage of the labile peroxide -O-O- bond (BDE of ~ 45 kcal mol^{-1})[136,137] producing transients $RO^{\bullet}$ and $HO^{\bullet}$, that are capable of reacting with skin proteins. For instance, allylic hydroperoxide **4.21** (Scheme 60) has been identified as a major autoxidation product of limonene **4.20** and has been reported to be a potent sensitiser.[344]

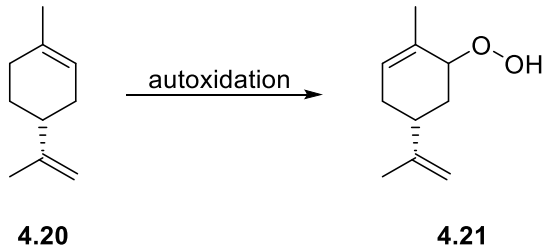

4.20 **4.21**

*Scheme 60. Oxidation of limonene **11** leading to an semi-stable allylic hydroperoxide **12**.*

Radical reactions initiated by the homolysis of terpene-derived hydroperoxides (including **4.21**) have been carried out recently, and intermediate radicals (both C- and O-centred) were characterised by spin trapping and EPR spectroscopy.[344–348] More recently, studies in this field were further expanded by investigating the iron-catalysed reactivity of allylic hydroperoxides **4.21** in the presence of protected amino acids and analysis by LC-MS.[344] The authors were able to identify adducts between the generated radicals and the biological target, thus demonstrating the potential of these radical to bind to skin proteins and cause antigenic structures. In all cases radical characterisation was achieved by either spin trapping or EPR spectroscopy. We believe that this relatively underexplored field provides an interesting new system to test the applicability of our radical traps and provide an alternative method of radical detection with a direct interest to the personal care and cosmetics industry.

4.8.1. Radical species from allylic hydroperoxides

Initial investigations on the allylic hydroperoxide **4.21** derived oxidation of protected amino acids were focused on replicating previous literature,[344] but using different starting substrates (Scheme 61).

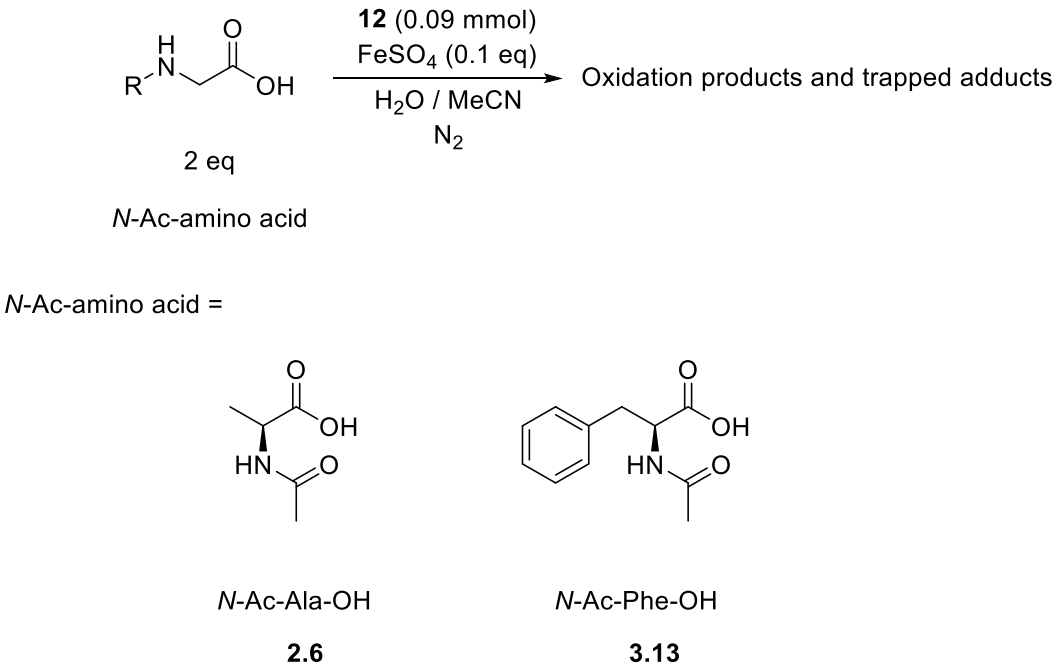

*Scheme 61. Reaction conditions for the iron-catalysed decomposition of allylic hydroperoxide **12**, and subsequent reactivity of the protected amino acids. Aliquots were collected every 24 h and were analysed immediately by LC-MS*

N-Ac-Ala-OH and *N*-Ac-Phe-OH were used as the biological targets in order to be able to directly compare our previous experimental findings on the $HO^{\bullet}$-induced oxidation, with our results here. Allylic hydroperoxide **4.21** was isolated in a one-step synthesis from H_2O_2 (50%) and (-)-carveol according to literature experimental procedure in a 40% yield.[344] Only limited spectroscopic data for the allylic hydroperoxide **4.21** were obtained (^{1}H-NMR) (more information, including the assignment of the ^{1}H-NMR in the experimental Chapter).[344]

Unlike our studies in the UV / H_2O_2 system, an excess of the biological target was used here to better resemble *in vivo* conditions. The amine group of the two amino acids was protected to mimic their structure when incorporated in peptides and proteins, and to avoid side reactions initiated by the N-terminus. $FeSO_4$ was used to cleave the labile -O-O- bond of **4.21**, as the iron-catalysed cleavage of the peroxide bond is well-established process that occurs in biological media, and therefore

emulates better real-life scenarios. The reductive cleavage of **4.21** by Fe(II) is likely to be a homolytic process yielding a transient alkoxyl radical **4.22** (Scheme 62).

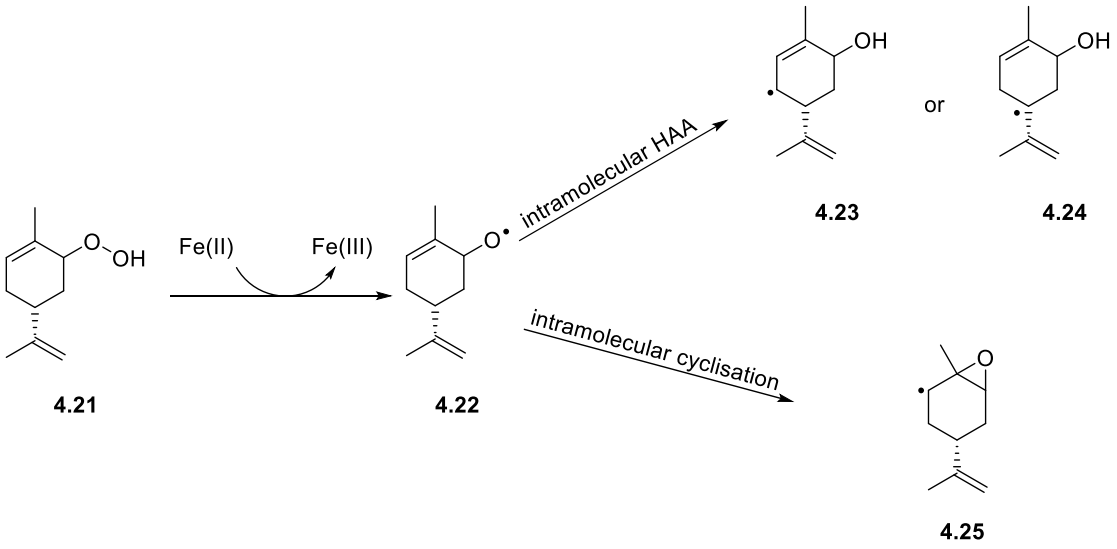

*Scheme 62. Reactivity of hydroperoxide **12** with Fe^{2+}, yielding initial O-centred radicals that in time can evolve into C-centred radicals.*

The transient alkoxyl **4.22** can evolve to a C-centred radical *via* two main unimolecular reaction pathways. It can either undergo intramolecular HAA to generate an allylic (**2.24**) or a tertiary (**4.25**) C-centred radical, or intramolecular addition to the double bond to generate an epoxide **4.25**. Alternatively, the alkoxyl radical **4.22** or any of the evolved C-centred radicals, can undergo radical-based reaction with the protected amino acids to generate non-radical adducts. It is noted that preliminary reactions were carried out under a N_2 atmosphere as the purpose of this study was to identify the short-lived radicals, and reaction with O_2 was not desirable.

4.8.2 Preliminary data and mechanistic insights

The iron-catalysed decomposition of allylic hydroperoxide **4.21** under the experimental conditions employed here is reported to be a slow process,[344] and thus, reactions were allowed to stir for 7 days with aliquots taken every 24 h. All reaction aliquots were analysed by DI-MS and LC-MS. Unfortunately, DI-MS were unsuccessful in this system, as no hydroperoxide **4.21**-derived products could be detected due to the very poor ionisation of **4.21**. Indeed, we note that both (-)-carveol (the precursor of **4.21**) and allylic hydroperoxide **4.21** ionised so inefficiently that high mM concentrations (> 50 mM) were required to even detect the pure compounds. LC-MS proved to be a more useful tool, and multiple hydroperoxide **4.21**-derived products were identified.

The reductive homolysis of hydroperoxide **4.21** yields an alkoxyl radical **4.22** that can evolve to different C-centred radicals (Scheme 62). In the case of *N*-Ac-Ala-OH, any of these radicals can abstract a hydrogen to generate C-centred radicals on the biological target. Since reactions were carried out in deaerated solvent, these radicals can accumulate and undergo dimerisation reactions or react further with the initiator. Selective scanning of LC-MS traces for the dimeric species of *N*-Ac-Ala-OH produced the following EIC (Figure 78A).

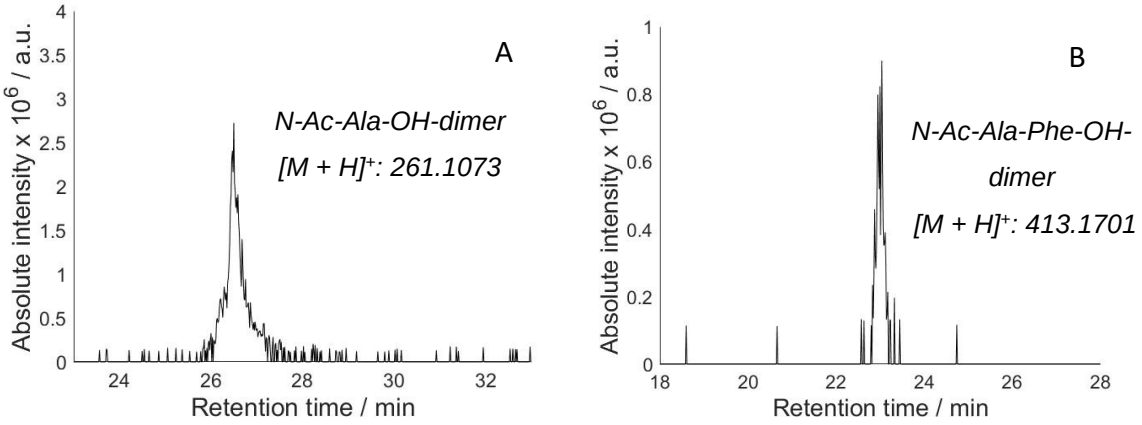

Figure 78. Representative EICs of LC-MS analysis, showing the formation of dimeric species on A) N-Ac-Ala-OH (24 h aliquot), and B) N-Ac-Phe-OH (24 h aliquot). Aliquots were analysed by LC-MS immediately after collection.

Dimerisation of *N*-Ac-Ala-OH appears to take place to a noticeable degree, with the peak emerging within the first 24 h of the reaction (Figure 78A). No *m*/*z* corresponding to potential non-radical adducts between *N*-Ac-Ala-OH and **12**-derived radicals could be identified. This likely is due to the relative stability of intermediate radicals. Indeed, *N*-Ac-Ala-OH C-centred radicals are relatively stable and are likely to be the most abundant radical in the system, thus dimerisation becomes prominent.

Based on the same mechanistic pathway, a dimerisation of *N*-Ac-Phe-OH was predicted to occur, and LC-MS chromatograms were investigated for the detection of the dimeric species (Figure 78B). In agreement with our mechanistic postulate, the detection of *N*-Ac-Phe-OH-dimer was successful (24 h). Furthermore, when *N*-Ac-Phe-OH was used as the biological substrate more non-radical products could be characterised (this is likely due to the more efficient ionisation in the positive ion MS of *N*-Ac-Phe-OH compared to *N*-Ac-Ala-OH).

The LC-MS chromatograms showed peaks that were related to the formation of *N*-Ac-Phe-OH adducts with **4.21**-derived radicals. More specifically, in agreement with literature MS data, the $[M + H]^+$ corresponding to a stable adduct between *N*-Ac-Phe-OH and radical **4.22** (or **4.23** / **4.24**) began to emerge within 24 h of the reaction (Figure 79A).

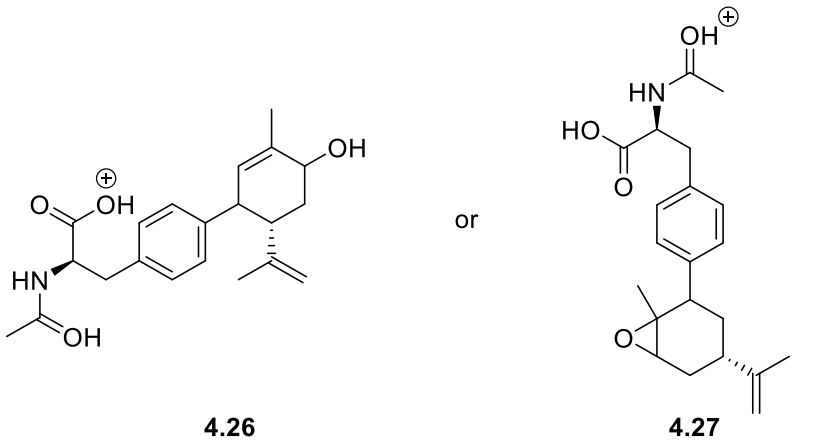

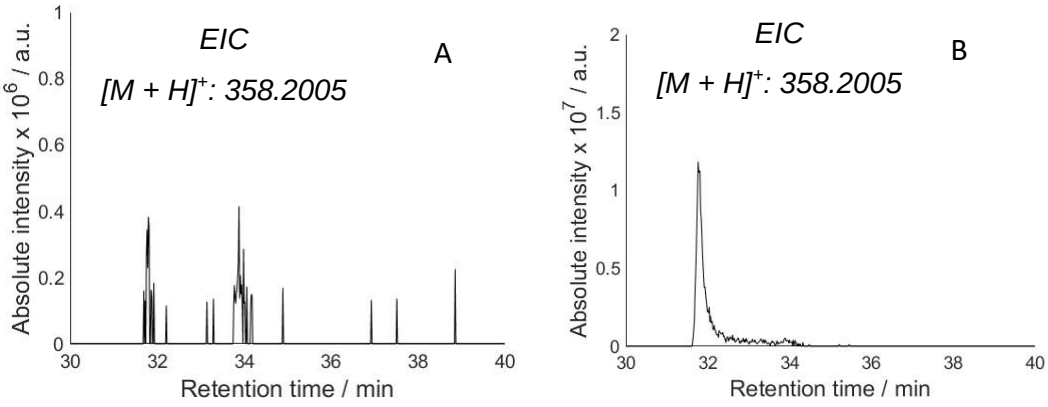

*Figure 79. Suggested chemical structures and $[M + H]^+$ for the adduct between N-Ac-Phe-OH and radicals derived from hydroperoxide **12**. LC-MS traces show representative EICs for the m/z of 358.2005 at A) 24 h, and B) 72 h. Aliquots were analysed by LC-MS immediately after collection.*

The generation of an adduct between *N*-Ac-Phe-OH and radicals derived from the homolysis of allylic hydroperoxide **4.21** is supported by the EIC chromatogram shown in Figure 79A and is consistent with literature data.[344] In fact, our analytical data suggest that two different adducts with the same $[M + H]^+$ are generated within 24 h of the reaction in similar relative intensity (first eluting at ~ 32 min and the second at ~ 34 min). This is not surprising, as reductive homolysis of hydroperoxide **4.21** yields multiple structurally different transients with the same mass (Scheme

62), and all of these radicals have the propensity to further react with *N*-Ac-Phe-OH. Unfortunately, it was not possible to further elucidate the chemical structure and assign each peak of Figure 79A to a specific adduct.

Interestingly, the compound responsible for the peak eluting at ~ 32 min continued to increase as the reaction progressed until it reached a maximum abundance at 72 h (Figure 79B). We note that at the same time, the compound responsible for the peak eluting at ~ 34 min plateaued (the peak is still there in Figure 79B with similar intensity as in Figure 79A). These data strongly indicate that while the two products appear to evolve at similar rates at the first stages of the reaction, this quickly changes, and one becomes significantly more prominent than the other.

In agreement with literature precedent, further investigation of the LC-MS chromatograms revealed another $[M + H]^+$ associated with *N*-Ac-Phe-OH. Specifically, it is reported that the epoxide adduct **4.27** is prone to nucleophilic addition of H_2O to produce the diol **4.28** (Figure 80; EIC at 72 h of reaction).

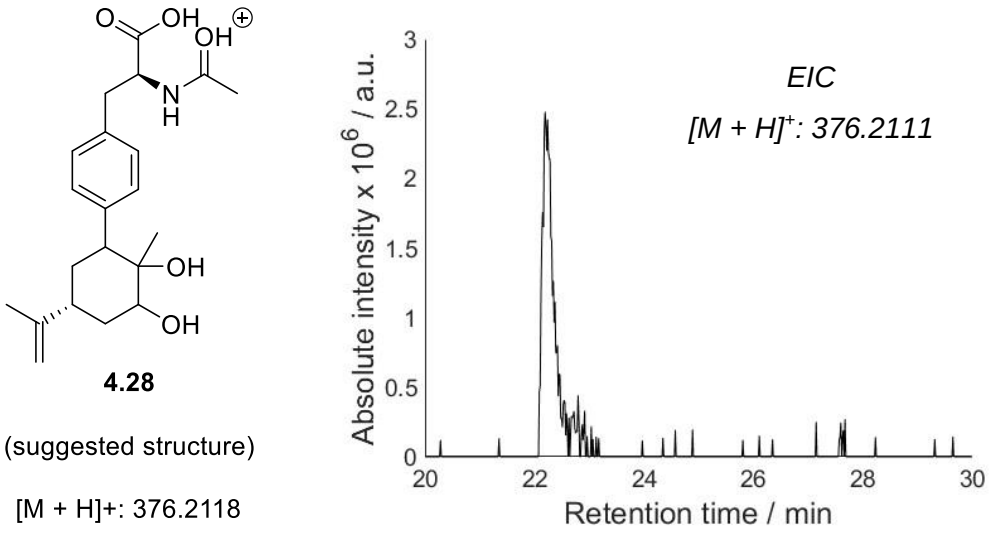

*Figure 80. Potential chemical structures and $[M + H]^+$ for the adduct between N-Ac-Phe-OH and radicals derived from hydroperoxide **12**. LC-MS traces show representative EICs for the m/z of 376.2111 at 72 h. Aliquots were analysed by LC-MS immediately after collection.*

The $[M + H]^+$ of the potential diol **4.28** was indeed present (Figure 80; LC-MS chromatogram of the reaction after 72 h). Interestingly, the acquired *m*/*z* of 376.2111 is not present at the first stages of the reaction (24 h) but is increasing in abundance thereafter. If the proposed chemical structure **4.28** and the mechanism for its formation are indeed correct, then this could provide an explanation as to why one of the peaks shown in Figure 79A is increasing over time and the other is plateauing. Indeed, this would mean that the peak eluting at 34 min in Figure 79A is due to the epoxide adduct **4.27**, and in time this converts to the diol adduct **4.28**. None of these adducts were detected when reactions were run in the absence of allylic hydroperoxide **4.28**. Lastly, in harmony with literature precedent no amino acid-derived oxidation products were detected under these experimental conditions.

4.8.3 Radical trapping

Encouraged by the successful detection of the allylic hydroperoxide **4.21**-derived adducts, we sought to investigate the trapping efficiency of our radical trap **4.1** under the same experimental conditions (Scheme 61). Therefore, reactions were repeated as earlier (i.e., 2 eq. of the biological target **2.6** or **3.13**, 1 eq. of allylic hydroperoxide **4.21** and 0.1 eq. of $FeSO_4$) with the addition of 0.1 eq. of trap **4.1** (more information in the Experimental Chapter; Section 5.4.10). LC-MS chromatograms were now scanned for adducts of the initiator **4.21** with radical trap **4.1** (Figure 81).

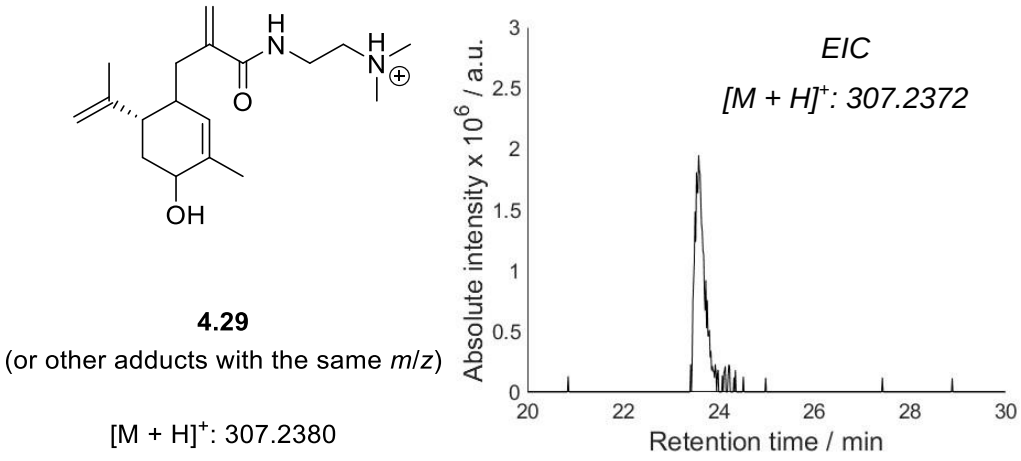

*Figure 81. Suggested chemical structure and $[M + H]^+$ of a stable non-radical adduct between the radical trap **4.1** and hydroperoxide **4.20**-derived radicals. LC-MS trace shows the EIC of the m/z of 307.2372 at 72 h. Aliquots were analysed by LC-MS immediately after collection.*

The EIC revealed that indeed an adduct associated with the radical trap **4.1** and the radicals derived from hydroperoxide **4.21** is present in the reaction mixtures. The peak eluting at ~ 24 min was not evident at the early stages of the reaction (24 h), but increased in abundance after 48 h, reaching the maximum concentration (Figure 81) at 72 h. It is noted that the $[M + H]^+$ of 307.2380 can be due to different compounds, as many of the hydroperoxide **4.21**-derived radicals have identical *m*/*z*. Unfortunately, no further elucidation of the exact chemical structure of this adduct is currently available. The detection of adduct **4.29** further corroborates that the previously detected adducts between the hydroperoxide **4.21**-derived radicals and *N*-Ac-Phe-OH are due to radical reactions.

Interestingly, no trap-related adduct with the diol **4.28** was detected. This outcome indicates that the acquired *m*/*z* of 376.2111 reported in Figure 80 is likely generated *via* a non-radical process, thus validating the literature mechanism proposal. Additionally, the hydroperoxide **4.21**-derived radicals abstract a hydrogen from the biological targets and generate C-centred radicals. In the absence of O_2 these radicals can accumulate to high concentrations and react with **4.1** to produce stable non-radical products. Considering this pathway, LC-MS chromatograms were now analysed for the characterisation of trapped C-centred adducts (Figure 82).

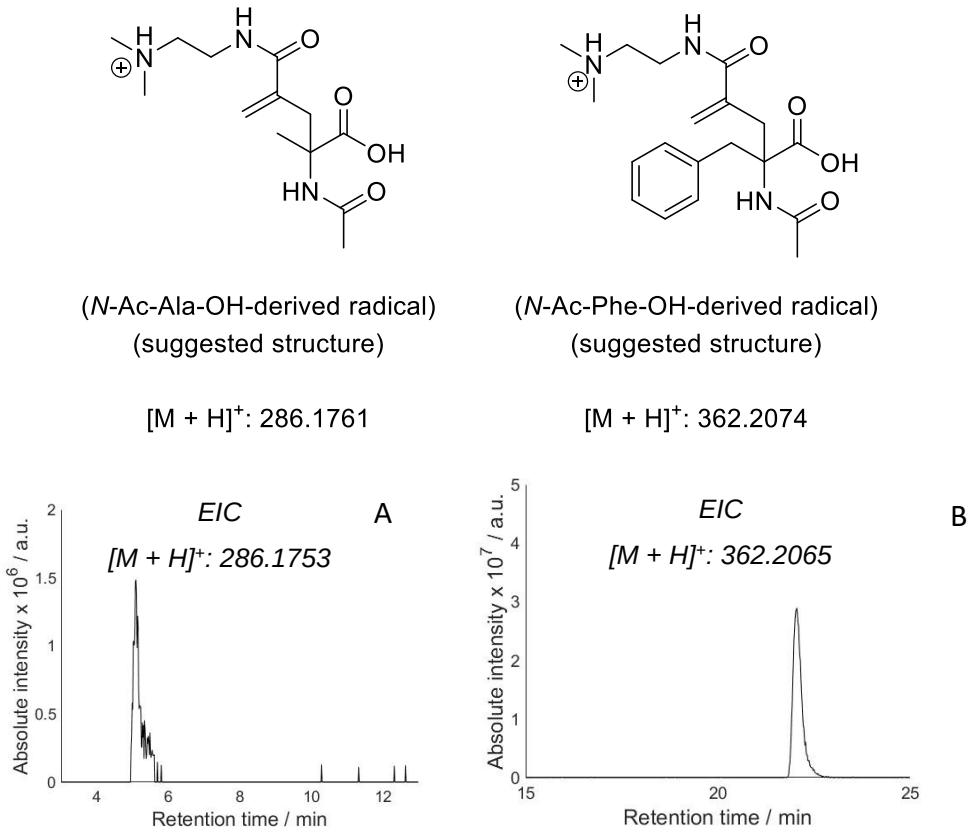

Figure 82. Suggested chemical structures and $[M + H]^+$ of trapped C-centred radicals on N-Ac-Ala-OH and N-Ac-Phe-OH with representative LC-MS EIC. Both EICs show the abundance at 72 h. Aliquots were analysed by LC-MS immediately after collection.

Consistently with our predictions, both trapped adducts associated with C-centred radicals on *N*-Ac-Ala-OH (Figure 82A) and *N*-Ac-Phe-OH (Figure 82B) were collected in relatively high abundance. Furthermore, in agreement with our previous results, the EIC of Figures 82A and 82B demonstrate the presence of the compounds at later stages of the reaction (72 h), as no evidence for their formation was obtained within the first 24 h (data not shown).

4.9 Chapter 4: Conclusions

A new approach for capturing and detecting short-lived radicals was developed previously in our group.[165–167] In this work its scope of application was further examined in the trapping of biological radicals. The scope and sensitivity of the new trapping method was investigated in the well-established ONOOH-mediated oxidation of a simple tyrosine-containing dipeptide, followed by the aerobic $HO^{\bullet}$-mediated oxidation of protected peptides. A wide range of peptide-derived radicals were successfully trapped and characterised. For *N*-Ac-Ala-Phe-OH and *N*-Ac-Ala-OH we were able to identify both C- and O-centred radicals. Using isotope exchange experiments we were able to separate, and thus conclusively assign, trapped radicals with the same $[M + H]^+$ (e.g., $ROO^{\bullet}$ from $RO^{\bullet}$ + OH).

Our results here are consistent with previous work in our group. Indeed, radical trap **4.1** has shown good efficiency at trapping C-centred and alkoxyl radicals, but not peroxyl radicals.[166,167] Trapping of peroxyl radicals with **4.1** is not as efficient, as these species react slowly with alkenes (see Section 4.6.2.2). The successful trapping and detection of peroxyl radicals, is thus depended on their steady state concentration. High steady state concentrations should allow their detection, and this was the case for *N*-Ac-Ala-Phe-OH and *N*-Ac-Ala-OH. On the contrary, reaction of HO radicals with *N*-Ac-Gly-Tyr-OH forms more stable radicals that do not undergo dioxygen addition, and as such, the steady state concentration of peroxyl radicals likely remains low. Nonetheless, both alkoxyl and peroxyl radicals were successfully trapped, and their presence was further confirmed by isotope exchange experiments. This is particularly important as biological O-centred radicals usually exist in low concentrations and their detection is very challenging.[59,104,349]

Lastly, we tested the feasibility of radical trap **4.1** to capture radicals generated from ROOH-initiated reactions. In this case C-centred radicals generated on *N*-Ac-Ala-OH and *N*-Ac-Phe-OH were successfully trapped with **4.1** and characterised by LC-MS. Moreover, we were able to detect initiator-derived radicals, thus further confirming the literature proposed mechanistic pathways.

Our results are in good agreement with previous literature work, where it was confirmed by EPR that reaction of Fe^{2+} with allylic hydroperoxide **4.21** generates both O- and C-centred radicals.[339]

The trapping of radicals arising from the reductive cleavage of terpene hydroperoxides was the closest system to realistic conditions that we have studied. Indeed, terpene hydroperoxides are believed to be present in the skin, and therefore radical initiation by Fe^{2+} (very common *in vivo*) could trigger radical chain reactions.[344,348] Unfortunately, due to time constraints, this system was not investigated further. In real systems, the generation of terpene hydroperoxides-derived radicals is likely followed by O_2 addition. Therefore, we believe in order to better emulate real-life scenarios, the effect of O_2 should be examined.

Chapter 5: Experimental

5.1 General

Unless otherwise stated, all reagents and solvents were purchased from commercial sources and used without further purification. A full list of chemicals used is provided in Section 5.2 Chemicals. Anhydrous solvents were obtained from an Innovative Technology Inc. PureSolv® solvent purification system.

Thin layer chromatography was carried out on Merck silica gel 60F254 pre-coated aluminium foil sheets and were visualised by staining with basic aqueous potassium permanganate. Flash column chromatography was carried out using slurry packed Fluka silica gel (SiO_2), 35–70 µm, 60 Å under a light positive pressure, eluting with the specified solvent system. ^{1}H and ^{13}C nuclear magnetic resonance (NMR) spectra were recorded in $CDCl_3$, DMSO-d^6, D_2O or MeOD-d^4 on a JEOL ECX400 spectrometer, operating at 400 MHz. Chemical shifts (δ) are quoted in parts per million (ppm). The residual solvent peaks were used as references in ^{1}H were δH 7.26 ppm, 2.50 ppm, 4.78 ppm and 3.31 ppm for $CDCl_3$, DMSO-d^6, D_2O and MeOD-d^4, respectively. Coupling constants (*J*) are reported in Hertz (Hz) to the nearest 0.1 Hz. The multiplicity abbreviations used are: s singlet, d doublet, t triplet, br broad, dd double doublet, dt double triplet, and m multiplet. Signal assignment was achieved by analysis of DEPT, COSY, HMQC and HMBC experiments where required. Mass spectra of synthesised compounds were recorded using positive or negative electrospray ionisation on a Bruker compact QTOF MS (compact) mass spectrometer (±0.001 *m/z* precision, 30000 resolution). Mass spectra of oxidation products and trapping reactions were recorded using positive electrospray ionisation (Pos ESI) on a high resolution solariX XR FTMS (solariX) mass spectrometer (±0.0001 *m/z* precision, >10^7 maximum resolution, mass accuracy 600 ppb (internal)), unless stated otherwise. All experiments and aqueous solutions were prepared using high-purity Milli-Q Water, or deuterium oxide (D_2O) that was supplied by Merck. All other solvents used were of analytical grade. For the hydroperoxide experiments, glassware was cleaned in concentrated nitric acid and thoroughly rinsed with Milli-Q water. This procedure was found to be essential for the removal of traces of iron.[148]

5.2 Chemicals

All chemicals in this list were used without further purification. *2,2,6,6*-Tetramethylpiperidine 1-oxyl (TEMPO•, 98%, Fluorochem), sodium sulfite (≥98%, Sigma-Aldrich), *O*-(benzotriazol-1-yl)-*N*,*N*,*N*′,*N*′-tetramethyluronium hexafluorophosphate (HBTU, 98%, Fluorochem), *N*,*N*-diisopropylethylamine (DIPEA, ≥99%, Fluorochem), sodium iodide (>99%, Thermo Scientific), methyl 2-(bromomethyl)acrylate (>97%, Fluorochem), ethylenediamine (99%, Fluorochem), acetic anhydride (>99%, Acros Organics), acetic acid (>99%, Fluorochem), *N*,*N*-dimethylethylenediamine (≥98%, Fluorochem), pentetic acid (99%, Sigma-Aldrich), isoamyl nitrite (≥ 95%, Fluorochem), hydrogen peroxide (30 wt.%, Fischer Chemical), hydrogen peroxide (50 wt.%, Fischer Chemical), (-)-carveol (mixture of isomers, 97%, Fluorochem), glycyl-L-tyrosine (Gly-Tyr-OH, ≥ 97%, Fluorochem), L-alanine-L-phenylalanine (Ala-Phe-OH, ≥ 97%, Fluorochem), *N*-acetyl-L-alanine (*N*-Ac-Ala-OH, ≥ 97%, Fluorochem), xylenol orange tetrasodium salt (XO, Merck), ammonium Fe(II) sulfate (≥ 98%, Merck), catalase from bovine liver (aqueous solution; > 30,000 units per mg of protein) was supplied by Sigma Aldrich, sulfuric acid (Fisher Scientific), nitric acid (Fisher Scientific). Water (LC-MS grade, ≥99.9%, Fischer Chemical), acetonitrile (LC-MS grade, ≥99.9%, Fischer Chemical), formic acid (LC-MS grade, ≥99%, Fischer Chemical), formic acid-d_2 (95 wt.% in D2O, 98% atom % D, Sigma-Aldrich) were used for MS characterisation.

5.3 Synthetic procedures

N-Ac-Gly-Gly-OH

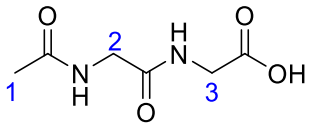

2.1

Gly-Gly-OH (2.0 g, 15.14 mmol, 1.0 eq.) was dissolved in aqueous NaOH solution (2 M; 15.0 mL). The solution was cooled at 0 °C and stirred. Then acetic anhydride (15.0 mL, 15.86 mmol, 1.1 eq.) was added dropwise while stirring at 0 °C. Upon complete addition, the solution was acidified to pH 2 with aqueous 2.0 M HCl solution and extracted with EtOAc (3 x 25 mL). The organic layers were combined, dried over $MgSO_4$, filtered and concentrated *in vacuo* to give the crude product as a white powder (1.97 g). The pure title compound 2.**1** was obtained as a white powder in a 67% yield (1.77 g, 10.14 mmol) after recrystallisation from H_2O/acetone.

^{1}H NMR (400 MHz, *D_2O*) δ ppm: 3.96 (2 H, s, H-2), 3.91 (2 H, s, H-3), 2.03 (3 H, s, H-1). Data are in agreement with the literature.[350] **HRMS** (ESI): $[M + H]^+$ HRMS acquired 175.0714, calculated 175.0713, $[M + Na]^+$ HRMS found 197.0533, calculated 197.0533.

N-Ac-Gly-Tyr-OH

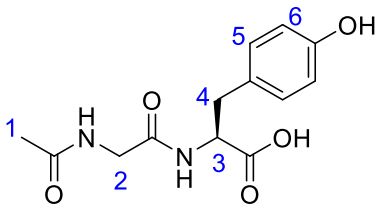

2.4

Gly-Tyr-OH (2.0 g, 8.39 mmol, 1 eq.) was dissolved in aqueous NaOH (2.0 N; 4.2 mL) and reaction was cooled to 0 °C. After 5 min, acetic anhydride (0.9 mL, 9.24 mmol, 1.1 eq.) dissolved in a mixture of THF (1.8 mL) and NaOH (4.0 N; 2.35 mL) was added dropwise over 45 min, while maintaining the pH at 11. Upon complete addition the reaction was continued to be stirred at 0 °C for another 1 h. After that, reaction was acidified with concentrated HCl to pH 1. The crude mixture was then concentrated to *in vacuo* to half volume before filtering (vacuum filtration). The precipitate was washed with ice-cold H_2O (20 mL), to afford the pure title compound **2.4** as a white powder in a 77% yield (1.8 g, 6.45 mmol).

^{1}**NMR** (400 MHz, *DMSO-d*^{6}) δ ppm: 8.09-7.95 (2 H, m, N-*H*), 7.04-6.92 (2 H, d, *J* 8.4 Hz, H-6), 6.70-6.58 (2 H, d, *J* 8.4 Hz, H-5), 4.37-4.27 (1 H, m, H-3), 3.73-3.66 (1 H, dd, *J* 15.0, 6.0 Hz, H-2), 3.62-3.55 (1 H, dd, *J* 15.0, 6.0 Hz, H-2) 2.93-2.86 (1 H, dd, *J* 14.0, 5.5 Hz, H-4), 2.80-2.70 (1 H, dd, *J* 14.0, 5.5 Hz, H-4), 1.82 (3 H, s, H-1). Spectroscopic data are in agreement with the literature.[351] **HRMS** (ESI): [M - H]$^-$ HRMS acquired: 279.0993, calculated: 279.0986.

N-Ac-Ala-Phe-OH

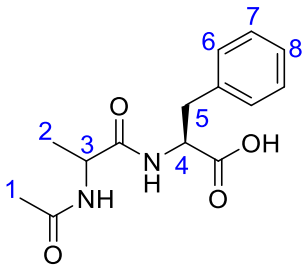

2.5

Ala-Phe-OH (2.0 g, 8.46 mmol, 1 eq.) was suspended in acetic acid (24.0 mL), and reaction was heated to 40 °C and stirred. Upon complete dissolution, acetic anhydride (0.9 mL, 9.24 mmol, 1.1 eq.) was added dropwise over 10 min. Upon complete addition of acetic anhydride, reaction was heated to 100 °C, and left stirring for 2 h. After this, reaction was concentrated *in vacuo* and a white powder was obtained. The crude mixture was suspended in Et_2O (10 mL) and filtered. The precipitate was washed with ice-cold H_2O (20 mL) and Et_2O (20 mL), to afford the purified title compound **2.5** as a white powder in a 59% yield (1.4 g, 5.03 mmol).

^{1}**NMR** (400 MHz, *MeOD-d*^{4}) δ ppm: 7.30-7.15 (5 H, m, H-6, H-7, H-8), 4.70-4.60 (1 H, m, H-3), 4.40-4.25 (1 H, m, H-4), 3.25-3.15 (1 H, m, H-5), 3.05-2.92 (1 H, m, H-5), 1.95-1.91 (3 H, m, H-1), 1.32-1.10 (3 H, m, H-2). Spectroscopic data are in agreement with the literature.[351] **HRMS** (ESI): $[M + Na]^+$ HRMS acquired: 301.1157, calculated: 301.1159.

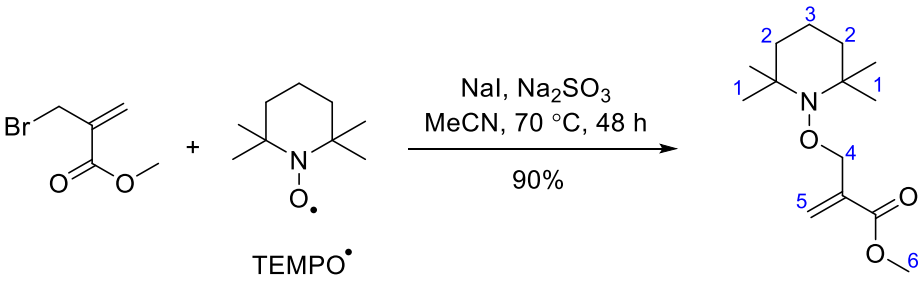

5.1

Methyl-2-(TEMPOmethyl)-acrylate

Methyl 2-(bromomethyl)acrylate (2.0 g, 11.17 mmol, 1.0 eq.), (2,2,6,6-tetramethylpiperidin-1-yl)oxyl (TEMPO•, 2.1 g, 13.44 mmol, 1.2 eq.), NaI (3.35 g, 22.35 mmol, 2.0 eq.), Na_2SO_3 (4.24 g, 33.64 mmol, 3.0 eq.) were dissolved in MeCN (100 mL) and placed in a flame-dried two-neck round bottom flask charged with a stirrer bar. This solution was sealed and purged thoroughly with N_2 before being heated to 70 °C, and was stirred for 48 h. MeCN was then removed *in vacuo*. H_2O (100 mL) was added and was extracted with EtOAc (3 × 100 mL). The organic layers were dried with $MgSO_4$, filtered and solvent removed *in vacuo*, yielding a crude orange oil (2.5 g). This was purified using flash silica column chromatography (1:99 MeOH: CH_2Cl_2) yielding the pure title compound **5.1** as a yellow oil in a 94% yield (2.68 g, 10.49 mmol)

^{1}**NMR** (400 MHz, *$CDCl_3$*) δ ppm: 6.32-6.26 (1 H, br. s, H-5), 5.94-5.89 (1 H, br. s, H-5), 4.53-4.47 (2 H, m, H-4), 3.76 (3 H, s, H-6), 1.65-1.45 (6 H, m, H-2, H-3), 1.18 (3 H, s, H-1), 1.12 (3 H, s, H-1). Spectroscopic data are in agreement with the literature.[167] **HRMS** (ESI): $[M + H]^+$ HRMS acquired: 256.1905, calculated: 256.1907.

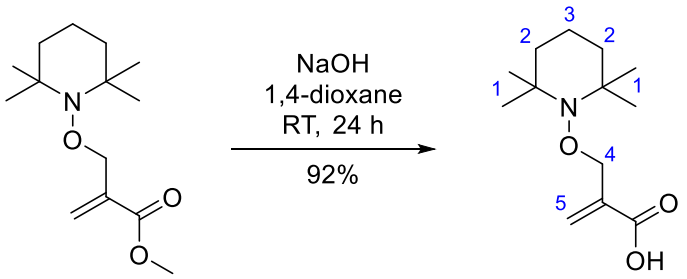

5.1 **5.2**

2-(TEMPOmethyl)-acrylic acid

2-([(2,2,6,6-Tetramethylpiperidin-1-yl)oxyl]methyl)acrylate **5.1** (2.50 g, 9.80 mmol, 1.0 eq.) was dissolved in 1,4-dioxane (50 mL), and aqueous NaOH (1.0 M; 50 mL) was added, and the solution was stirred for 24 h. The resultant solution was acidified (pH 5) with aqueous HCl (2.0 M), and the crude mixture was extracted with EtOAc (3 × 50 mL). The organic layers were washed with brine (1 x 40 mL), dried with $MgSO_4$, filtered and solvent removed *in vacuo*, yielding a crude golden oil. This was purified using flash silica column chromatography (0.1:4:96 acetic acid:MeOH:CH_2Cl_2) yielding the pure title compound **5.2** as a yellow oil in 92% yield (2.18 g, 9.01 mmol).

^{1}**NMR** (400 MHz, *$CDCl_3$*) δ ppm: 6.41 (1 H, br. S., H-5), 5.98 (1 H, br. S., H-5), 4.53 (2 H, br. S., H-4), 1.68-1.28 (6 H, m, H-2, H-3), 1.19 (3 H, s, H-1), 1.15 (3 H, m, H-1). Spectroscopic data are in agreement with the literature.[167] **HRMS** (ESI): $[M + H]^+$ HRMS acquired: 242.1752, calculated: 242.1751. $[M + Na]^+$ HRMS acquired: 264.1574, calculated: 264.1570.

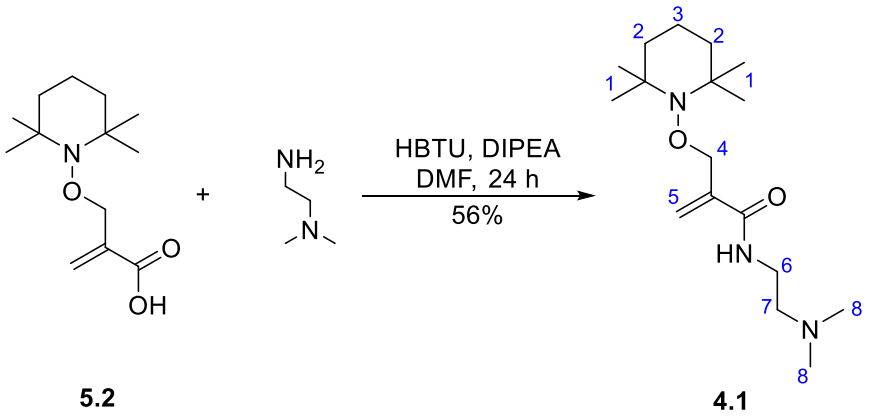

5.2 **4.1**

22 (600 mg, 2.49 mmol, 1.0 eq.) was added to a flask, and it was dissolved in DMF (10.0 mL). To this flask, HBTU (1.04 g, 2.74 mmol, 1.1 eq.), DIPEA (643 mg, 4.98 mmol, 2.0 eq.), and *N,N*-dimethylethylenediamine (220 mg, 2.49 mmol, 1.0 eq.) were added, and reaction was left to stir for 24 h. After this, the solvent was removed *in vacuo*. Saturated aqueous $NaHCO_3$ (10 mL) was added, and the crude mixture was extracted with EtOAc (3 × 10 mL). The combined organic layers were washed with brine (1 × 10 mL). The organic layer was dried with MgSO4, filtered and solvent removed *in vacuo* yielding the crude product. This was then purified using flash silica column chromatography (2:4:96 NaOH:MeOH:CH_2Cl_2) yielding the pure title compound **4.1** in a 56% yield (435 mg, 1.39 mmol)

^{1}**NMR** (400 MHz, *CDCl*$_3$) δ ppm: 7.00 (1 H, br. s., N-*H*), 6.05 (1 H, dt, *J* 1.4, 1.1, H-5), 5.50 (1 H, dt, 1.4, 0.6, H-5), 4.9 (1 H, dd, *J* 1.1, 0.6 H-4), 3.42 (2 H, t, *J* 5.6, H-6), 2.44 (2 H, t, , *J* 5.6 H-7), 2.20 (6 H, s, H-8), 1.65-1.40 (6 H, m, H-2, H-3), 1.18 (3 H, s, H-1), 1.10 (3 H, m, H-1). Spectroscopic data are in agreement with the literature.[167]

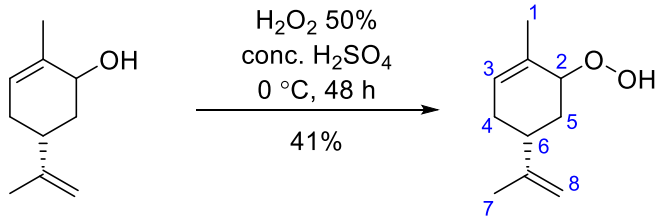

5.3 (-)-carveol

4.21 2-hydroxyperoxylimonene

Hydrogen peroxide (50%, 7.1 mL) was added to a round-bottom flask charged with a stirrer bar, and the flask was cooled at 0 °C. To this flask, a few drops of conc. H_2SO_4 were added, and the mixture allowed to stir for a few minutes. Then, (-)-carveol **5.3** (97%, 500 mg, 3.28 mmol, 1.0 eq.) was added, and the mixture was allowed to stir for 48 h at 0°C. After 48 h, the reaction mixture was allowed to warm to RT, before extracting with pentane (5 x 20 mL). The organic layers were combined, dried over MgSO4, filtered, and concentrated *in vacuo* to remove excess solvent. The crude product was collected as a yellow oil and was purified by flash silica column chromatography on a neutralised silica gel 4:1 pentane:Et_2O) yielding the pure title compound **4.21** in a 41% yield (227 mg, 1.35 mmol, mixture of diastereomers) as a colourless oil.

^{1}**NMR** (400 MHz, *$CDCl_3$*) δ ppm: 5.75-5.68 (1 H, m, H-3), 5.62-5.55 (1 H, m, H-3), 5.48-5.38 (1 H, m, H-2), 5.28-5.20 (1 H, m, H-2), 4.76-4.66 (2 H, m, H-8), 2.35-2.25 (1 H, m, H-6), 2.24-2.14 (1 H, m, H-5), 1.99-1.75 (3 H, m, H-4, H-5), 1.73-1.66 (6 H, m, H-1, H-7). To the best of our knowledge, this is the correct ^{1}H-NMR assignment of the molecule. Our spectroscopic data are slightly different from the one reported in the literature.[344,348]

5.4 Experimental protocols

5.4.1 General irradiation conditions

Aqueous solutions of substrates (5 mM for *N*-Ac-Gly-Gly-OH, 1 mM for all others) were exposed to UV light in the presence of aqueous H_2O_2 (100 mM), using a Philips HPK 125 W high pressure Hg lamp with a H_2O filter (5 cm) which provides broad-band UV light.[352,353] The light output from this HP lamp provides maximum energy at 365 nm with substantial radiation also at 435, 404, 313 and 253 nm.[354] All irradiations were carried out in H_2O or D_2O.

5.4.2 $HO^{\bullet}$-mediated generation and quantification of hydroperoxides

Hydroperoxides were generated by irradiation (5.4.1). The reactions were carried out in a quartz Schlenk tube (50 mL final reaction volume; open to air). The glassware was placed 1 cm in front of the UV lamp, and the irradiance at the sample location was 32 mW cm^{-2}. Aliquots (1 mL) were taken before the UV exposure and then at the indicated timestamps. Aliquots were treated with catalase (aqueous solution, 10 µL; activity 3150 U mL^{-1}) immediately after cessation of irradiation to decompose residual H_2O_2. After catalase treatment (15 minutes) the samples were diluted (5 mL final volume), frozen in liquid N_2 and stored in the freezer. Aliquots containing the hydroperoxides were thawed on the day of analysis and were analysed by the FOX-assay (5.5.1). For *N*-Ac-Ala-OH (**2.6**), reactions were carried out 6 times (as opposed to triplicate for *N*-Ac-Gly-Gly-OH (**2.1**), *N*-Ac-Gly-Tyr-OH (**2.4**) and *N*-Ac-Ala-Phe-OH (**2.5**)) to account for the higher errors in the weekly variations of the calibration curve.

5.4.3 Sunlight-induced decay of *N*-Ac-Gly-Gly-OH-derived hydroperoxides

At the end of the irradiation (5.4.1), the remainder of the solution (45 mL) was treated with catalase (10 µL; similarly to the hydroperoxide quantification Section 5.4.2). After 15 min, the H_2O_2-free solutions were exposed to a lamp that simulates sunlight for 120 min. The irradiance at the sample location was 100 W cm^{-2}, and the output spectrum was AM1.5G which refers to the standard spectrum of the solar output at Earth's surface. The output is from 290 to 1250 nm, with a maximum at 500 nm. Aliquots (1 mL) were taken at the indicated timestamps and treated as in 5.4.2 to determine the total hydroperoxide content.

5.4.4 UV-induced decay of hydroperoxides

At the end of the irradiation (5.4.1), the remainder of the solution (45 mL) was treated with catalase (10 µL; similarly to the hydroperoxide quantification Section 5.4.2). After 15 min, the H_2O_2-free solutions were exposed to the same UV lamp (5.4.1) for 2 min. Aliquots were taken at the indicated timestamps and treated as in 5.4.2 to determine the total hydroperoxide content.

5.4.5 Thermal treatment of irradiated solutions

At the end of the irradiation (5.4.1), the remainder of the solution (45 mL) was treated with catalase (10 µL; similarly to the hydroperoxide quantification Section 5.4.2). After 15 min, the H_2O_2-free solutions were incubated at 61, 82 or 100 °C for 30 min. Aliquots were taken at the indicated timestamps and were treated as in 5.4.2 to determine the total hydroperoxide content. In addition, one aliquot (0.01 mL diluted to 1 mL for *N*-Ac-Gly-Tyr-OH (**2.4**) and *N*-Ac-Ala-Phe-OH (**2.5**), and 0.1 mL diluted to 1 mL for *N*-Ac-Ala-OH (**2.6**)) was analysed by LC-MS to determine the parent substrate concentration (5.4.5).

5.4.6 $HO^{\bullet}$-mediated oxidation of 4 and 6 in the presence of antioxidants

The four catechol-based antioxidants were supplied as isolated compounds (powders) by P&G. In addition, 6 rosemary extracts (powders or oils) were supplied as mixture of compounds by P&G. For all antioxidants (both isolated and extracts), fresh stock solutions in MeOH:H_2O were prepared the day of analysis. Irradiations were carried out according to general procedure 5.4.1. The reactions were carried out in a quartz cuvette (3 mL final reaction volume; open to air). The glassware was placed 10 cm in front of the UV lamp. Samples were exposed to UV light for 2 min and were analysed (undiluted) by LC-MS (5.5.6) immediately after cessation of irradiation.

5.4.7 Sodium borohydride treatment

Photo-generated hydroperoxides were reduced by treatment with solid $NaBH_4$ (1 mg per mL of solution). Solutions were left to incubate in the dark for 1 h, before lowering the pH of the solutions to 2 using aq. 1 M HCl, to neutralise the remaining $NaBH_4$. The pH of the solutions was then restored to 6 using aq. 1 M NaOH. The total hydroperoxide content was determined by FOX-assay and showed complete disappearance of hydroperoxides. This procedure was followed both for the reduction of hydroperoxides generated on the peptides (Chapter 2), and hydroperoxides generated on the antioxidants (Chapter 3).

5.4.8 ONOOH synthesis and reactions

5.4.8.1 Synthesis

ONOOH was synthesised according to a well-established protocol.[331] H_2O_2 (30%, 5 mL) was diluted in H_2O to 50 mL final volume, before cooling the solution at 0 °C. To this solution 5 N NaOH (9 mL), and pentetic acid (5 mL, 0.05 M in 0.05 N NaOH) was added and the solution was stirred. The solution was then further diluted in H_2O to 100 mL final volume. This solution was then mixed with isoamyl nitrite (6.8 mL), and was stirred for 8 h at 0 °C. The reaction progress was monitored by taking aliquots (1 mL) every 1 h, centrifuging to separate the aqueous from the organic layer, diluting the aqueous phase x 1000 with 0.1 N NaOH, and measuring the ONOOH concentration spectroscopically at 302 nm (ε_{302} = 1670 M^{-1} cm^{-1}). Upon maximum formation of ONOOH (7-8 h), the mixture was extracted with CH_2Cl_2 (6 x 50 mL), and the aqueous phase was collected. Pure ONOOH was obtained upon purification with flash column chromatography filled with granular MnO_2. The column was washed with H_2O (first) and 0.5 N NaOH (second). The first 10 mL were discarded (colourless solution), and then pure ONOOH was collected (yellow solution).

5.4.8.2 Reactions

Reactions were carried out at various concentrations of ONOOH (5 – 500 µM). ONOOH was allowed to react with *N*-Ac-Gly-Tyr-OH (5 – 50 µM), in strongly buffered (0.1 M phosphate buffer pH 7.4) solutions and in the presence of trap **4.1** (5 – 500 µM). All reagents were mixed, and allowed to react for 30 min at RT. All reactions were analysed by LC-MS (5.5.7).

5.4.9 $HO^{\bullet}$-mediated oxidation of 2.4, 2.5 and 2.6 in the presence of radical trap 4.1.

Irradiations were carried out according to general procedure 5.4.1 and conditions as in 5.4.2. Radical trap **4.1** (0.1 mM) was added to the reactions. Samples were frozen in liquid N_2 and stored in the freezer immediately after cessation of irradiation. Samples were thawed the day of analysis. Samples were analysed by DI-MS (5.5.2) and LC-MS (5.5.3)

5.4.10 Reaction of 2.6 and 3.13 with allylic hydroperoxide 4.20

Substrate **2.6** or **3.13** (2 eq.), allylic hydroperoxide **4.20** (1 eq.), and $FeSO_4$ heptahydrate (0.1 eq.) were dissolved in a deoxygenated 1:1 mixture of H_2O/MeCN so that final concentrations were (in a 5 mL reaction), 35.6, 17.8 and 1.78 (all in mM), respectively. Reactions were also run under the same conditions, but with the addition of radical trap **4.1** (0.1 eq., 1.78 mM). The reactions were rigorously stirred under N_2 at RT for 7 days (as per literature protocol),[344] with aliquots taken every 24 h. Aliquots were diluted (x 10) and analysed immediately by LC-MS (5.5.8).

5.5 Analysis protocols

5.5.1 FOX-assay

Hydroperoxides were quantified following a modified version of the FOX assay.[64] A fresh solution (assay solution) containing 4-5 mM ammonium Fe(II) sulfate and 4 mM Xylenol orange in 0.5 M H_2SO_4 was prepared every day and passed through a 0.45 μm syringe filter to remove any undissolved matter. Ammonium Fe(II) sulfate was dissolved directly in H_2SO_4 as aerobic Fe(II) oxidation is significantly slower under acidic pH. The assay solution was added to the desired peroxide sample (0.25 mL of assay solution for 5 mL of peroxide solution). The samples were gently mixed and incubated in the dark for 30 minutes. After that time the absorbance at 560 nm was recorded. The data were analysed using the calibration standard curve and peroxides levels are reported as H_2O_2 equivalents. The calibration curve was constructed using H_2O_2 standard solutions according to a well-established literature protocol and can be found in Appendix.[149]

5.5.2 Direct injection MS analysis

Direct injection MS characterisation (DI-MS) was performed using a solariX XR FTMS mass spectrometer in positive-ion mode ESI (*m/z* ±0.001 precision, 30000 resolution, 1-50 Hz scan speed). Mass spectra were recorded over an *m/z* range of *m/z* 100-1000, averaging multiple scans (16). Ion transfer time (ToF) was set to 0.6 ms. In general, ESI settings were as follows: drying gas flow = 2.0 L min^{-1}; nebulizer pressure: 2.0 bar; dry temperature: 180 °C, capillary voltage = 4500 V; spray shield voltage = -500 V; skimmer voltage = 15 V. For standard MS (including D2O exchange), other settings used were: injection speed = 2 µL min^{-1}; ion accumulation time = 0.2 s; drying gas temperature = 180 °C. The MS instrument was calibrated daily using a dilute solution of sodium trifluoroacetate (NaTFA) in a 1:1 MeCN/H_2O mixture in ESI. Samples were injected in the spectrometer (2 µL min^{-1}) until stable signal was detected (typically within 5 min). A mass spectrum was then recorded, and the spectrometer was reflushed with the 1:1 MeCN/H_2O mixture and the procedure was repeated. Accepted random *m/z* error was < 0.0000 - 0.0010. For the isotope-exchange experiments, the solariX XR FTMS mass spectrometer allowed a definitive separation and detection between the fully deuterated products, and the ^{13}C satellite peaks. In the event where this was not possible, then this is fully acknowledged and discussed appropriately in the text.

5.5.3 LC-MS Analysis - General

Separation of samples was performed by LC-MS using an Agilent 1200 liquid chromatography machine equipped with a reverse phase 2.7 μm Waters Correct T3 (150 × 3 mm) column and coupled to a SolariX XR FTMS 9.4T mass spectrometer. Samples were separated at 25 °C with a flow rate of 0.2 mL min^{-1} by gradient elution, and 1 scan with a 0.2 s accumulation time. Elution solvents were: A) 0.1% formic acid in H_2O and B) 0.1% formic acid in MeCN. Gradient elution was different based on the system (Sections 5.5.4 to 5.5.8). General ESI settings (unless otherwise stated) were as follows: drying gas flow = 4.0 L min^{-1}; nebulizer pressure: 4.0 bar; dry temperature: 240°C, capillary voltage = 4500 V; spray shield voltage = -500 V; skimmer voltage = 15 V.

5.5.4 Separation and analysis of oxidised samples for Chapter 1

All oxidised solutions were analysed by DI-MS (5.5.2) and LC-MS (5.5.3) with gradient elution as reported in Table 1.

Table 3. Gradient elution for LC-MS separation used in 6.5.4. Elution solvents consisted of A) 0.1% formic acid in H_2O and B) 0.1% formic acid in MeCN.

Time / min	% A	% B
0	100	0
5	100	0
10	90	10
15	90	10
25	70	30
30	70	30
35	95	5
40	100	0
45	100	0

5.5.5 Peptide calibration curves

Calibration curves for *N*-Ac-Gly-Tyr-OH (**2.4**), *N*-Ac-Ala-Phe-OH (**2.5**), *N*-Ac-Ala-OH (**2.6**) and *N*-Ac-Phe-OH (**3.13**) were constructed by separating the parent peptides by LC-MS (5.5.3), with a gradient elution (5.5.4). Liquid chromatography – mass spectrometry (LC-MS) calibration curves were constructed by preparing the most concentrated sample of the substrates (0.1 mM for *N*-Ac-Gly-Tyr-OH (**2.4**)**,** *N*-Ac-Ala-Phe-OH (**2.5**) and *N*-Ac-Phe-OH (**3.13**), and 1 mM for *N*-Ac-Ala-OH (**2.6**)), and then preparing serial dilutions (0.02 – 0.08 mM for *N*-Ac-Gly-Tyr-OH (**2.4**)**,** *N*-Ac-Ala-Phe-OH (**2.5**), and *N*-Ac-Phe-OH (**3.13**), and 0.2 – 0.8 mM for *N*-Ac-Ala-OH (**2.6**)). The method afforded excellent calibration curves ($R^2 > 0.997$ in all cases). For *N*-Ac-Gly-Tyr-OH (**2.4**)**,** *N*-Ac-Ala-Phe-OH (**2.5**) and *N*-Ac-Phe-OH (**3.13**), the UV detector was used, and the calibration curves were constructed by integrating the peak of the peptides. For *N*-Ac-Ala-OH (**2.6**)**,** the total ion count (TIC) of the $[M + H]^+$ extracted ion chromatogram (EIC) was used. All four calibration curves can be found in the Appendix. Daily and weekly variations of the calibration curves were assessed by repeating LC-MS injections with fresh solutions for all diluted samples.

5.5.6 Separation and analysis of oxidised samples for Chapter 2

Oxidised solutions containing antioxidants were analysed and separated by LC-MS (5.5.3) with a gradient elution. The gradient is given in Table 2. ESI settings were as follows: drying gas flow = 4.0 L min^{-1}; nebulizer pressure: 2.0 bar; dry temperature: 240°C. For reactions run in D_2O, the same gradient was used, but elution solvents were A) 0.1% formic acid-d_2 in D_2O, and B) 0.1% formic acid-d_2 in MeCN.

Table 4. Gradient elution for LC-MS separation used in 6.5.6. Elution solvents consisted of A) 0.1% formic acid in H_2O and B) 0.1% formic acid in MeCN.

Time / min	% A	% B
0	100	0
5	100	0
10	70	30
15	70	30
25	50	50
35	50	50
40	30	70
45	30	70
50	100	0
60	100	0

5.5.7 Separation and analysis of ONOOH- and HO•-induced oxidised samples for Chapter 3

Oxidised solutions containing the substrates and radical trap **4.1** were analysed by DI-MS (5.5.2) and LC-MS (5.5.3) with gradient elution as reported in Section 5.5.4. When high **7** concentrations were used (≥ 0.1 µM), a waste-segment was added in the separation method, that allowed excess (unreactive) trap to be filtered out, and not injected in the MS instrument (contamination).

5.5.8 Separation and analysis of hydroperoxide-induced oxidised samples for Chapter 3

Oxidised solutions were analysed by LC-MS (5.5.3) with a gradient elution. The gradient elution is given in Table 3. When radical trap **4.1** was used a waste segment was added (5.5.7). ESI settings were as follows: drying gas flow = 10.0 L min^{-1}; nebulizer pressure: 3.0 bar; dry temperature: 325°C.

Table 5. Gradient elution for LC-MS separation used in 6.5.8. Elution solvents consisted of A) 0.1% formic acid in H_2O and B) 0.1% formic acid in MeCN.

Time / min	% A	% B
0	100	0
5	100	0
15	70	30
25	70	30
35	10	90
45	10	90
55	90	10
60	100	0

5.5.9 MS/MS studies

For MS/MS, He was used as the collision gas for collision-induced dissociation (CID) experiments to generate fragments, with a normalized collision energy of 10 or 15%. Detected ions on MS analysis with masses $[M + 32 + H]^+$ (potential hydroperoxides) and $[M + 16 + H]^+$ (potential alcohols) were subjected to MS/MS and the resulting fragments ions were analysed.

5.5.10 Deuterium exchange studies

Irradiated solutions (1 mL) were diluted (×100) in D_2O. Solutions were left in the dark for 1 h before analysis by direct injection MS and LC-MS as indicated previously (Sections 5.5.2 and 5.5.3). A 1 h incubation in D_2O was determined to be sufficient to exchange all labile H of the starting substrates (reagent in excess) with D atoms. Alternatively, the reactions were performed in D_2O (instead of Milli-Q H_2O) to enable more concentrated solutions to be injected (while ensuring complete exchange of all labile H). The isotope exchange protocol was followed as such in all three Chapters.

5.5.11 Hair source and treatment

Light blonde human hair for the testing was purchased from International Hair Importers & Products, Glendale, NY. The treatment of human hair was carried out by Jennifer M. Marsh, and Lijuan Li (Procter and Gamble). Tresses of hair (1.5 g, 15 cm) were either subjected to sunlight or heat or a combination of both and then sampled for biomarker analysis (3 tresses per test, 3 samples of hair taken per tress). Sun exposure was simulated by irradiation with an Atlas Ci3000+ weather-o-meter (Atlas, Chicago, Illinois, US). An internal and outer quartz filter was used to simulate broad-spectrum, outdoor daylight with a specific irradiance of 1.48 W/m^2 at 420 nm. During the irradiation process, temperature, and relative humidity (RH) were kept constant at 35 °C and 80% RH, respectively. Heat application was via a flat-iron at 200°C, 5 cycles of 3 passes.

5.5.12 Biomarker Measurement

The biomarker measurement was done by Jennifer M. Marsh, and Lijuan Li (Procter and Gamble). Samples (0.5 g) of hair from treated tresses were cut and placed into 50 mL tubes with 5 mL of water added. Tubes with hair and water were mixed on a multi-tube vortex shaker for 60 min at 2500 rpm. Water portion was then transferred from the tubes by pipette into glass scintillation vials. A 10 mg/mL solution of MALDI matrix (alpha-cyano-4-hydroxy cinnamic acid) was mixed with the hair extract samples in a 1:1 volume ratio. A 1 µL of this solution was used to spot onto the MALDI plate and MALDI MS spectra was acquired (1000 shots). Intensity of the UV damage marker peptide at m/z 1278 was measured.

Chapter 6: Appendix

Contents

6.1 NMR and MS data

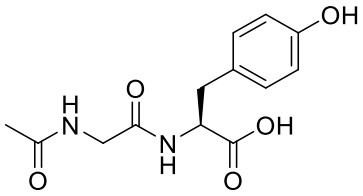

N-Ac-Gly-Tyr-OH

2

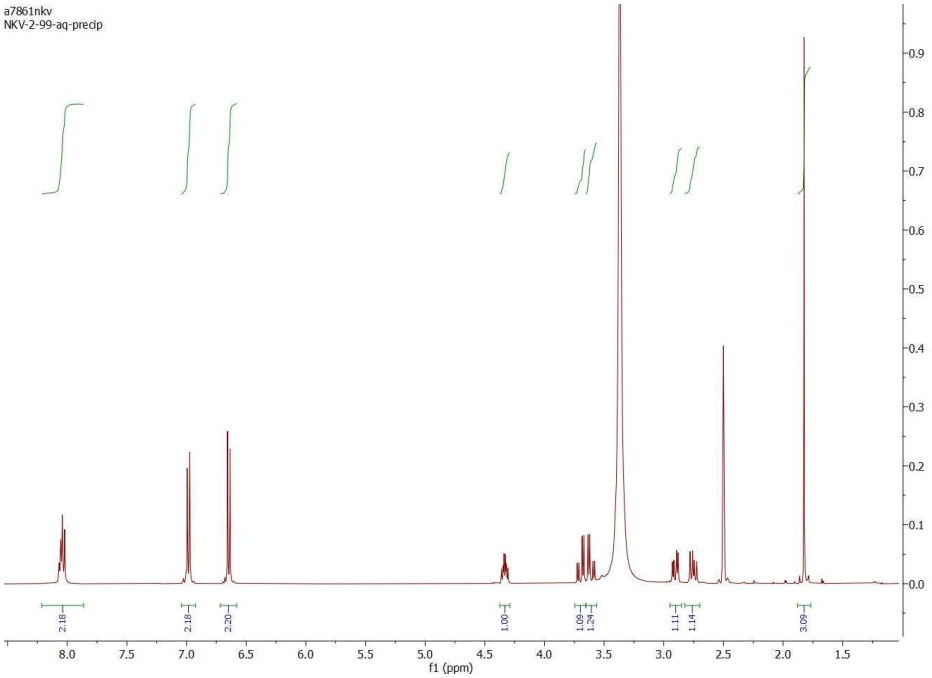

York - Chemistry - Mass Spectrometry Service Report *NKV-2-99-EtOAc recryst_vc83724nv*

Analysis Information

Analysis Filename	vc83724nv_P1-A-9_01_19513.d	Acquisition Date	22/06/2020 14:31:07
Method	ESI_low mass neg_2c1s.m	Instrument	compact
Submission Name	vc83724nv	ESI	Negative

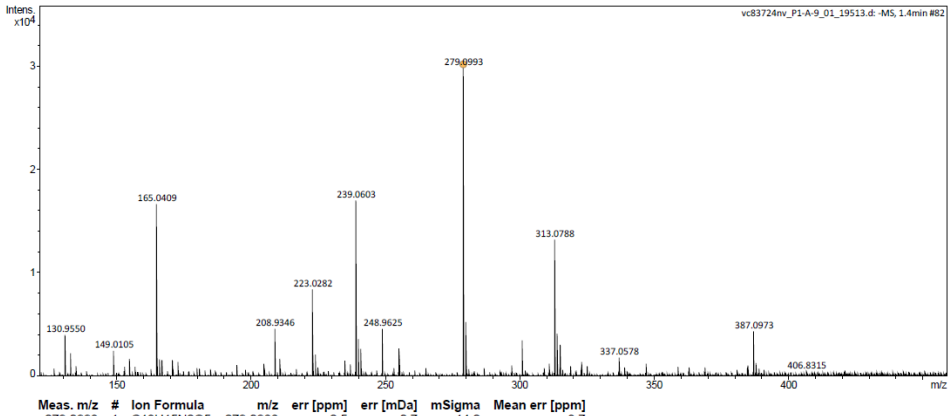

Meas. m/z	#	Ion Formula	m/z	err [ppm]	err [mDa]	mSigma	Mean err [ppm]
279.0993	1	C13H15N2O5	279.0986	-2.5	-0.7	14.2	-3.7

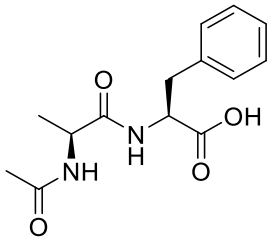

N-Ac-Ala-Phe-OH

3

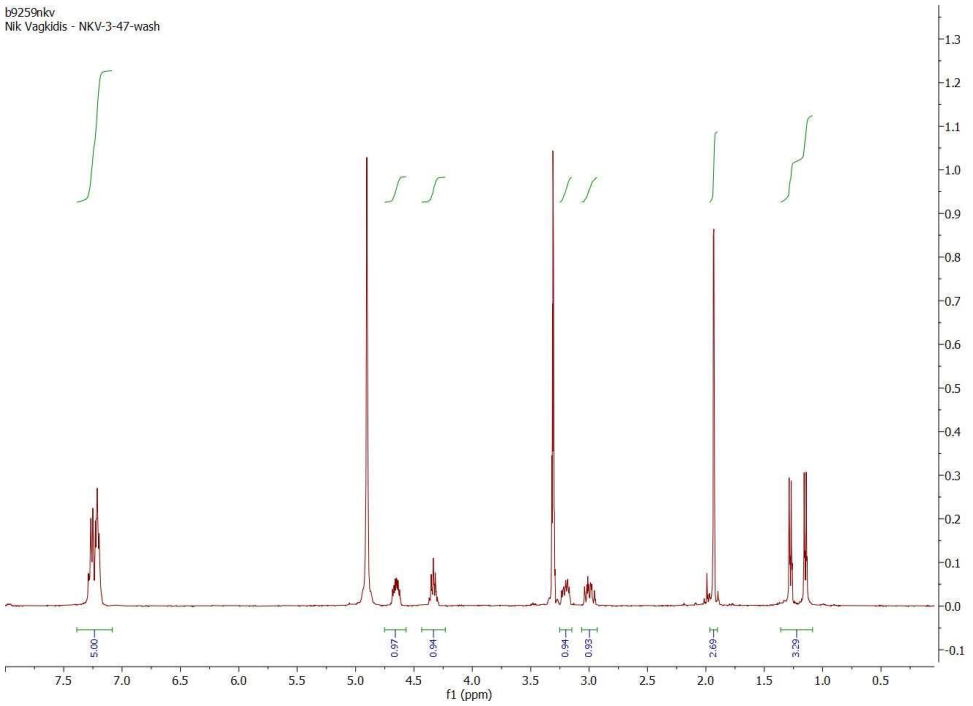

York - Chemistry - Mass Spectrometry Service Report

NKV-3-47-Et2O wash_vc88447nv

Analysis Information

Analysis Filename	vc88447nv_P1-E-7_01_24767.d	Acquisition Date	18/02/2021 13:44:46
Method	ESI_low mass_2c1s.m	Instrument	compact
Submission Name	vc88447nv	ESI	Positive

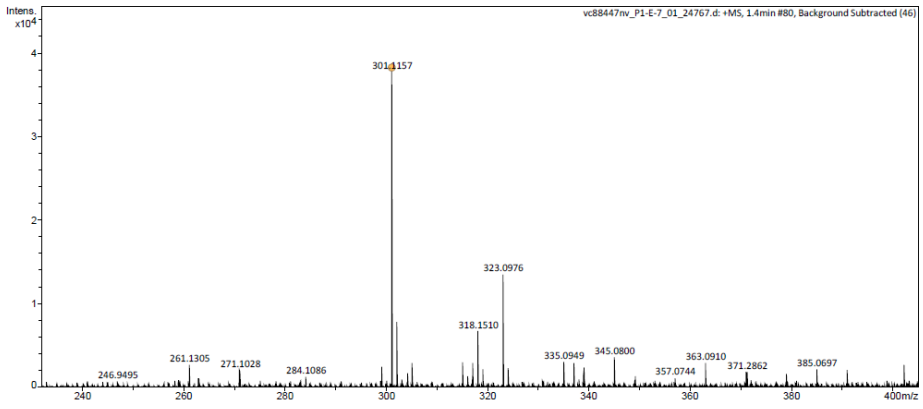

Meas. m/z	#	Ion Formula	m/z	err [ppm]	err [mDa]	mSigma	Mean err [ppm]
301.1157	1	C14H18N2NaO4	301.1159	0.5	0.1	26.2	0.9

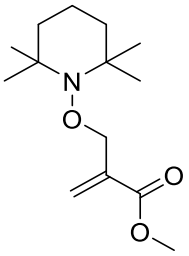

21

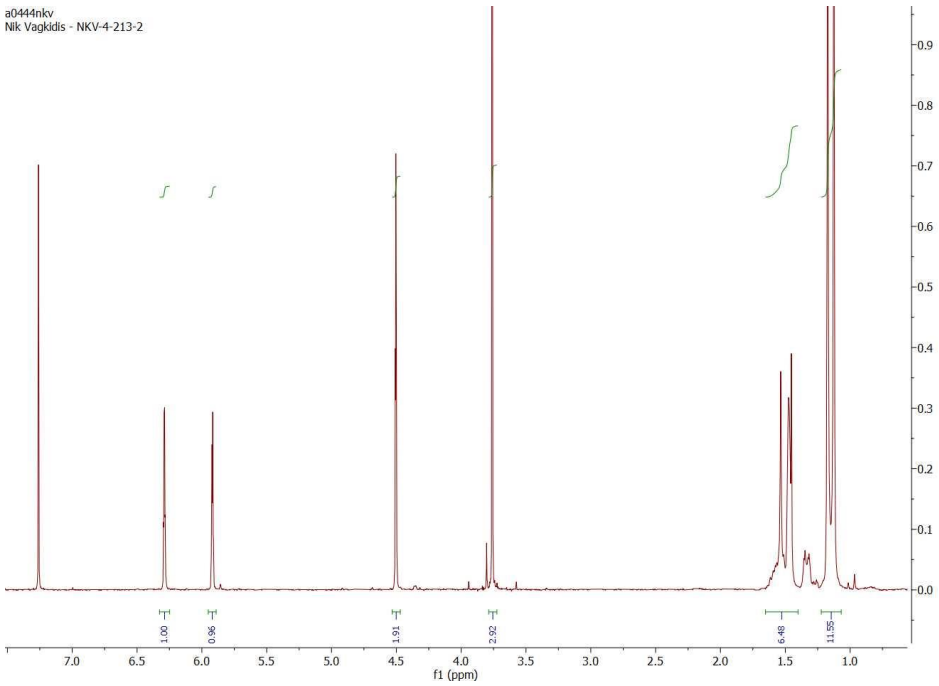

York - Chemistry - Mass Spectrometry Service Report

NKV-3-45 col_vc88329nv

Analysis Information

Analysis Filename	vc88329nv_P1-E-2_01_24643.d	Acquisition Date	12/02/2021 12:21:51
Method	ESI_low mass_2c1s.m	Instrument	compact
Submission Name	vc88329nv	ESI	Positive

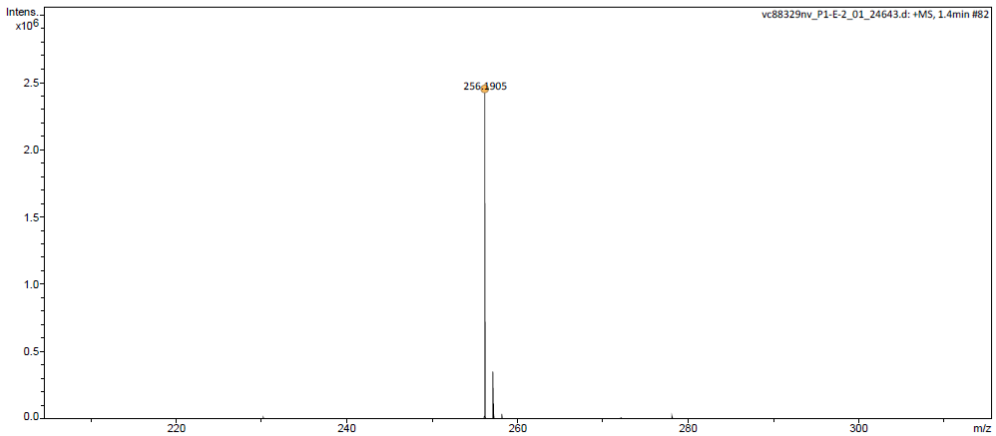

Meas. m/z	#	Ion Formula	m/z	err [ppm]	err [mDa]	mSigma	Mean err [ppm]
256.1905	1	C14H26NO3	256.1907	0.8	0.2	7.5	0.0

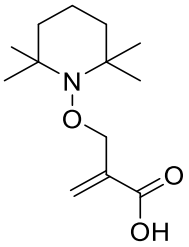

22

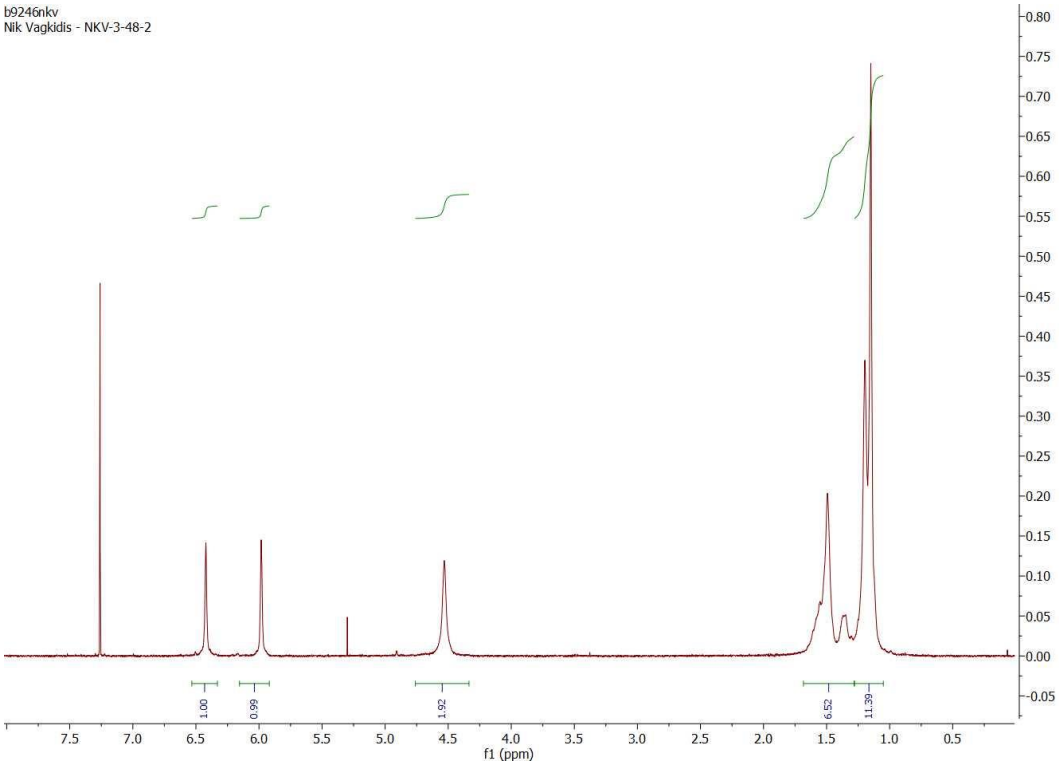

York - Chemistry - Mass Spectrometry Service Report

NKV-3-48-col_vc88448nv

Analysis Information

Analysis Filename	vc88448nv_P1-E-8_01_24768.d	Acquisition Date	18/02/2021 13:47:45
Method	ESI_low mass_2c1s.m	Instrument	compact
Submission Name	vc88448nv	ESI	Positive

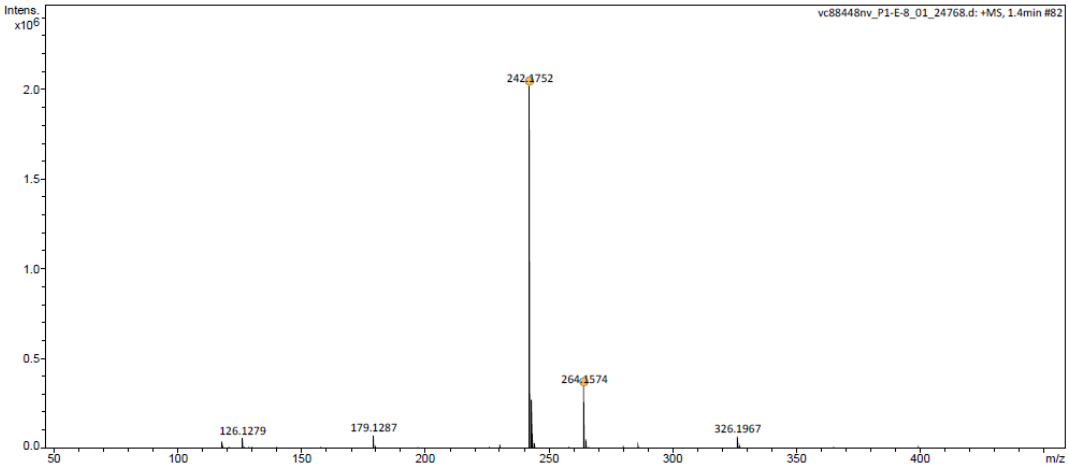

Meas. m/z	#	Ion Formula	m/z	err [ppm]	err [mDa]	mSigma	Mean err [ppm]
242.1752	1	C13H24NO3	242.1751	-0.5	-0.1	8.2	-1.1
264.1574	1	C13H23NNaO3	264.1570	-1.3	-0.3	3.3	-2.1

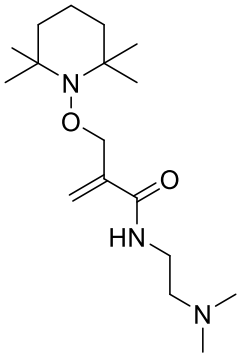
N
O
O
HN
N

7

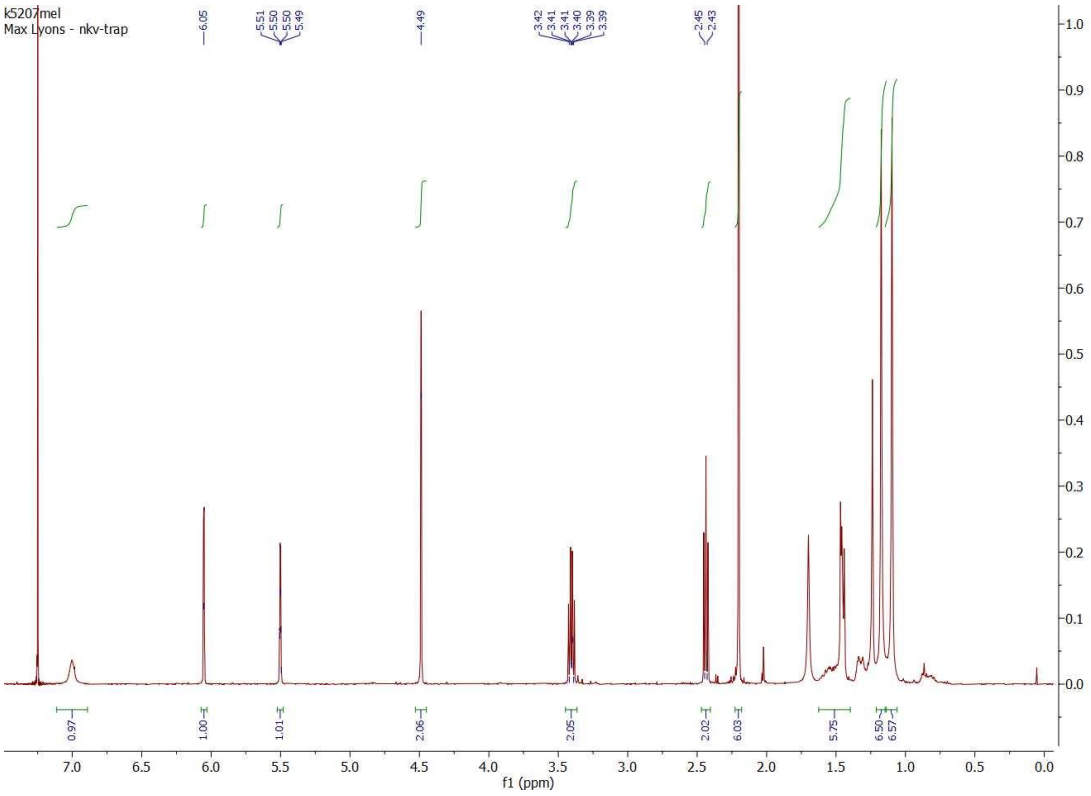
k5207mel
Max Lyons - nkv-trap
6.05
5.51
5.50
5.50
5.49
4.49
3.42
3.41
3.41
3.40
3.39
3.39
2.45
2.43
0.97
1.00
1.01
2.06
2.05
2.02
6.03
5.75
6.50
6.57
f1 (ppm)

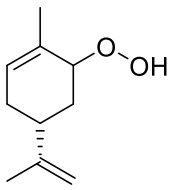
O
OH

12

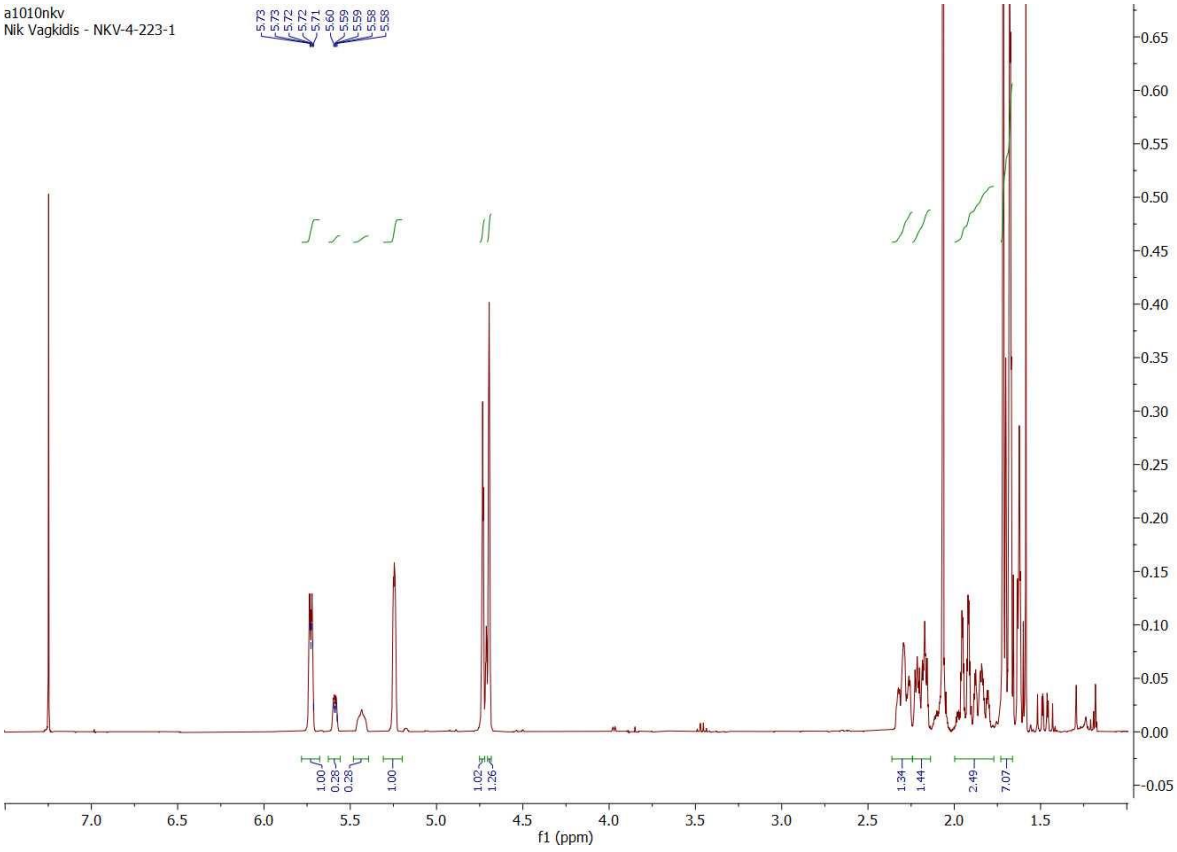
a1010nkv
Nik Vagkidis - NKV-4-223-1
5.73
5.73
5.72
5.72
5.71
5.60
5.59
5.59
5.58
5.58
1.00
0.28
0.28
1.00
1.02
1.26
1.34
1.44
2.49
7.07
f1 (ppm)

6.2 Kinetic model

Reactions, reactions rate constants, activation energies and corresponding references used for the design of the kinetic model. For the peroxide decomposition (reactions 9 and 10), rate constants were determined experimentally in our lab using *N*-Ac-Gly-Gly-OH as a model peptide (Section 5.4.3 and 5.4.4)

#	Reaction	Rate constant (M^{-1} s^{-1} or s^{-1})	Activation energy (kcal mol^{-1})	Reference
(1)	Hair + sunlight $\longrightarrow$ $In^{\bullet}$	10^{-10}	n/a	n/a
(2)	$Pr + In^{\bullet} \longrightarrow Pr^{\bullet}$ + Inactive molecule	10^{5}	n/a	n/a
(3)	$Pr^{\bullet} + O_2 \longrightarrow PrOO^{\bullet}$	10^{9}	28	350
(4)	$PrOO + Pr^{\bullet} \longrightarrow PrOOH + Pr^{\bullet}$	10^{3}	9	127
(5)	$PrOO^{\bullet} \longrightarrow$ Imine + $HO_2^{\bullet}$	10^{2}	9	127
(6)	$2\ PrOO^{\bullet} \longrightarrow$ Non-radical products	2×10^{4}	8.8	127
(7)	$2\ PrOO^{\bullet} \longrightarrow PrOOPr + O_2$	10^{3}	8.8	127
(8)	$2\ PrOO^{\bullet} \longrightarrow 2\ PrO^{\bullet} + O_2$	9×10^{3}	8.8	127
(9)	$PrOOH \longrightarrow PrO^{\bullet} + HO^{\bullet}$	10^{-5}	n/a	n/a
(10)	$PrOOPr \longrightarrow 2\ PrO^{\bullet}$	10^{-5}	n/a	n/a
(11)	$PrO + Pr^{\bullet} \longrightarrow PrOH + Pr^{\bullet}$	10^{6}	4.5	350
(12)	$PrO^{\bullet} \longrightarrow Pr^{\bullet}$ + Carbonyl	10^{6}	15.3	350
(13)	$PrO^{\bullet} + PrOOH \longrightarrow PrOH + PrOO^{\bullet}$	10^{6}	4.5	350
(14)	$PrO^{\bullet} \longrightarrow {}^{\bullet}PrOH$	10^{6}	4.5	350
(15)	${}^{\bullet}PrOH + O_2 \longrightarrow {}^{\bullet}OOPrOH2$	10^{9}	28	350
(16)	${}^{\bullet}OOPrOH2 \longrightarrow$ Carbonyl + $HO_2^{\bullet}$	10^{2}	9	127
(17)	$2\ PrO^{\bullet} \longrightarrow$ Non-radical products	10^{6}	4.5	350
(18)	$Pr + HO^{\bullet} \longrightarrow Pr^{\bullet} + H_2O$	10^{10}	15	88
(19)	$Pr + HO_2^{\bullet} \longrightarrow Pr^{\bullet} + H_2O_2$	10^{4}	15	351
(20)	$2\ HO^{\bullet} \longrightarrow H_2O_2$	10^{10}	15	88
(21)	$2\ HO_2^{\bullet} \longrightarrow H_2O_2 + O_2$	9×10^{6}	4.77	352
(22)	$HO^{\bullet} + HO_2^{\bullet} \longrightarrow H_2O + O_2$	10^{10}	15	88

6.3 *N*-Ac-Gly-Gly-OH-hydroperoxides decomposition

Fitting of the data to first order kinetics to determine the *k* of decomposition, A) Sunlight exposure and B) incubation at 100 °C.

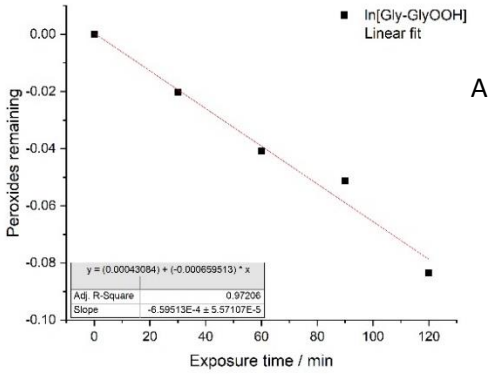

A

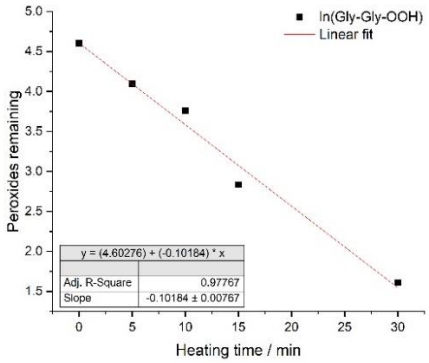

B

6.4 Calibration curves

6.4.1 FOX-assay

Net absorbance of solutions of H_2O_2 (concentrations of 1 to 20 µM) in the standard FOX-assay. Results are the mean ± the standard error of three measurements (the error bars fall within the data points).

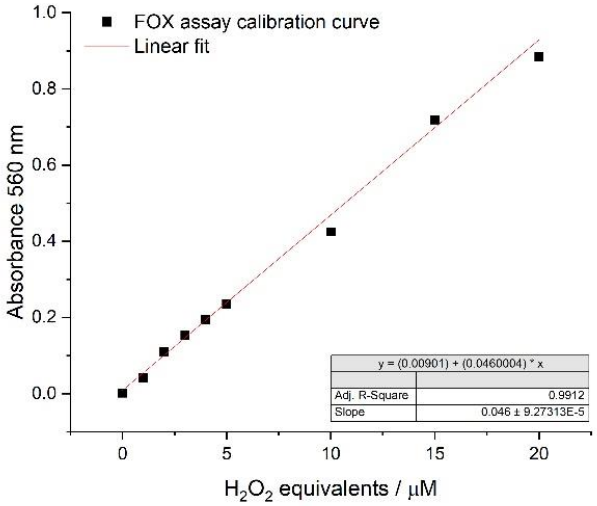

6.4.2 Peptides standard curves

Calibration curves was constructed using LC-MS for all four substrates. For *N*-Ac-Gly-Tyr-OH (A), *N*-Ac-Ala-Phe-OH (B), and *N*-Ac-Phe-OH (D) the UV detector was used for the quantification. For *N*-Ac-Ala-OH (C) the total ion current (TIC) was used for the quantification.

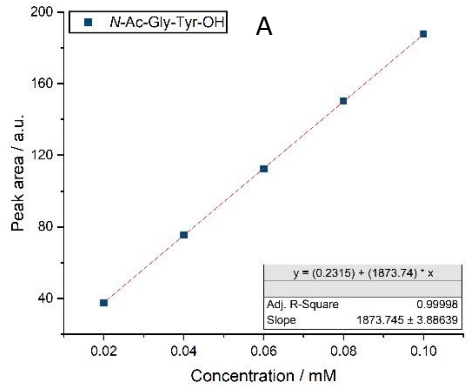

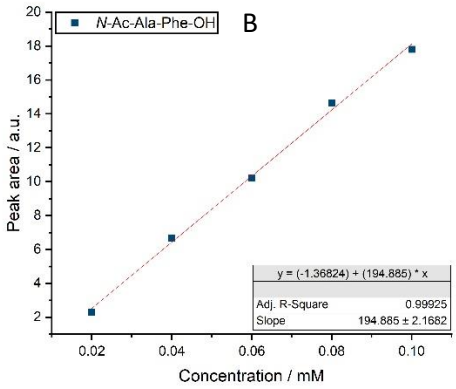

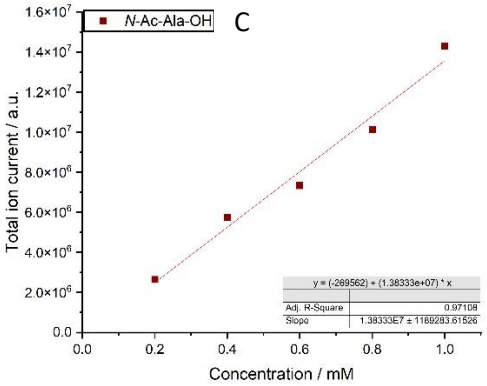

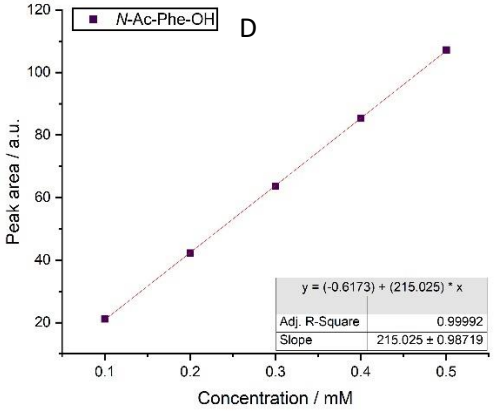

6.5 Control reactions MS data

6.5.1 Chapter 1

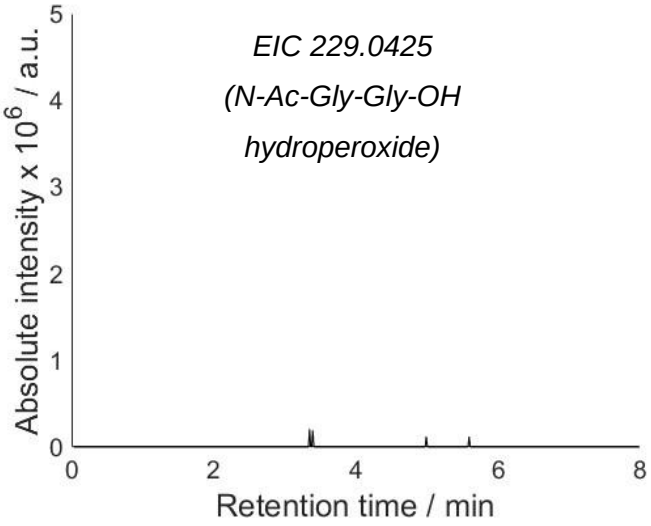

Figure S1. EIC of 229.0425. Aqueous solutions H_2O_2 (100 mM) and N-Ac-Gly-Gly-OH (5 mM) were incubated in the dark for 60 min.

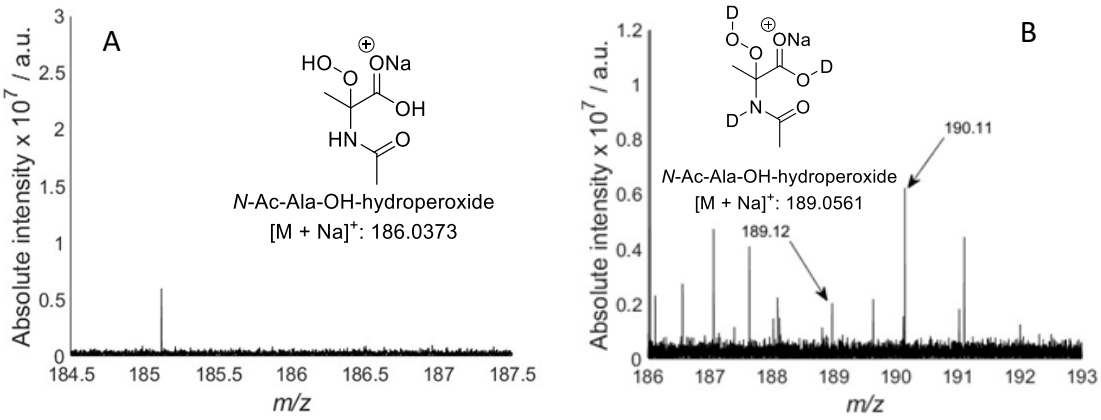

Figure S2. A) DI-MS spectra of aqueous solutions of H_2O_2 (100 mM) and N-Ac-Ala-OH (1 mM) incubated in the dark for 2 min. DI-MS spectra of aqueous solutions of H_2O_2 (100 mM) and N-Ac-Ala-OH (1 mM) exposed to UV light for 2 min (reaction run in D_2O). Figures is zoomed in to show the m/z area where the expected N-Ac-Ala-OH-derived hydroperoxides would be detected.

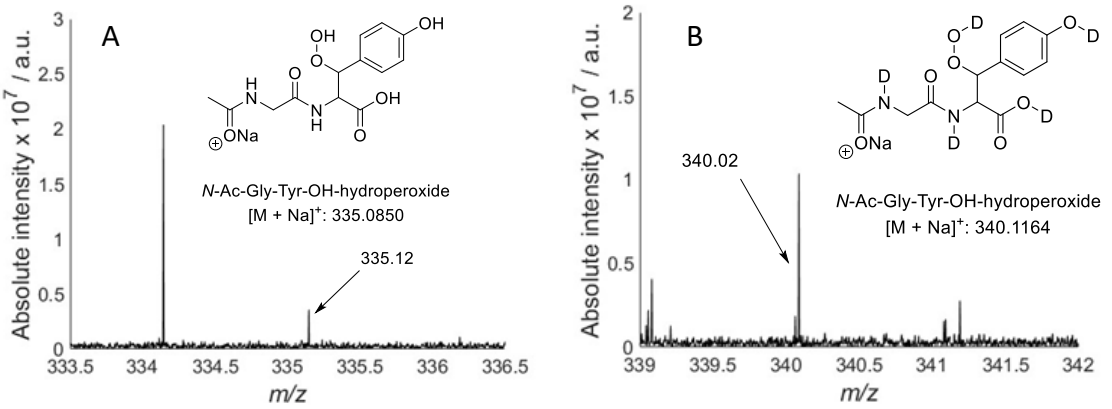

Figure S3. A) DI-MS spectra of aqueous solutions of H_2O_2 (100 mM) and N-Ac-Gly-Tyr-OH (1 mM) incubated in the dark for 2 min. B) DI-MS spectra of aqueous solutions of H_2O_2 (100 mM) and N-Ac-Gly-Tyr-OH (1 mM) exposed to UV light for 2 min (reaction run in D_2O). Figures are zoomed in to show the m/z area where the expected N-Ac-Gly-Tyr-OH-derived hydroperoxides would be detected.

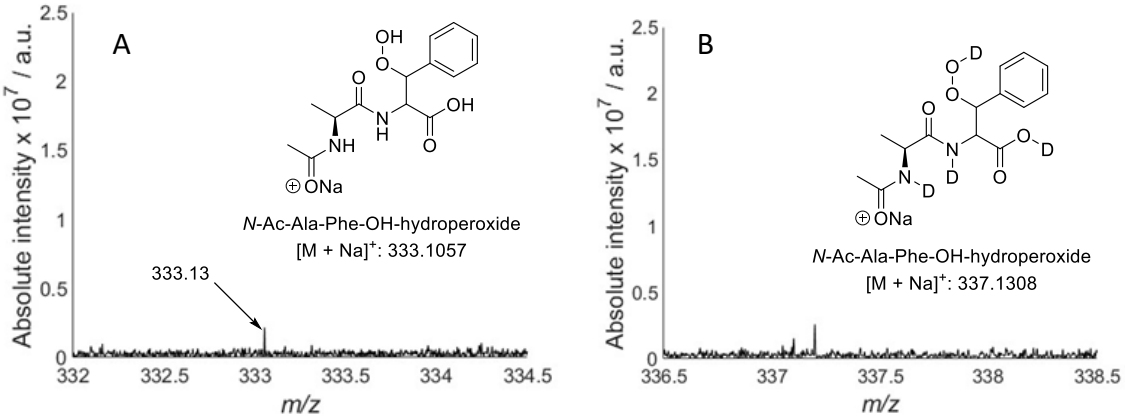

Figure S4. A) DI-MS spectra of aqueous solutions of H_2O_2 (100 mM) and N-Ac-Ala-Phe-OH (1 mM) incubated in the dark for 2 min. B) DI-MS spectra of aqueous solutions of H_2O_2 (100 mM) and N-Ac-Ala-Phe-OH (1 mM) exposed to UV light for 2 min (reaction run in D_2O). Figures are zoomed in to show the m/z area where the expected N-Ac-Ala-Phe-OH-derived hydroperoxides would be detected.

6.6 Trapped adducts MS data

6.6.1 Peroxynitrite project

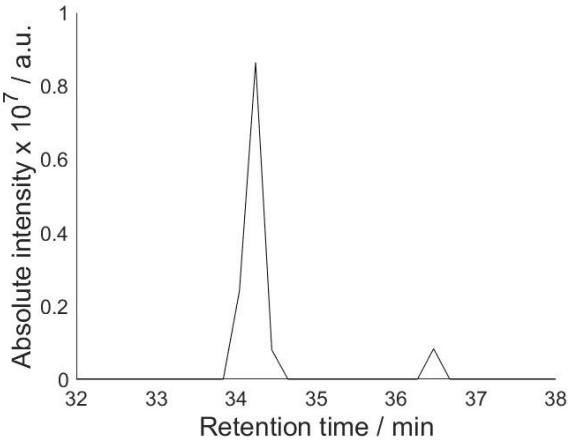

*Figure S5. LC-MS analysis. EIC of 328.2595. The m/z corresponds to the allylic radical **9** (Scheme 56)trapped as a TEMPO-adduct.*

6.6.2 *N*-Ac-Ala-OH

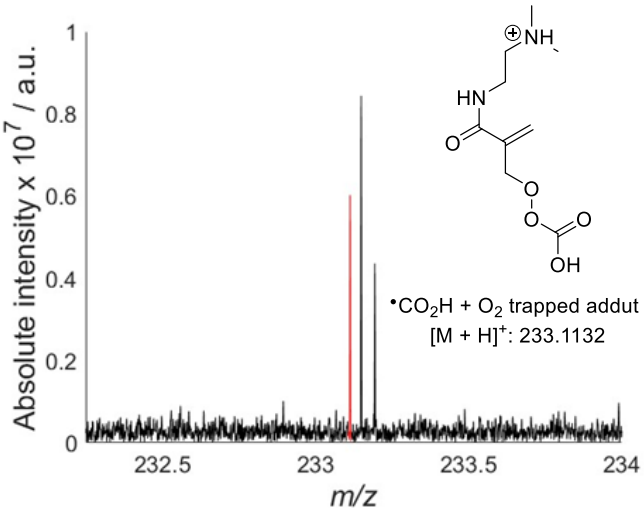

*Figure S6. DI-MS Spectra. The fragmentation mechanism of Scheme 58 releases a $^{\bullet}CO_2H$, which can rapidly add to dioxygen. Highlighted in red is the m/z corresponding to the resulting peroxyl radical trapped with **4.1**.*

6.6.3 *N*-Ac-Ala-Phe-OH

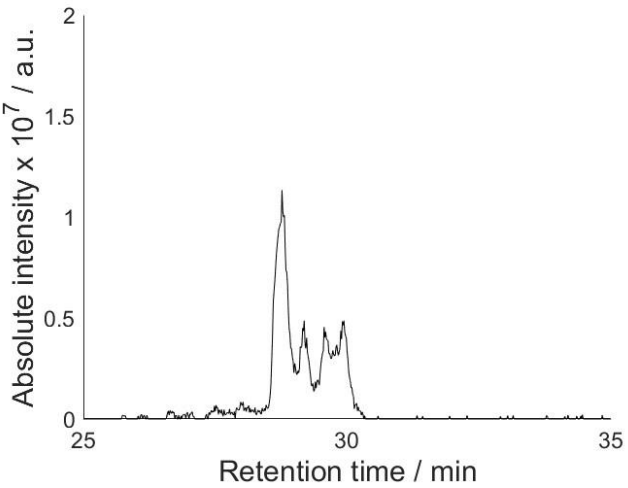

*Figure S7. LC-MS Analysis. EIC of 433.2444. The m/z corresponds to potential C-centred radicals generated on N-Ac-Ala-Phe-OH trapped with **4.1**. The radical is generated via HAA by HO• from N-Ac-Ala-Phe-OH.*

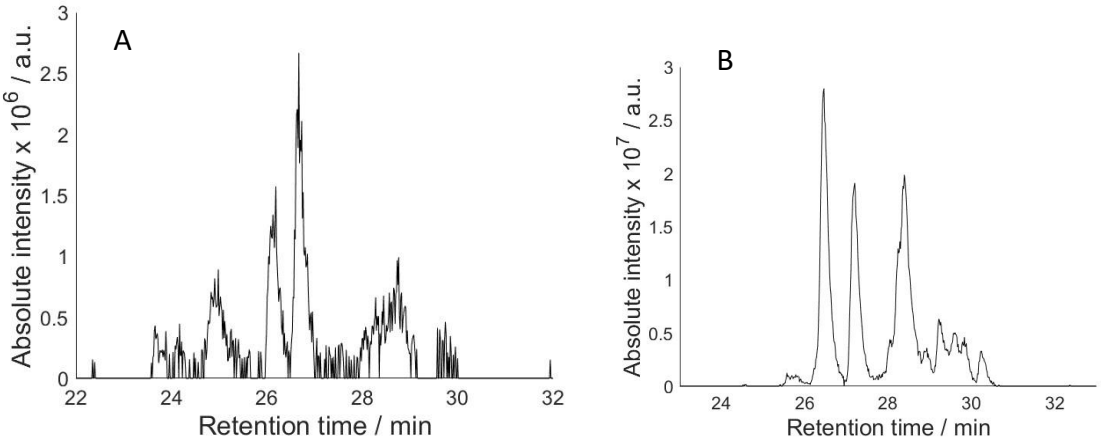

*Figure S8. LC-MS Analysis. A) EIC of 421.2444. The m/z corresponds to potential peroxyl radicals generated on N-Ac-Ala-Phe-OH trapped with **4.1**. B) EIC of 405.2496. The m/z corresponds to potential alkoxyl radicals generated on N-Ac-Ala-Phe-OH trapped with 7. The radicals are generated via the ET mechanism of Scheme 60, leading to the radical decarboxylation of N-Ac-Ala-Phe-OH.*

6.6.4 *N*-Ac-Gly-Tyr-OH

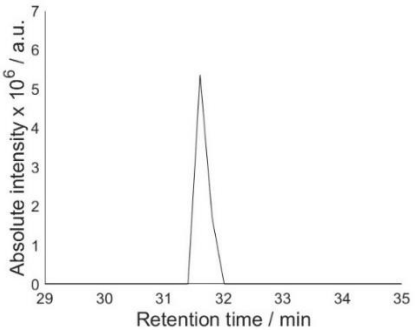

*Figure S9. LC-MS Analysis. EIC of 435.2244. The m/z corresponds to potential C- or O-centred radicals generated on N-Ac-Gly-Tyr-OH trapped with **4.1**. The radical is generated via HAA by HO• from N-Ac-Gly-Tyr-OH.*

6.7 Degradation products MS data

6.7.1 Chapter 1 and 3

6.7.1.1 N-Ac-Ala-OH

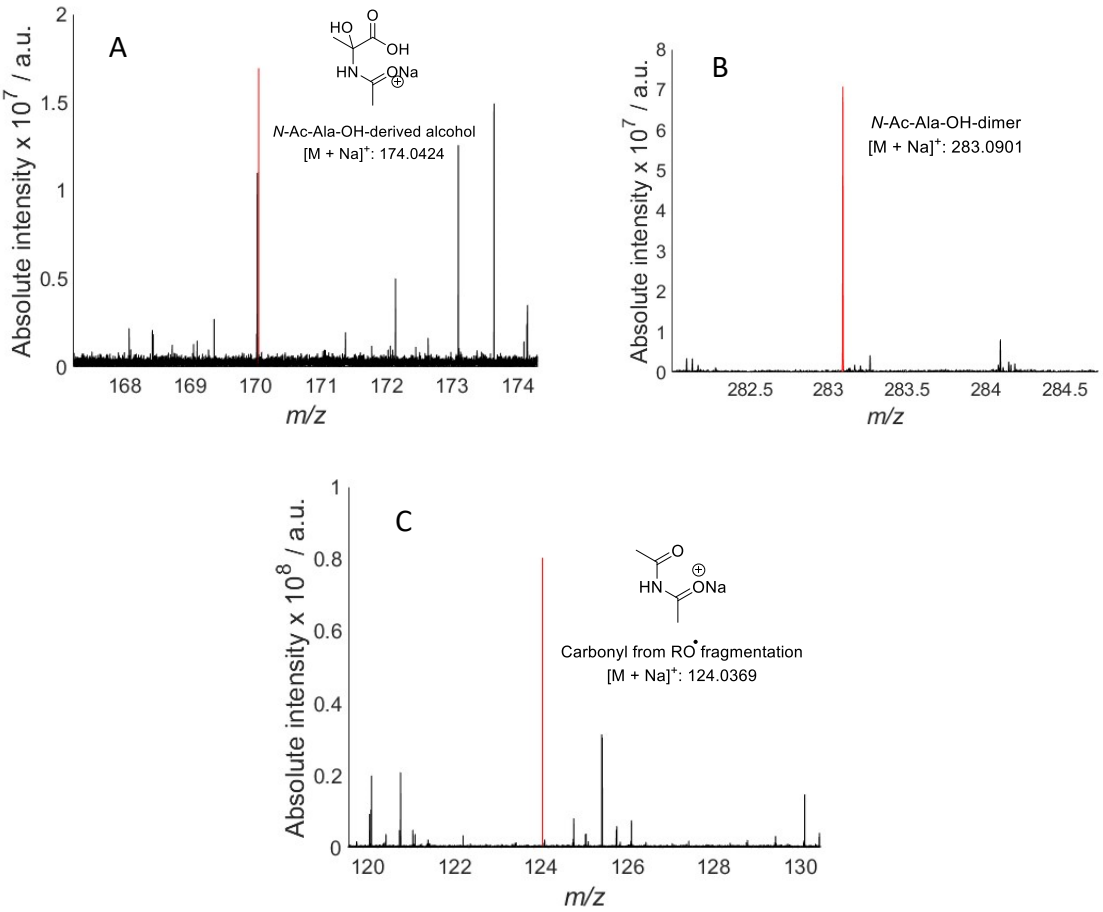

Figure S10. DI-MS spectra of irradiated samples of H_2O_2 (aq. solution; 100 mM) in presence of N-Ac-Ala-OH (aq. solution; 1 mM). A) The m/z of N-Ac-Ala-OH-derived alcohols is highlighted in red. B) The m/z of the dimeric species is highlighted in red, and C) he m/z of carbonyls, resulting from fragmentation of tertiary alkoxyl radicals is highlighted in red (mechanism is given in Scheme 58). The figures is zoomed in to show the m/z area where the expected products would be detected.

6.7.1.2 N-Ac-Ala-Phe-OH

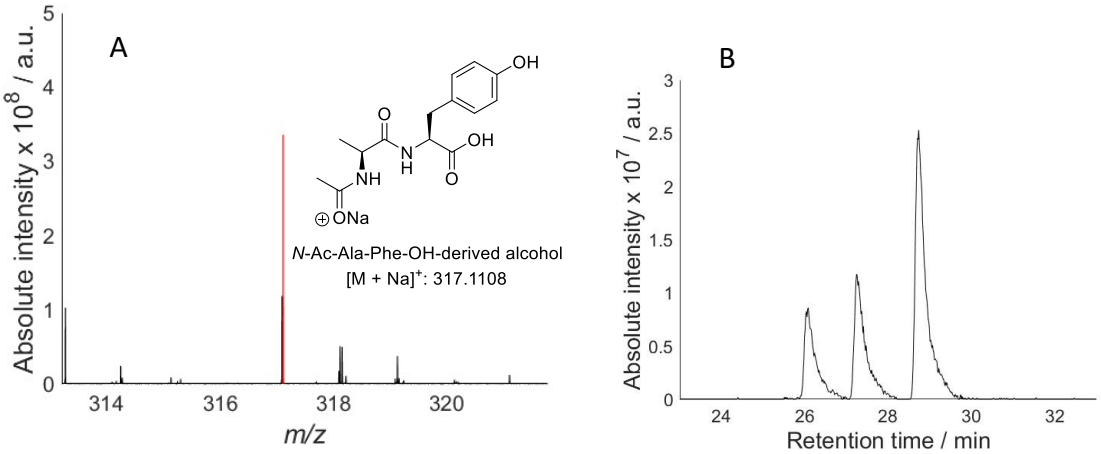

Figure S11. MS data of irradiated samples of H_2O_2 (aq. solution; 100 mM) in presence of N-Ac-Ala-Phe-OH (aq. solution; 1 mM). A) DI-MS spectra. The m/z of potential N-Ac-Ala-Phe-OH-derived alcohols is highlighted in red. B) LC-MS Data. EIC of 317.1108.

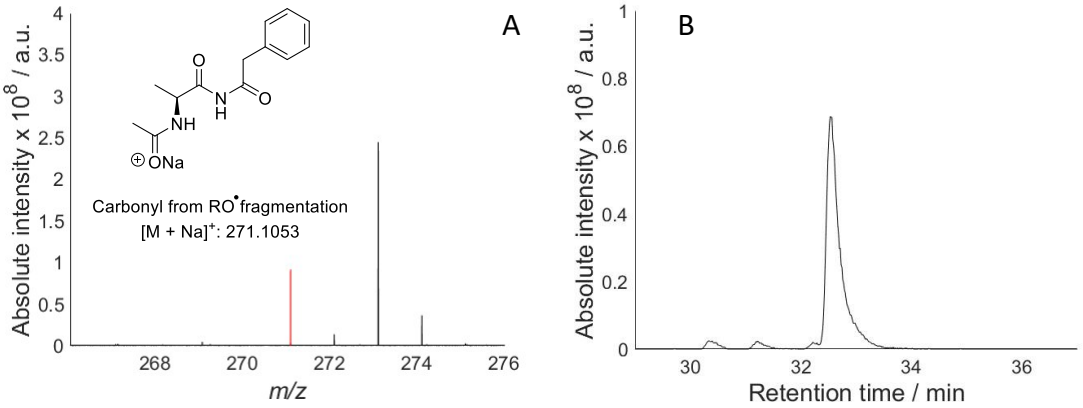

Figure S12. MS data of irradiated samples of H_2O_2 (aq. solution; 100 mM) in presence of N-Ac-Ala-Phe-OH (aq. solution; 1 mM). A) DI-MS spectra. The m/z of N-Ac-Ala-Phe-OH-derived carbonyls (mechanism in Scheme 58) is highlighted in red. B) LC-MS Data. EIC of 271.1053.

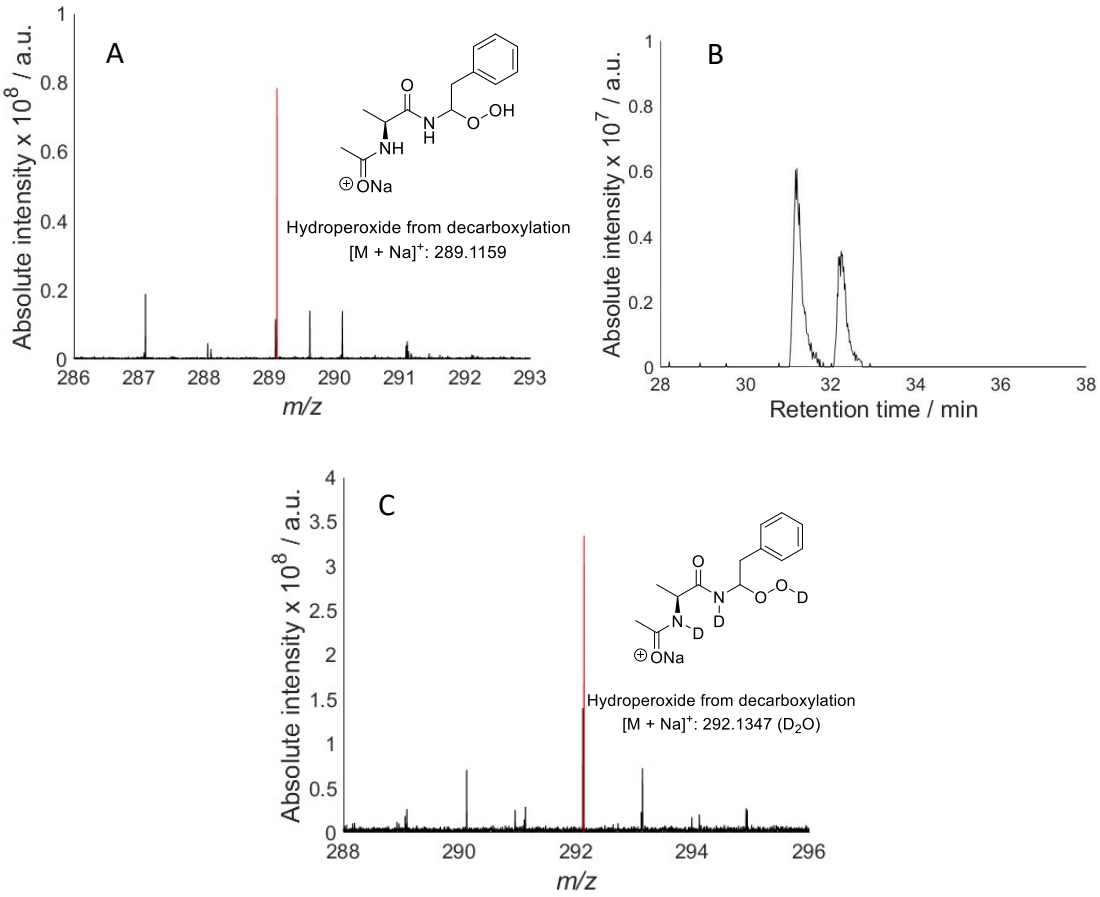

Figure S13. MS data of irradiated samples of H_2O_2 (aq. solution; 100 mM) in presence of N-Ac-Ala-Phe-OH (aq. solution; 1 mM). A) DI-MS spectra. The m/z of potential N-Ac-Ala-Phe-OH-derived hydroperoxides, arising from the fragmentation mechanism of Scheme 58 and subsequent O_2 addition is highlighted in red. B) LC-MS Data. EIC of 289.1159. The two peaks in the LC-MS trace likely indicate that the signal is also due to an alcohol that has been previously hydroxylated.

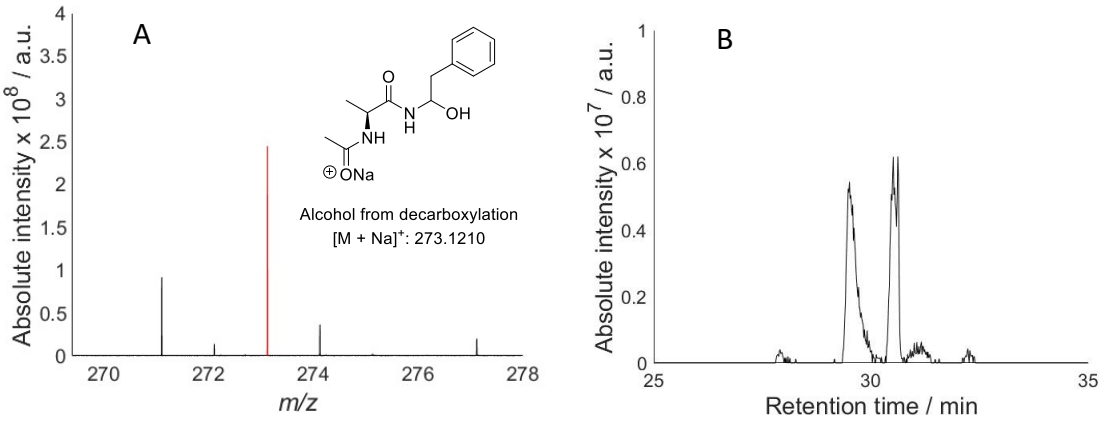

Figure S14. MS spectra of irradiated samples of H_2O_2 (aq. solution; 100 mM) in presence of N-Ac-Ala-Phe-OH (aq. solution; 1 mM). A) DI-MS Spectra. The m/z of potential alcohols, resulting from the radical decarboxylation (Scheme 60) is highlighted in red. B) LC-MS Spectra. EIC of 273.1210. The two peaks in the LC-MS trace likely indicate that the signal is also due to previous hydroxylation.

6.7.1.3 N-Ac-Gly-Tyr-OH

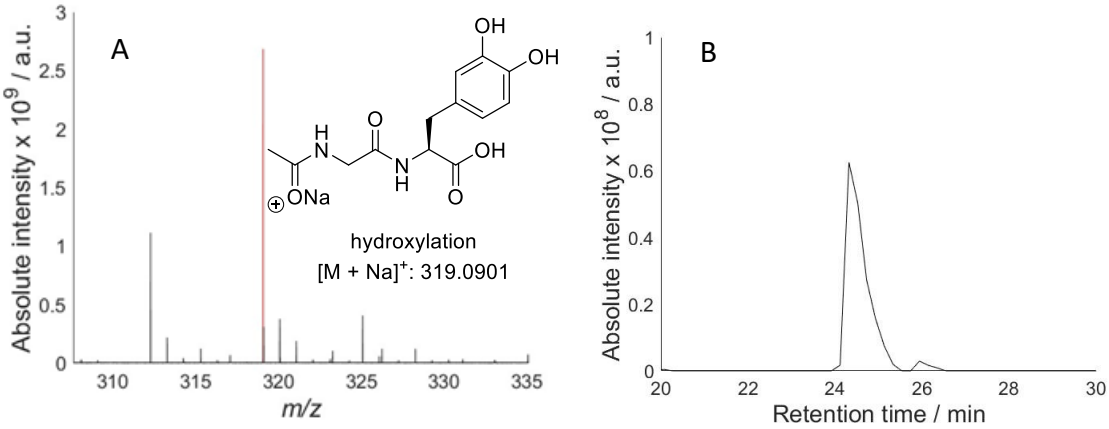

Figure S15. MS data of irradiated samples of H_2O_2 (aq. solution; 100 mM) in presence of N-Ac-Gly-Tyr-OH (aq. solution; 1 mM). A) DI-MS spectra. The m/z of potential N-Ac-Gly-Tyr-OH-derived alcohols is highlighted in red. B) LC-MS Data. EIC of 319.0901

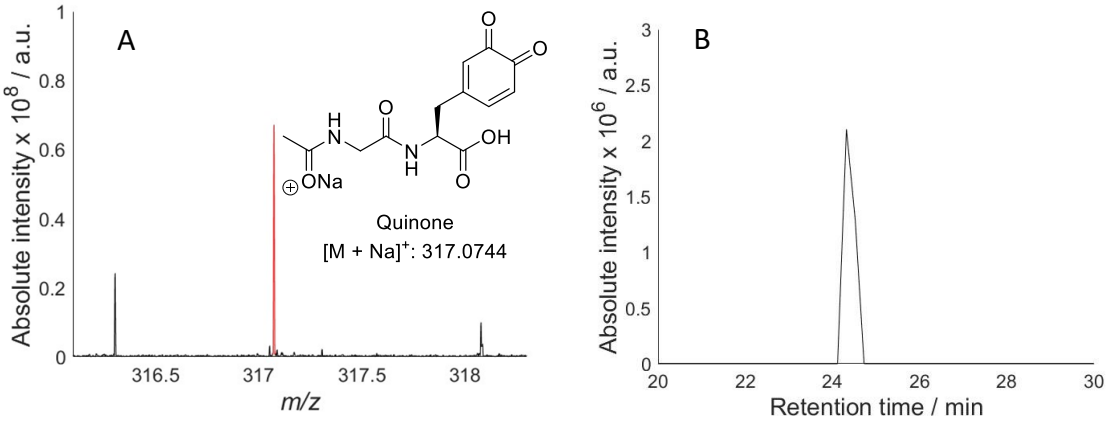

Figure S16. MS data of irradiated samples of H_2O_2 (aq. solution; 100 mM) in presence of N-Ac-Gly-Tyr-OH (aq. solution; 1 mM). A) DI-MS spectra. The m/z of potential N-Ac-Gly-Tyr-OH-derived quinones is highlighted in red. B) LC-MS Data. EIC of 317.0744

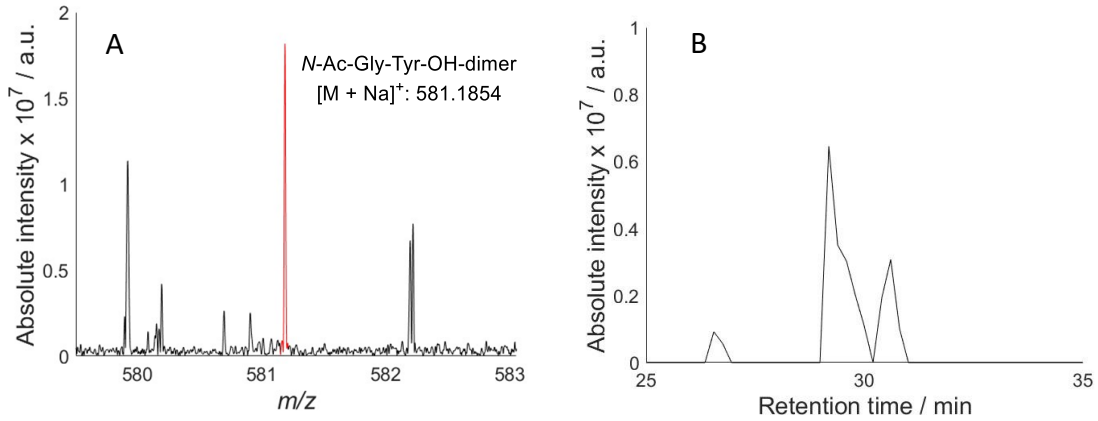

Figure S17. MS data of irradiated samples of H_2O_2 (aq. solution; 100 mM) in presence of N-Ac-Gly-Tyr-OH (aq. solution; 1 mM). A) DI-MS spectra. The m/z of potential N-Ac-Gly-Tyr-OH-dimer is highlighted in red. B) LC-MS Data. EIC of 581.1854

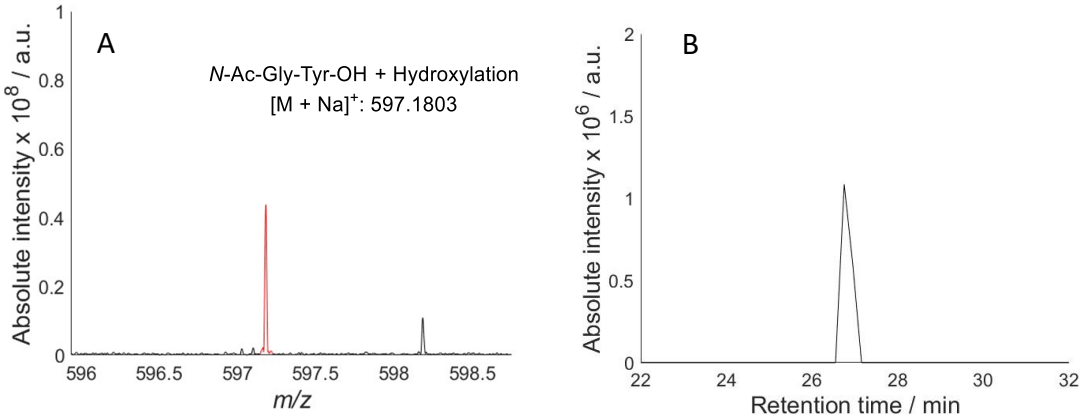

Figure S18. MS data of irradiated samples of H_2O_2 (aq. solution; 100 mM) in presence of N-Ac-Gly-Tyr-OH (aq. solution; 1 mM). A) DI-MS spectra. The m/z of potential dimer between N-Ac-Gly-Tyr-OH and DOPA is highlighted in red. B) LC-MS Data. EIC of 597.1803.

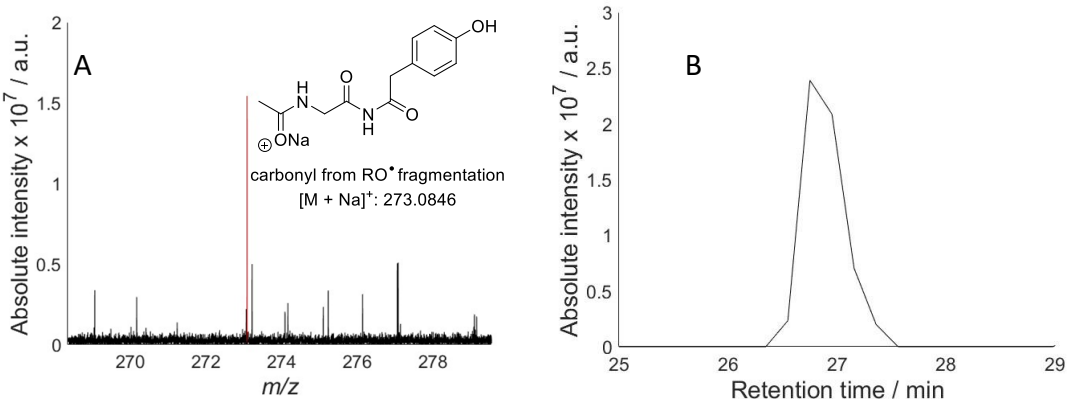

Figure S19. MS data of irradiated samples of H_2O_2 (aq. solution; 100 mM) in presence of N-Ac-Gly-Tyr-OH (aq. solution; 1 mM). A) DI-MS spectra. The m/z of potential N-Ac-Gly-Tyr-OH-derived carbonyl from the fragmentation mechanism of Scheme 58 is highlighted in red. B) LC-MS Data. EIC of 273.084

6.7.2 Chapter 2

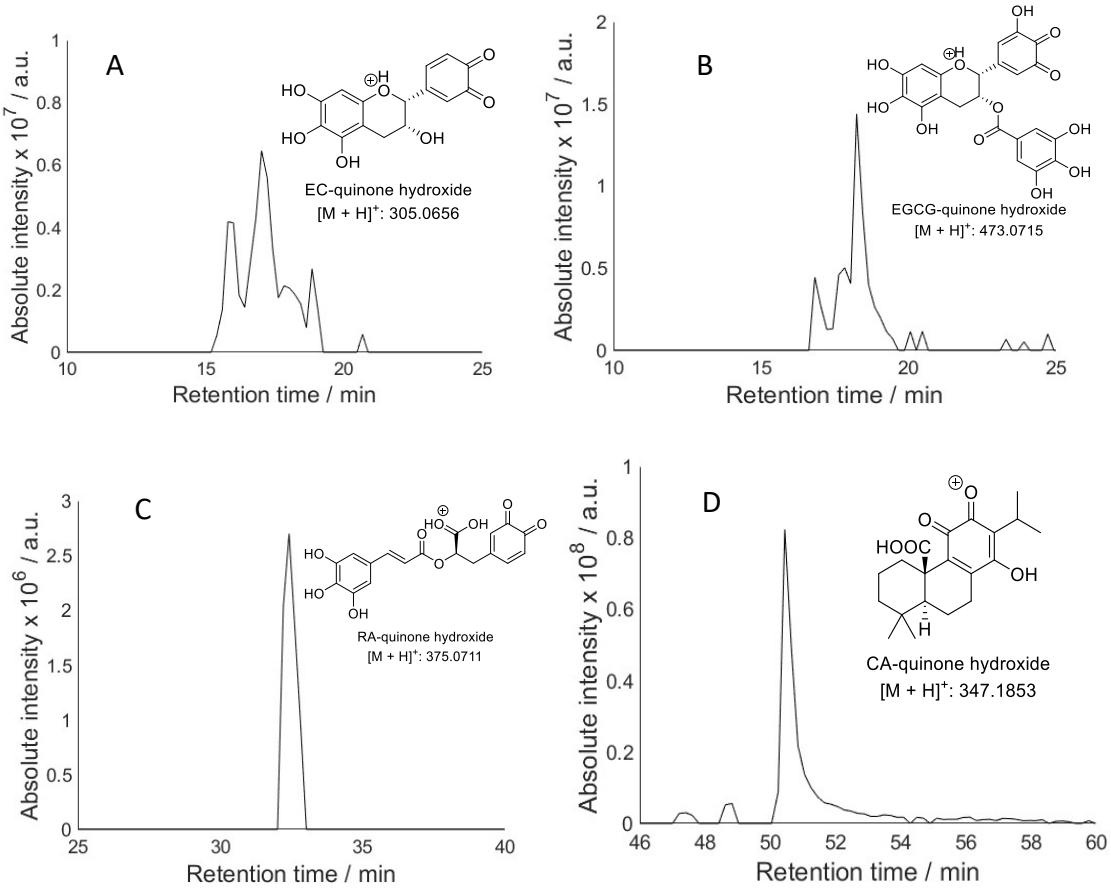

Figure S20. LC-MS Data. EICs of the $[M + H]^+$ of potential overoxidised quinones. A) EIC of 305.0656 (EC-quinone hydroxide), B) EIC of 473.0715 (EGCG-quinone hydroxide), EIC of 375.0711 (RA-quinone hydroxide), and D) EIC of 347.1853 (CA-quinone hydroxide). Figures shows one of the possible isomers.

Abbreviations

Ac	acetyl
Ala	alanine
AH	antioxidant
aq.	aqueous
AAPH	2,2'-Azobis(2-methylpropionamidine)
AIBN	2,2'-Azobis(2-methylpropionitrile)
BDE	bond dissociation energy
br	broad
Bu	butyl
BHT	3,5-Di-tert-4-butylhydroxytoluene
Boc	tert-butyloxycarbonyl
CA	carnosic acid
CAGR	compound annual growth
CID	collision-induced dissociation
Cys	cysteine
DNA	deoxyribonucleic acid
DMF	dimethylformamide
DI-MS	direct injection – mass spectrometry
DIPEA	*N*,*N*-diisopropylethylamine
DOPA	3,4-dihydroxyphenylalanine
DMPO	5,5-dimethyl-1-pyrroline N-oxide
d	doublet
EPR	electron paramagnetic resonance
ESR	electron spin resonance
ET	electron transfer
ESI	electrospray ionisation
EC	epicatechin
EGCG	epigallocatechin gallate
eq.	equivalents
EIC	extracted ion chromatogram
FOX	ferrous oxidation - xylenol orange
Gly	glycine
HAA	Hydrogen atom transfer

HBTU	O-(benzotriazol-1-yl)-N,N,N’,N’-tetramethyluronium hexafluorophosphate
$In^{\bullet}$	initiation radical (kinetic model)
J	coupling constant
KAP	keratin-associated proteins
LC-MS	liquid chromatography – mass spectrometry
m/*z*	mass to charge ratio
MS	mass spectrometry
MS/MS	tandem mass spectrometry
M	unfragmented molecule
NMR	nuclear magnetic resonance
ORAC	oxygen radical absorbance capacity
ppm	parts per million
Phe	phenylalanine
P.B.	phosphate buffer
P&G	Procter and Gamble
Pr	protein
RA	rosmarinic acid
ROS	reactive oxygen species
RNA	ribonucleic acid
RT	room temperature
s	Singlet (NMR)
t	*tert*
TIC	total ion current
ToF	time-of-flight
Trp	tryptophan
Tyr	tyrosine
TEMPO	(2,2,6,6-tetramethylpiperidin-1-yl)oxyl
UV	ultraviolet
Val	valine
Vis	visible
VOC	volatile organic compound
XO	xylenol orange

References

1 • Global hair care industry 2012-2025 | Statista, https://www.statista.com/statistics/254608/global-hair-care-market-size/, (accessed 23 April 2020).

2 Haircare Global Industry Guide 2013-2022 - Marketline, https://store.marketline.com/report/mlig180078-06--haircare-global-industry-guide-2013-2022/#tab-list-of-figures, (accessed 23 April 2020).

3 F. J. Wortmann, in *Handbook of Textile Fibre Structure*, Woodhead Publishing, 2009.

4 D. R. Graham and K. W. Statham, *J. Soc. Dye.*, 1956, **72**, 434–438.

5 A. S. Inglis and F. G. Lennox, *Text. Res. J.*, 1963, **33**, 431–435.

6 K. S. la Fleur, *Text. Res. J.*, 1948, **18**, 39–41.

7 J. S. Ingham, *J. Soc. Dye.*, 1954, **70**, 227–229.

8 A. C. S. Nogueira, L. E. Dicelio and I. Joekes, *Photochem. Photobiol. Sci.*, 2006, **5**, 165–169.

9 S. Ratnapandian, S. B. Warner and Y. K. Kamath, *J. Cosmet. Sci*, 1998, **49**, 309–320.

10 C. Pande and J. Jachowicz, *J. Soc. Cosmet. Chem.*, 1993, **44**, 109–122.

11 R. M. Trüeb, *Int. J. Cosmet. Sci.*, 2015, **37**, 25–30.

12 J. M. Wood, H. Decker, H. Hartmann, B. Chavan, H. Rokos, J. D. Spencer, S. Hasse, M. J. Thornton, M. Shalbaf, R. Paus and K. U. Schallreuter, *FASEB J.*, 2009, **23**, 2065–2075.

13 D. I. Pattison, A. S. Rahmanto and M. J. Davies, *Photochem. Photobiol. Sci.*, 2012, **11**, 38–53.

14 M. Feughelman, *J. Appl. Polym. Sci.*, 2001, **83**, 489–507.

15 L. N. Jones, *Clin. Dermatol.*, 2001, **19**, 95–103.

16 J. A. Swift, in *Practical Modern Hair Science*, eds. A. C. Kozlowski and B. W. Budzynski, Allured Pub Corp, 1st edn., 2012.

17 V. Trunova, N. Parshina and V. Kondratyev, *J. Synchrotron. Radiat.*, 2003, **10**, 371–375.

18 N. Saito and T. Morishima, *Arch. Dermatol. Res.*, 1991, **283**, 7–9.

19 A. C. Santos Nogueira and I. Joekes, *J. Cosmet. Sci.*, 2007, **58**, 385–391.

20 W. Cao, X. Zhou, N. C. McCallum, Z. Hu, Q. Z. Ni, U. Kapoor, C. M. Heil, K. S. Cay, T. Zand, A. J. Mantanona, A. Jayaraman, A. Dhinojwala, D. D. Deheyn, M. D. Shawkey, M. D. Burkart, J. D. Rinehart and N. C. Gianneschi, *J. Am. Chem. Soc.*, 2021, **143**, 2622–2637.

21 G. E. Rogers, *Int. J. Dev. Biol.*, 2004, **48**, 163–170.

22 R. D. B. Fraser and T. P. MacRae, *Biosci. Rep.*, 1983, **3**, 517–525.

23 B. Wang, W. Yang, J. McKittrick and M. A. Meyers, *Prog. Mater. Sci.*, 2016, **76**, 229–318.

24 P. Y. Chen, J. McKittrick and M. A. Meyers, *Prog. Mater. Sci.*, 2012, **57**, 1492–1704.

25 L. Pauling, R. B. Corey and H. R. Branson, *PNAS*, 1951, **37**, 205–211.

26 W. G. Crewther, L. M. Dowling, P. M. Steinert and D. A. D. Parry, *Int. J. Biol. Macromol.*, 1983, **5**, 267–274.

27 C. C. Chou and M. J. Buehler, *Biomacromolecules*, 2012, **13**, 3522–3532.

28 E. Fernández, C. Barba, C. Alonso, M. Martí, J. L. Parra and L. Coderch, *J. Photochem. Photobiol. B*, *Biol.*, 2012, **106**, 101–106.

29 K. R. Millington and J. M. Marsh, *Int. J. Cosmet. Sci.*, 2020, **42**, 174–184.

30 M. J. Davies and R. J. W. Truscott, *J. Photochem. Photobiol. B*, *Biol.*, 2001, **63**, 114–125.

31 M. A. Rogers, L. Langbein, S. Praetzel-Wunder, H. Winter and J. Schweizer, *Int. Rev. Cytol.*, 2006, **251**, 209–263.

32 J. A. Swift, *Scanning Microsc.*, 1979, **2**, 83–88.

33 R. C. Clay and K. Cook, *J. Am. Chem. Soc.*, 1940, **62**, 2709–2710.

34 D. Creed, *Photochem. Photobiol.*, 1984, **39**, 537–562.

35 C. R. Robbins and C. H. Kelly, *Text. Res. J.*, 1970, **40**, 891–896.

36 D. Creed, *Photochem. Photobiol.*, 1984, **39**, 563–575.

37 D. Creed, *Photochem. Photobiol.*, 1984, **39**, 577–583.

38 G. H. Beaven and E. R. Holiday, *Adv. Protein. Chem.*, 1952, **7**, 319–386.

39 W. F. Forbes and W. E. Savige, *Photochem. Photobiol.*, 1962, **1**, 1–13.

40 O. Mozziconacci, B. A. Kerwin and C. Schöneich, *J. Phys. Chem. B*, 2010, **114**, 3668–3688.

41 O. Mozziconacci, V. Sharov, T. D. Williams, B. A. Kerwin and C. Schöneich, *J. Phys. Chem. B*, 2008, **112**, 9250–9257.

42 T. Nauser and C. Schöneich, *J. Am. Chem. Soc.*, 2003, **125**, 2042–2043.

43 A. Rauk, D. Yu, J. Taylor, G. V. Shustov, D. A. Block and D. A. Armstrong, *Biochemistry*, 1999, **38**, 9089–9096.

44 A. Rauk, D. Yu and D. A. Armstrong, *J. Am. Chem. Soc.*, 1998, **120**, 8848–8855.

45 F. M. Welle, H. D. Beckhaus and C. Rüchardt, *J. Org. Chem.*, 1997, **62**, 552–558.

46 T. Nauser, G. Casi, W. H. Koppenol and C. Schöneich, *J. Phys. Chem.B*, 2008, **112**, 15034–15044.

47 C. Schöneich, *Free Radic. Res.*, 2016, **50**, 143–149.

48 C. Schöneich, *Chem. Res. Toxicol.*, 2008, **21**, 1175–1179.

49 C. L. Hawkins and M. J. Davies, *Biochim. Biophys. Acta Bioenerg.*, 2001, **1504**, 196–219.

50 D. B. Wetlaufer, *Adv. Protein. Chem.*, 1963, **2**, 303–390.

51 R. V. Bensasson, E. J. Land and T. G. Truscott, *Excited States and Free Radicals in Biology and Medicine*, Oxford University Press, 1993.

52 Y. Saito, H. Tachibana, H. Hayashi and A. Wada, *Photochem. Photobiol.*, 1981, **33**, 289–295.

53 E. P. L. Hunter, M. F. Desrosiers and M. G. Simic, *Free Radic. Biol. Med.*, 1989, **6**, 581–585.

54 L. R. Karam, M. Dizdaroglu and M. G. Simic, *Int. J. Radiat. Biol.*, 1984, **46**, 715–724.

55 F. Jin, J. Leitich and C. Von Sonntag, *J. Chem. Soc., Perkin Trans. 2*, 1993, **2**, 1583–1588.

56 G. Boguta and A. M. Dancewicz, *Radiat. Phys. Chem.*, 1982, **20**, 359–363.

57 M. J. Davies, *Biochem. Biophys. Res. Commun.*, 2003, **305**, 761–770.

58 A. Wright, W. A. Bubb, C. L. Hawkins and M. J. Davies, *Photochem. Photobiol.*, 2002, **76**, 35–46.

59 M. J. Davies, *Biochem. J.*, 2016, **473**, 805–825.

60 J. M. Gebicki, *Redox Report.*, 1997, **3**, 99–110.

61 S. Fu, S. Gebicki, W. Jessup, J. M. Gebicki and R. T. Dean, *Biochem. J.*, 1995, **311**, 821–827.

62 S. L. Fu and R. T. Dean, *Biochem. J.*, 1997, **324**, 41–48.

63 S. Fu, L. A. Hick, M. M. Sheil and R. T. Dean, *Free Radic. Biol. Med.*, 1995, **19**, 281–292.

64 P. E. Morgan, D. I. Pattison, C. L. Hawkins and M. J. Davies, *Free Radic. Biol. Med.*, 2008, **45**, 1279–1289.

65 M. J. Davies, *Biochim. Biophys. Acta Proteins Proteom.*, 2005, **1703**, 93–109.

66 P. E. Morgan, D. I. Pattison and M. J. Davies, *Free Radic. Biol. Med.*, 2012, **52**, 328–339.

67 M. J. Davies, *Photochem. Photobiol. Sci.*, 2004, **3**, 17–25.

68 A. Wright, C. L. Hawkins and M. J. Davies, *Redox Rep.*, 2000, **5**, 159–161.

69 P. Di Mascio, G. R. Martinez, S. Miyamoto, G. E. Ronsein, M. H. G. Medeiros and J. Cadet, *Chem. Rev.*, 2019, **119**, 2043–2086.

70 S. Criado, A. T. Soltermann, J. M. Marioli and N. A. García, *Photochem. Photobiol.*, 1998, **68**, 453–458.

71 M. Hayyan, M. A. Hashim and I. M. Alnashef, *Chem. Rev.*, 2016, **116**, 3029–3085.

72 Z. Kozmér, E. Arany, T. Alapi, E. Takács, L. Wojnárovits and A. Dombi, *Radiat. Phys. Chem.*, 2014, **102**, 135–138.

73 M. C. Foti, *J. Pharm. Pharmacol.*, 2010, **59**, 1673–1685.

74 B. H. J. Bielski, D. E. Cabelli, R. L. Arudi and A. B. Ross, *J. Phys. Chem. Ref. Data.*, 1985, **14**, 1041–1100.

75 G. Cohen and R. E. Heikkila, *J. Biol. Chem.*, 1974, **249**, 2447–2452.

76 M. F. R. G. Dias, A. M. De Almeida, P. M. R. Cecato, A. R. Adriano and J. Pichler, *Int. J. Trichology*, 2014, **6**, 95–99.

77 H. Orru, C. Andersson, K. L. Ebi, J. Langner, C. Åström and B. Forsberg, *Eur. Respir. J.,* 2013, **41**, 285–294.

78 H. Salonen, T. Salthammer and L. Morawska, *Environ, Int.*, 2018, **119**, 503–514.

79 J. Kobza and M. Geremek, *Int. J. Environ. Res. Public Health*, 2021, **18**, 1473-1493.

80 B. Ryffel, J. Hamacher, S. Manoussa Ethel Fanny, F. Erard, J. Zhang, Y. Wei and Z. Fang, *Front. Immunol.*, 2019, **10**, 2518.

81 K. Ikehata, N. Jodeiri Naghashkar and M. Gamal El-Din, *Ozone Sci. Eng.*, 2006, **28**, 353–414.

82 V. K. Sharma and N. J. D. Graham, *Ozone Sci. Eng.*, 2010, **32**, 81–90.

83 J. A. Lloyd, J. M. Spraggins, M. V Johnston and J. Laskin, *J. Am. Soc. Mass. Spectrom.*, 2006, **17**, 1289.

84 E. D. A M Biochem, Y. Yamamoto, E. Niki, H. Shiokawa and Y. Kamiya, *J. Org. Chem.*, 1979, **44**, 2137–2142.

85 J. Dai, Y. Zhang, J. Wang, X. Li, Z. Lu, Y. Cai and X. Qian, *Rapid Commun. Mass Spectrom.*, 2005, **19**, 1130–1138.

86 W. H. Koppenol and J. Butler, *Adv. Free Radic. Biol. Med.*, 1985, **1**, 91–131.

87 G. R. Buettner, *Arch. Biochem. Biophys.*, 1993, **300**, 535–543.

88 D. M. Miller, G. R. Buettner and S. D. Aust, *Free Radic. Biol. Med.*, 1990, **8**, 95–108.

89 G. V. Buxton, C. L. Greenstock, W. P. Helman and A. B. Ross, *J. Phys. Chem. Ref. Data.*, 1988, **17**, 513–886.

90 M. J. Davies and R. T. Dean, *Radical-mediated protein oxidation : from chemistry to medicine*, Oxford University Press, 1977.

91 E. R. Stadtman and R. L. Levine, *Amino Acids*, 2003, **25**, 207–218.

92 E. Hayon, T. Ibata, N. N. Lichtin and M. Simic, *J. Am. Chem. Soc.*, 1970, **92**, 3898–3903.

93 M. G. Simic, *J. Agric. Food. Chem.,* 1978, **26**, 6-14.

94 G. N. R. Tripathi, *J. Am. Chem. Soc.*, 1998, **120**, 4161–4166.

95 T. Masuda, K. Yoshihara, H. Shinohara and M. Kondo, *J. Radiat. Res.*, 1976, **17**, 106–110.

96 J. J. Pignatello, E. Oliveros and A. MacKay, *Crit. Rev. Environ. Sci. Technol.*, 2006, **36**, 1–84.

97 K. J. Davies, *J. Biol. Chem.*, 1987, **262**, 9895–9901.

98 W. M. Garrison, *Chem. Rev.*, 1987, **87**, 381–398.

99 C. J. Easton, *Chem. Rev*., 1997, **97**, 53-82.

100 E. Blokker, M. ten Brink, J. M. van der Schuur, T. A. Hamlin and F. M. Bickelhaupt, *ChemistryEurope*, 2023, e202300006.

101 J. Uranga, O. Lakuntza, E. Ramos-Cordoba, J. M. Matxain and J. I. Mujika, *Phys. Chem. Chem. Phys.*, 2016, **18**, 30972–30981.

102 N. Karpel Vel Leitner, P. Berger and B. Legube, *Environ. Sci. Technol.*, 2002, **36**, 3083–3089.

103 Z. I. Watts and C. J. Easton, *J. Am. Chem. Soc.*, 2009, **131**, 11323–11325.

104 C. L. Hawkins and M. J. Davies, *J. Chem. Soc. Perkin Trans. 2*, 1998, 2617–2622.

105 E. R. Stadtman, *Annu. Rev. Biochem.*, 1993, **62**, 797–821.

106 G. Xu and M. R. Chance, *Chem. Rev.*, 2007, **107**, 3514–3543.

107 K. R. Lynn and J. W. Purdie, *Int. J. Radiat. Phys. Chem.*, 1976, **8**, 685–689.

108 R. C. Armstrong and A. J. Swallow, *Radiat. Res.*, 1969, **40**, 563–579.

109 S. Solar, *Radiat. Phys. Chem.*, 1985, **26**, 103–108.

110 M. G. Simic, E. Gajewski and M. Dizdaroglu, *Radiat. Phys. Chem.*, 1984, **24**, 465–473.

111 J. Chrysochoos, *Radiat. Res.*, 1968, **33**, 465–479.

112 S. Solar, W. Solar and N. Getoff, *J. Phys. Chem.*, 1984, **88**, 2091–2095.

113 C. Von Sonntag, *J. Chem. Soc., Perkin Trans. 2*, 2001, 264–268.

114 X. R. Liu, M. M. Zhang, B. Zhang, D. L. Rempel and M. L. Gross, *Anal. Chem.*, 2019, **91**, 9238–9245.

115 I. Cudina and Lj. Josimovic, *Radiat. Res.*, 1987, **109**, 206–215.

116 C. Houée-Lévin, K. Bobrowski, L. Horakova, B. Karademir, C. Schöneich, M. J. Davies and C. M. Spickett, *Free Radic. Res.*, 2015, **49**, 347–373.

117 S. P. Gieseg, J. A. Simpson, T. S. Charlton, M. W. Duncan and R. T. Dean, *Biochemistry*, 1993, **32**, 4780–4786.

118 S. Luo, Z. Wei, R. Spinney, F. A. Villamena, D. D. Dionysiou, D. Chen, C. J. Tang, L. Chai and R. Xiao, *J. Hazard. Mater.*, 2018, **344**, 1165–1173.

119 K. M. Bansal and R. W. Fessenden, *Radiat. Res.*, 1976, **67**, 1–8.

120 S. Steenken, C. J. Warren and B. C. Gilbert, *J. Chem. Soc., Perkin Trans. 2*, 1990, **2**, 335–342.

121 D. Wang, H. P. Schuchmann and C. Sonntag von, *Z. Naturforsch. – J. Chem. Sci.*, 1993, **48**, 761–770.

122 J. E. Bennett, D. M. Brown and B. Mile, *Trans. Faraday Soc.,* 1970, **66**, 397–405.

123 J. E. Bennett, *J. Chem. Soc., Faraday Trans.*, 1990, **86**, 3247–3252.

124 S. Abramovitch and J. Rabani, *J. Phys. Chem.*, 1976, **80**, 1562–1565.

125 E. Bothe, M. N. Schuchmann, D. Schulte-Frohlinde and C. von Sonntag, *Photochem. Photobiol.*, 1978, **28**, 639–643.

126 Y. Ilan, J. Rabani and A. Henglein, *J. Phys. Chem.*, 1976, **80**, 1558–1562.

127 J. Rabani, D. Klug-Roth and A. Henglein, *J. Phys. Chem.*, 1974, **78**, 2089–2093.

128 P. Neta, R. E. Huie and A. B. Ross, *J. Phys. Chem. Ref. Data.*, 1990, **19**, 413–513.

129 C. López-Alarcón, A. Arenas, E. Lissi and E. Silva, *Biomol. Concepts*, 2014, **5**, 119–130.

130 L. Batt, *Int. Rev. Phys. Chem*., 1987, **6**, 53– 90

131 B. C. Gilbert, H. A. H. Laue, R. O. C. Norman and R. G. G. Holmes, *J. Chem. Soc., Perkin Trans.s 2*, 1976, 1047–1052.

132 H. A. Headlam, A. Mortimer, C. J. Easton and M. J. Davies, *Chem. Res. Toxicol.*, 2000, **13**, 1087–1095.

133 H. A. Headlam and M. J. Davies, *Free Radic. Biol. Med.*, 2002, **32**, 1171–1184.

134 J. Neuzil, J. M. Gebicki and R. Stocker, *Biochem. J.*, 1993, **293**, 601–606.

135 R. T. Dean, S. Fu, R. Stocker and M. J. Davies, *Biochem. J.*, 1997, **324**, 1–18.

136 R. D. Bach, P. Y. Ayala and H. B. Schlegel, *J. Am. Chem. Soc.*, 1996, **118**, 12758-12765.

137 R. D. Bach and H. B. Schlegel, *J. Phys. Chem*, 2020, **124**, 4742-4751.

138 M. J. Davies, S. Fu and R. T. Dean, *Biochem. J.*, 1995, **305**, 643–649.

139 M. J. Davies, *Arch. Biochem. Biophys.*, 1996, **336**, 163–172.

140 J. A. Simpson, S. Narita, S. Gieseg, S. Gebicki, J. M. Gebicki and R. T. Dean, *Biochem. J.*, 1992, **282**, 621–624.

141 S. Gebicki and J. M. Gebicki, *Biochem. J.*, 1993, **289**, 743–749.

142 S. Robinson, R. Bevan, J. Lunec and H. Griffiths, *FEBS Lett.*, 1998, **430**, 297–300.

143 W. Jessup, R. T. Dean and J. M. Gebicki, *Meth. Enzymol.*, 1994, **233**, 289–303.

144 C. Gay, J. Collins and J. M. Gebicki, *Anal. Biochem.*, 1999, **273**, 149–155.

145 S. P. Wolff, *Meth. Enzymol.*, 1994, **233**, 182–189.

146 C. Gay, J. Collins and J. M. Gebicki, *Redox Rep.*, 1999, **4**, 327–328.

147 R. Bou, R. Codony, A. Tres, E. A. Decker and F. Guardiola, *Anal. Biochem.*, 2008, **377**, 1–15.

148 C. Gay and J. M. Gebicki, *Anal. Biochem.*, 2000, **284**, 217–220.

149 C. L. Hawkins, P. E. Morgan and M. J. Davies, *Free Radic. Biol. Med.*, 2009, **46**, 965–988.

150 M. Gracanin, C. L. Hawkins, D. I. Pattison and M. J. Davies, *Free Radic. Biol. Med.*, 2009, **47**, 92–102.

151 V. V. Agon, W. A. Bubb, A. Wright, C. L. Hawkins and M. J. Davies, *Free Radic. Biol. Med.*, 2006, **40**, 698–710.

152 G. E. Ronsein, M. C. Bof De Oliveira, M. H. Gennari De Medeiros and P. Di Mascio, *J. Am. Soc. Mass. Spectrom.*, 2009, **20**, 188–197.

153 G. E. Ronsein, M. C. B. Oliveira, S. Miyamoto, M. H. G. Medeiros and P. Di Mascio, *Chem. Res. Toxicol.*, 2008, **21**, 1271–1283.

154 S. Gebicki, G. Bartosz and J. M. Gebicki, *Biochem. Soc. Trans.*, 1995, **23**, 249S-249S.

155 M. Baasandorj, D. K. Papanastasiou, R. K. Talukdar, A. S. Hasson and J. B. Burkholder, *Phys. Chem. Chem. Phys.*, 2010, **12**, 12101–12111.

156 P. Gray, A. Williams and P. Gray, *Chem. Rev.*, 1959, **59**, 239–328.

157 R. M. Trüeb, *Int. J. Trichology*, 2009, **1**, 6–14.

158 R. L. Willson, *Oxidative Stress*, Academic Press, London, 1985.

159 J. M. Marsh, M. G. Davis, M. J. Flagler, Y. Sun, T. Chaudhary, M. Mamak, D. W. McComb, R. E. A. Williams, K. D. Greis, L. Rubio and L. Coderch, *Int. J. Cosmet. Sci.*, 2015, **37**, 532–541.

160 P. C. Arck, R. Overall, K. Spatz, C. Liezman, B. Handjiski, B. F. Klapp, M. A. Birch-Machin and E. M. J. Peters, *FASEB J.*, 2006, **20**, e908–e920.

161 P. R. Groves, PhD Thesis, University of York, 2017.

162 M. F. R. G. Dias, *Int. J. Trichology*, 2015, **7**, 2-15.

163 F. Shahidi, P. K. Janitha and P. D. Wanasundara, *Crit. Rev. Food. Sci. Nutr.*, 1992, **32**, 67–103.

164 C. A. Rice-Evans, N. J. Miller and G. Paganga, *Trends Plant Sci.*, 1997, **2**, 152–159.

165 A. J. Grantham, PhD Thesis, University of York, 2017.

166 P. J. H. Williams, PhD Thesis, University of York, 2022.

167 P. J. H. Williams, G. A. Boustead, D. E. Heard, P. W. Seakins, A. R. Rickard and V. Chechik, *J. Am. Chem. Soc.,* 2022, **144**, 15969-15976.

168 W. Zhang, S. Xiao and D. U. Ahn, *Crit. Rev. Food Sci. Nutr.*, 2013, **53**, 1191–1201.

169 C. A. Gay and J. M. Gebicki, *Anal. Biochem.*, 2003, **315**, 29–35.

170 S. Miyamoto, G. E. Ronsein, F. M. Prado, M. Uemi, T. C. Corrêa, I. N. Toma, A. Bertolucci, M. C. B. Oliveira, F. D. Motta, M. H. G. Medeiros and P. Di Mascio, *IUBMB Life*, 2007, **59**, 322–331.

171 C. F. Cruz, M. M. Fernandes, A. C. Gomes, L. Coderch, M. Mart, S. M. Endez, L. Gales, N. G. Azoia, U. Shimanovich and A. Cavaco-Paulo, *Int. J. Cosmet. Sci*., 2013, **35**, 244-249

172 R. M. Trüeb, *Int. J. Cosmet. Sci.*, 2021, **43**, S9–S13.

173 L. A. Beoy, W. J. Woei and Y. K. Hay, *Trop. Life Sci. Res.*, 2010, **21**, 91–99.

174 Z. H. Wang, X. L. Li, Z. Q. Yang and M. Xu, *Biol. Trace Elem. Res.*, 2010, **137**, 280–288.

175 D. F. Mielewski, D. R. Bauer and J. L. Gerlock, *Polym. Degrad. Stab.*, 1991, **33**, 93–104.

176 J. Lemaire, R. Arnaud and J. L. Gardette, *Pure Appl. Chem.*, 1983, **55**, 1603–1614.

177 T. Ojeda, A. Freitas, K. Birck, E. Dalmolin, R. Jacques, F. Bento and F. Camargo, *Polym. Degrad. Stab.*, 2011, **96**, 703–707.

178 M. L. Andersen, M. Gundermann, B. P. Danielsen and M. N. Lund, *J. Agric. Food. Chem.*, 2017, **65**, 10820–10828.

179 L. P. De Oliveira, D. Hudebine, D. Guillaume and J. J. Verstraete, *Oil Gas Sci. Technol.*, 2016, **71**, 1–49.

180 S. Fajardo, García-Galvan, F. R., V. Barranco, J. C. Galvan and S. F. Batlle, in *Physico-Chemical Wastewater Treatment and Resource Recovery*, edited by R. Farooq and Z. Ahmad, InTech, 2017, Chapter 2.

181 P. Kralik, H. Kusic, N. Koprivanac and A. Loncaric Bozic, *J. Chem. Eng.*, 2010, **158**, 154–166.

182 S. Katare, J. M. Caruthers, W. N. Delgass and V. Venkatasubramanian, *Ind. Eng. Chem. Res.,* 2004, **43**, 3484-3512.

183 A. K. Burnham, *Global Chemical Kinetics of Fossil Fuels*, Springer Cham, 2017.

184 G. Litwinienko and K. U. Ingold, *Acc. Chem. Res.*, 2007, **40**, 222–230.

185 D. W. Snelgrove, J. Lusztyk, J. T. Banks, P. Mulder and K. U. Ingold, *J. Am. Chem. Soc.*, 2001, **123**, 469–477.

186 T. Masuda, K. Yoshihara, H. Shinohara and M. Kondo, *J. Radiat. Res.*, 1976, **17**, 106–110.

187 D. P. Nelson and L. A. Kiesow, *Anal. Biochem.*, 1972, **49**, 474–478.

188 S. Goldstein, D. Aschengrau, Y. Diamant and J. Rabani, *Environ. Sci. Technol.*, 2007, **41**, 7486–7490.

189 H. Kušić, N. Koprivanac, A. L. Božić and I. Selanec, *J. Hazard. Mater.*, 2006, **136**, 632–644.

190 J. C. Crittenden, S. Hu, D. W. Hand and S. A. Green, *Water Res.*, 1999, **33**, 2315–2328.

191 P. E. Morgan, R. T. Dean and M. J. Davies, *Free Radic. Biol. Med.*, 2004, **36**, 484–496.

192 E. P. L. Hunter, M. F. Desrosiers and M. G. Simic, *Free Radic. Biol. Med.*, 1989, **6**, 581–585.

193 A. J. Grosvenor, J. Marsh, A. Thomas, J. A. Vernon, D. P. Harland, S. Clerens and J. M. Dyer, *Photochem. Photobiol.*, 2016, **92**, 144–149.

194 I. O. Aruoma, *J. Am. Oil Chem. Soc.*, 1998, **75**, 199–212.

195 N. Maddu, in *Antioxidants*, edited by E. Shalaby and T. Brzozowski, InTech, 2019, Chapter 20.

196 V. Lobo, A. Patil, A. Phatak and N. Chandra, *Pharmacogn. Rev.*, 2010, **4**, 118–126.

197 G. Martemucci, C. Costagliola, M. Mariano, L. D'andrea, P. Napolitano and A. G. D'Alessandro, *Oxygen*, 2022, **2**, 48–78.

198 A. Rahal, A. Kumar, V. Singh, B. Yadav, R. Tiwari, S. Chakraborty and K. Dhama, *Biomed. Res. Int.*, 2014, **2014**, 1-19

199 H. Boeing, A. Bechthold, A. Bub, S. Ellinger, D. Haller, A. Kroke, E. Leschik-Bonnet, M. J. Müller, H. Oberritter, M. Schulze, P. Stehle and B. Watzl, *Eur. J. Nutr.*, 2012, **51**, 637–663.

200 T. C. Wallace, R. L. Bailey, J. B. Blumberg, B. Burton-Freeman, C. y. O. Chen, K. M. Crowe-White, A. Drewnowski, S. Hooshmand, E. Johnson, R. Lewis, R. Murray, S. A. Shapses and D. D. Wang, *Crit. Rev. Food Sci. Nutr.*, 2020, **60**, 2174–2211.

201 K. Mellendick, L. Shanahan, L. Wideman, S. Calkins, S. Keane and C. Lovelady, *Nutrients*, , 2018, **10**, 136-151.

202 H. Cena and P. C. Calder, *Nutrients*, 2020, **12**, 334-349.

203 K. A. Steinmetz and J. D. Potter, *J. Am. Diet. Assoc.*, 1996, **96**, 1027–1039.

204 A. Subar and B. Patterson, *Nutr Cancer*, 1992, **18**, 1–29.

205 W. Mullen, J. Mcginn, M. E. J. Lean, M. R. Maclean, P. Gardner, G. G. Duthie, T. Yokota, ⊥ And and A. Crozier, *J. Agric. Food Chem*., 2002, **50**, 5191-5196.

206 M. A. Eastwood, *QJM*, 1999, **92**, 527–530.

207 J. Pokorný, *Eur. J. Lipid Sci. Technol.*, 2007, **109**, 629–642.

208 R. Sotler, B. Poljšak, R. Dahmane, T. Jukić, D. Pavan Jukić, C. Rotim, P. Trebše and A. Starc, *Acta Clin. Croat.*, 2019, **58**, 726–736.

209 S. Azam, N. Hadi, N. U. Khan and S. M. Hadi, *Toxicol. Vitro*, 2004, **18**, 555–561.

210 L. Y. Lu, N. Ou and Q.-B. Lu, *Sci. Rep.*, 2013, **3**, 1–11.

211 I. Gutiérrez-Del-río, S. López-Ibáñez, P. Magadán-Corpas, L. Fernández-Calleja, Á. Pérez-Valero, M. Tuñón-Granda, E. M. Miguélez, C. J. Villar and F. Lombó, *Antioxidants.* 2021*,* **10***,* 1264-1297.

212 A. Zeb, *J. Food Biochem.*, 2020, **44**, e13394-e13416.

213 R. Franco, G. Navarro and E. Martínez-Pinilla, *Antioxidants*, 2019, **8**, 542-551.

214 E. Yi, J. Y. Hong and E. S. Yoo, *Text. Res. J.*, 2010, **80**, 2124–2131.

215 K. H. Hong, *Fibers Polym.*, 2015, **16**, 565–571.

216 M. S. Brewer, *Compr. Rev. Food Sci. Food Saf.*, 2011, **10**, 221–247.

217 H. Sies, *Redox Biol.*, 2015, **4**, 180–183.

218 K. U. Ingold, *Chem. Rev.*, 1961, **61**, 563–589.

219 D. W. Wilson, P. Nash, H. Singh, K. Griffiths, R. Singh, F. De Meester, R. Horiuchi and T. Takahashi, *Antioxidants*, 2017, **6**, 81-101.

220 M. Carocho, P. Morales and I. C. F. R. Ferreira, *Trends Food Sci Technol*, 2018, 71, 107–120.

221 Y. J. Moon, L. Wang, R. Dicenzo and M. E. Morris, *Biopharm. Drug Dispos.,* 2008, **29**, 205–217.

222 B. N. Moore and R. R. Julian, *Phys. Chem. Chem. Phys.*, 2012, **14**, 3148–3154.

223 M. Lucarini, G. F. Pedulli and M. Cipollone, *J. Org. Chemi.*, 1994, **59**, 5063–5070.

224 V. D. Kancheva, *Eur. J. Lipid Sci. Technol.*, 2009, **111**, 1072–1089.

225 R. Tsao, *Nutrients*, 2010, **2**, 1231–1246.

226 D. B. Mcphail, R. C. Hartley, P. T. Gardner and G. G. Duthie, *J. Agric. Food Chem*., 2003, **51**, 1684-1690.

227 M. Lucarini, P. Pedrielli, G. F. Pedulli, S. Cabiddu and C. Fattuoni, *J. Org. Chem.*, 1996, **61**, 9259–9263.

228 P. Mulder, H. G. Korth, D. A. Pratt, G. A. DiLabio, L. Valgimigli, G. F. Pedulli and K. U. Ingold, *J. Phys. Chem. A Chem.*, 2005, **109**, 2647–2655.

229 M. Lucarini, G. F. Pedulli and M. Guerra, *Chem. Eur. J.*, 2004, **10**, 933–939.

230 M. Altarawneh, B. Z. Dlugogorski, E. M. Kennedy and J. C. Mackie, *J. Phys. Chem. A Chem.*, 2010, **114**, 1098–1108.

231 M. I. De Heer, H. G. Korth and P. Mulder, *J. Org. Chem.*, 1999, **64**, 6969–6975.

232 J. S. Wright, E. R. Johnson and G. A. DiLabio, *J. Am. Chem. Soc.*, 2001, **123**, 1173–1183.

233 A. N. Panche, A. D. Diwan and S. R. Chandra, *J. Nutr. Sci.*, 2016, **5**, 1–15.

234 E. R. Sherwin, *J. Am. Oil Chem. Soc.*, 1978, **55**, 809–814.

235 L. Valgimigli, R. Amorati, M. G. Fumo, G. A. DiLabio, G. F. Pedulli, K. U. Ingold and D. A. Pratt, *J. Org. Chem.*, 2008, **73**, 1830–1841.

236 W. Korytowski, B. Pilas, T. G. Truscottg, -T Sarna, E. J. Land and B. Kalyanaraman, *Arch. Biochem. Biophys.*, 1988, **266**, 277–284.

237 R. Amorati, A. Baschieri, G. Morroni, R. Gambino and L. Valgimigli, *Chem. Eur. J.*, 2016, **22**, 7924–7934.

238 L. R. C. Barclay, M. R. Vinqvist, K. Mukai, S. Itoh and H. Morimoto, *J. Org. Chem.*, 1993, **58**, 7416–7420.

239 D. Loshadkin, V. Roginsky and E. Pliss, *Int. J. Chem. Kinet.*, 2002, **34**, 162–171.

240 V. Roginsky, T. Barsukova, D. Loshadkin and E. Pliss, *Chem. Phys. Lipids*, 2003, **125**, 49–58.

241 A. Pezzella, O. Crescenzi, L. Panzella, A. Napolitano, E. J. Land, V. Barone and M. D'Ischia, *J. Am. Chem. Soc.*, 2013, **135**, 12142–12149.

242 J. K. Dohrmann and B. Bergmann, *J. Phys. Chem.*, 1995, **99**, 1218–1227.

243 A. Alsoufi, M. Altarawneh, B. Z. Dlugogorski, E. M. Kennedy and J. C. Mackie, *J. Mol. Struct.*, 2010, **958**, 106–115.

244 R. Amorati, F. Ferroni, M. Lucarini, G. F. Pedulli and L. Valgimigli, *J. Org. Chem.*, 2002, **67**, 9295–9303.

245 S. Steenken, P. Neta and S. Steenken2, *J Phys Chem*., 1979, **83**, 1134-1137.

246 Y. N. Wang and L. A. Eriksson, *Theor. Chem. Acc.*, 2001, **106**, 158–162.

247 V. Lukeš, A. Kováčová and H. Hartmann, *J. Mol. Liq*., 2022, **360**, 1-10.

248 Y. Song and G. R. Buettner, *Free Radic. Biol. Med.*, 2010, **49**, 919–962.

249 S. Alavi Rafiee, R. Farhoosh and A. Sharif, *Eur. J. Lipid Sci. Technol.*, 2018, **120**, 1800319-1800327.

250 K. Shimizu, R. Kondo, K. Sakai, N. Takeda, T. Nagahata and T. Oniki, *Lipids*, 2001, **36**, 1321–1326.

251 M. Hiasa, M. Kurokawa, K. Ohta, T. Esumi, H. Akita, K. Niki, Y. Yagi, N. Echigo, D. Hatakeyama and T. Kuzuhara, *Food Res. Int.*, 2013, **54**, 72–80.

252 K. Mukai, S. Nagai and K. Ohara, *Free Radic. Biol. Med.*, 2005, **39**, 752–761.

253 V. Tavasi, R. P. A. Bettens and L. P. Leong, *J. Phys. Chem. A Chem.*, 2009, **113**, 3068–3077.

254 J. Alanko, A. Riutta, I. Mucha, H. Vapaatalo and T. Metsä-Ketelä, *Free Radic. Biol. Med.*, 1993, **14**, 19–25.

255 V. Thavasi, L. P. Leong and R. P. A. Bettens, *J. Phys. Chem. A Chem.*, 2006, **110**, 4918–4923.

256 E. A. Pillar-Little, R. C. Camm and M. I. Guzman, *Environ. Sci. Technol.*, 2014, **48**, 14352–14360.

257 Ji. Yue, Y. Side, L. Weizhen and Z. Dayuan, *Sci. China Chem.*, 1998, **41**, 295–300.

258 M. F. Dario, R. Pahl, J. R. De Castro, F. S. De Lima, T. M. Kaneko, C. A. S. O. Pinto, A. R. Baby and M. V. R. Velasco, *J. Photochem. Photobiol. B Biol.*, 2013, **120**, 142–147.

259 Y. Chen, Q. Li, W. P. Zhang, J. J. Cui and X. J. Wu, *Adv. Mat. Res.*, 2013, **821**, 28–31.

260 E. Fernández, B. Martínez-Teipel, R. Armengol, C. Barba and L. Coderch, *J. Photochem. Photobiol. B Biol.*, 2012, **117**, 146–156.

261 M. A. Alboreadi, · Manal, M. Al-Najdawi, · Qais, B. Jarrar and · Said Moshawih, *Adv. Trad. Med.*, 2022, **22**, 155–161.

262 J. Terao, M. Piskula and Q. Yao, *Arch. Biochem. Biophys.*, 1994, **308**, 278–284.

263 Y. J. Cai, L. P. Ma, L. F. Hou, B. Zhou, L. Yang and Z. L. Liu, *Chem. Phys. Lipids*, 2002, **120**, 109–117.

264 Z. Q. Liu, L. P. Ma, B. Zhou, L. Yang and Z. L. Liu, *Chem. Phys. Lipids*, 2000, **106**, 53–63.

265 S. V. Jovanovic, S. Steenken, M. Tosic, B. Marjanovic and M. G. Simic, *J. Am. Chem. Soc.*, 1994, **116**, 4846–4851.

266 T. Masuda, Y. Inaba and Y. Takeda, *J. Agric. Food Chem.*, 2001, **49**, 5560–5565.

267 Y. Zhang, J. P. Smuts, E. Dodbiba, R. Rangarajan, J. C. Lang and D. W. Armstrong, *J. Agric. Food Chem.*, 2012, **60**, 9305–9314.

268 M. Loussouarn, A. Krieger-Liszkay, L. Svilar, A. Bily, S. Birtić and M. Havaux, *Plant Physiol.*, 2017, **175**, 1381–1394.

269 S. Valcic, A. Muders, N. E. Jacobsen, D. C. Liebler and B. N. Timmermann, *Chem. Res. Toxicol.*, 1999, **12**, 382–386.

270 S. Sang, S. Tian, H. Wang, R. E. Stark, R. T. Rosen, C. S. Yang and C. T. Ho, *Bioorg. Med. Chem.*, 2003, **11**, 3371–3378.

271 M. Mochizuki, S. I. Yamazaki, K. Kano and T. Ikeda, *Biochim. Biophys. Acta Gen. Subj.*, 2002, **1569**, 35–44.

272 J. Tan, W. J. C. De Bruijn, A. Van Zadelhoff, Z. Lin and J. P. Vincken, *J. Agric. Food Chem.*, 2020, **68**, 13879–13887.

273 J. Treml and K. Šmejkal, *Compr. Rev. Food Sci. Food Saf.*, 2016, **15**, 720–738.

274 B. Krimmel, F. Swoboda, S. Solar and G. Reznicek, *Radiat. Phys. Chem.*, 2010, **79**, 1247–1254.

275 K. Ulbert, *Nature,* 1962, **195**, 175–175.

276 J. M. Marsh, R. Iveson, M. J. Flagler, M. G. Davis, A. B. Newland, K. D. Greis, Y. Sun, T. Chaudhary and E. R. Aistrup, *Int. J. Cosmet. Sci.*, 2014, **36**, 32–38.

277 K. Kondo, M. Kurihara, N. Miyata, T. Suzuki and M. Toyoda, *Free Radic. Biol. Med.*, 1999, **27**, 855–863.

278 N. Zhu, T. C. Huang, Y. Yu, E. J. LaVoie, C. S. Yang and C. T. Ho, *J. Agric. Food Chem.*, 2000, **48**, 979–981.

279 M. Polovka, V. Brezová and A. Staško, *Biophys. Chem.*, 2003, **106**, 39–56.

280 D. H. Truong, T. C. Ngo, N. T. A. Nhung, D. T. Quang, T. L. A. Nguyen, D. Khiri, S. Taamalli, F. Louis, A. El Bakali and D. Q. Dao, *RSC Adv.*, 2022, **12**, 1499–1514.

281 N. Erkan, G. Ayranci and E. Ayranci, *Food Chem.*, 2008, **110**, 76–82.

282 H. Boulebd, *Phytochemistry*, 2021, **12**, 1499-1514.

283 K. Schwarz and W. Ternes, *Z. Lebensm. Unters. Forsch.*, 1992, **195**, 99–103.

284 J. Z. Xu, S. Ying, V. Yeung, Q. Chang, Y. Huang and Z.-Y. Chen, *J. Nutr*., 2004, **91**, 873-881.

285 H. Ishimoto, A. Tai, M. Yoshimura, Y. Amakura, T. Yoshida, T. Hatano and H. Ito, *Biosci. Biotechnol. Biochem.*, 2012, **76**, 395–399.

286 I. F. F. Benzie and J. J. Strain, *Anal. Biochem.*, 1996, **239**, 70–76.

287 I. F. F. Benzie and J. J. Strain, *Meth. Enzymol.*, 1999, **299**, 15–27.

288 M. Zhang, L. Vervoort, M. Moalin, A. Mommers, C. Douny, G. J. M. den Hartog and G. R. M. M. Haenen, *Free Radic. Biol. Med.*, 2018, **124**, 31–39.

289 K. Kondo, M. Kurihara, N. Miyata, T. Suzuki and M. Toyoda, *Arch. Biochem. Biophys.*, 1999, **362**, 79–86.

290 S. A. B E van Acker, M. J. de Groot, D.-J. van den Berg, M. N. J L Tromp, G. Donné-Op den Kelder, W. J. F van der Vijgh and A. Bast, *Chem. Res. Toxicol*., 1996, **9**, 1305-1312.

291 H. Cao, W. X. Cheng, C. Li, X. L. Pan, X. G. Xie and T. H. Li, *J. Mol. Struct*., 2005, **719**, 177– 183.

292 A. Fujimoto and T. Masuda, *Food Chem.*, 2012, **132**, 901–906.

293 G. Cao, H. M. Alessio and R. G. Cutler, *Free Radic. Biol. Med.*, 1993, **14**, 303–311.

294 M. K. Roy, M. Koide, T. P. Rao, T. Okubo, Y. Ogasawara and L. R. Juneja, *Int. J. Food Sci. Nutr.*, 2010, **61**, 109–124.

295 P. T. Gardner, D. B. McPhail and G. G. Duthie, *J. Sci. Food Agric.*, 1998, **76**, 257–262.

296 P. Oyetakinwhite, H. Tribout and E. Baron, *Oxid. Med. Cell Longev*., 2012, **2012**, 560682-560692.

297 S. C. Moldoveanu and R. Oden, *ACS Omega*, 2021, **6**, 9982-9988.

298 K. F. Pirker, J. F. Severino, T. G. Reichenauer and B. A. Goodman, *Biotechnol. Annu. Rev.*, 2008, **14**, 349–401.

299 L. M. de Macedo, É. M. Dos Santos, L. Militão, L. L. Tundisi, J. A. Ataide, E. B. Souto and P. G. Mazzola, *Plants*, 2020, **9**, 651-663.

300 A. M. Hosking, M. Juhasz and N. Atanaskova Mesinkovska, *Skin Appendage Disord.*, 2019, **5**, 72.

301 M. M. Aboulwafa, F. S. Youssef, H. A. Gad, A. E. Altyar, M. M. Al-Azizi and M. L. Ashour, *Antioxidants*, 2019, **8**, 455-492.

302 D. Xu, M. J. Hu, Y. Q. Wang and Y. L. Cui, *Molecules.* 2019, **24**, 1123-1138.

303 T. Benali, I. Jaouadi, R. Ghchime, N. El Omari, K. Harboul, K. Hammani, M. Rebezov, M. A. Shariati, M. S. Mubarak, J. Simal-Gandara, G. Zengin, M. N. Park, B. Kim, S. Mahmud, L. H. Lee and A. Bouyahya, *Antioxidants,* 2022, **11**, 1842-1861.

304 L. J. Kirschenbaum, X. Qu and E. T. Borish, *J. Soc. Cosmet. Chem.*, 2000, **51**, 169–182.

305 S. Sachdev and K. J. A. Davies, *Free Radic. Biol. Med.*, 2008, **44**, 215–223.

306 M. J. Davies, *Methods*, 2016, **109**, 21–30.

307 M. M. Roessler and E. Salvadori, *Chem. Soc. Rev.*, 2018, **47**, 2534–2553.

308 E. G. Janzen, *Acc. Chem. Res.*, 1971, **4**, 31–40.

309 V. Chechik, E. Carter and D. Murphy, *Electron Paramagnetic Resonance*, Oxford University Press, Oxford, UK, 2016.

310 M. Brustolon and G. Giamello, *Electron Paramagnetic Resonance a Practitioner's Toolkit*. Hoboken, N.J: Wiley, 2009.

311 F. Nami, P. Gast and E. J. J. Groenen, *Appl. Magn. Reason.*, 2016, **47**, 643.

312 G. Lassmann, L. A. Eriksson, F. Himo, F. Lendzian and W. Lubitz, J*. Phys. Chem. A Chem*., 1999, **103**, 1283–1290.

313 M. J. Davies and A. Puppo, *Biochem. J.*, 1992, **281**, 197.

314 M. J. Davies, B. C. Gilbert, C. Hazlewood and N. P. Polack*, J. Chem. Soc., Perkin Trans. 2*, 1995, **0**, 13–21.

315 F. Leinisch, K. Ranguelova, E. F. Derose, J. Jiang and R. P. Mason, *Chem. Res. Toxicol.*, 2011, **24**, 2217–2226.

316 S. E. Gomez-Mejiba, Z. Zhai, M. C. Della-Vedova, M. D. Muñoz, S. Chatterjee, R. A. Towner, K. Hensley, R. A. Floyd, R. P. Mason and D. C. Ramirez, *Biochim. Biophys. Acta Gen. Subj.*, 2014, **1840**, 722–729.

317 R. P. Mason and D. Ganini, *Free Radic. Biol. Med.*, 2019, 131, 318–331.

318 D. C. Ramirez and R. P. Mason, *Curr. Protoc. Toxicol.*, 2005, **24**, 17.7.1-17.7.18.

319 R. P. Mason, *Redox Biol.*, 2016, **8**, 422–429.

320 R. P. Mason, *Free Radic. Biol. Med.*, 2004, **36**, 1214–1223.

321 K. M. Nash, A. Rockenbauer and F. A. Villamena, *Chem. Res. Toxicol.*, 2012, **25**, 1581–1597.

322 D. V. Avila, K. U. Ingold, J. Lusztyk, W. R. Dolbier and H. Q. Pan, *J. Org. Chem.*, 1996, **61**, 2027–2030.

323 M. Hartmann, Y. Li and A. Studer, *Org. Biomol. Chem.*, 2015, **14**, 206–210.

324 S. Bartesaghi and R. Radi, *Redox Biol.*, 2018, **14**, 618–625.

325 G. Ferrer-Sueta, N. Campolo, M. Trujillo, S. Bartesaghi, S. Carballal, N. Romero, B. Alvarez and R. Radi, *Chem. Rev.*, 2018, **118**, 1338–1408.

326 R. Radi, *J. Biol. Chem.*, 2013, **288**, 26464–26472.

327 L. G. Lorentzen, C. Y. Chuang, A. Rogowska-Wrzesinska and M. J. Davies, *Redox Biol.*, 2019, **24**, 101226.

328 R. Radi, *PNAS*, 2018, **115**, 5839–5848.

329 B. Alvarez and R. Radi, *Amino Acids*, 2003, **25**, 295–311.

330 W. A. Prütz, H. Mönig, J. Butler and E. J. Land, *Arch. Biochem. Biophys.*, 1985, **243**, 125–134.

331 R. M. Uppu and W. A. Pryor, *Anal. Biochem.*, 1996, **236**, 242–249.

332 J. Chateauneuf, J. Lusztyk and K. U. Ingold, *J. Org. Chem*, 1988, **53**, 1629–1632.

333 S. Gligorovski, R. Strekowski, S. Barbati and D. Vione, *Chem. Rev.*, 2015, **115**, 13051–13092.

334 H. Yu, G. Liu, B. Dong, R. Jin and J. Zhou, *J. Chem. Eng*., 2021, **424**, 130359-130370.

335 Y. Wang, J. Sun, J. Qiao, J. Ouyang and N. Na, *Anal. Chem.*, 2018, **90**, 45.

336 R. J. Oreilly, A. Karton and L. Radom, *J. Phys. Chem. A*, 2011, **115**, 5496–5504.

337 X. M. Pan, M. N. Schuchmann and C. Von Sonntag, *J. Chem. Soc., Perkin Trans. 2*, 1993, **0**, 289–297.

338 L. M. Dorfman, I. A. Taub and R. E. Bühler, *J. Chem. Phys.*, 1962, **36**, 3051–3061.

339 F. Jin, J. Leitich and C. von Sonntag, *J. Photochem. Photobiol. A Chem.*, 1995, **85**, 101–109.

340 J. A. Howard, *Can. J. Chem.*, 1972, **50**, 2298.

341 P. C. Wong, D. Griller and J. C. Scaiano, *J. Am. Chem. Soc.*, 1982, **104**, 5106–5108.

342 M. S. Bin Mohd Yusof, J. X. Siow, N. Yang, W. X. Chan and Z. H. Loh, *Phys. Chem. Chem. Phys.*, 2022, **24**, 2800–2812.

343 Y. Zubavichus, M. Zharnikov, A. Shaporenko, O. Fuchs, L. Weinhardt, C. Heske, E. Umbach, J. D. Denlinger and M. Grunze, *J. Phys. Chem. A*, 2004, **108**, 4557–4565.

344 D. Kao, A. Chaintreau, J. P. Lepoittevin and E. Giménez-Arnau, *J. Org. Chem.*, 2011, **76**, 6188–6200.

345 E. Giménez Arnau, L. Haberkorn, L. Grossi and J. P. Lepoittevin, *Tetrahedron*, 2002, **58**, 5535–5545.

346 E. Giménez-Arnau, L. Haberkorn, L. Grossi and J. P. Lepoittevin, *Tetrahedron*, 2008, **64**, 5680–5691.

347 S. G. H. Johansson, K. Emilsson, M. Grøtli and A. Börje, *Chem. Re.s Toxicol.*, 2010, **23**, 677–688.

348 S. Johansson, E. Giménez-Arnau, M. Grøtli, A. T. Karlberg and A. Börje, *Chem. Res. Toxicol.*, 2008, **21**, 1536–1547.

349 E. R. Stadtman and R. L. Levine, *Amino Acids*, 2003, **25**, 207–218.

350 A. Radzicka and R. Wolfenden, *J. Am. Chem. Soc.*, 1996, **118**, 6105–6109.

351 Drauz K., Knaup G., Groeger U., *N-acyl Dipeptides and their Compositions*, US Patent No. US5534538A, 1996

352 D. P. Dickinson, S. W. Evans, M. Grellier, H. Kendall, R. N. Perutz, B. Procacci, S. Sabo-Etienne, K. A. Smart and A. C. Whitwood, *Organometallics*, 2019, **38**, 626–637.

353 B. Procacci, S. B. Duckett, M. W. George, M. W. D. Hanson-Heine, R. Horvath, R. N. Perutz, X. Z. Sun, K. Q. Vuong and J. A. Welch, *Organometallics*, 2018, **37**, 855–868.

354 HPK125W - Hi-Tech Lamps, Inc., https://www.hi-techlamps.com/hpk125w/, (accessed 23 February 2020).